

## **Investigating and reversing T-cell dysfunction in the E-TCL1 mouse model of chronic lymphocytic leukaemia (CLL)**

McClanahan, Fabienne

The copyright of this thesis rests with the author and no quotation from it or information derived from it may be published without the prior written consent of the author

For additional information about this publication click this link.

<http://qmro.qmul.ac.uk/jspui/handle/123456789/8761>

Information about this research object was correct at the time of download; we occasionally make corrections to records, please therefore check the published record when citing. For more information contact [scholarlycommunications@qmul.ac.uk](mailto:scholarlycommunications@qmul.ac.uk)

Investigating and reversing T-cell  
dysfunction in the E $\mu$ -TCL1 mouse  
model of chronic lymphocytic leukaemia  
(CLL)

Fabienne McClanahan

A thesis submitted for the degree of Doctor of Philosophy  
Queen Mary University of London

November 2014

Centre for Haemato-Oncology  
Barts Cancer Institute

**Abstract**

Chronic lymphocytic leukaemia (CLL) is the most common adult leukaemia, and despite recent introduction of targeted therapies, remains incurable. An important hallmark of CLL is severe immune deficiency, including the failure to mount effective anti-tumour immune responses. This can partly be explained by insufficient antigen presentation, but also by the existence of complex CLL-induced T-cell defects. Based on the cancer immuno-editing hypothesis that the immune system not only protects a host against tumour formation but can also be compromised to actively provide a pro-tumour microenvironment, modulating cancer-induced T-cell defects could restore the full anti-tumour response and result in more durable clinical responses.

The immune checkpoint molecules PD-1 (expressed on activated immune effector cells) and PD-L1 (expressed on antigen-presenting and microenvironmental cells including tumour cells) have emerged as important mediators of T-cell suppression. Several studies suggest that PD-L1/PD-1 inhibitory signalling in CLL might be overcome by the immune modulatory drug lenalidomide. Furthermore, directly targeting PDL-1/PD-1 interactions produces significant responses in solid cancers. However, similar studies are notably absent in CLL, and the effect of PDL-1/PD-1 blockade on restoring cancer-induced immune dysfunction is not understood.

Transgenic E $\mu$ -TCL1 mice have been extensively validated as an adequate preclinical model of aggressive human CLL, and our group showed their suitability to mirror T-cell defects observed in human CLL. Using the E $\mu$ -TCL1 model, this dissertation project substantially extends our previous characterization of CLL-induced T-cell dysfunction and evaluates the functional impact of PD-L1/PD-1 inhibitory signalling both in parallel with disease development and in different microenvironments.

The findings to be described here demonstrate that developing CLL is associated with specific T-cell subset alterations, phenotypic changes, and functional defects that are very similar in peripheral blood and secondary lymphoid organs. In addition to PD-L1, PD-L2 is identified as a potential mediator of inhibitory signalling in CLL. CD8<sup>+</sup> T cells in leukaemic mice are characterised as a functionally heterogeneous population, in which subsets of cells are able to exert effector functions despite PD-1 expression. *In vivo* lenalidomide treatment repairs selected phenotypic alterations and immune synapse formation, and a PD-L1 IgG blocking antibody effectively controls disease and reverses global T-cell defects even in cells expressing PD-1. In sum, this work provides a strong rationale to explore PD-L1/PD-1 targeting in CLL clinical trials, potentially in combination with novel agents.

**Statement of Work Undertaken**

I, Fabienne McClanahan, confirm that the research included within this thesis is my own work or that where it has been carried out in collaboration with, or supported by others, that this is duly acknowledged below and my contribution indicated. Previously published material is also acknowledged below. I attest that I have exercised reasonable care to ensure that the work is original, and does not to the best of my knowledge break any UK law, infringe any third party's copyright or other Intellectual Property Right, or contain any confidential material. I accept that the College has the right to use plagiarism detection software to check the electronic version of the thesis. I confirm that this thesis has not been previously submitted for the award of a degree by this or any other university. The copyright of this thesis rests with the author and no quotation from it or information derived from it may be published without the prior written consent of the author.

All sources of information have been properly referenced.

Initial TCL1 mouse breeding pairs were provided by Prof. Carlo Croce of the Ohio State University Columbus.

From April 15<sup>th</sup> 2013, the day-to-day breeding and maintenance of mice was assisted by Mr Shaun Miller. Selected animal interventions were performed by Shaun Miller, the Animal Technician Service (ATS) to include Mrs Julie Andow Cleaver, Mr Hagen Schmitt, and Mrs Tracy Chapman-Perkins, or by the Biological Services Unit (BSU) staff member Mr Arif Mustafa under my direction and following experimental procedures, plans and standard operation procedures that I have established.

Lenalidomide was extracted from capsules donated by CLL patients no longer on treatment, and was purified in the OSU College of Pharmacy by Dr. Chia-Hsien Wu.

Mass spectrometry was performed by Mr Essam Ghazaly.

Flow sorting was performed by Dr. Guglielmo Rossignoli and Mr William Day.

Statistical analyses were performed by me but after consultation with Dr. Donna Neuberg of the Dana Faber Cancer Institute Boston.

Work described in Chapter 7 (Potential of *in vivo* lenalidomide) and Chapter 8 (Potential of *in vivo* PD-L1 blockade) was performed in collaboration with Dr. Martina Seiffert (Group Leader, Department of Molecular Genetics), Prof. Peter Lichter (Centre Lead) and Mr Bola Hanna (Ph.D. student) of the German Cancer Research Center (DKFZ), Heidelberg, Germany. Within this collaboration, I provided the planning of mouse numbers and experimental set-up, conducted the adoptive transfers with donor

cells from transgenic mice aged in our colony, applied experimental substances and monitored mice daily. Samples from mice reaching experimental endpoints were shared. Information on mouse and CLL characteristics (*i.e.* mouse morphometry, photographs, CLL loads in organs) was shared. Mr Hanna conducted the majority of his experiments in our facilities and with my assistance, to examine the effect of *in vivo* treatment on restoring myeloid defects observed in leukaemic mice. Additional experiments on shared samples were performed in the DKFZ laboratory, but were related to myeloid defects. No results of these experiments are used in this thesis. In addition, I provided Mr Hanna with access to leukaemic TCL1 mice aged in our colony and samples from mice with CLL after adoptive transfer to allow him to characterize myeloid defects in this context.

A handwritten signature in black ink, appearing to read 'Fabienne McClanahan', with a long horizontal flourish extending to the right.

05/02/2015

**Dedication**

To John, Carmen, Volker, Corinne and David.

**Acknowledgements**

This work was funded by a Mildred-Scheel Postdoctoral Fellowship awarded by Deutsche Krebshilfe (salary 2011-2013), by the Virtual Helmholtz Institute "VH404 - Resistance in Leukaemia" (salary and consumables, 2013-2015), and by the Kenneth Street Endowment Fund (consumables, 2011-2015).

My sincere thanks go to my primary supervisor, John Gribben, for his mentorship, guidance and inspiration. He provided the necessary structures for the project, and introduced me into a great network of CLL experts. I deeply value his unconditional support and the freedom to pursue my goals, his trust, patience and encouragement, the opportunities to attend and present at national and international conferences and meetings, and the chance to write articles and contribute to a haematology text book with him. I would also like to thank my secondary supervisor, Melania Capasso, for all her patient and kind support, and her advice on my projects and career development.

A very special thanks to Shaun Miller and John Riches for their support in science and life and for becoming such great comrades.

Other people at Barts Cancer Institute who have helped me greatly in the last three years are Guglielmo Rossignoli, Will Day, Julie Andow Cleaver, Tracy Chaplin Perkins, Hagen Schmitt, Arif Mustafa, Eleni Kotsiou, Essam Ghazaly, Cristina Ghirelli, Elayne Hondares Viera, Juliana Candido, Foggy Andrew Clear, Sameena Iqbal, Li Jia, David Taussig, Tom Butler, Paul Greaves and Simon Hallam – you all rock!

I am very grateful to Prof. Carlo Croce for inviting me to work in his laboratory at the Ohio State University for 3 months in 2013, which was a unique opportunity to gain insight into a different research environment and allowed me to develop the idea for the TLR7/miRNA/PD-L1 project. I would also like to thank the CLL Research Consortium and all CRC collaborators for their feedback, mice and reagents and for fantastic meetings in San Diego and at ASH. I am also much obliged to our German collaborators Peter Lichter, Daniel Mertens and Martina Seiffert.

Finally, I would like to thank my 2013 TRTH mentors and peers, for a difficult but fantastic mentorship programme and for making me believe in myself.

**Publications****Original articles:**

**McClanahan F\***, Hanna B\*, Miller S, Clear AJ, Lichter P, Gribben JG\*, Seiffert M\*. *Immune Checkpoint Blockade Prevents Immune Dysfunction and Leukemia Development in a Mouse Model of Chronic Lymphocytic Leukemia*. Currently under review for Blood. \*Equal contribution

Riches JC, O'Donovan CJ, Kingdon SJ, **McClanahan F**, Clear AJ, Neubergh DS, Werner L, Croce CM, Ramsay AG, Rassenti LZ, Kipps TJ, Gribben JG. *Trisomy 12 Chronic Lymphocytic Leukemia cells exhibit functional upregulation of integrin signaling that is modulated by NOTCH1 mutations*. Blood. 2014 Jun 26;123(26):4101-10.

Riches JC, Davies JK, **McClanahan F**, Fatah R, Iqbal S, Agrawal S, Ramsay AG, Gribben JG. *T cells from CLL patients exhibit features of T-cell exhaustion but retain capacity for cytokine production*. Blood 2013;121:1612-21.

**Book contributions:**

**McClanahan F**, Gribben JG. Chapter 78: *Functions of T lymphocytes: T-cell receptors for antigen*. In: Williams Hematology, 9<sup>th</sup> Edition, in press.

**Review articles:**

**McClanahan F**, Gribben JG. *Overcoming Immunodeficiency in Chronic Lymphocytic Leukaemia: current knowledge and perspectives*. EMJ Hema. 2014;1:70-79.

**McClanahan F**, Gribben JG. *Transplantation in chronic lymphocytic leukemia: Does it still matter in the era of novel targeted therapies?* Hematol Oncol Clin North Am, 2014; 28(6):1055-1071.

**Commentaries:**

**McClanahan F**, Gribben JG. *Immunotherapeutic approaches have the potential to brighten the future not only for patients with del(17p13.1), but for all CLL patients*. Oncology (Williston Park). 2012 Nov;26(11):1055, 1058.

**Meeting abstracts:**

**McClanahan F**, Calore F, Zanesi N, Gribben JG, Croce CM. *Aberrant PD-L1 Expression in CLL As a Result of Adaptive Immune Resistance Mediated By Tumor-Secreted Circulating miRNA Binding to Toll-like Receptor 7*. Blood 2014; 122:Abstract 716 (Oral presentation).

Hanna B\*, **McClanahan F\***, Miller S, Clear AJ, Lichter P, Gribben JG, Seiffert M. *Immune Checkpoint Blockade with Anti-PD-L1 Prevents Immune Dysfunction and CLL Development in the TCL1 Adoptive Transfer Mouse Model*. Blood 2014; 122:Abstract 717 (Oral presentation). \*Equal contribution

Hanna B, **McClanahan F**, Zaborsky N, Dürr C, Kalter V, Egle A, Gribben J, Lichter P, Seiffert M. *Targeting Dysfunctional Myeloid Cells Delays Disease Development and Improves Immune Function in a CLL Mouse Model*. Blood 2014; 122:Abstract 3298 (Poster presentation).

Dürr C, Hanna B, **McClanahan F**, Clear AJ, Zenz T, Stilgenbauer S, Gribben JG, Lichter P, Seiffert M. *The Flavonoid Wogonin Reduces CLL Cell Survival in Vitro and Leukemia Development in Eμ-TCL1 Mice By Targeting Aberrant TNF Receptor Signaling*. Blood 2014; 122:Abstract 1966 (Poster presentation).

**McClanahan F**, Riches JC, Miller S, Ghazaly E, Day WP, Capasso M, Gribben JG. *PD-1/PD-L1 mediated T-cell dysfunction in CLL is not absolute and can be at least partially reversed in vivo by the immune-modulatory drug lenalidomide*. Oncology Research and Treatment 2014; 37(Supplement 5):Abstract V732 (Oral presentation).

Hanna B, **McClanahan F**, Zaborsky N, Dürr C, Gschwend V, Stilgenbauer S, Egle A, Gribben J, Lichter P, Seiffert M. *CLL induces severe skewing in the myeloid compartment in patients and in the TCL1 mouse model*. Haematologica 2014 99 (supplement 1) Abstract S660 (Oral presentation).

**McClanahan F**, Miller S, Riches JC, Ghazaly E, Day WP, Capasso M, Gribben JG. *T-Cell Dysfunction In CLL Is Mediated Not Only By PD-1/PD-L1 But Also By PD-1/PD-L2 Interactions - Partial Functionality Is Maintained In PD-1 Defined CD8 Subsets and This Can Be Further Promoted By Ibrutinib Treatment*. Blood 2013; 122:Abstract 4120 (Poster presentation).

O'Donovan C., Ramsay AG, **McClanahan F**, Rassenti L, Kipps TJ, Gribben JG, Riches JC. *Trisomy 12 CLL Cells Have High Surface Expression Of Integrins Involved In Lymphocyte Trafficking But This Does Not Translate Into Improved LFA-1-Mediated Motility*. Blood 2013; 122:Abstract 4159 (Poster presentation).

Riches JC, Sangaralingam A, Chaplin T, **McClanahan F**, Iqbal S, Agrawal SG, Ramsay AG, Gribben JB. *NK Cells From CLL Patients Exhibit Down-Regulation Of Interferon Response Genes That Can Be Reversed With Lenalidomide*. Blood 2013; 122: Abstract 4131 (*Poster presentation*).

Chen SS, Herndon TM, Emson C, Riches JC, **McClanahan F**, Tong T, Yan XJ, Patten PEM, Gribben JB, Wiestner A, Chiorazzi N. *Intraclonal Complexity Of CLL Fractions In Cell Proliferation Rates, Gene Expression Signatures, and Responses To Autologous T-Cell Help In Peripheral blood and Secondary Lymphoid Tissues*. Blood 2013; 122: Abstract 115 (*Oral presentation*).

**McClanahan F**, Riches JC, Miller S, Durance C, Petty R, Capasso M, Gribben JG. *PD-1/PD-L1 axis-mediated T-cell dysfunction and CLL are causally related but partial functionality is maintained and potentially reversible in PD-1 defined CD8 subsets*. *iwCLL meeting 2013* (*Oral presentation*).

**McClanahan F**, Ghirelli C, Greaves P, Riches JC, Coutinho R, Ramsay AG, Gribben JG. *Inhibitory Ligands CD200, CD270, CD274 and CD276 Are Expressed On Eμ-TCL1 Transgenic Mouse Splenocytes and Are of Potential Relevance to Impaired T-Cell Function in Vivo*. Blood 2013; 120: Abstract 313 (*Oral presentation*).

Riches JC, Davies JK, **McClanahan F**, Iqbal S, Fatah R, Agrawal S, Ramsay AG, Gribben JG. *Characterizing Immunophenotypic And Functional Pseudo-exhaustion in T Cells From CLL Patients: The Impact of Lenalidomide*. Blood 2012; 120: Abstract 564 (*Oral presentation*).

Riches JC, Davies JK, **McClanahan F**, Iqbal S, Fatah R, Agrawal S, Ramsay AG, Gribben JG. *Identification of an expanded population of terminally differentiated CD8+ T cells with a novel phenotypic and functional profile in patients with CLL*. Haematologica 2012; 97 (supplement 1) Abstract 1099 (*Oral presentation*).

**Table of Contents**

Abstract .....	2
Statement of Work Undertaken.....	3
Dedication .....	5
Acknowledgements.....	6
Publications .....	7
Table of Contents .....	10
List of Figures .....	15
List of Tables .....	17
Abbreviations.....	18
1 Background .....	25
1.1 Chronic lymphocytic leukaemia .....	25
1.1.1 Epidemiology and clinical features of the disease.....	25
1.1.2 Clinical staging and prognosis .....	25
1.1.3 Current treatment options and unmet needs.....	27
1.1.4 Immune dysfunctions in CLL.....	33
1.2 Murine models of CLL.....	39
1.2.1 E $\mu$ -TCL1 mouse model.....	39
1.2.1.1 Generation and disease characteristics .....	39
1.2.1.2 Suitability to mirror the biology of human CLL.....	41
1.2.1.3 Suitability as a preclinical tool to test <i>in vivo</i> efficacy of substances.....	42
1.2.2 Alternative genetically engineered murine models of CLL.....	43
1.2.3 TCL1 model-based crosses with other murine models.....	45
1.2.4 Xenograft models of CLL.....	46
1.3 PD-L1/PD-1 immune checkpoint interactions.....	47
1.3.1 PD-L1/ PD-1 in physiological immune responses .....	47
1.3.2 PD-L1 and PD-1 inhibitory signalling and adaptive immune resistance in cancer.....	53
1.4 Generating anticancer immunity harnessing T cell responses .....	56
1.4.1 Potential of novel agents to correct immune defects in CLL.....	57
1.4.2 PD-L1 and PD-1 blockade in cancer.....	59
1.5 Summary.....	62
2 Hypothesis and aims of the project.....	63
3 Materials and Methods .....	64
3.1 Mice and animal procedures.....	64
3.1.1 Ethical considerations relating to animal work .....	64
3.1.2 Breeding and standard maintenance of mice.....	65

3.1.3	Haematology testing.....	66
3.1.4	Processing of mouse organs into single cell suspension .....	66
3.1.5	Adoptive transfer of syngeneic mouse cells .....	67
3.1.6	Application of experimental substances.....	67
3.2	Cell thawing procedures .....	68
3.3	Cell separation procedures.....	68
3.3.1	Positive selection of CLL and B cells .....	68
3.3.2	Negative selection of T cells .....	69
3.4	Flow cytometry .....	69
3.4.1	Surface staining.....	69
3.4.2	Intracytoplasmic and intranuclear staining .....	70
3.4.3	Absolute numbers.....	71
3.4.4	Flow cytometry based functional T-cell assays .....	72
3.4.4.1	Cell stimulation for functional assays .....	72
3.4.4.2	Proliferation assays .....	72
3.4.4.2.1	CFSE labelling of lymphocyte for <i>in vitro</i> proliferation assay.....	72
3.4.4.2.2	Intranuclear ki67 .....	73
3.4.4.2.3	EdU incorporation.....	73
3.4.4.3	CD107a degranulation assay.....	74
3.4.5	Flow Sorting .....	74
3.4.6	Controls.....	74
3.4.7	Data acquisition and analysis .....	75
3.5	Immune synapse formation assay .....	76
3.5.1	Cell conjugation assays.....	76
3.5.2	Staining for confocal microscopy .....	77
3.5.3	Confocal microscopy and image analysis .....	77
3.6	Statistical considerations .....	78
4	Breeding and maintenance of TCL1 mice and induction of disease by adoptive transfer.....	79
4.1	Specific introduction .....	79
4.2	Goals and objectives .....	79
4.3	Specific methods .....	80
4.3.1	Genotyping .....	80
4.3.2	Follow-up by haematology testing.....	80
4.3.3	Adoptive transfer experiments .....	81
4.4	Results .....	81
4.4.1	Genomic PCR and TCL1 sequence analysis .....	81
4.4.2	Haematology testing and anatomic sites of disease .....	82

4.4.3	Adoptive transfer experiments .....	84
4.5	Discussion .....	90
5	Investigation of T-cell dysfunction in TCL1 mice on the B6 background....	92
5.1	Specific introduction .....	92
5.2	Goals and objectives .....	94
5.3	Specific methods and materials .....	94
5.3.1	Mice and examined organs.....	94
5.3.2	Multicolour flow cytometry for cell surface markers.....	96
5.3.3	Multicolour flow cytometry for intracellular cytokines/effector function.....	98
5.3.4	Multicolour flow cytometry for <i>in vivo</i> proliferation.....	101
5.4	Results .....	102
5.4.1	CLL progressively develops in transgenic TCL1 mice but shows considerable biological diversity, and can be consistently induced by AT in peripheral blood and secondary lymphoid organs.....	102
5.4.2	Developing CLL is associated with significant changes in relative and absolute numbers of T-cell subsets in spleen .....	103
5.4.3	CLL-specific T-cell subset changes are recapitulated in blood.....	109
5.4.4	CLL-specific T-cell subset changes are recapitulated in bone marrow....	111
5.4.5	T-cell subset changes exhibit particular patterns in lymph nodes.....	113
5.4.6	Developing CLL and CD3+, CD4+, CD8+ subset changes are significantly correlated with each other .....	115
5.4.7	Developing CLL leads to characteristic functional changes in T-cell intracellular cytokines and effector cytotoxicity function .....	116
5.4.8	Developing CLL is accompanied by increasing T-cell proliferation.....	120
5.4.9	Developing CLL is accompanied by impaired ability of autologous B and T cells to form immunological synapses.....	121
5.5	Summary of phenotypic and functional T-cell defects developing with progressing CLL .....	122
5.6	Discussion .....	124
6	PD-L1/ PD-1 mediated T-cell dysfunction and T-cell exhaustion in TCL1 mice on the B6 background .....	130
6.1	Specific introduction .....	130
6.2	Goals and objectives .....	133
6.3	Specific methods and materials .....	133
6.3.1	Mice and examined organs.....	133
6.3.2	Multicolour flow cytometry for inhibitory ligand expression on normal and malignant B cells.....	135
6.3.3	Comparison of gene-expression profiles from T-cell subsets in deposited data.....	136
6.3.4	Multicolour flow cytometry for surface expression of T-cell exhaustion markers .....	137

6.3.5	Multicolour flow cytometry for intracellular cytokines/effector function in AT experiments unmasking the effect of ageing .....	138
6.3.6	Flow sorting of PD-1 subsets for immune synapse formation assays.....	140
6.4	Results .....	142
6.4.1	Inhibitory ligands CD200, CD270, CD274 (PD-L1) and CD276 are expressed on murine CLL cells but only CD274 and CD276 are significantly upregulated compared to normal B cells .....	142
6.4.2	Highly aberrant PD-L1 and PD-L2 expression are exclusive to malignant CLL cells and develop in the context of advancing disease regardless of microenvironment .....	144
6.4.3	Molecular signature of exhausted T-cells from LCMV infection model is represented in murine CLL T cells but similarities to functional effector cells are maintained.....	146
6.4.4	Typical exhaustion phenotype is modelled in TCL1 mice but is confounded by ageing .....	148
6.4.5	Aberrant PD-1 expression by CD3+CD8+ T cells develops largely regardless of microenvironment.....	152
6.4.6	Randomized AT experiments unmask the effect of ageing .....	153
6.4.6.1	Confirmation of CLL-induced specific T-cell phenotype in both WT and TCL1 recipients .....	153
6.4.6.2	CLL induces aberrant expression of surface exhaustion markers .....	155
6.4.6.3	CLL induces altered cellular survival cytokine profile indicating switch from IL-7 to IL-2 dependency.....	158
6.4.6.4	CLL T-cells maintain certain effector functions such as cytokine production and degranulation despite PD-1 expression .....	159
6.4.6.5	The ability to form immunological synapses is significantly impaired in PD-1 <sup>high</sup> compared to PD-1 <sup>low</sup> cells.....	164
6.4.7	PD-1 expressing normal T cells have markedly different effector functions than PD-1 expressing CLL T cells .....	166
6.4.8	Summary of PD-L1/PD-1 mediated T-cell dysfunction and T-cell exhaustion in TCL1 mice .....	170
6.5	Discussion .....	172
7	Potential of <i>in vivo</i> lenalidomide treatment to restore T-cell function in TCL1 mice .....	179
7.1	Specific introduction .....	179
7.2	Goals and objectives .....	182
7.3	Specific methods and materials .....	182
7.3.1	Mice and randomization procedure.....	182
7.3.2	Drug preparation and stability .....	183
7.3.3	Multicolour flow cytometry for cell surface markers.....	186
7.3.4	Multicolour flow cytometry for intracellular cytokines/effector function.....	187
7.3.5	Immune synapse formation assays.....	187
7.3.6	<i>Ex vivo</i> lenalidomide treatment of autologous murine B and T cells.....	187

7.3.7	<i>Ex vivo</i> PD-L1 and PD-1 blockade.....	188
7.4	Results .....	190
7.4.1	<i>In vivo</i> lenalidomide treatment does not result in effective CLL control and has no effect on aberrant PD-L1 and PD-L2 expression .....	190
7.4.2	Lack of CLL control is reflected by persistence of typical CLL-induced aberrant T-cell phenotype .....	191
7.4.3	<i>In vivo</i> lenalidomide treatment prevents development of typical CLL-induced exhaustion-like T-cell phenotype .....	193
7.4.4	<i>In vivo</i> lenalidomide treatment does not restore key T-cell effector functions.....	194
7.4.5	<i>In vivo</i> lenalidomide treatment improves immune synapse formation which can be further improved by additional <i>ex vivo</i> PD-L1 blockade .....	196
7.4.6	Lenalidomide is detectable in tissues and plasma of treated mice .....	199
7.5	Summary of effect of <i>in vivo</i> lenalidomide treatment on T-cell dysfunction and T-cell exhaustion in TCL1 mice .....	200
7.6	Discussion .....	202
8	Potential of <i>in vivo</i> PD-L1 blockade to restore T-cell dysfunction .....	208
8.1	Specific introduction .....	208
8.2	Goals and objectives .....	210
8.3	Specific methods and materials .....	211
8.3.1	Mice and <i>in vivo</i> treatment.....	211
8.3.2	Multicolour flow cytometry for cell surface markers.....	211
8.3.3	Multicolour flow cytometry for intracellular cytokines/effector function.....	213
8.3.4	Immune synapse formation assays.....	214
8.4	Results .....	214
8.4.1	<i>In vivo</i> anti-PD-L1 treatment effectively controls CLL and prevents PD-L2 expression on normal B cells.....	214
8.4.2	<i>In vivo</i> anti-PD-L1 treatment prevents development of the typical CLL-induced aberrant T-cell phenotype.....	217
8.4.3	<i>In vivo</i> anti-PD-L1 treatment prevents development of typical CLL-induced exhaustion-like T-cell phenotype .....	219
8.4.4	<i>In vivo</i> anti-PD-L1 treatment corrects key T-cell effector functions.....	220
8.4.5	<i>In vivo</i> anti-PD-L1 treatment corrects key effector functions attributed to PD-1 expression.....	223
8.5	Summary of effect of <i>in vivo</i> PD-L1 blockade on T-cell dysfunction and T-cell exhaustion in TCL1 mice.....	225
8.6	Discussion .....	226
9	Overall Discussion.....	231
10	Appendix .....	238
11	References .....	240

## List of Figures

<b>Figure 1:</b> BCR signalling pathway and targets for molecular inhibitors .....	30
<b>Figure 2:</b> Summary of genetically engineered models crossed with TCL1 mice .....	45
<b>Figure 3:</b> Effect of PD-1 ligation on intracellular targets in T cells.....	52
<b>Figure 4:</b> Validation of genotyping procedure and protocol to maintain TCL1 mice ....	82
<b>Figure 5:</b> Results of routine haematology testing in TCL1 and WT mice .....	83
<b>Figure 6:</b> Anatomic sites of CLL in TCL1 transgenic mice .....	83
<b>Figure 7:</b> Longitudinal follow-up of disease development in recipient mice after AT ...	85
<b>Figure 8:</b> Comparison of AT into young TCL1 transgenic and WT recipients. ....	87
<b>Figure 9:</b> Improvement of AT model by reducing the number of i.v. injections.....	88
<b>Figure 10:</b> Reproducibility of and survival after AT.....	90
<b>Figure 11:</b> Optimization of CCR7 4B.12 antibody.....	97
<b>Figure 12:</b> Gating strategy to identify naive vs. antigen-experienced effector, memory, central memory and effector memory CD8 T cells.....	98
<b>Figure 13:</b> Gating strategy for functional T-cell assays.....	100
<b>Figure 14:</b> Gating strategy for EdU <i>in vivo</i> proliferation. ....	101
<b>Figure 15:</b> CLL development in ageing TCL1 mice and after AT in blood and secondary lymphoid organs .....	103
<b>Figure 16:</b> T-cell subset changes in ageing TCL1 mice and after AT in spleen .....	106
<b>Figure 17:</b> Confirmation of T-cell subset changes in spleen .....	108
<b>Figure 18:</b> Confirmation of T-cell subset changes in ageing TCL1 and WT mice and after AT in peripheral blood.....	111
<b>Figure 19:</b> T-cell subset changes in bone marrow.....	113
<b>Figure 20:</b> T-cell subset changes in lymph nodes .....	114
<b>Figure 21:</b> Statistical correlations between CLL and T-cell subsets.....	115
<b>Figure 22:</b> Intracellular cytokine production by CD4+ and CD8+ cell subsets.....	117
<b>Figure 23:</b> Effector cell function in antigen experienced cells .....	119
<b>Figure 24:</b> Proliferation in T-cell subsets .....	120
<b>Figure 25:</b> Proliferation of healthy B and CLL cells <i>in vivo</i> .....	121
<b>Figure 26:</b> Development of immune synapse formation. ....	122
<b>Figure 27:</b> Heatmap summary of p-values describing differences in functional T-cell subsets .....	123
<b>Figure 28:</b> Overview of mice to assess expression of inhibitory ligands on spleen CLL and normal B cells.....	134
<b>Figure 29:</b> Gating strategy to assess expression of inhibitory ligands .....	136
<b>Figure 30:</b> Flow sorting of CD8+ T cells according to PD-1 expression.....	141
<b>Figure 31:</b> Expression of CD200, CD270, CD274 and CD276 on CLL/B cells.....	143
<b>Figure 32:</b> Development of PD-L1/PD-L2 expression alongside advancing CLL in different organs.....	145
<b>Figure 33:</b> Comparison of gene expression profiles between deposited data.....	147
<b>Figure 34:</b> PD-1 surface expression on naïve/antigen-experienced CD3+CD8+ spleen cells .....	149
<b>Figure 35:</b> Surface expression of other exhaustion markers on naïve/antigen- experienced CD3+CD8+ cells from spleen.. ..	150
<b>Figure 36:</b> Surface expression of CD160 on naïve/antigen-experienced CD3+CD8+ cells from spleen.....	151
<b>Figure 37:</b> Heatmap summary of p-values describing differences in relative and absolute changes of cell subsets expressing typical exhaustion markers .....	152
<b>Figure 38:</b> Development of PD-1 expression on CD3+CD8+ T cells alongside advancing CLL in different organs .....	153
<b>Figure 39:</b> Confirmation of CLL-specific T-cell phenotype in AT mice .....	154
<b>Figure 40:</b> CLL-induced aberrant expression of PD-1 on CD3+CD8+ cells. ....	155
<b>Figure 41:</b> CLL-induced aberrant expression of KLRG-1, 2B4 and LAG-3 on CD3+CD8+ cells.....	156

<b>Figure 42:</b> CLL-induced expression of CD160 on CD3+CD8+ cells. ....	157
<b>Figure 43:</b> CLL-induced expression of IL-2 and IL-7 cytokine receptors on CD3+CD8+ cells. ....	159
<b>Figure 44:</b> Intracellular cytokine production by CD4+ and CD8+ subsets. ....	161
<b>Figure 45:</b> Intracellular cytokine production and degranulation in PD-1 subsets. ....	163
<b>Figure 46:</b> CD3+CD8+ T-cell proliferation by CFSE dilution. ....	164
<b>Figure 47:</b> Immune synapse formation between murine B cells and T cells. ....	165
<b>Figure 48:</b> Associations between PD-1 expression and effector functions in T cells from healthy mice and TCL1 mice with developing CLL. ....	169
<b>Figure 49:</b> CLL load in mice assigned to vehicle and lenalidomide treatment. ....	183
<b>Figure 50:</b> Mass spectrometric analysis of lenalidomide. ....	185
<b>Figure 51:</b> <i>Ex vivo</i> lenalidomide treatment of autologous murine B and T cells. ....	188
<b>Figure 52:</b> Saturation curves of blocking PD-L1 and PD-1 antibodies. ....	189
<b>Figure 53:</b> Effect of <i>in vivo</i> lenalidomide treatment on CLL progression and PD-L1 and PD-L2 expression on CLL cells. ....	191
<b>Figure 54:</b> T-cell phenotype in lenalidomide/vehicle treated mice. ....	192
<b>Figure 55:</b> Exhaustion surface markers in lenalidomide/vehicle treated mice. ....	193
<b>Figure 56:</b> T-cell effector function in lenalidomide/vehicle treated mice. ....	195
<b>Figure 57:</b> T-cell effector function in PD-1 <sup>high</sup> and PD-1 <sup>low</sup> CD8 T cells from lenalidomide/vehicle treated mice. ....	196
<b>Figure 58:</b> Immune synapse formation between autologous T and CLL/B cells. ....	197
<b>Figure 59:</b> Effect of <i>ex vivo</i> PD-L1/PD-1 blockade on immune synapse formation. ....	198
<b>Figure 60:</b> Confirmation of drug concentrations by mass spectrometry. ....	200
<b>Figure 61:</b> <i>In vitro</i> blockade with PD-L1 clone 10F.9G2 affects binding of PD-L1 clone MIH5. ....	212
<b>Figure 62:</b> Effect of <i>in vivo</i> aPD-L1 treatment on disease development. ....	215
<b>Figure 63:</b> Effect of <i>in vivo</i> aPD-L1 treatment on PD-L1 and PD-L2 expression. ....	216
<b>Figure 64:</b> Prevention of typical CLL-induced aberrant T-cell phenotype in CD3+, CD4+ and CD8+ cells by <i>in vivo</i> anti-PD-L1 treatment. ....	217
<b>Figure 65:</b> Prevention of typical CLL-induced aberrant T-cell phenotype in CD3+CD8+ naïve and antigen experienced cells by <i>in vivo</i> anti-PD-L1 treatment. ....	218
<b>Figure 66:</b> Prevention of typical CLL-induced exhaustion-like phenotype in CD3+CD8+CD44+ cells by <i>in vivo</i> anti-PD-L1 treatment. ....	220
<b>Figure 67:</b> Prevention of typical CLL-induced CD4+ cytokine production by <i>in vivo</i> anti-PD-L1 treatment. ....	221
<b>Figure 68:</b> Prevention of typical CLL-induced effector cell defects by <i>in vivo</i> anti-PD-L1 treatment. ....	222
<b>Figure 69:</b> Differences in effector function between PD-1 <sup>high</sup> and PD-1 <sup>low</sup> cells in anti-PD-L1 and isotype treated mice. ....	225

## List of Tables

<b>Table 1:</b> Overview of parameters included into the Rai and Binet staging systems. ...	26
<b>Table 2:</b> Development of expanded IgM+CD5+ B-cell population in TCL1 mice .....	40
<b>Table 3:</b> Summary of alternative genetically engineered murine models of CLL. ....	44
<b>Table 4:</b> Summary of preclinical studies highlighting the effects of novel substances on the immune system and the microenvironment. ....	59
<b>Table 5:</b> Summary of clinical trials using single agent PD-L1 blockade. ....	60
<b>Table 6:</b> Summary of clinical trials using single agent PD-1 blockade. ....	61
<b>Table 7:</b> Overview of adoptive transfer experiments .....	84
<b>Table 8:</b> Summary of all cohorts of mice to validate and further characterize T-cell defects in spleen and other organs. ....	95
<b>Table 9:</b> Summary of flow antibodies to assess T-cell subsets in relation to CLL. ....	96
<b>Table 10:</b> Summary of flow antibodies to assess T-cell function in relation to CLL. ....	99
<b>Table 11:</b> Summary of changes in absolute numbers of T-cell subsets in spleen (I). ....	107
<b>Table 12:</b> Summary of changes in absolute numbers of T-cell subsets in spleen (II) .....	109
<b>Table 13:</b> Summary of results of statistical Spearman correlation coefficient analyses for all examined organs according to CD3, 4 and 8 subset .....	116
<b>Table 14:</b> Summary of flow antibodies to assess inhibitory ligand expression .....	135
<b>Table 15:</b> Summary of flow antibodies assess T-cell exhaustion in relation to CLL. ....	138
<b>Table 16:</b> Summary of flow antibodies to assess T-cell function in relation to CLL. ...	139
<b>Table 17:</b> Summary of p-values of comparisons between mice injected with B cells compared to mice injected with CLL cells for expression of exhaustion markers.....	157
<b>Table 18:</b> Medians/ranges of effector cell ratios for WT, TCL1 and AT mice. ....	169
<b>Table 19:</b> Overview of flow panel to phenotype T-cell subsets, exhaustion markers, cytokine receptors, CLL and inhibitory ligands in spleen and peripheral blood.....	186
<b>Table 20:</b> Summary of p-values of comparisons of T-cell subsets between lenalidomide and vehicle treated mice for spleen and peripheral blood.....	192
<b>Table 21:</b> Summary of p-values of comparisons between lenalidomide and vehicle treated mice and healthy WT mice with and without additional <i>ex vivo</i> lenalidomide treatment, <i>ex vivo</i> PD-L1/PD-1 antibody blockade, and isotype blocking antibodies. ....	199
<b>Table 22:</b> Overview of flow panel to phenotype T-cell subsets, exhaustion markers, CLL and inhibitory ligands in mouse tissues. ....	213
<b>Table 23:</b> Summary of p-values of comparisons of specific MFIs for PD-L1 and PD-L2 between anti-PD-L1 and isotype treated mice and healthy WT mice.....	216
<b>Table 24:</b> Summary of p-values for T-cell subset comparisons between anti-PD-L1 and isotype treated mice and healthy WT mice.....	219
<b>Table 25:</b> Summary of p-values for comparisons of T-cell surface exhaustion markers between anti-PD-L1 and isotype treated mice and healthy WT mice.....	220
<b>Table 26:</b> Summary of p-values of comparisons of key T-cell effector functions between anti-PD-L1 and isotype treated mice and healthy WT mice.....	222
<b>Table 27:</b> Summary of p-values of comparisons of key T-cell effector function markers according to PD-1 expression between anti-PD-L1 and isotype treated mice .....	225
<b>Table 28:</b> Gene list of overlapping genes in CLL T cell and exhausted/ effector/ memory T cell signature.....	239

**Abbreviations**

ADCC	Antibody-dependent cellular cytotoxicity
AF	Alexa-Fluor
AMC	Absolute monocyte count
AML	Acute myeloid leukaemia
AP-1	Activator protein 1
APC	Antigen presenting cell
APC	Allophycocyanin
APRIL	A proliferation-inducing ligand
AT	Adoptive transfer
ATM	Ataxia telangiectasia mutated
ATS	Animal technician service
B6	C57BL/6 (mouse strain)
BAD	Bcl-2-associated death promoter
BAFF	B-cell activating factor
BAX	Bcl-2-associated X protein
BCL2	B-cell lymphoma 2
BCL-XL	B-cell lymphoma-extra large
BCR	B-cell receptor
BID	BCL-2 Interacting Domain
BIRC3	Baculoviral IAP repeat containing 3
BLIMP1	B-lymphocyte-induced maturation protein 1
BLNK	B-cell linker protein
BM	Bone marrow
BP	Base pair
BR	Bendamustin, rituximab
BSA	Bovine serum albumin
BSU	Biological services unit
BTK	Bruton's tyrosine kinase
C3H	B6C3H-F1 (mouse strain)
CAR	Chimeric antigen receptor
CCL	C-C motif ligand
CCR	C-C motif receptor
CD	Cluster of differentiation
CDC	Complement-dependent cytotoxicity
CDK	Cyclin dependent kinase

CDR	Common deleted region
CFSE	Carboxyfluorescein diacetate succinimidyl ester
CI	Confidence interval
CLL	Chronic lymphocytic leukaemia
CM	Central memory
CMAC	7-amino-4-chloromethylcoumarin
CMML	Chronic myelomonocytic leukaemia
CMV	Cytomegalovirus
CR	Complete remission
CRBN	Cereblon
CRC	CLL Research Consortium
CSK	C-terminal Src kinase
CTLA4	Cytotoxic T-lymphocyte-associated protein 4
CXCL	CXC Motif Ligand
CXCR	CXC Motif Receptor
Cy7	Cyanine 7
DAG	Diacylglycerol
DAPI	4'6-diamidino-2-phenylindole
DC	Dendritic cell
DDB1	DNA damage binding protein 1
DLBCL	Diffuse large B cell lymphoma
DLEU1/2	Deleted in lymphocytic leukemia 1/2 (non-protein coding)
DLT	Dose limiting toxicity
DMSO	Dimethylsulphoxide
DNA	Deoxyribonucleic acid
DNMT	DNA methyltransferase
EBV	Epstein–Barr virus
ECOG	Eastern Cooperative Oncology Group performance status
EDTA	Ethylenediamine tetra-acetate
EdU	5-ethynyl-2'-deoxyuridine
EFS	Event free survival
EM	Effector memory
eNAMPT	Extracellular nicotinamide phosphoribosyltransferase
EOMES	Eomesodermin
ERK	Extracellular signal-regulated kinases
FACS	Fluorescence activated cell sorting
FasL	Fas Ligand

FCR	Fludarabine, cyclophosphamide, rituximab
FCS	Fetal calf serum
FDA	US Food and Drug Administration
FISH	Fluorescence <i>in situ</i> hybridisation
FITC	Fluorescein isothiocyanate
FL	Follicular lymphoma
FLT3	FMS-like tyrosine kinase 3 receptor
FMO	Fluorescence minus one
Foxp3	Forkhead box P3
FSC	Forward scatter
FZD-6	Frizzled-6
GCLLSG	German CLL Study Group
G-CSF	Granulocyte-colony stimulating factor
GDP	Guanosine diphosphate
GEF	Guanine exchange factor
GEP	Gene expression profile
GM-CSF	Granulocyte-macrophage colony-stimulating factor
GTP	Guanosine triphosphate
GvHD	Graft- <i>versus</i> -host disease
GvL	Graft- <i>versus</i> -leukaemia/lymphoma
HCDR3	Third complementarity-determining region of the heavy chain
HIV	Human immunodeficiency virus
HLA	Human leucocyte antigen
hpf	High-power field
HS-1	Haematopoietic cell-specific Lyn substrate-1
HSCT	Allogeneic haematopoietic stem cell transplantation
HVEM	Herpes virus entry mediator
hWT	Healthy wild type
IDO	Indoleamine 2,3-dioxygenase
IFN- $\gamma$	Interferon- $\gamma$
IgVH	Immunoglobulin variable region heavy chain
IgVL	Immunoglobulin variable region light chain
IHC	Immunohistochemistry
IKZF1/3	Ikaros family zinc finger protein 1/3
IL	Interleukin
IMiDs	Immunomodulatory drugs
i.p.	Intraperitoneal

IP3	Inositol trisphosphate
IQR	Interquartile range
IRF	Interferon regulatory factor
ITAM	Immunoreceptor tyrosine-based activation motif
ITIM	Immunoreceptor tyrosine-based inhibitory motif
ITSM	Immunoreceptor tyrosine-based switch motif
i.v.	Intravenous
JNK	Jun N-terminal kinase
KIR	Killer immunoglobulin-like receptor
KLRG1	Killer cell lectin-like receptor subfamily G member 1
LAG3	Lymphocyte-activation gene 3
LAMP1	Lysosomal-associated membrane protein 1
LAT	Linker of activated T-cells
LCK	Lymphocyte-specific protein tyrosine kinase
LC-MS	Liquid chromatography mass spectrometry
LCMV	Lymphocytic choriomeningitis virus
LEAF	Low Endotoxin, Azide-Free
LFA1	Leucocyte function antigen 1
LN	Lymph node
LPS	Lipopolysaccharide
MAP	Mitogen-associated protein
MAPK	Mitogen-associated protein kinase
MBG	Mouse betaglobin
MBL	Monoclonal B-cell lymphocytosis
MCL1	Induced myeloid leukemia cell differentiation protein
MDR	Minimal deleted region
MDS	Myelodysplastic syndrome
MDSCs	Myeloid-derived suppressor cells
MFI	Median Fluorescence Intensity
MHC	Major histocompatibility complex
MIF	Macrophage migration inhibitory factor
miRNA	MicroRNA
MNC	Mononuclear cells
MTD	Maximum tolerated dose
mTOR	Mammalian target of rapamycin
MYD88	Myeloid differentiation primary response gene (88)
NAD	Nicotinamide adenine dinucleotide

NFAT	Nuclear factor of activated T-cells
NFκB	Nuclear factor κ light chain enhancer of activated B cells
NHL	Non Hodgkin Lymphoma
NK	Natural killer
NLC	Nurse like cells
NOD	Non-obese diabetic (mouse strain)
NOS	Nitric oxide synthase
NPM	Nucleophosmin
n.s.	Not-significant
NSCLC	Non–small-cell lung cancer
NSG	NOD/SCID x IL2rg <sup>-/-</sup> mice
OFAR	Rituximab, oxaliplatin, cytarabine, fludarabine
ORR	Overall response rate
OS	Overall survival
PB	Peripheral blood
PBMCs	Peripheral blood mononuclear cells
PBS	Phosphate-buffered saline
PCR	Polymerase chain reaction
PD-1	Programmed death-1
PD-L1	Programmed death ligand-1
PD-L2	Programmed death ligand-2
PE	Phycoerythrin
PerCP	Peridinin-chlorophyll-protein
PFA	Paraformaldehyde
PFS	Progression free survival
PI3K	Phosphoinositide 3-kinase
PIP2	Phosphatidylinositol 4,5-bisphosphate
PIP3	Phosphatidylinositol-3,4,5-triphosphate
PKCθ	Protein kinase C θ
PLCγ	Phospholipase C γ
PMA	Phorbol myristate acetate
PMBL	Primary mediastinal B-cell lymphoma
PMT	Photomultiplier tube
PR	Partial response
PtC	Phosphatidylcholine
PTEN	Phosphatase and tensin homolog
RAP1GAP	Rap1 GTPase-activating protein 1

RCC	Renal cell cancer
RDX	Radixin
RHOA	Ras homolog gene family, member A
RNA	Ribose nucleic acid
ROR1	Receptor tyrosine kinase–like orphan receptor 1
RR	Response rate
RT	Room temperature
SAE	Serious adverse events
scFv	Single chain variable region moieties
SCID	Severe combined immunodeficiency
SD	Standard deviation
SD	Stable disease
SEB	Staphylococcal enterotoxin B
SF3B1	Splicing factor 3B subunit 1
SH-2	Src homology 2
SH-3	Src homology 3
siRNA	Short interfering RNA
shRNA	Short hairpin RNA
SIV	Simian immunodeficiency virus
SKP-2	S-phase kinase-associated protein 2
SLL	Small lymphocytic lymphoma
SLP76	Src homology 2 domain-containing leukocyte protein of 76 kDa
SOCS1	Suppressor of cytokine signalling 1
SSC	Side scatter
STAT	Signal transducers and activators of transcription
SYK	spleen tyrosine kinase
TAMs	Tumour-associated macrophages
TBD	Thalidomide binding domain
TBET	T box expressed in T-cells
TCL1	T cell leukemia/lymphoma 1
TCR	T-cell receptor
T <sub>EMRA</sub>	Effector cells with 45RA expression
TFH	Follicular helper T cells
TFR	Tumour flare reaction
TGFβ	Transforming growth factor-β
Th1	T helper 1 cell
Th17	T helper 17 cell

Th2	T helper 2 cell
TIM3	T cell immunoglobulin mucin-3
TLR	Toll-like receptor
TNF- $\alpha$	Tumour necrosis factor $\alpha$
TP53	Tumour-suppressor protein 53
TPL	Transplantation
TRAF2	TNF receptor-associated factor 2
TRAIL	Tumour necrosis factor-related apoptosis-inducing ligand
TReg	CD4+CD25 <sup>hi</sup> regulatory T-cells
WASP	Wiskott–Aldrich Syndrome protein
WBC	White blood cell
WT	Wild type
XID	X-linked immunodeficiency
ZAP70	Zeta-chain T-cell receptor-associated protein kinase

## 1 Background

### 1.1 Chronic lymphocytic leukaemia

#### 1.1.1 Epidemiology and clinical features of the disease

Chronic lymphocytic leukaemia (CLL) is the most common adult leukaemia in Western countries with an age-adjusted incidence rate of about 5 cases per 100,000 men and women per year<sup>1, 2</sup>. With a median age at diagnosis of 72 years, CLL is predominantly a disease of the elderly, although 1/3 of patients are diagnosed at or below 65 years of age. CLL is characterised by the progressive accumulation of mature B lymphocytes within blood, bone marrow, lymph nodes and spleen, leading to lymphocytosis, lymphadenopathy and organomegaly. The diagnosis is based on the combination of lymphocyte morphology and the presence of at least 5,000 circulating clonal CD19+CD20+IgM+IgD+ B lymphocytes/ $\mu$ L blood persisting for more than three months; additional characteristics of the CLL immunophenotype are the expression of CD5, CD23, and kappa or lambda light chain restriction<sup>3, 4</sup>. The findings of less than 5,000 circulating clonal B lymphocytes/ $\mu$ L in the absence of palpable lymphadenopathy fulfil the criteria for a diagnosis of monoclonal B-cell lymphocytosis (MBL), whereas those patients with lymphadenopathy fulfil the criteria for a diagnosis of small lymphocytic lymphoma (SLL)<sup>5</sup>. Although all cases of CLL appear to be preceded by MBL, the majority of individuals with MBL have a low risk of developing a haematological malignancy, largely depending on the number of monoclonal B lymphocytes detected<sup>6, 7</sup>. As CLL proceeds, constitutional symptoms and occasionally extranodal infiltrates are observed. Another CLL hallmark is immune suppression and deficiency, a feature which will be further discussed in Chapter 1.1.4. Clinical features are generally highly variable, and while many patients are asymptomatic and never require any treatment, the features and course of disease can be very aggressive in specific subgroups of patients.

#### 1.1.2 Clinical staging and prognosis

To identify patients with poorer risk disease, several staging and prognosis systems have been developed. Clinically, the two most established prognostic staging systems are the Rai<sup>8</sup> and Binet<sup>9</sup> classifications, which are based on physical examination and blood counts (see Table 1). Patients with low-risk disease (*i.e.* Rai stage 0, Binet stage A) generally have a median survival of up to 17 years. This is significantly shortened in patients with intermediate-risk (*i.e.* Rai stage I or II, Binet stage B) and high-risk

disease (*i.e.* Rai stage III or IV, Binet stage C) to 5 to 8 years and to less than 2 years, respectively.

<b>Rai Staging System</b>		
<b>stage</b>	<b>simplified 3-Stage System</b>	<b>clinical features</b>
0	low risk	lymphocytosis in blood and bone marrow only
I	intermediate risk	lymphocytosis + lymphadenopathy
II		lymphocytosis + splenomegaly/hepatomegaly
III	high risk	lymphocytosis + anaemia
IV		lymphocytosis + thrombocytopenia
<b>Binet Staging System</b>		
<b>group</b>		<b>clinical features</b>
A		< 3 involved lymph node areas, no anaemia or thrombocytopenia
B		≥ 3 involved lymph node areas, no anaemia or thrombocytopenia
C		haemoglobin <10g/dl and/or platelets <100,000/ $\mu$ l $\pm$ lymphadenopathy/ organomegaly

**Table 1: Overview of parameters included into the Rai and Binet staging systems.**

With the improved understanding of disease biology and mechanisms of pathogenesis, a variety of additional prognostic factors have emerged over the last 10 to 15 years. These include patient-related characteristics (*e.g.* age, performance status and co-morbidities) and disease-related biomarkers. However, only a few biomarkers have been prospectively validated. These include immunoglobulin heavy chain variable region (IgVH) gene mutation analysis<sup>10, 11</sup>, CD38<sup>10</sup> and ZAP-70 expression<sup>12</sup>, and cytogenetic abnormalities determined by fluorescence *in situ* hybridisation (FISH)<sup>13</sup>. Among the latter, deletion of the chromosome region 17p13.1 (del17p) is of high prognostic importance, as patients with this abnormality typically require therapy within one year of diagnosis and have a median overall survival (OS) of just 32 months due to poor response to standard immunochemotherapy<sup>13</sup>. However, selected retrospective data indicate that a minority of patients with del17p might experience an indolent course despite the mutation<sup>14</sup>. The general lack of chemosensitivity in this subset is biologically explained by the absence of the tumour suppressor protein TP53, the locus for which is located on the short arm of chromosome 17<sup>15</sup>. This deletion is often accompanied by inactivating mutations of the second allele of *TP53*, leading to a complete loss of TP53 function<sup>16, 17</sup>. Other cytogenetic abnormalities commonly observed in CLL include deletion of 11q22.3 (del11q), trisomy of chromosome 12, and deletion of 13q14 (del13q) as the sole abnormality<sup>13</sup>; median survival times for patients in these groups were found to be 79, 114, 111, and 133 months, respectively. Potentially critical genes within the affected regions of these chromosomes include

*DLEU2*/mir15a/miR15-1 for del13q<sup>18</sup>, *NOTCH1* for trisomy 12<sup>19</sup>, and *RDX* and *ATM* for del11q<sup>20</sup>. More recently, *SF3B1*, *BIRC3* and *MYD88* have been identified to be recurrently mutated in CLL<sup>21-23</sup>, and several retrospective studies indicate that these mutations appear to be enriched in cohorts of patients with high-risk characteristics and poor response to conventional therapy<sup>24-26</sup>.

As many prognostic markers were identified and validated in small, retrospective, and heterogeneously treated cohorts of patients, efforts are now being focused on combining individual markers into a more accurate and powerful prognostic score. Rossi and colleagues integrated mutational and cytogenetic data from 1,274 CLL patients to identify four hierarchical subgroups<sup>27</sup>. These included high-risk patients with *TP53* and/or *BIRC3* abnormalities with a 10-year survival of 29%; intermediate-risk patients with *NOTCH1* and/or *SF3B1* mutations and/or del11q (10-year survival 37%); low-risk patients with trisomy 12 or normal cytogenetics (10-year survival 57%); and very low-risk patients with del13q as a sole abnormality (10-year survival 69.3%). A recent study developed a more clinically applicable comprehensive prognostic index for OS combining disease stage, biological markers, and patient-related factors from 1,948 CLL patients participating in phase III trials of the German CLL Study Group (GCLLSG)<sup>28</sup>. Using multivariate modelling, they identified 8 factors as being independently associated with inferior survival from study entry. These included del17p and del11q, elevated serum thymidine kinase and  $\beta$ 2 microglobulin, unmutated IgVH, ECOG performance status greater than 0, male gender and age over 60 years. While such sophisticated and comprehensive prognostic scores contribute significantly to increasing the predictive value of currently available biomarkers, their day-to-day application in clinical practise is still limited by the lack of availability of specialized assays and laboratories, as well as economic constraints.

### 1.1.3 Current treatment options and unmet needs

As there is no reliable curative approach, the decision to begin treatment of CLL is based on the development of symptoms and disease activity<sup>29, 30</sup>. Factors guiding the choice of treatment include physical fitness, the presence of comorbidities, and validated biological prognostic factors such as IgVH mutation status and cytogenetic abnormalities. In young patients without significant comorbidities, immunochemotherapy approaches (chemotherapy plus a monoclonal antibody) are typically used as front-line treatment. The current standard is fludarabine, cyclophosphamide and the anti-CD20 antibody rituximab (FCR)<sup>31, 32</sup>. While this regimen

leads to high overall response rates (ORR) and a long progression-free survival (PFS), it is unsuitable for certain subgroups of patients including those with *TP53* abnormalities<sup>13, 33, 34</sup> and elderly patients with comorbidities who are typically unable to tolerate toxicities associated with FCR<sup>35</sup>. In the latter, chlorambucil is a widely accepted therapeutic option, and the combination with rituximab is generally well tolerated and improves PFS<sup>36, 37</sup>. Another option is the combination of rituximab with bendamustine (BR); a Phase II trial by the GCLLSG found an ORR of 88%, which translated into an event free survival (EFS) of almost 34 months. This combination produced only very moderate toxicities, making it particularly suitable for elderly CLL patients<sup>38</sup>. A direct comparison between FCR and BR is currently being conducted in an ongoing Phase III trial. A recently published pivotal Phase III trial by the GCLLSG showed that the type 2 anti-CD20 antibody obinutuzumab (GA101) was superior to rituximab when each was combined with chlorambucil<sup>39</sup>. Another anti-CD20 monoclonal antibody is the fully humanized agent ofatumumab, which shows high efficacy in untreated and relapsed/refractory patients, and even in patients pre-treated with rituximab<sup>40-42</sup>. A recently published direct preclinical *in vitro* and *in vivo* comparison of obinutuzumab with rituximab and ofatumumab demonstrated that obinutuzumab was superior to rituximab and ofatumumab in the induction of direct cell death and antibody-dependent cellular cytotoxicity (ADCC), showed slower internalization rate upon binding to CD20, and induced superior *in vivo* anti-tumour efficacy, but was 10 to 1,000 times less potent in mediating complement-dependent cytotoxicity (CDC)<sup>43</sup>.

To capitalize on the success of rituximab, a variety of monoclonal antibodies is currently being tested in preclinical studies, for example against receptor tyrosine kinase-like orphan receptor 1 (ROR-1)<sup>44</sup> or CD44<sup>45</sup>, or has been introduced to the treatment of CLL. Among those, the anti-CD52 monoclonal antibody alemtuzumab and combinations of this with chlorambucil, high-dose corticosteroids, rituximab, and FCR appeared to be able to overcome the negative impact of *TP53* abnormalities in the first-line treatment setting (both in terms of its predictive value and its effect on the response to treatment)<sup>46-49</sup>. However, alemtuzumab-containing approaches are associated with severe haematological and non-haematological toxicities and infectious complications, making them unsuitable for the majority of CLL patients. In the relapsed setting, the management of patients with *TP53* abnormalities is even more challenging. Several clinical studies demonstrated that FCR and combinations with high-dose corticosteroids, alemtuzumab or alternative regimens consisting of rituximab, oxaliplatin, cytarabine and fludarabine (OFAR) have only limited and short-term

efficacy and are associated with high toxicity rates<sup>50-56</sup>. Thus, identifying new strategies for the del17p and *TP53* mutated CLL patient subsets remains especially urgent.

A great deal of work has therefore been focused on identifying agents that can provide anti-tumour activity in the absence of functional p53. These efforts led to the development of the cyclin dependent kinase (CDK) inhibitor flavopiridol and the second-generation CDK inhibitor dinaciclib. In several studies flavopiridol has demonstrated potent clinical activity even in the highest risk CLL subsets, and has provided benefit to patients lacking other options<sup>57, 58</sup>. However, due to its rapid induction of tumour cell death, this agent carries the risk of acute tumour lysis syndrome that can be fatal without proper monitoring and intervention. To reduce this risk, CDK inhibitors have been combined with cytoreductive therapies. In a recently published phase I study, the combination of flavopiridol with cyclophosphamide and rituximab was tolerable and active in high-risk CLL patients, and tumour lysis syndrome was not observed<sup>59, 60</sup>. Regardless, concerns persist, and widespread clinical application of CDK inhibitors in CLL appears unlikely at this time.

After many years without a significant clinical breakthrough, CLL researchers have recently been able to capitalize on laboratory data showing the importance of B-cell receptor (BCR) signalling in CLL tumour cell survival and proliferation. BCR activation is a central stimulus in CLL cells, and promotes their survival by activating multiple downstream kinases such as Bruton's tyrosine kinase (BTK), spleen tyrosine kinase (Syk), ZAP-70, Src family kinases, and phosphatidylinositol 3-kinase (PI3K)<sup>61, 62</sup>. These events drive the expression of pro-survival molecules, in part via activation of transcription factors such as NF- $\kappa$ B. An overview of BCR signalling pathways and targets is provided in Figure 1.

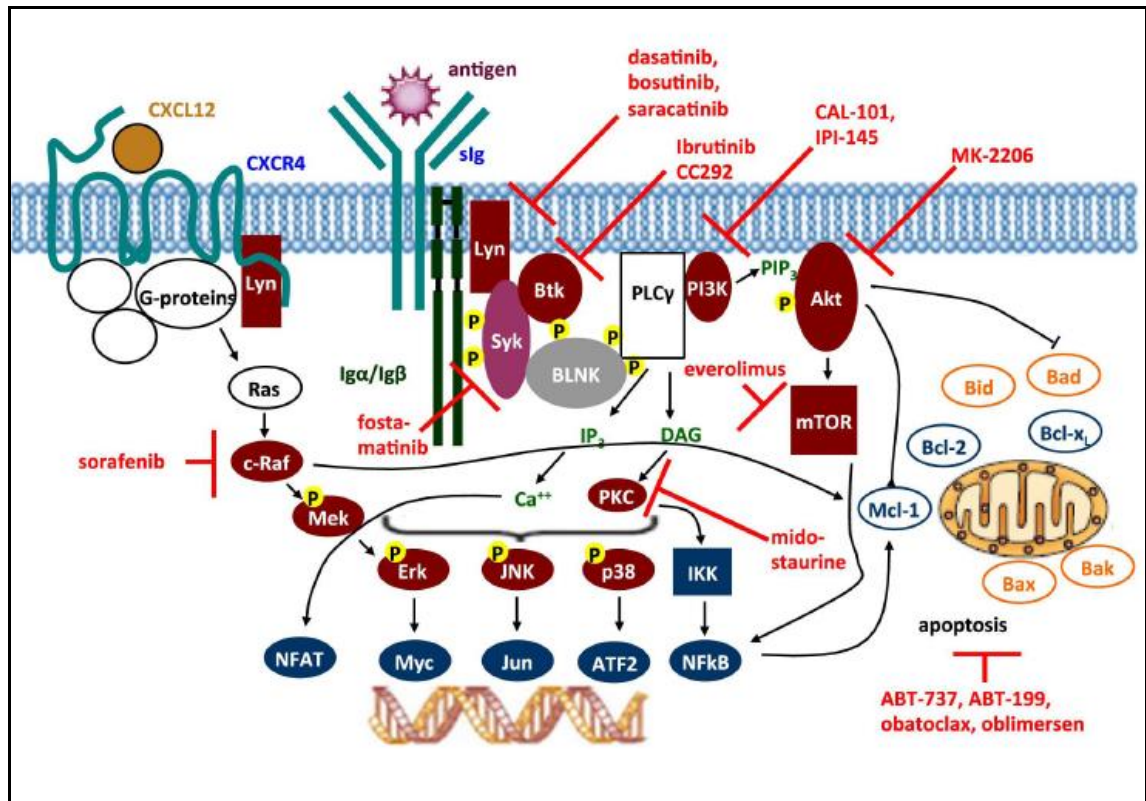


**Figure 1: BCR signalling pathway and targets for molecular inhibitors:** Engagement of the BCR by antigen induces phosphorylation of immune receptor tyrosine-based activation motifs (ITAMs) within the cytoplasmic domains of immunoglobulins, which is primarily mediated by the Src family kinase Lyn. This results in the recruitment and activation of the tyrosine kinase Syk. Activated Syk forms a membrane-associated complex with other tyrosine kinases such as Lyn and BTK, and adapter molecules such as B-cell linker protein (BLNK). This complex mediates the activation of downstream signalling pathways such as PI3K and phospholipase Cy2 (PLC $\gamma$ 2). PI3K generates the second messenger phosphatidylinositol-3,4,5-triphosphate (PIP $_3$ ), which recruits molecules such as Akt. PLC $\gamma$ 2 activation leads to the release of intracellular calcium and subsequent activation of protein kinase C (PKC). These events lead in turn to activation of mitogen activated protein kinases (MAPKs) including extracellular signal regulated kinase (ERK), c-JUN NH $_2$ -terminal kinase (JNK) and p38 MAPK. Activation of PKC also increases expression of the transcription factor NF $\kappa$ B, while the rise in intracellular calcium causes activation of nuclear factor of activated T cells (NFAT). *Figure taken from Hallek 2013*<sup>63</sup>.

Recent clinical studies convincingly show that agents inhibiting BCR signalling are well tolerated and very active, even in patients with relapsed and fludarabine-refractory CLL and/or those with *TP53* abnormalities. To date, the most clinically successful BCR pathway inhibitor is the BTK inhibitor ibrutinib. In addition to blocking BCR-associated anti-apoptosis pathways, ibrutinib interferes with BCR- and chemokine-mediated homing and retention of CLL cells in the protective lymph node and bone marrow microenvironments<sup>64-66</sup>. In a phase I/II study of ibrutinib in 85 heavily pre-treated patients with relapsed or refractory CLL, the ORR was 71%, with a PFS of 75% and an OS of 83% at 26 months. Importantly, these responses were independent of the presence of del17p<sup>67</sup>. Ibrutinib monotherapy is also very well tolerated and effective in

treatment-naïve elderly CLL patients, producing an ORR of 71% in this population<sup>68</sup>. To validate these early encouraging results, a randomized phase III study of 391 relapsed/refractory CLL patients demonstrated that ibrutinib significantly improved ORR (42.6% vs. 4.1%,  $P < 0.001$ ) as well as PFS and OS compared to ofatumumab monotherapy, and was able to overcome the adverse effect of del17p<sup>69</sup>.

Idelalisib (formerly known as GS-1101 and CAL-101) is an inhibitor of the PI3K regulatory subunit p110 $\delta$  that is involved in CLL cell survival, clonal expansion and retention in lymphoid tissues<sup>70, 71</sup>. In a phase I study of 54 heavily pre-treated patients with relapsed/refractory CLL, including patients with del17p, 81% achieved nodal responses with an ORR of 72% and a very acceptable safety profile<sup>72</sup>. A phase III trial was then initiated on 220 patients with relapsed CLL that compared idelalisib in combination with rituximab to rituximab plus placebo<sup>73</sup>. Due to overwhelming improvement in efficacy in the idelalisib arm, the study was interrupted after the first interim analysis. The ORR was 81% and 13% for the idelalisib combination and the rituximab monotherapy, respectively; at 12 months, OS was 92% *versus* 80%, and PFS 93% *versus* 46%, respectively.

The BCL-2 family of proteins controls apoptosis by modulating mitochondrial stability. A delicate balance of anti-apoptotic (e.g. BCL-2, BCL-XL, MCL-1) and pro-apoptotic (e.g. BAD, BAX, NOXA) family members is essential to normal immune system function. In many tumour types including CLL, this balance is disrupted to aberrantly promote cell survival. BCL-2 antagonists such as navitoclax (previously ABT-263) and GDC-0199 (previously ABT-199) have been developed to restore apoptosis by interfering with BCL-2 protein-protein interactions, thus blocking its mitochondria-stabilizing activity. In a phase I study of navitoclax in 29 patients with relapsed/refractory CLL, lymphocytosis was reduced by more than 50% in 19 of 21 patients with baseline lymphocytosis, and partial response (PR) or disease stabilization was achieved in almost half of the patients, including those with del17p<sup>74</sup>. The newer agent GDC-0199 is even more promising, as it is more specific for BCL-2 and lacks the platelet-depleting activity of navitoclax.

Lenalidomide is an especially unusual drug in CLL due to its ability to modulate immune responses<sup>75</sup>. A derivative of thalidomide, lenalidomide was recently found to interact with cereblon, a component of a multiprotein E3 ubiquitin ligase complex. This interaction alters the proteasomal degradation of certain proteins, including the transcription factors IKZF-1 and 3<sup>76</sup>. However, lenalidomide has very little direct cytotoxic activity against CLL cells, and appears to work primarily by enhancing anti-tumour immunity in effector cells, suggesting pleiotropic effects on immune cells<sup>77-81</sup>.

Several clinical trials have demonstrated that lenalidomide, both as a single agent and in combination with rituximab or corticosteroids, has activity in untreated and relapsed/refractory CLL, including in patients with del17p<sup>82-90</sup>. However, lenalidomide occasionally produces serious toxicities including immune-mediated tumour flare reactions, impeding its clinical development<sup>78, 91</sup>.

Combinations of all of these agents are currently being investigated in randomized and non-randomized clinical trials with immunochemotherapy and with other novel agents. While early results are encouraging, especially in the combination setting, it is yet to be seen if these will translate into long-lasting remissions and disease control. Further emphasizing the inadequacy of monotherapy even with effective targeted agents, recent reports show that a subset of patients develop resistance to ibrutinib therapy due to mutations within BCR pathway components, and similar resistance mechanisms to other substances are likely to arise as well<sup>92</sup>.

The only curative treatment option in CLL to date is allogeneic haematopoietic stem cell transplantation (HSCT). HSCT takes advantage of the graft-*versus*-leukaemia (GvL) effect mediated by differentiated transplanted immune effector cells, which are able to mount an anti-tumour immune response and induce long-lasting clinical remission<sup>93</sup>. Additional observations supporting GvL activity in CLL include decreased relapse rates in patients who develop graft *versus* host disease (GvHD)<sup>94, 95</sup>, and increased relapse rates in recipients of T-cell depleted allografts<sup>96</sup>. However, HSCT is only applicable to a minority of CLL patients, as patients are typically of advanced age at presentation. In addition, it is associated with significant treatment related mortality and morbidity, largely due to chronic graft *versus* host disease (cGvHD)<sup>24, 97-99</sup>. Internationally accepted guidelines suggest that HSCT is indicated in patients who are fit enough, have a suitable matched donor, have 17p deletion or *TP53* mutations, or relapsed quickly after chemo-immunotherapy<sup>100</sup>. As described above, several new agents are in clinical trials or have recently been approved for CLL that demonstrate impressive and durable responses in high-risk patients who might be candidates for transplant. Thus, HSCT must always be considered in view of other, potentially less toxic therapies that could be offered. The choice of HSCT *versus* a novel agent is one that must be gauged on a patient-by-patient basis, and this will change as data mature on the use of these novel agents in CLL<sup>101</sup>.

#### 1.1.4 Immune dysfunctions in CLL

As introduced in Chapter 1.1.1, immune dysfunction is a major hallmark of CLL. This can be related both to the disease and to the treatments administered. Clinical manifestations include severe and recurrent infections, hypogammaglobulinaemia, autoimmune anaemia and thrombocytopenia, and poor responses to vaccination<sup>102</sup>. Infectious complications pose an enormous challenge in the management of CLL patients, and retrospective analyses indicate they are the main cause of increased morbidity and mortality, accounting for up to 50% of CLL-related deaths<sup>103-105</sup>. Disease-related immune suppression is significantly aggravated by treatment with steroids and immunochemotherapy; in fact, a main risk factor for infectious complications in CLL patients is the number of previous chemotherapeutic regimens<sup>106, 107</sup>.

Several quantitative and qualitative immune defects have been described in CLL to date, which include both humoral and cellular immunity. Early data implied that an impaired complement system might be involved in the pathophysiology of CLL and its associated immune defects<sup>108</sup>. Complement plays a crucial role in the control of some bacterial infections, as opsonisation with complement is necessary for clearance by neutrophils. Although CLL patients appear to have normal concentrations of complement factors, a defect in C3b binding to certain bacteria has been reported<sup>108</sup>. In another study, reduced activity of the classical complement pathway predicted shortened survival<sup>109</sup>.

Cellular immune defects are observed in nearly all immune subsets. Among B cells, the most clinically apparent defect is hypogammaglobulinaemia, the severity of which tends to increase with the duration and stage of disease<sup>110-112</sup>. It has been proposed that hypogammaglobulinaemia might be the result of IL-4 mediated abnormal CD30/CD30L interactions, leading to impaired isotype switching and increased sensitivity of normal B cells to FasL-mediated cell death<sup>113</sup>. Early studies indicate that clonal CLL cells have a limited ability to present antigen to T cells<sup>114, 115</sup>, largely due to an inadequate costimulatory capacity<sup>116, 117</sup>, leading to the failure of T-cell responses. A wide range of immune defects have been described in the T-cell compartment itself. Several studies demonstrated that despite reduced relative numbers of CD3+, CD4+ and CD8+ T cells because of the relative expansion of CLL cells in lymphocytes, absolute T-cell numbers are actually increased in CLL patients, and this increase correlates with disease stage<sup>118-125</sup>. This increase in CD3+ T cells was found to be primarily due to a relative expansion of CD3+CD8+ T cells over CD3+CD4+ T cells, leading to a reduction of the typical CD4+/CD8+ ratio. It is hypothesized that this might be attributed to the higher sensitivity of CD4+ T-cell subtypes to CLL-induced Fas-

mediated cell death<sup>126</sup>. Another potential explanation for the “loss” of CD4+ T cells in the blood is migration into secondary lymphoid organs towards CLL-secreted cytokines. An early study by Pizzolo *et al.* described that CD4+ T cells are the predominant subtype in the bone marrow of CLL patients<sup>127</sup>. This accumulation might be chemokine-mediated, as activated CD40L+CD4+ T cells in bone marrow and lymph nodes express CCR4, the receptor for the CLL cell-released chemokine CCL22, and are predominantly found in proliferation centres of secondary lymphoid organs (so-called pseudofollicles), a hallmark histopathology finding in CLL describing the microanatomical tissue sites where CLL proliferation occurs<sup>128, 129</sup>. Chemo-attracted CD40L+CD4+ T cells are therefore likely to provide pro-survival and costimulatory signals to CLL cells, leading to the progressive accumulation of malignant cells. Another study linked CD38 expression by CLL cells to interactions with CD4+ T cells within pseudofollicles and found that CD38 expression was higher in tissues that contain pseudofollicles and was subject to dynamic changes in response to contact with activated CD4+ T cells<sup>130</sup>. Peripheral blood CD4+ cell subsets were later described to be skewed towards central memory (CM) and effector memory (EM) cells, which was more pronounced in patients with unmutated IgVH compared to mutated IgVH status and correlated with shorter treatment-free survival, but not CD38 expression or cytogenetic risk groups<sup>131</sup>. Interestingly, CD4+ memory cells were superior to CD4+ naive cells in protecting CLL cells from apoptosis, probably via IL-4 secretion, indicating that even outside of pseudofollicles, CLL survival is promoted by CD4+ T cells.

Among CD8+ T cells, subsets were also found to be skewed towards CCR7- effector cells compared to healthy controls<sup>132-135</sup>. Recently, multidimensional scaling (principal coordinates analysis) was applied to form a T-cell score integrating 24 circulating T-cell subsets to describe the evolution of T-cell phenotypes from MBL to advanced stage CLL<sup>136</sup>. Distinct T-cell scores were found for different stages of CLL development, even at the MBL stage, and changes were apparent during disease progression and after treatment. This important finding highlights the dynamic alterations of T-cell phenotypes as a response to the presence of disease. Consequently, these T-cell scores were also of prognostic value; patients with higher scores had significantly shorter time to treatment compared to those with low T-cell scores, and scores also correlated with established prognostic markers such as IgVH status and cytogenetic aberrations. Changes in the score were mainly driven by specific T-cell subsets such as CD4+CD25<sup>hi</sup> regulatory T-cells (TRegs), CD3+CD56+ NKT cells and  $\gamma\delta$  T cells, although terminally differentiated T<sub>EMRA</sub> CD8+ subsets at the expense of effector-

memory subsets were confirmed to contribute to high T-cell scores in patients with advanced disease.

In addition to CD4+ and CD8+ subset characteristics, a number of alterations in the surface expression of T-cell activation markers have been reported. These include increased expression of CD57, CD69, HLA-DR, killer immunoglobulin-like receptors (KIRs) and CD94, and decreased expression of CD62L and CD28<sup>137-139</sup>. CD57+ T cells especially appear to represent clonal or oligoclonal populations, probably as a result of chronic activation by CLL-associated antigens<sup>140-142</sup>. Another major factor influencing lymphoid subsets in healthy individuals is CMV infection<sup>143</sup>. Indeed, expanded populations of CMV-specific CD4+ and CD8+ T cells have been reported in CMV+ CLL patients<sup>144-146</sup>. Work from our group demonstrated that CD8+ T cells from CMV+ CLL patients appeared shifted towards a T<sub>EMRA</sub> phenotype, while CMV- patients predominantly exhibit an EM phenotype (as described above)<sup>133</sup>. In line with previous observations, a similar shift was also observed in CMV+ healthy controls, indicating that altered CD8+ subset composition was unrelated to CMV serostatus. Chronic T-cell activation has been extensively studied in patients with viral infections, where chronic antigenic stimulation leads to failed T-cell immune responses and the ongoing replication of virus-specific effector T cells. This is associated with a number of progressive phenotypic and functional T-cell changes, such as a hierarchical loss of effector CD8+ T-cell function and the expression of inhibitory surface receptors such as PD-1 and CTLA-4, which has been termed T-cell exhaustion<sup>147</sup>. Our group demonstrated that T cells from CLL patients actually carry features of T-cell exhaustion, such as an increased surface expression of CD244, CD160, and PD-1, especially in the expanded population of effector T cells<sup>133</sup>. In addition, CD8+ T cells exhibited proliferative and cytotoxic functional defects, but had an increased production of IFN- $\gamma$ , TNF- $\alpha$  and TBET, and normal IL-2 production. Similar to T-cell subsets, impaired T-cell function was unrelated to CMV serostatus. This was also explored from a slightly different angle by Kater's group, who found that although global T-cell defects indeed occur in CLL patients, CMV-specific antiviral T-cell responses appear to be uncompromised<sup>148</sup>.

Overall, these findings highlight the range of functional T-cell defects and imply a high degree of heterogeneity of the T-cell population in CLL. In addition, they expand the previous notion of cytokine production by T cells in CLL, which was based on a dichotomous Th-1 *versus* Th-2 cytokine skewing. Impaired or aberrant classical Th1 and Th2 cytokine production, *i.e.* IFN- $\gamma$  and IL-2 (Th-1 response), and IL-4, IL-5 and IL-10 (Th-2 response) and their correlation with clinical course and outcome have been

investigated in several clinical and translational studies<sup>149-151</sup>. Some studies suggested that T cells in CLL were skewed towards Th-2 responses, with an increase in IL-4 and IL-6 producing T-cell subsets<sup>152-155</sup>. Both IL-4 and IL-6 have been demonstrated to induce CLL cell proliferation and to protect CLL cells from apoptosis *in vitro*, probably via an increase of BCL-2 expression<sup>156</sup> as well as enhanced STAT6 levels and phosphorylation<sup>157</sup>. In addition, IL-6 serum levels, along with IL-10, are increased in CLL patients and correlate with OS<sup>149</sup>. Similar to IL-4 and IL-6, IL-10 has anti-apoptotic properties *in vitro*<sup>158</sup>. In contrast, significant evidence demonstrates that IFN- $\gamma$ , TNF- $\alpha$ , and IL-2 are upregulated in CLL T cells and correlate with disease stage<sup>159-164</sup>. These cytokines have also been demonstrated to induce CLL cell proliferation and to protect CLL cells from apoptosis *in vitro*<sup>165, 166</sup>. The biological situation is likely to be much more complex, and cytokines certainly exert their functions in a dynamic network rather than against or from single cells. To account for this complexity, groups of cytokines and chemokines have been analysed within the context of networks<sup>167</sup>. Three clusters of highly correlated but differentially expressed cytokines were identified. These included cytokines that had previously been implied in CLL, but also new molecules relevant to CLL biology such as CCL17, CXCL11, IL-5 and IL-17. However, these were evaluated in serum, and not attributed to specific T-cell subsets, therefore also accounting for cytokines/chemokines released by CLL and/or other cells. Considering the increasing evidence of the complexity of networks of cytokines and chemokines between CLL cells and the microenvironment<sup>168</sup>, determining cytokine secretion by specific cell subsets and under *in vitro* stimulation conditions might therefore no longer be sufficient. Indeed, CLL cells were recently described to bear functional and phenotypic resemblance to IL-10-producing regulatory B10 cells<sup>169</sup>. Another study found IL-10 secretion by B cells to be linked to surface CD5 expression, controlled by transcription factors STAT3 and NFAT2, suggesting a CD5-triggered autocrine feedback mechanism to maintain protective cytokine production<sup>170</sup>.

A major effort of our group has been to investigate the underlying molecular mechanisms of T-cell dysfunction in CLL patients<sup>171</sup>. We demonstrated that both CD4+ and CD8+ T cells from patients with CLL show multiple differentially expressed genes when compared to these cells from age-matched healthy donors, indicating that global T-cell defects occur on a molecular level. Deregulated genes were enriched in pathways of T-cell proliferation, differentiation, vesicle trafficking, and actin cytoskeleton formation and included *cdc42*, *PIK4CB*, *RAB35* and *ARPC1B*, all of which are key regulators of the formation and stabilisation of the immune synapse. Most importantly, very similar alterations in gene expression could be induced in normal

allogeneic T cells after direct contact with CLL cells in co-culture, indicating that the presence of the malignant CLL cell drives the observed T-cell changes. The global nature of molecular T-cell defects was confirmed by Di Ianni *et al.*, who demonstrated that peripheral blood T cells from CLL patients showed deregulated genes involved mainly in cell differentiation, proliferation, survival, apoptosis, cytoskeleton formation, vesicle trafficking and T-cell activation<sup>172</sup>. A recently published study demonstrated by gene expression profiling and subsequent gene enrichment analysis that differentially expressed genes in CD3+ T cells from CLL patients were enriched in the signature of publicly available combined CD8+ EM/CM T cells<sup>135</sup>.

Subsequently, our group demonstrated the inappropriate functional response of T cells to antigen presenting cells (APCs) due to their inability to effectively regulate actin remodelling and to recruit key cytoskeletal signalling molecules such as Lck, Cdc42, WASp, filamin-A and dynamin-2, using immune synapse formation assays and confocal microscopy<sup>77</sup>. Consistent with our gene expression studies, these defects could be induced in normal allogeneic T cells by co-culturing them in direct cell-cell contact with CLL cells. More recently, impaired actin remodelling was found to be mediated by activation of the Rho GTPases RhoA, Cdc42, and Rac1<sup>79</sup>, which also led to impaired LFA-1 mediated T-cell adhesion and migration<sup>81</sup>.

Several groups have highlighted the importance of other T-cell subsets as components of the CLL microenvironment, such as CD4+CXCR5+ circulating follicular helper T cells (Tfh) and IL-17 producing Th17 cells. Tfh cells of a Tfh-th2 and a Tfh-th17 phenotype were significantly increased in the peripheral blood of CLL patients compared to healthy controls, especially in patients with advanced stage disease<sup>173</sup>. Moreover, higher Th17 and IL-17A values were associated with less advanced clinical stage of CLL, and also inversely correlated with numbers of TRegs<sup>174, 175</sup>. An increase in TRegs is implicated in advanced stage disease and correlates with shorter time to treatment<sup>136, 176, 177</sup>. This expansion can be explained by a combination of increased formation, facilitated by CD27-CD70 interactions in lymph node proliferation centres, and decreased sensitivity to drug-induced apoptosis because of a shifted Noxa:BCL-2 balance<sup>178</sup>. In addition, both CD4+ and CD8+ T cells in CLL aberrantly express surface and cytoplasmic CTLA4 (CD152)<sup>179</sup>, which is an essential marker to define TRegs and plays an important functional role in limiting T-cell immune responses<sup>180, 181</sup>.

Another immune subset with functional and numerical alterations in CLL, especially in advanced disease, is natural killer (NK) cells. In earlier work, NK cells were reported to have a reduced ability to lyse leukaemia cell lines because of a lack of cytoplasmic granules<sup>182, 183</sup>. This could be restored by IL-2, which also resulted in increased

granularity of the large granular lymphocyte subset<sup>184</sup>. In contrast, a more recent publication indicated that peripheral NK cells from CLL patients maintain partial functionality and are able to degranulate and exert ADCC, although some variability was observed<sup>185</sup>. Proposed mechanisms by which CLL cells impair NK cell function include inhibition via soluble factors<sup>186, 187</sup> and cell surface receptors HLA-G<sup>188</sup> or 4-1BB ligand<sup>189</sup>. In patients with early stage CLL and in those with mutated IgVH, higher NK-cell numbers are observed, with a higher NK:CLL cell ratio being predictive of longer time to treatment<sup>190</sup>. Moreover, numbers of CD3<sup>+</sup>CD16<sup>+</sup>CD56<sup>+</sup> NKT cells appear to be important in CLL, as a reduction in numbers was associated with disease progression and a higher risk of death<sup>191</sup>.

Aberrant numbers and functional defects are also observed in plasmacytoid dendritic cells, which were recently found to have markedly reduced IFN- $\alpha$  production via decreased expression of FMS-like tyrosine kinase 3 receptor (Flt3) and Toll-like receptor 9 (TLR9), as well as in granulocytes, which exhibited impaired phagocytic and bactericidal function, migration and chemotaxis through lysozyme and myeloperoxidase deficiencies and altered secretion of TNF-superfamily proteins<sup>192-195</sup>.

Several studies have focused on monocytes and macrophages in CLL. A recently published study found an increased absolute number of monocytes in CLL patients compared to healthy controls, which were skewed towards non-classical Tie-2-expressing monocytes<sup>196</sup>. Gene expression analysis performed in this study revealed an altered composition and deregulation of genes involved in phagocytosis and inflammation, such as *RAP1GAP*, tubulins and *CDC42EP3*, which resulted functionally in inhibited proliferation of T cells in contact with CLL monocytes. Healthy donor monocytes increased migration and up-regulated CD16, *RAP1GAP*, IL-10, IL-8 and MMP9 while down-regulating *PTGR2* in response to leukemic cells or conditioned media. The clinical relevance of peripheral absolute monocyte count (AMC) has been demonstrated by the finding that patients with low AMC had a shorter time to treatment and evidence of immune dysregulation leading to increased mortality<sup>197</sup>. In addition, patients with high AMC also had a shorter time to treatment compared to intermediate AMC patients. In another study on 29 patients with previously untreated early to intermediate stage CLL prior to therapy with alemtuzumab, rituximab and G-CSF, monocytes were found to have decreased expression of HLA-DR and CD86, suggesting decreased antigen-presenting capacity and reduced immune stimulatory capacity<sup>198</sup>. Higher HLA-DR<sup>lo/neg</sup> monocyte levels were associated with shorter time to disease progression, while the number of total monocytes did not influence time to progression. This was further extended in a recently published study by Jitschin *et*

*al.*<sup>199</sup>. The authors found significantly increased levels of circulating CD14+HLA-DR<sup>lo</sup> cells which express myeloid markers such as CD11c, CD13, CD33, adhesion molecules CD11b and CD62L, and receptors associated with promotion and activation of myeloid cells such as TNF-receptor type 2/CD120b, and showed phenotypic and functional features linking them to the myeloid-derived suppressor cells (MDSCs), a heterogeneous population that shares certain characteristics including an aberrant myeloid phenotype and the ability to suppress T cells.

Proposed mechanisms by which CLL cells polarize monocytes/macrophages and affect their function include the production and release of soluble factors. One such example is macrophage migration inhibitory factor (MIF), a proinflammatory and immunoregulatory chemokine; patients with advanced stage CLL show a trend toward higher MIF levels compared with patients with early-stage CLL<sup>200</sup>. A second example is extracellular nicotinamide phosphoribosyltransferase (eNAMPT), a rate-limiting enzyme in NAD biosynthesis with cytokine/adipokine-like properties<sup>201</sup>. Furthermore, MDSCs were found to exert immune regulatory functions on T cells via indoleamine 2,3-dioxygenase (IDO)<sup>199</sup>. Early *in vitro* evidence for a tumour-supporting role of monocytes was based on the observation that peripheral blood monocytes from CLL patients could be differentiated *ex vivo* into nurse-like cells (NLC), which protect CLL cells from spontaneous or drug-induced apoptosis through multiple interactions regulated by soluble or cell-surface molecules such as CXCL12, CXCL13, BAFF, APRIL, CD31, plexin-B1 and activation of the BCR signalling cascade<sup>168, 202, 203</sup>. Gene expression analyses suggested that NLC bear resemblance to tumour-associated macrophages (TAMs)<sup>204, 205</sup>, which are alternatively activated M2 macrophages with IL-10<sup>high</sup>IL-12<sup>low</sup> cytokine secretion, poor antigen-presenting capacity, immunosuppressive effects and pro-angiogenic properties. *In vivo*, a population of CD68+CD14+ cells resembling TAMs/NLC can be found in the spleen and lymphoid tissues of CLL patients<sup>206, 207</sup>.

## 1.2 Murine models of CLL

### 1.2.1 E $\mu$ -TCL1 mouse model

#### 1.2.1.1 Generation and disease characteristics

T-cell leukaemia/lymphoma protein (*TCL1*) expression in humans is restricted to subsets of immature cells within the T and B lymphoid lineage (*i.e.* pre-B cells, immature IgM expressing B cells, early triple negative T-cell progenitors), while it functions as an oncogene in leukaemic cells carrying a t(14;14)(q11;q32) translocation or an inv(14)(q11;q32) inversion<sup>208</sup>. *TCL1* is located on chromosome 14q32.1 and

consists of the *TCL1A* (HGNC ID 11648)<sup>209</sup> and the *TCL1B* (HGNC ID 11649) genes<sup>210, 211</sup>. The E $\mu$ -TCL1 (hereafter abbreviated to TCL1) mouse model, one of the most established preclinical models for CLL using immune competent mice, was derived by placing the entire human *TCL1* coding region under the control of a mouse IgV<sub>H</sub> promoter and a IgH- $\mu$  enhancer<sup>212</sup>, which results in specific expression of TCL1 in immature and mature B cells<sup>213</sup>. Originally, two TCL1<sup>+wt</sup> founders on the B6C3 background were obtained and further bred to study the expression of TCL1 and the course and characteristics of disease in transgenic TCL1<sup>+wt</sup> offspring compared to non-transgenic litter-mates. At 6 month of age, transgenic mice exhibited an expanded B220<sub>low</sub>+/IgM+ population in the peripheral blood. This population co-expressed CD5 and Mac-1/CD11b, was also present in bone marrow, peritoneal cavity and spleen, and expanded with age (see Table 2). Non-transgenic controls showed a normal distribution of B-cell populations, and peripheral T-cell subsets were comparable between transgenic mice and controls. After 13 to 18 months, 100% of transgenic mice became visibly ill with hepatosplenomegaly, lymphadenopathy and high white blood cell (WBC) counts, all of which are hallmarks of human CLL. At the endpoint, spleen weights ranged from 1.5 to 2.3 g (normal spleen weight .07  $\pm$  .01 g), and the WBC count was 1.8x10<sup>8</sup> per  $\mu$ L of blood (normal value  $\sim$ 2.8x10<sup>6</sup>).

age	% IgM+CD5+ B cells		
	bone marrow	peritoneal cavity	spleen
2 months	1	45	4
4 months	2	46	9
8 months	43	74	69
control: WT 4 months	>1	20	1

**Table 2: Development of expanded IgM+CD5+ B-cell population over time and in different organs in TCL1 mice.** Adapted from Bichi *et al.*<sup>212</sup>; *Abbreviations:* WT = wild type.

Despite a 100% penetrance, the long latency of TCL1-driven leukaemia is an obvious disadvantage of this model. Several groups therefore demonstrated that this obstacle can be overcome by adoptive transfer of murine CLL cells from leukaemic TCL1 mice into healthy recipients, which leads to faster and less variable disease development<sup>214-216</sup>. A similar approach uses a TCL1 leukaemia cell line established from the original TCL1 transgenic colony: 2x10<sup>7</sup> cells from a leukaemic TCL1 mouse with oligoclonal autoantigen phosphatidylcholine (PtC) reactive cells were injected into two severe combined immunodeficiency (SCID) mice, and serially transferred into other SCID mice for a total of 3 transfers<sup>217</sup>. This led to the outgrowth of cells expressing an autoantigen-

specific B-cell receptor, superior autoantigen binding, and a more aggressive course of disease.

### 1.2.1.2 Suitability to mirror the biology of human CLL

Since its creation in 2002, the TCL1 model has been validated by several groups as an adequate tool to depict the biology of aggressive human CLL B cells. One of the earliest studies demonstrated that it replicates aspects of the molecular B-cell receptor V-region rearrangement characteristics of aggressive, unmutated human CLL<sup>218</sup>. This included minimal levels of IgVL and IgVH somatic hypermutation, biased VHDJ<sub>H</sub> and VLJ<sub>L</sub> rearrangements and CDR3 characteristics, as well as stereotypical BCR usage between sets of leukaemic clones. In addition, immunoglobulins from leukaemic mice were found to resemble auto-antibodies and antibodies reactive with microbial antigens, suggesting this might be driven by (auto)-antigens. Another study using extensive cross-species epigenetic analyses confirmed that epigenetic alterations seen in human CLL, such as the aberrant methylation of promoter sequences containing the binding sites for the transcription factor FOXD3, were recapitulated in CLL cells from TCL1 mice at various stages of disease progression<sup>219</sup>. More recently, CLL cells from TCL1 mice were found to mirror phenotypic and functional aspects of human CLL cells competent to produce IL-10, suggesting a similarity of human and murine CLL cells to regulatory B10 cells<sup>169</sup>.

Work from our group also validated the appropriateness of the TCL1 model to mirror CLL-induced T-cell defects in humans<sup>216</sup>. With the development of CLL, TCL1 transgenic mice exhibited various functional T-cell defects such as decreased *in vivo* antigen-specific activation, suppressed proliferation, and impaired induction of idiotype-specific CD8<sup>+</sup> cytotoxic T cells. Gene-expression profiling of CD4<sup>+</sup> and CD8<sup>+</sup> T cells from TCL1 mice with CLL, compared to young TCL1 mice without CLL and wild-type mice, revealed several differentially expressed genes in both CD4<sup>+</sup> and CD8<sup>+</sup> cells. With increasing tumour burden, the changes in gene-expression profiles in CD4<sup>+</sup> and CD8<sup>+</sup> cells became more evident and correlated well with findings in human CLL cells. A causal relationship between CLL and T-cell dysfunction was demonstrated by injecting CLL cells from leukaemic TCL1 mice into young transgenic mice without the disease. After just 7 days, gene-expression profile changes of CD4<sup>+</sup> and CD8<sup>+</sup> cells in mice receiving the leukaemic cell transfer were comparable to those seen in TCL1 mice that developed CLL with age. Comparative analysis of gene-expression profiles of humans and mice using RESOURCERER, a database for annotating and linking

microarray resources within and across species, detected 50 overlapping differentially expressed genes, which were mainly involved in pathways of cell proliferation and activation, vesicle formation and protein trafficking, and actin cytoskeleton pathways. As in human CLL, these defects resulted in an impaired immune synapse formation. Another study examined CD4+ and CD8+ T-cell changes and subset compositions in lymph nodes and peripheral blood of TCL1 mice<sup>220</sup>. This work demonstrated that, as in human CLL, absolute T-cell numbers were increased in mice with manifest leukaemia compared to age-matched wild-type controls, that cells were shifted from naïve to antigen-experienced T cells, and that these cells were of a clonal character. The shift from naïve to antigen-experienced CD8+ T cells was recently confirmed by another study in the peritoneal cavity of 7 month old TCL1 mice with early stage leukaemia<sup>135</sup>.

Finally, adoptive transfer studies indicated that the TCL1 model might also be suitable to study the tumour-promoting role of the microenvironment *in vivo*. Protein kinase C (PKC)- $\beta$ II deficient mice were found to be unsusceptible to adoptive transfer of CLL cells from leukaemic TCL1 mice, indicating that the expression of PKC- $\beta$ II and the subsequent activation of NF- $\kappa$ B in bone marrow stromal cells are prerequisites to support the survival of malignant B cells<sup>221</sup>.

In summary, a broad body of evidence supports the use of the TCL1 model and adoptive transfer of TCL1 leukaemia cells to wild-type mice to investigate the biology of CLL. However, immunological studies in mice generally must be interpreted within the context of age and genetic background strain, as both ageing<sup>222, 223</sup> and genetics<sup>224, 225</sup> have been demonstrated to play a major role in shaping the immune response.

### **1.2.1.3 Suitability as a preclinical tool to test *in vivo* efficacy of substances**

Several studies have demonstrated that the TCL1 model is very suitable to mirror clinical responses to therapy observed in human CLL patients, thus validating it as a preclinical tool to evaluate novel drugs and treatment combinations. An initial study confirmed that transformed murine lymphocytes express relevant therapeutic targets such as BCL-2, MCL-1, AKT, PDK1, and DNMT1, but have a wild-type p53 status<sup>215</sup>. In this work, treatment with low dose fludarabine led to a modest but significant survival advantage and reduced lymphocytosis, but mice became eventually completely resistant to fludarabine treatment. More recently, a direct comparison between treatment with fludarabine and actinomycin D, a p53-independent inducer of apoptosis targeting MCL-1 and BCL-2, indicated that actinomycin D was more effective than fludarabine in reducing tumour load and prolonging survival<sup>226</sup>. Other studies have

demonstrated responses of leukaemic mice to a variety of other substances such as agents targeting components of the BCR signalling pathway<sup>64, 65, 214, 227, 228</sup>, as well as agents targeting novel pathways or cellular mechanisms<sup>229-231</sup>. In addition, TCL1 mice are a suitable tool to investigate anti-tumour strategies targeted at the repair of the immune system. Our group has previously demonstrated that T-cell immune synapse deficiencies could be repaired by *ex vivo* treatment of murine cells with lenalidomide. In another study, anti-CD40 antibody and CpG oligonucleotide treatment increased anti-tumour macrophage responses against T-cell depleted TCL1 donor cells and resulted in a significant retardation of tumour growth and prolonged survival of mice<sup>232</sup>.

### 1.2.2 Alternative genetically engineered murine models of CLL

Several alternative genetically engineered mouse models of CLL are described in the literature. These include models mimicking genetic lesions in CLL, as well as models with over-expression or targeted deletion of oncogenes or microRNAs. The most frequent genetic lesion in CLL associated with an indolent course of disease is del13q14<sup>13</sup>. Therefore, transgenic mouse models with targeted deletion of the minimal deleted region (MDR) including *DLEU1*, *DLEU2* and the *miR-15a/16-1* cluster<sup>233</sup> and the common deleted region (CDR) of the corresponding murine 14qC3 locus have been created<sup>234</sup>. These mice developed a spectrum of lymphoproliferative disorders, including MBL and CD5- non-Hodgkin lymphoma (NHL), with the phenotype and severity of the developing disease being dependent on the size of the deleted region. While both MDR and CDR deleted mice first exhibited a leukaemic population at the age of 6 to 18 months and succumbed to disease after 12 to 18 months, similar to TCL1 mice, the percentage of CLL-like disease in relation to MBL or NHL was higher in CDR deleted mice.

Additional genetically engineered models are based on the targeted deletion of TNF-receptor family components, and include *BCL-2/TRAF2DN*<sup>235</sup>, *APRIL*<sup>236</sup> and *Myc/BAFF* transgenic mice<sup>237</sup>. To provide insights into the *in vivo* biology of microRNAs, a plethora of mouse models based on the over-expression or targeted deletion of microRNAs have been described. This was pioneered by studies in the New Zealand Black strain, a model of sporadic late-onset CLL-like disease linked to a genetic abnormality in the microRNA *miR-15a/16-1* locus<sup>238-240</sup>. The role of *miR-15a/16-1* in CLL was further elucidated in the context of studies targeting murine 14qC3 described above<sup>233</sup>. Compared to MDR deleted mice, *miR-15a/16-1* deleted mice had a longer time to CLL development and longer disease latency, with mice developing a similar spectrum of

lymphoproliferative disorders. In another model, *miR-29a* over-expression led to a markedly expanded CD5+ population detectable at 2 month of age in 85% of transgenic mice, but only 20% of mice developed frank leukaemia and died of disease at about 2 years of age<sup>241</sup>. Other microRNA-based models using *miR-155*<sup>242</sup>, the *miR-17-19* cluster<sup>243, 244</sup>, or *miR-125b*<sup>245</sup> largely fail to mirror the course of disease or immunophenotype of CLL. A recently described murine model of CLL is based on the over-expression of ROR1, an oncoembryonic antigen found on CLL cells, but not on normal adult tissues<sup>246</sup>. However, only 5% of transgenic mice developed CLL. In contrast, CLL penetrance was significantly improved and reached 100% in models of *IRF4*<sup>-/-</sup>*Vh11* deletion<sup>247</sup> and simian virus 40 (SV40) T antigen transgenic mice<sup>248</sup>. Key characteristics of these models are summarized in Table 3.

Most of these genetically engineered murine models of CLL are inferior to the TCL1 model with regards to disease penetrance. This can likely be attributed to the strong oncogenic function of TCL1 on multiple cellular targets such as the serine/threonine kinase AKT pathway<sup>249</sup>, the NF- $\kappa$ B pathway<sup>250, 251</sup>, and the DNA methyltransferases DNMT3A and DNMT3B<sup>252</sup>. The high disease penetrance in *IRF4*<sup>-/-</sup>*Vh11*<sup>247</sup> and E $\mu$ -SV40 T<sup>248</sup> is most likely related to the presence of exogenous factors accelerating B-cell transformation, but this leads to skewing of the IgVH repertoire, which is not representative of human CLL.

model based on:	time to leukaemia (months)	age of death (months)	% disease penetrance	comments
<b>genetic lesions</b>				
MDR 14qC3 <sup>233</sup>	6-18	12-18	~22	mice also developed MBL and NHL
CDR 14qC3 <sup>234</sup>	6-18	12-18	~50	
<b>TNFR family signalling</b>				
Bcl-2xTRAF2 DN mice <sup>235</sup>	9-15	~14	80	
APRIL Tg mice <sup>236</sup>	>9	12-15	40	
Myc/Baff Tg mice <sup>237</sup>	3	10	~80	male gender bias
<b>microRNA</b>				
miR15a/16- <sup>233</sup>	12-18	15-18	~20	see above
IgH-E $\mu$ -miR-29 <sup>241</sup>	12-24	24-26	20	
<b>other</b>				
E $\mu$ -ROR1 <sup>246</sup>	>15	>15	5	
IRF4 <sup>-/-</sup> Vh11 <sup>247</sup>	5-10	>9	100	
E $\mu$ -SV40 T <sup>248</sup>	<5	<10	100	

**Table 3: Summary of disease characteristics in alternative genetically engineered murine models of CLL.**

### 1.2.3 TCL1 model-based crosses with other murine models

To study the mechanisms of putative targets involved in CLL pathobiology and progression, the TCL1 model has been crossed with a variety of other genetically modified models. For examples, crosses between TCL1 and  $XID^{228}$ ,  $pkc\beta^{-/-}$  or  $pkc\beta^{+/-}$ <sup>253</sup>,  $dnrag1$  transgenic<sup>254</sup>,  $TIR8^{-/-}$ <sup>255</sup>,  $IRE-1$   $XBP1^{256}$ ,  $TP53^{-/-}$ <sup>257</sup>,  $ID4^{-/-}$ <sup>258</sup> and  $ROR1^{246}$  mice have highlighted the effects of receptor signalling and tumour suppressors or oncogenes on disease onset and progression. Other crosses with transgenic  $APRIL^{259}$ ,  $BAFF^{260}$ ,  $MIF^{-/-}$ <sup>200</sup>,  $CD44^{-/-}$ <sup>261</sup>,  $fzd6^{-/-}$ <sup>262</sup>,  $\rho h o H^{-/-}$ <sup>263</sup> and  $h s 1^{-/-}$  mice<sup>264</sup> have significantly contributed to the understanding of microenvironmental interactions and cytoskeleton formation and cell trafficking. Figure 2 provides an overview of mouse models crossed with TCL1 mice.

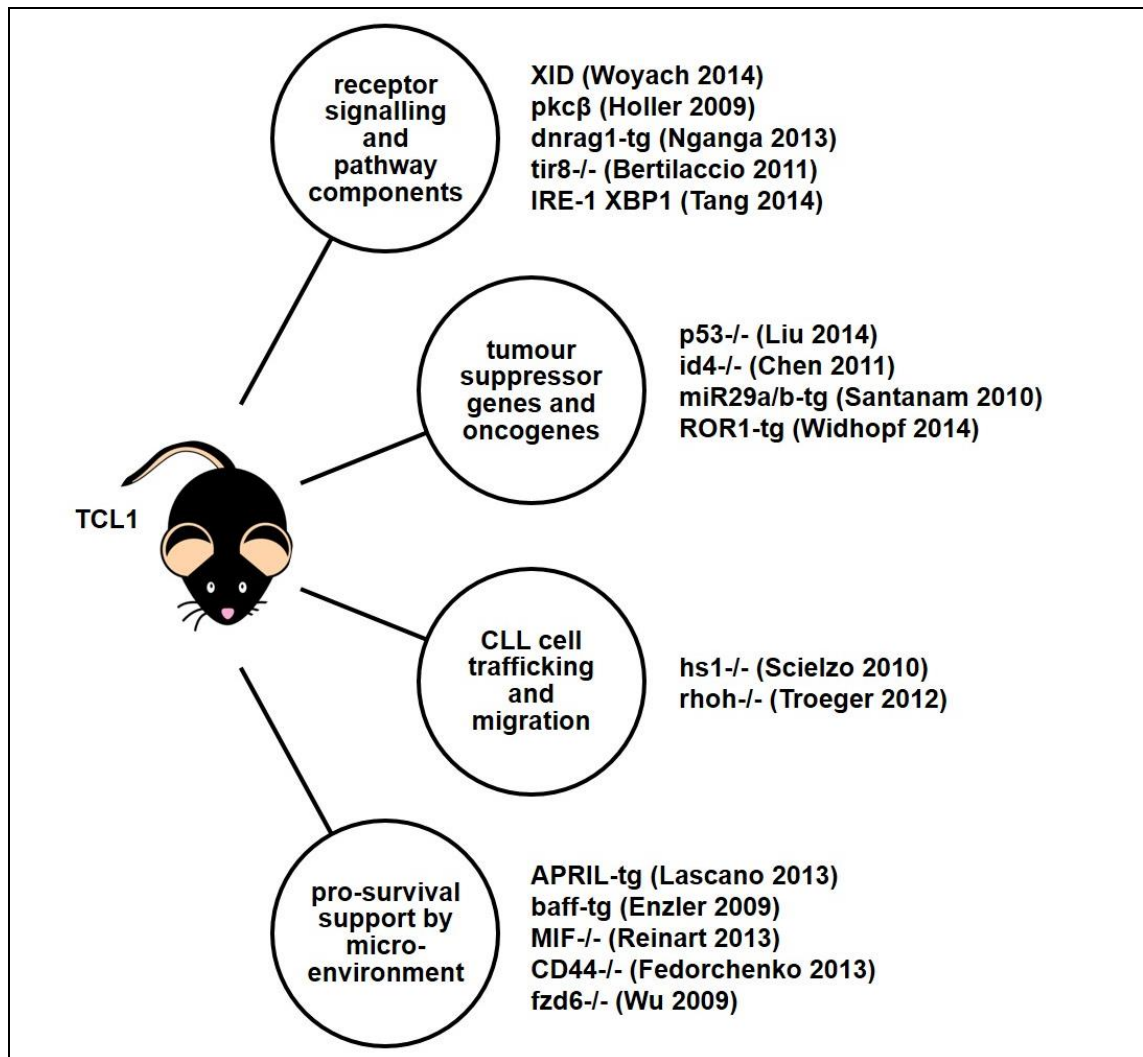


**Figure 2: Summary of genetically engineered mouse models crossed with TCL1 mice to investigate effects of putative targets on disease development and progression.** Adapted from Simonetti *et al.*<sup>265</sup>; Abbreviations: tg – transgenic.

#### 1.2.4 Xenograft models of CLL

A variety of xenograft models using primary CLL cells or CLL-like cell lines have been described<sup>266</sup>. In general, xenograft models using primary mature CLLs from peripheral blood are hampered by the observations that circulating CLL cells do not engraft well, that they are rejected by the host if recipients are immune competent mice, and that immune compromised mice such as SCID mice can develop CD5- EBV-driven B-cell tumours unrelated to human CLL<sup>267, 268</sup>. In addition, engraftment of human CLL cells appears to be influenced by T cells; early studies demonstrated that intraperitoneal (i.p.) injection of CLL cells into lethally irradiated BALB/c or beige/nude/Xid (BNX) mice which were radioprotected with bone marrow from NOD/SCID mice led to generally enhanced engraftment of CLL in the peritoneal cavity in the absence of T cells<sup>269, 270</sup>. Further studies improved the engraftment of human CLL cells by combinations of i.p. and intravenous (i.v.) injections, but confirmed that the expansion of CLL cells was influenced by T cells, suggesting a role for T cells in controlling the expansion of leukaemic B cells *in vivo*<sup>271, 272</sup>. In contrast, another study using completely lymphocyte deficient NSG mice (NOD/SCID x IL2rg<sup>-/-</sup>) observed engraftment and proliferation of CLL after co-transfer with autologous T cells and allogeneic antigen presenting cells. However, CLL disappeared after approximately 3 months, coincident with the onset of lethal T-cell mediated GvHD, indicating a dual functional role of T cells in this context<sup>273</sup>. Another study injected newborn NSG mice with immature CD34<sup>+</sup>CD38<sup>-</sup> stem cells from bone marrow from CLL patients<sup>274</sup>. CD34<sup>+</sup> cells gave rise to a high number of polyclonal B-cell progenitors, but their maturation into B cells was restricted to monoclonal or oligoclonal CLL-like cells, which were independent from the original CLL clones as evidenced by different IGVH-DJ rearrangements. This indicates that the propensity to generate clonal B cells has already been acquired at the stem cell stage and is independent of oncogenic events. The NSG xenograft model has also been used for the preclinical testing of drug efficacy *in vivo*<sup>275</sup>. After i.v. transplantation of CLL peripheral blood mononuclear cells into NSG recipients pre-treated with busulfan, mice were treated with ibrutinib. This reduced CLL tumour burden by promoting the emigration of CLL cells from solid tissues and by blocking CLL cell proliferation.

Altogether, xenograft models are appropriate tools to identify the genetic basis, development and evolution of CLL and to conduct rapid drug testing, while mostly falling short of depicting the complex associations and interactions between CLL cells and the microenvironment. The NSG xenograft model might be an exception to this, as a recently published study indicated that spleens from NSG xenografted mice are suitable to mirror the role of human lymph nodes in activating B-cell receptor and NFκB

pathways in CLL cells, which leads to increased CLL cell proliferation and activation<sup>275</sup>. However, the complexity of long-term host immune responses in the context of developing disease can only be adequately modelled in immune competent mice. This makes the TCL1 model, along with the reasons discussed above (*i.e.* 100% penetrance of the disease and great biological similarity to human CLL) the most suitable model system currently available to investigate and explore potential strategies targeted at restoring anti-tumour immune responses.

### 1.3 PD-L1/PD-1 immune checkpoint interactions

#### 1.3.1 PD-L1/ PD-1 in physiological immune responses

The primary signal in T cells is generated after presentation of antigen by major histocompatibility complex molecules (MHC) and recognition by the T-cell receptor. In addition, accessory receptors are required during T-cell priming, activation, expansion, effector function and contraction to modulate T-cell signalling pathways and to prevent destructive autoimmune responses to self-tissues. Accessory T-cell molecules mostly belong to the immunoglobulin superfamily and include CD28 and CTLA-4, which are both receptors for CD80 and CD86<sup>276</sup>. CD28 is constitutively expressed by T cells and is essential for T-cell activation. Following co-ligation of CD28, the Src kinases Lck and Fyn phosphorylate a tyrosine within an ITAM in the cytoplasmic domain of CD28, allowing the latter to bind and to activate PI3K via its Src homology 2 (SH-2) domain. CD28 signalling also facilitates GTP/GDP exchange on Ras, resulting in activation of the MAP kinase pathway, activation of Akt kinase, and activation of the adapter protein Vav and the associated Rac pathway. These signals enhance the transcription of IL-2 and the stability of IL-2 transcripts, thereby stimulating T-cell proliferation<sup>277</sup>. In contrast, CTLA-4 is only expressed by most T-cell types after activation, and transmits a negative signal<sup>276</sup>. Instead of an ITAM, CTLA-4 possesses an immunoreceptor tyrosine inhibitory motif (ITIM) in its cytoplasmic domain. Ligation of CTLA-4 induces tyrosine phosphorylation of the ITIM, which, in turn, recruits the tyrosine phosphatase SHP-2 that can deactivate the phosphorylated ITAMs of the  $\zeta$  chains of the T-cell receptor complex. CTLA-4<sup>-/-</sup> mice develop a fatal lymphoproliferative disorder that is characterized by massive cell activation and infiltration into tissues, indicating that CTLA-4 serves as an essential brake on T-cell activation<sup>278</sup>.

An important member of the CD28 family is CD279 (Programmed Death-1, PD-1). PD-1 was first described in 1992 in apoptosis-induced murine cells<sup>279</sup>. The human PD-1 gene was soon after mapped to chromosome 2q37.3 and was demonstrated to share

70% homology at the nucleotide level and 60% homology at the amino acid level with the murine PD-1 gene, translating into a 288 amino acid type I transmembrane protein containing an intracellular tyrosine domain<sup>280, 281</sup>. After expression of PD-1 mRNA was found to be restricted to thymus in adult mice, several studies examined the expression of PD-1 protein in lymphoid tissues. In thymus and normal murine lymphoid tissues PD-1 was expressed at very low levels, while CD4-CD8<sup>-</sup> cells were enriched for PD-1-expressing  $\gamma\delta$  T cells as well as PD-1-negative  $\gamma\delta$  T cells which upregulated PD-1 after stimulation with CD3 antibody. These observations indicate that PD-1 expression is restricted during T cell differentiation and can be induced at stages preceding clonal selection<sup>282</sup>. The notion of PD-1 as a marker of activated T cells was confirmed by further studies demonstrating increased PD-1 expression on mature T cells after *in vivo* stimulation with CD3 and *in vitro* stimulation with CD3, PHA and PMA/Ionomycin<sup>283</sup>. Moreover, PD-1 expression could also be induced on B cells by anti-IgM stimulation.

The functional relevance of PD-1 was subsequently discovered in a number of studies using PD-1<sup>-/-</sup> mice. Initial studies indicated a role of PD-1 in increasing proliferative responses of B cells after anti-IgM stimulation *in vitro*<sup>284</sup>. In addition, PD-1<sup>-/-</sup> mice showed increased serum levels of IgG2b, IgA and IgG3, while IgM and IgG1 were comparable with control mice, indicating a role of PD-1 in B-cell differentiation and isotype class switching. The involvement of PD-1 in the maintenance of peripheral self-tolerance as a negative regulator of immune responses was first suggested by the observation that aged C57BL/6 PD-1<sup>-/-</sup> mice spontaneously developed auto-immune diseases such as lupus-like proliferative arthritis and glomerulonephritis, and exhibited strong and ongoing T-cell receptor mediated proliferative responses to the stimulation with specific antigen-presenting cells<sup>285</sup>. The same group demonstrated autoimmune dilated cardiomyopathy in BALB/c PD-1<sup>-/-</sup> mice<sup>286</sup>.

The PD-1 ligand PD-L1 (CD247, B7-H1) was first discovered as a member of the B7 family with T-cell stimulatory effects after T-cell receptor engagement in the presence of IL-2<sup>287</sup>. In contrast, Freeman and colleagues found that engagement of PD-1 by PD-L1 led to a dose-dependent inhibition of T-cell receptor-mediated proliferation and IFN- $\gamma$  and IL-10 cytokine secretion, which was not observed in T cells from PD-1<sup>-/-</sup> mice<sup>288</sup>. Interestingly, the outcome of PD-L1/PD-1 interactions was demonstrated to be dependent on the strength of the T-cell receptor and CD28 costimulation signals: under conditions of suboptimal T-cell receptor engagement, minimal proliferation was observed in the absence of costimulation, while the addition of increasing concentrations of soluble anti-CD28 antibody led to an up to 30-fold increase in proliferation. Under these conditions, activation of T cells in the presence of PD-L1

resulted in an 80% reduction in proliferation, and a maximal level of CD28 costimulation was required to rescue the inhibition of proliferation mediated by PD-L1 stimulation. In contrast, under saturating conditions of T-cell receptor activation, PD-L1-mediated inhibition of T-cell proliferation was only observed in the absence of CD28 costimulation, indicating that increasing levels of T-cell receptor or CD28 signalling can circumvent the inhibitory effects of PD-1 ligation at the activation stage. The same group later compared T-cell activation and cytokine production of PD-1-deficient *versus* PD-1/B7-1 (CD80) double-deficient T cells to PD-L1 ligation and of CD28/CTLA-4 double-deficient *versus* CD28/CTLA-4/PD-L1 triple-deficient T cells to B7-1 (CD80) ligation<sup>289</sup>. These studies revealed a specific functionally relevant interaction between the two B7 family members CD80 and PD-L1, resulting in inhibitory signals, diminished expression of cell-surface activation markers, decreased T-cell proliferation and reduced cytokine production, therefore adding a new dimension to the immunoregulatory interactions within the B7:CD28 family of costimulatory molecules.

PD-L1 mRNA expression follows very distinct patterns: in contrast to CD80 and CD86, PD-L1 mRNA was found to be constitutively expressed by non-lymphoid, parenchymal organs such as the heart, placenta, skeletal muscle, and lung, while mRNA expression could be induced in APCs, including human peripheral blood CD14<sup>+</sup> monocytes, dendritic cells, activated B cells and to a certain extent by CD3<sup>+</sup> T cells themselves after stimulation with IFN- $\gamma$ <sup>287, 288</sup>. On a protein level, PD-L1 was detected in a variety of haematopoietic cell types, including a minor proportion of splenic T and B cells, the majority of pre-B cells and myeloid cells in bone marrow, and subsets of thymocytes<sup>290</sup>. In addition, a significant proportion of immature lineage-marker-negative and c-Kit-positive bone marrow cells containing stem cells were found to express PD-L1. Following two-day mitogenic concanavalin A or LPS stimulation, PD-L1 surface expression could be detected in all lymphocyte subsets. Another study confirmed constitutive PD-L1 expression on freshly isolated murine splenic T cells, B cells, macrophages, and dendritic cells, and upregulation on T cells by anti-CD3 stimulation, on macrophages by LPS, IFN- $\gamma$ , GM-CSF, or IL-4, and on dendritic cells by IFN- $\gamma$ , GM-CSF, or IL-4<sup>291</sup>.

The second ligand for PD-1 is PD-L2 (CD273, B7-DC). Similar to PD-L1/PD-1, engagement of PD-1 by PD-L2 inhibited T-cell receptor mediated proliferation and cytokine production of CD4<sup>+</sup> T cells<sup>292</sup>. At low antigen concentrations, PD-L2/PD-1 interactions counteracted costimulatory CD28 signals, but reduced cytokine production only without inhibiting T-cell proliferation at high antigen concentrations. Compared with PD-L1, PD-L2 protein expression was found to be more restricted to subsets of

macrophages and dendritic cells stimulated with IFN- $\gamma$ , GM-CSF, or IL-4<sup>291</sup>, whereas another study found PD-L2 expression to be absent in haematopoietic cells<sup>290</sup>. Early murine studies using PD-L1<sup>-/-</sup> and PD-L2<sup>-/-</sup> mice confirmed that PD-L1 and PD-L2 have largely overlapping functions in inhibiting IL-2 and IFN- $\gamma$  production during T-cell activation, but that PD-L1 expression on parenchymal cells appears to be a more important mediator of tissue tolerance<sup>293</sup>. Other studies using PD-L1<sup>-/-</sup> mice observed a spontaneous accumulation of CD8<sup>+</sup> T cells in the liver, leading to accelerated hepatocyte damage in experimental autoimmune hepatitis<sup>294</sup>, and confirmed the role of PD-L1 in negatively regulating both CD4<sup>+</sup> and CD8<sup>+</sup> T cells<sup>295</sup>. In a murine model of asthma, the severity of airway hyperreactivity and airway inflammation was significantly greater in PD-L2<sup>-/-</sup> mice compared with wild-type mice and increased IL-4 production by NKT cells, while PD-L1<sup>-/-</sup> mice showed significantly reduced airway hyperreactivity and enhanced production of IFN- $\gamma$  by NKT cells, reflecting the expression of PD-L2 on lung dendritic cells<sup>296</sup>. In contrast, diminished IFN- $\gamma$  immune responses suggesting a positive costimulatory function of PD-L2 were observed in another line of PD-L2<sup>-/-</sup> mice<sup>297</sup>.

Several studies have contributed to elucidating the molecular mechanisms by which PD-L1/PD-L2/ PD-1 influence T-cell activation. Karwacz *et al.* demonstrated that PD-1 ligation facilitates the down-modulation of the T-cell receptor by increasing expression of the E3 ubiquitin ligase Cbl-b, which is essential to downmodulate T-cell receptors as part of a normal immune response<sup>298</sup>. As early intracellular signalling pathways, PD-1 ligation was found to attenuate T-cell receptor induced CD3 $\zeta$  chain and ZAP-70 phosphorylation, leading to impaired IL-2 production and T-cell proliferation via PKC $\theta$  signalling<sup>299</sup>. A key element in the mediation of PD-1 inhibition of T-cell receptor signalling is the binding and consecutive phosphorylation of SHP-2 to the cytoplasmic tail of PD-1, which contains both an ITIM and an immunoreceptor tyrosine-based switch motif (ITSM)<sup>292</sup>: SHP-2 phosphorylation after PD-1 engagement inactivates PI3K, which in turns inactivates Akt, a serine/threonine kinase that promotes T-cell activation, proliferation, and survival and induces IL-2 expression<sup>300</sup>. Mutation studies have demonstrated that this is mediated by binding of SHP-2 to ITSM<sup>301</sup>, and while either SHP-1 or SHP-2 can function as mediators when artificially co-localized to T-cell receptor microclusters, only SHP-2 is recruited physiologically<sup>302</sup>. In addition, there are several mechanisms by which PD-1 engagement leads to impaired immune synapse formation. Firstly, SHP-2 can also inhibit integrin signalling, which may partially account for the destabilization of the immune synapse<sup>303</sup>. In addition, Src family kinases Csk and Lck can be recruited to ITSM and ITIM, which leads to PI3K/ Akt deactivation. As

LFA-1 mediated T cell/ B cell conjugation requires signalling through Lck<sup>304</sup>, Lck dephosphorylation after PD-1 ligation interferes with the formation of the immunological synapse. Planar bilayer systems demonstrated that physical co-localization of PD-1 to T-cell receptor microclusters was sufficient for destabilization of the immune synapse and efficient at inhibiting T-cell receptor signalling independent of PD-1 ITSM phosphorylation<sup>302</sup>: Following engagement of both T-cell receptor and PD-1, 98% of activated T-cell receptor microclusters contained PD-1, while in the absence of PD-L1 ligation, PD-1 localized away from microclusters and allowed T-cell activation.

Mechanisms of PD-1 concentration at the immunological synapse with dendritic cells were elucidated by another study<sup>305</sup>. Similarly to CD28 and CTLA-4, ligand binding led to the recruitment of PD-1 to the synapse of CD4<sup>+</sup> T cells forming conjugates with peptide-pulsed activated splenic dendritic cells. It was suggested that PD-L2 was the preferred ligand for PD-1 recruitment to the immunological synapse in this context, but it is likely that this finding solely reflects the expression pattern of PD-L1 and PD-L2 on this cell type. However, another study describing the kinetics and relative affinities of the interactions between PD-L1, PD-L2 and PD-1 found a 2-6-fold higher affinity and different association/ dissociation kinetics for interaction of PD-L2 and PD-1 compared to interactions of PD-L1 and PD-1<sup>306</sup>.

Both PD-L2/PD-1 and PD-L1/PD-1 signals inhibit T-cell proliferation by blocking cell cycle progression, as evidenced by an increased number of cells in the G0/G1 phase and a corresponding decrease in those in S/G2 phase<sup>292</sup>. This was more pronounced by the engagement of PD-1 by PD-L1 than by PD-L2. As the underlying molecular mechanism for PD-1 mediated cell cycle arrest, the suppression of SKP2 transcription via PI3K/Akt inhibition and impaired RAS/MEK/ERK signalling was identified<sup>307</sup>. SKP2 encodes for a recognition component of the ubiquitin E3-ligase complex Skp, Cullin, F-box containing complex (SCF), and PD-1 induced down-regulation of Skp2 prevents the ubiquitination and degradation of p27 (kip1) during the induction of cell cycle allowing cell cycle progression. In addition, PD-1 ligation prevented Smad3 transcription factor phosphorylation, which increased the abundance of the G1 phase cell cycle inhibitor p15 (INK4) and repressed the CDK-activating phosphatase Cdc25A, resulting in inhibition of CDK2, CDK4, and CDK6 essential for progression through the G1 and S phases of the cell cycle<sup>308</sup>. Interestingly, exposure of cells to IL-2 restored activation of MEK/ERK signalling, but not Akt signalling, and only partially restored SKP2 expression<sup>307</sup>. In addition, p38 and JNK activation remained unaffected, indicating that PD-1 signalling selectively targets T-cell receptor signalling pathways rather than representing a global abrogation.

PD-1 was also described as having an effect on T-cell survival by impacting apoptotic genes. This is primarily mediated via PI3K inhibition, which attenuates expression of the antiapoptotic gene BCL-x<sub>L</sub><sup>309</sup>. Another study found lower levels of the pro-apoptotic molecule Bim in antigen-primed CD8+ T cells in PD-L1 deficient mice, while the engagement of activated CD8+ T cells by a plate-bound PD-L1 fusion protein led to the upregulation of Bim and increased cell death<sup>310</sup>. As the Bim/Bcl-2 balance is critical for maintaining naive and memory T-cell homeostasis, PD-1 engagement might negatively regulate T-cell memory by enhancing the depletion of effector T cells through the upregulation of Bim. A simplified overview of intracellular targets in T cells affected by PD-1 ligation is depicted in Figure 3.

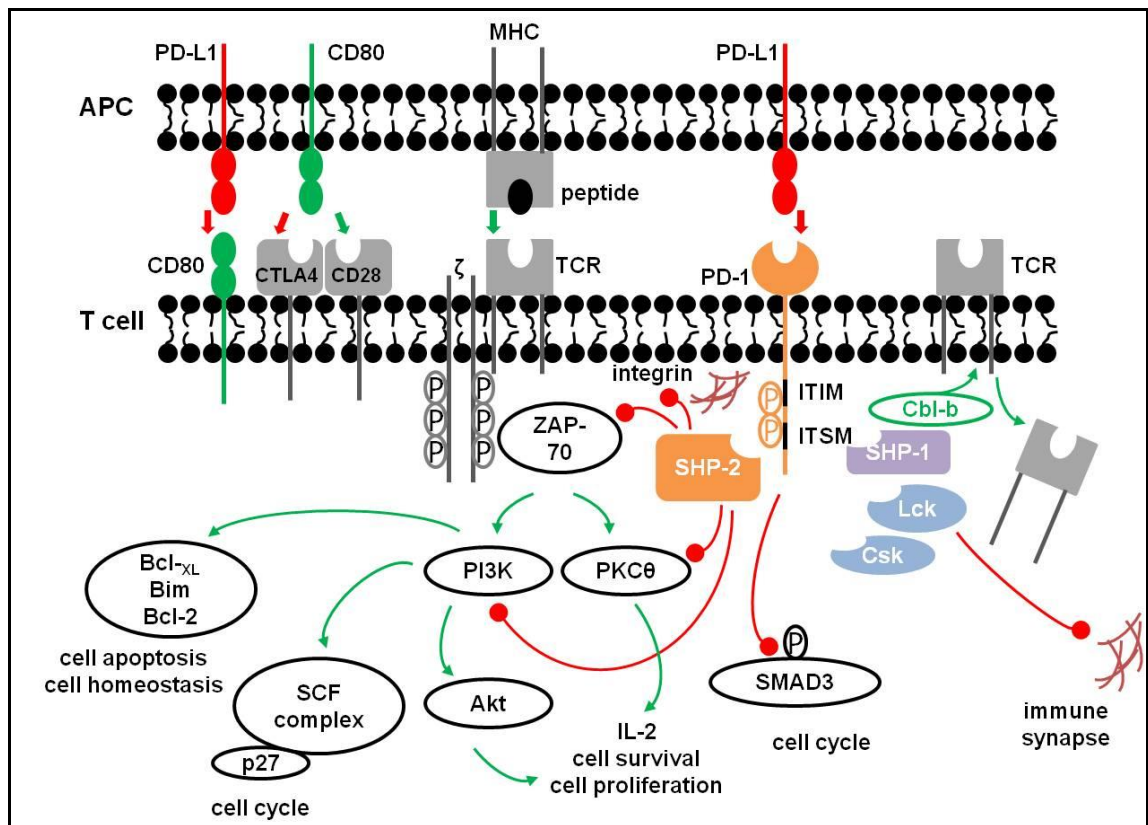


**Figure 3: Effect of PD-1 ligation on intracellular targets in T cells:** The role of PD-1 is to guarantee T-cell homeostasis by limiting T-cell activation and proliferation. PD-1 co-localizes with the T-cell receptor (TCR) to microclusters following its ligation with PD-L1. PD-1 mediated Cbl-b activation increases the internalization of the TCR. PD-1 ligation directly inhibits proximal TCR signalling by blocking phosphorylation of the ZAP70/CD3 $\zeta$  signalosome. As a key molecule, SHP-2 is recruited to the PD-1 intracytoplasmic ITSM domain, leading to the inactivation of PI3K, Akt and integrin, which results in impaired IL-2 production and T-cell proliferation. ITSM and ITIM also recruit the tyrosine kinases Csk and Lck, affecting PI3K/Akt signalling and destabilizing the immune synapse. Cell cycle arrest is mediated via Akt signalling, promoting accumulation of Smad3, and by SCF complex-mediated impaired degradation of p27. Apoptosis and impaired cell homeostasis is mediated via PI3K and Bcl-2 family proteins.

### 1.3.2 PD-L1 and PD-1 inhibitory signalling and adaptive immune resistance in cancer

While the physiological role of PD-1 is to guarantee T-cell homeostasis and to prevent autoimmunity by limiting T-cell activation and proliferation, aberrant PD-L1 expression is often used by tumour cells to provide a pro-tumour microenvironment by suppressing T-cell effector functions. Soon after the discovery of PD-L1, several studies described aberrant PD-L1 expression on tumour cell lines and primary tumour cells. One of the earliest studies characterizing the protein expression found that a variety of murine leukaemic lines of T-, B-, and myeloid lineages expressed PD-L1<sup>290</sup>. Another study detected surface PD-L1 expression on human lung and ovarian carcinoma cell lines<sup>311</sup>. PD-L1 expression was also observed in both the cytoplasm and on the plasma membrane of a variety of primary solid tumours using immunohistochemistry<sup>311-314</sup>. Of note, considerable intra-tumour heterogeneity was found, and not all cells within a tumour expressed PD-L1.

Aberrant PD-L1 expression is also utilized by haematological malignancies. For example, our group has demonstrated that PD-L1 is upregulated on primary tumour cells in patients with CLL, follicular lymphoma (FL) and diffuse large B cell lymphoma (DLBCL)<sup>79</sup>. Aberrant PD-L1 expression by tumour cells is also observed in mantle cell lymphoma<sup>315</sup>, Hodgkin Lymphoma (HL)<sup>316</sup>, primary mediastinal B-cell lymphoma (PMBL)<sup>317</sup> and on CD34+ blasts cells from MDS<sup>318</sup>, CMML and AML patients<sup>319</sup>, especially patients with AML M5<sup>320</sup>, and multiple myeloma<sup>321</sup>. Of note, high PD-L1 expression on tumour cells, along with increased PD-1 expression on tumour-specific CD8+ T cells, has also been described in patients with relapsed leukaemia after HSCT<sup>322</sup>.

Immunohistochemistry-based studies also observed inverse correlations between PD-L1 expression by solid tumour cells and tumour-infiltrating lymphocytes, particularly CD8+ T cells<sup>312, 314</sup>. This association, however, appears to be dependent on the tumour type, as another study in oesophageal cancer failed to recapitulate this correlation<sup>313</sup>. The functional relevance of PD-L1 expression by tumour cells was first demonstrated by the finding that cancer-associated PD-L1 increased the apoptosis of antigen-specific human T-cell clones *in vitro*<sup>311</sup>. Congruently, immunized PD-L1 deficient mice showed an increased expansion of effector CD8+ T cells and a delayed T-cell contraction followed by the emergence of a protective CD8+ T-cell memory capable of completely rejecting tumour metastases in the lung<sup>310</sup>. Similar observations have been made in haematological malignancies: in a PMBL cell line, both wild-type PD-L1 expression and a newly identified fusion product between the MHC class II transactivator CIITA and

PD-L1/ PD-L2 genes negatively regulated Jurkat T-cell activation<sup>317</sup>. In another study, the presence of PD-L1 blocking antibody and shRNA knockdown of PD-L1 in SP53 and Granta 519 cells significantly increased the proliferation of allogeneic T cells<sup>315</sup>. The *in vivo* relevance was demonstrated by the finding that in SCID mice with established mantle cell lymphoma, the downregulation of PD-L1 on lymphoma cells resulted in higher sensitivity to killing by lymphoma-specific cytotoxic effector memory T cells and led to improved survival. In HL, culturing bulk tumour cells in the presence of anti-PD-L blocking antibodies led to augmented IFN- $\gamma$  production<sup>316</sup>. Blocking PD-1/PD-L1 interactions also restored the proliferative activity of leukaemia-specific CD8+ memory T cells in patients who relapsed after HSCT<sup>322</sup>.

Using a functional siRNA screening approach in the CLL-like cell line MEC-1, work from our group has demonstrated that knockdown of PD-L1, as well as silencing of CD200 (OX2), CD276 (B7-H3) and CD270 (TNF receptor, TNFR-superfamily 14), reverse impairment of T-cell actin dynamics via regulation of members of the Rho family of GTPases, including RhoA, Rac1 and Cdc42<sup>79</sup>. In primary CLL cells, neutralizing antibodies against these targets increased F-actin polymerization, measured by immune synapse formation assays, with the combination of antibodies against all four ligands yielding the largest effect on immune synapse repair. This translated into significantly improved normal donor CD8+ T cell killing function using third-party normal donor allogeneic B cells as antigen-presenting cells after primary coculture with CLL cells, which could be further improved by addition of lenalidomide to the coculture. Antibodies targeting co-receptors on T cells receiving the immunosuppressive signal from the tumour, namely against CD200R, CD272 and PD-1, also improved synapse formation and T-cell effector function. This inhibitory ligand-induced impairment of T-cell actin dynamics was also observed in FL and DLBCL, as well as in solid carcinoma cells, indicating that immunomodulating processes in CLL might serve as a model for other malignancies.

Studies of tumour cell lines or primary tumour cells have also contributed considerably to elucidate the mechanisms leading to PD-L1 over-expression. For example, frequent cytogenetic alterations in PMBL and HL involve chromosome 9p<sup>323</sup>. This is also the coding region for *PD-L1* and *PD-L2* along with *JAK2*, which encodes a tyrosine kinase, and *SMARCA2*, which encodes a putative chromatin regulator. Rosenwald *et al.* demonstrated that elevated transcription of *PD-L1* and *PD-L2* were a characteristic feature of PMBL with chr 9p alterations<sup>324</sup>. This was confirmed by molecular studies in HL, which found *PD-L1* and *PD-L2* to be key targets at the 9p24.1 amplification peak in nodular sclerosing HL cell lines<sup>325</sup>. In classical HL, the extended 9p24.1 amplification

region included the *JAK2* locus, leading to increased protein expression and activity, induction of PD-L1 transcription and enhanced sensitivity to JAK2 inhibition. In EBV positive HL, matrix protein 1 (MP1) and latent membrane protein 2A (LMP2A) enhanced the transcriptional activity of *PD-L1* and *PD-L2*, indicating that the expression of *PD-L* genes is possibly caused by latent virus-associated membrane proteins<sup>316</sup>. PD-L1 was also found to be regulated by the oncogenic, chimeric nucleophosmin (NPM)/ anaplastic lymphoma kinase (ALK) in NPM+/ALK+ T-cell lymphoma via the STAT3 transcription factor, indicating a direct link between an oncoprotein and the immunosuppressive cell-surface protein PD-L1<sup>326</sup>. At the translational level, PD-L1 expression appears to be suppressed by the *PTEN* gene: mutated PTEN was found to activate S6K1, which shifts PD-L1 mRNA to polysomes, increasing the translation of PD-L1 mRNA and its plasma expression<sup>327</sup>. As another regulator at the translational level, miRNA513 was described, which is complementary to the 3' UTR of PD-L1 and prevents PD-L1 mRNA translation<sup>328</sup>.

Interestingly, several of these mechanisms lead to the increased production of IFN- $\gamma$ . On the other hand, cancer-associated PD-L1 expression in response to IFN- $\gamma$  has been described in several malignancies, for example in mantle cell lymphoma<sup>315</sup>, multiple myeloma<sup>321</sup>, AML<sup>329</sup> and MDS blasts<sup>318</sup>, where this induction was associated with the activation of NF- $\kappa$ B and nearly completely blocked by an NF- $\kappa$ B inhibitor. Lee *et al.* demonstrated that interferon regulatory factor-1 (IRF-1) is primarily responsible for the constitutive PD-L1 expression as well as for the IFN- $\gamma$  -mediated PD-L1 upregulation in a human lung cancer cell line A549, with AG490, a Janus activated kinase/signal transducer and activator of transcription inhibitor, greatly abolishing the responsiveness of A549 cells to IFN- $\gamma$  by reducing the IRF-1 transcription<sup>330</sup>. However, PD-L1 induction on cancer cells was also observed in response to stimulation with IL-10 in mantle cell lymphoma<sup>315</sup> and to toll-like receptors (TLR) ligands<sup>321, 329</sup>. In addition, as described in chapter 1.3.1, PD-L1 can be induced in various other non-tumour cell types of the microenvironment, whereas constitutive aberrant PD-L1 expression is a characteristic of certain cells of the tumour microenvironment such as MDSCs<sup>199, 331</sup>.

These observations have prompted the formulation of the “adaptive immune resistance” hypothesis<sup>332</sup> – under the pre-requisite of a tumour being immunogenic, immune and bystander cells produce cytokines such as TNF- $\alpha$  and IFN- $\gamma$  as a result of activation by a tumour, which prompts the upregulation of PD-L1 by both the tumour and the tumour microenvironment. As a result, immune effector cells are suppressed, and the tumour is protected from anti-tumour immune responses and is able to

promote further immune suppression by additional immune escape mechanisms such as the downregulation of surface molecules or evasion into sanctuary and growth-supporting niches. Moreover, other activated immune cells such as NKT cells<sup>333</sup>, B cells<sup>334</sup> or dendritic cells<sup>335</sup> also can express PD-1 and can hence be suppressed by PD-L1 ligation.

#### **1.4 Generating anticancer immunity harnessing T cell responses**

Hanahan and Weinberg famously proposed six hallmarks of cancer in 2000, which comprise biological capabilities acquired during tumour development due to genome instability<sup>336</sup>. Considering the rapidly building evidence of the central role of the immune system in tumour formation and progression, the authors since revisited these hallmarks<sup>337</sup>. Most if not all tumour types are now recognized to rely on immune suppression and evasion for their survival, and tumour cells in many cases actually subvert immune components to support their growth. In view of the cancer immunoediting hypothesis whereby an individual is protected from cancer through the elimination and immunogenic modification of cancer cells<sup>338</sup>, cancer immunotherapy is a very attractive approach. When properly established, anti-tumour immune surveillance is exquisitely capable of eliminating tumour cells, and in fact is probably the most likely route to achieving cures or at least long-term control of cancer. The ability of HSCT to produce cures in a subset of CLL patients, as described in chapter 1.1.3, provides one illustration of the remarkable potential of the immune system. However, HSCT remains a risky option due to the immune-depleting conditioning regimens and GvHD, and thus alternative, safer methods of establishing anti-tumour immune responses are being aggressively pursued.

An especially exciting new and active immunotherapy approach is chimeric antigen receptor (CAR) T-cell therapy. CAR technology has recently emerged as a promising strategy to specifically target malignant cells using precisely engineered T cells. The successful construction of a chimeric T-cell receptor was first described over 20 years ago<sup>339</sup>. Considerable progress has been made since then, to the point that at some centres the generation of CAR T-cells is nearly routine. CARs are generally made up of an antigen-recognizing receptor coupled to a signalling molecule or molecules that activate the T cell expressing the CAR<sup>340</sup>. The antigen receptors most commonly incorporated into CARs are single chain variable region moieties (scFv) that consist of the light chain and the heavy chain variable regions of a monoclonal antibody joined by a peptide linker. The scFv portion is linked to a transmembrane domain followed by a

tyrosine-based activation motif such as that from CD3 $\zeta$ . In initial studies, CARs were designed to contain a single cytoplasmic signalling domain derived most commonly from the TCR-derived CD3 $\zeta$  chain (first generation CARs). Second generation CARs contained additional cytoplasmic signalling domains, and third generation CARs now include more than one costimulatory signalling domain in addition to the CD3 $\zeta$  chain to enhance T-cell proliferation and survival. As for monoclonal antibodies, attractive CAR targets in CLL include CD19, CD20 and ROR1. In part because of the uncertainty regarding antigen selection, the optimal clinical approach to treating patients with CAR-T cells is not yet understood. Several Phase I/II clinical trials of anti-CD19 CAR-T cells have been initiated, and clinical activity is promising but not widespread (reviewed in <sup>341</sup>). One of the most impressive results was seen in a heavily pre-treated CLL patient with del17p and *TP53* mutation, who entered a complete remission after receiving second-generation anti-CD19 CAR T cells after conditioning with pentostatin and cyclophosphamide, while experiencing no acute side effects<sup>342</sup>.

Despite the promise of CAR T cells, there are several obstacles that must be overcome. First, as no single tumour-associated antigen is expressed by all tumour types, scFv encoded by CAR genes need to be constructed for each potential antigen. These target antigens must be carefully selected to avoid “on-target, off-organ” effects that can occur when the antigen is also expressed and recognized on non-malignant tissues and organs. Other issues include the paucity of such targets, the inability of current CARs to target more than one antigen which could promote the preferential growth of more aggressive antigen-negative tumour cells, manufacturing complexities and costs, and the inability to derive sufficient cells from some patients<sup>343, 344</sup>. In addition, CAR T-cell therapy can be associated with severe complications such as cytokine release syndrome, which is potentially lethal, and prolonged loss of normal B-cells<sup>345, 346</sup>. It has also become clear that the success of CAR therapy is highly dependent on the inclusion of lympho-reducing conditioning chemotherapy as well as CAR design<sup>346-349</sup>.

#### **1.4.1 Potential of novel agents to correct immune defects in CLL**

As highlighted in Chapter 1.1.3, several novel agents have shown very promising activity even in high-risk CLL patients. In addition to eliminating malignant cells via inhibition of specific targets or tyrosine kinases, they partly appear to have the potential to correct CLL-associated immune defects. For example, the BTK inhibitor ibrutinib also affects BCR- and chemokine-controlled retention and homing of CLL cells in their

growth- and survival-supporting lymph node and bone marrow microenvironment<sup>64-66</sup>. Thus, malignant B cells are driven out of their protective niches and are more accessible to cytotoxic therapy and potentially other immune cells. Recently published preclinical data indicates that ibrutinib also irreversibly binds the BTK isoform ITK, which is expressed in T cells, and can therefore be potentially used to correct T-cell based immune responses<sup>350</sup>.

Other novel agents that appear to affect signalling pathways involved in cell survival, clonal expansion and malignant cell retention in lymphoid tissues include idelalisib, an inhibitor of PI3K $\delta$ , CXCR4 antagonists, as well as inhibitors of Syk protein kinase, RAF/MEK/ERK, and BCL2.

A summary of key preclinical studies highlighting the effects of these substances on the immune system and the microenvironment in CLL is provided in Table 4. Especially lenalidomide has been demonstrated to have pleiotropic effects on several effector cell subsets of the immune system, probably accounting for the anti-tumour immune responses observed in CLL. This will be described in detail in Chapter 7.1.

target	name of compound(s)	published effects on the immune system/microenvironment in preclinical <i>in vitro</i> and <i>in vivo</i> models
<b>CXCR4/ CXCL12 mediated chemotaxis</b>	T140, TC14012, TN14003, plerixafor (AMD3100)	<ul style="list-style-type: none"> <li>antagonize the antiapoptotic effect of CXCL12 and stromal cell-mediated protection of CLL cells<sup>351</sup></li> <li>combination with passive (<i>i.e.</i> monoclonal anti-CD20/CD52 antibodies) but not active (<i>i.e.</i> activated T cells) immunotherapy as a promising potential treatment concept<sup>352</sup></li> </ul>
<b>SYK protein kinase</b>	R406, PRT318, P505-15	<ul style="list-style-type: none"> <li>reduces CLL migration towards CXCL12 and adhesion to VCAM-1<sup>353</sup></li> <li>antagonizes CLL cell survival in NLC co-cultures, inhibits BCR-dependent secretion of CCL3 and CCL4 by CLL cells, inhibits CLL migration towards CXCL12, CXCL13<sup>354</sup></li> </ul>
<b>TEC family kinases (BTK, ITK)</b>	ibrutinib	<ul style="list-style-type: none"> <li>inhibits BCR-controlled signalling and integrin <math>\alpha(4)\beta(1)</math>-mediated adhesion to fibronectin and VCAM-1, inhibits CXCL12-, CXCL13-, and CCL19-induced signalling, adhesion, and migration of primary CLL cells<sup>66</sup></li> <li>inhibits migration in response to tissue homing chemokines (CXCL12, CXCL13), down-regulates secretion of BCR-dependent chemokines (CCL3, CCL4) by CLL cells both <i>in vitro</i> and <i>in vivo</i><sup>65</sup></li> <li>blocks survival signals provided from the microenvironment including soluble factors (CD40L, BAFF, IL-6, IL-4, and TNF-<math>\alpha</math>), fibronectin engagement, and stromal cell contact<sup>64</sup></li> <li>ITK as an irreversible T-cell target of ibrutinib, driving a Th1-selective pressure<sup>350</sup></li> </ul>
<b>PI3K<math>\delta</math></b>	idelalisib (GS-1101, CAL-101)	<ul style="list-style-type: none"> <li>abrogates protection from spontaneous apoptosis induced by B cell-activating factors CD40L, TNF-<math>\alpha</math>, and fibronectin, decreases activated T-cell production of various inflammatory and antiapoptotic cytokines<sup>355</sup></li> <li>inhibits CLL cell chemotaxis toward CXCL12 and CXCL13 and migration beneath stromal cells, down-regulates secretion of chemokines in stromal cocultures and after BCR triggering, reduces survival signals derived from the BCR or from NLC<sup>70</sup></li> </ul>
<b>RAF/MEK/ ERK</b>	sorafenib	<ul style="list-style-type: none"> <li>inhibits RAF and ERK activation by NLC or stromal cells<sup>356</sup></li> <li>blocks migratory and microenvironmental survival signals in CLL cells<sup>357</sup></li> </ul>
<b>Bcl2</b>	AT-101	<ul style="list-style-type: none"> <li>induces similar extent of down-regulation of Mcl-1 and apoptosis in CLL lymphocytes cultured in suspension or on stroma<sup>358</sup></li> </ul>

**Table 4: Summary of key preclinical studies highlighting the effects of novel substances on the immune system and the microenvironment.**

#### 1.4.2 PD-L1 and PD-1 blockade in cancer

As discussed in Chapter 1.3.2, a variety of tumour types utilizes PD-L1/PD-1 immune checkpoints to their advantage to escape anti-tumour immune responses. Therefore, several clinical trials using PD-L1 or PD-1 antibody blockade have been initiated or are currently ongoing, mostly in heavily pre-treated or advanced disease stage patients. Key clinical trials using PD-L1 or PD-1 antibody blockade as a single therapy are summarized in Table 5 (PD-L1 blockade) and Table 6 (PD-1 blockade). Collectively, these trials have yielded very promising results: PD-L1/PD-1 antibodies were generally well tolerated and associated with a low incidence of serious adverse events (SAEs), while producing significant and in some cases durable responses in heavily pre-treated

patients with advanced stage cancers. Although a direct comparison has not been conducted yet, PD-1 blockade appears to be slightly superior to PD-L1 blockade based on objective response rates, while potentially being associated with a higher frequency of SAEs.

Although preclinical data strongly suggest that inhibiting PD-L1/PD-1 interactions might also be effective in haematological malignancies (see Chapter 1.3.2), few clinical trials using PD-L1/PD-1 antibodies as single agents have been conducted. To date, anti-PD-1 antibodies have been administered to patients with DLBCL after autologous haematopoietic stem-cell transplantation<sup>359</sup>, and to patients with relapsed FL in combination with rituximab<sup>360</sup>. These trials will be further discussed, with a focus on the effect of PD-1 blockade on immune effector cells, in Chapter 8.1.

compound	study design	no of pts	tumour types	remarks	key findings
<b>PD-L1 blockade</b>					
BMS-936559 <sup>361</sup>	Phase I	207	<ul style="list-style-type: none"> <li>• NSCLC</li> <li>• melanoma</li> <li>• colorectal cancer</li> <li>• RCC</li> <li>• ovarian cancer</li> <li>• pancreatic cancer</li> <li>• gastric cancer</li> <li>• breast cancer</li> </ul>	application until CR or confirmed disease progression	<ul style="list-style-type: none"> <li>• SAE grade 3/4 in 9% of pts</li> <li>• RR melanoma 9/52 pts</li> <li>• RR RCC 2/17 pts</li> <li>• RR NSCLC 5/49 pts</li> <li>• Response duration &gt;1 year in 8/16 pts with at least 1 year follow-up</li> </ul>

**Table 5: Summary of key findings of clinical trials using single agent PD-L1 blockade.** Abbreviations: pts – patients; NSCLC - non-small-cell lung cancer; RCC - renal cell cancer; CR – complete response; SAE – serious adverse events; RR – response rate.

compound	study design	no pts	tumour types	remarks	key findings
<b>PD-1 blockade</b>					
CT-011 (pidilizumab) <sup>362</sup>	Phase I dose escalation	17	<ul style="list-style-type: none"> <li>AML</li> <li>MDS</li> <li>NHL (incl. 3 CLL)</li> </ul>	first in-human study	<ul style="list-style-type: none"> <li>well tolerated (DLT not reached)</li> <li>stabilization of disease</li> <li>cumulative survival at 21 days 76% (95% CI 48-90)</li> <li>mean OS 25±27 weeks (range 1.7 to &gt;77)</li> <li>SD in ~1/3 of pts</li> <li>1 CR</li> </ul>
MDX-1106 (BMS-936558/ ONO-4538, nivolumu- mab) <sup>363</sup>	Phase I dose escalation	39	<ul style="list-style-type: none"> <li>metastatic melanoma</li> <li>colorectal cancer</li> <li>castrate-resistant prostate cancer</li> <li>NSCLC</li> <li>RCC</li> </ul>	in n=9 pts, tumour PD-L1 expression ~ likelihood of response to treatment	<ul style="list-style-type: none"> <li>well tolerated (1 SAE: inflammatory colitis)</li> <li>1 CR</li> <li>2 PR</li> <li>stabilisation of disease in 3 pts</li> </ul>
MDX-1106 (BMS-936558/ ONO-4538, nivolumu- mab) <sup>364</sup>	multiple dose trial	296	<ul style="list-style-type: none"> <li>advanced melanoma</li> <li>NSCLC</li> <li>castrate-resistant prostate cancer</li> <li>RCC</li> <li>colorectal cancer</li> </ul>	no objective response in pts with PD-L1 negative tumours (n=17), but 36% response in pts with PD-L1 positive tumours (n=25)	<ul style="list-style-type: none"> <li>SAE grade 3/4 (esp. pulmonary toxicity) in 14% of pts</li> <li>MTD not reached</li> <li>RR NSCLC 18%</li> <li>RR melanoma 28%</li> <li>RR RCC 27%</li> </ul>
MDX-1106 (BMS-936558/ ONO-4538, nivolumu- mab) <sup>365</sup>	update from <sup>364</sup>	107	<ul style="list-style-type: none"> <li>advanced melanoma</li> </ul>	OS outcomes in patients with melanoma	<ul style="list-style-type: none"> <li>median OS 16.8 months</li> <li>1-year OS 62%</li> <li>2-year OS 43%</li> <li>among pts with tumour regressions: median response duration 2 years</li> <li>71% maintained responses off-therapy for &gt;16 weeks (range 16 to &gt;56)</li> </ul>
MK-3475 (lambrolizu- mab) <sup>366</sup>	Phase I	135	<ul style="list-style-type: none"> <li>advanced malignant melanoma</li> </ul>	responses regardless of pretreatment with CTLA-4 antibody ipilimumab	<ul style="list-style-type: none"> <li>well tolerated</li> <li>objective clinical RR: 38% (95% CI 25-44)</li> <li>overall median PFS &gt;7 months</li> </ul>
MK-3475 (lambrolizu- mab, pembrolizu- mab) <sup>367</sup>	expansion cohort from <sup>366</sup>	173	<ul style="list-style-type: none"> <li>advanced melanoma with disease progression after ≥2 doses ipilimumab</li> </ul>	2 mg/kg (n=89) or 10 mg/kg (n=84)	<ul style="list-style-type: none"> <li>well tolerated at both doses</li> <li>overall RR 26% at both doses</li> </ul>

**Table 6: Summary of key findings of clinical trials using single agent PD-1 blockade.**

*Abbreviations:* DLT – dose limiting toxicity; CI - confidence interval; OS – overall survival; SD – stable disease; CR – complete response; pts – patients; PR – partial response; NSCLC - non-small-cell lung cancer; RCC - renal cell cancer; CR – complete response; SAE – serious adverse events; RR – response rate; MTD – maximum tolerated dose; PFS – progression-free survival.

## 1.5 Summary

CLL is incurable using currently available standard immunochemotherapy approaches, but several novel agents show activity even in high-risk CLL patients. However, CLL-associated immune dysfunction remains a very serious clinical problem. This is caused by a variety of humoral and cellular immune defects, the majority of which is responsible for providing a pro-tumour and immune-suppressive tumour microenvironment. As CLL is now understood as a disease that closely interacts with its microenvironment, targeting these interactions is a very attractive treatment approach. Novel target molecules in this context are immune checkpoints, which under physiological conditions regulate the activation of immune effector cells to maintain self-tolerance and prevent autoimmunity. PD-1 and its ligands PD-L1 and potentially PD-L2 constitute one of the most prominent immune checkpoint ligand/receptor axes mediating CLL-associated immune dysfunction. Establishing anti-tumour immune surveillance mechanisms via targeting of PD-L1/PD-1 is a novel and potentially powerful strategy to eliminate tumour cells, and in fact might be a route to achieving cures or at least long-term control of CLL.

## 2 Hypothesis and aims of the project

The central hypothesis of this thesis project is that specific T-cell defects result from the interaction of malignant CLL cells with the immune system, and that repairing the defects in T-cell function will be required to activate an effective T-cell mediated anti-tumour immune response. Using the TCL1 mouse model, the major aims are:

1. *To further characterize the nature of PD-L1/PD-1 mediated T-cell dysfunctions in the context of developing CLL and within different microenvironments*

Initial work on T-cell dysfunction in the TCL1 model has been conducted using TCL1 mice on the B6C3H-F1 genetic background. As this potentially prevents crosses with other transgenic mice, which will be an essential component of future work of the group, we have backcrossed TCL1 mice to a pure C57BL/6 genetic background, greatly increasing the value of this model for immunological studies. However, the effects of CLL on T cells in this new strain require thorough assessment to confirm that this model remains valid. My first aim is therefore to compare T-cell dynamics and dysfunctions of TCL1 mice on the B6C3H-F1 background to TCL1 mice on the backcrossed C57BL/6 background at different stages of CLL to validate both backgrounds for the investigation of T-cell dysfunctions and to characterize T-cell defects in the direct context of advancing CLL. Additional aims are the characterization of T-cell subsets in different CLL-affected compartments to assess the impact of the microenvironment, and to explore changes in effector T-cell function alongside developing CLL. Considering the growing body of evidence suggesting a central role of PD-L1 and PD-1 in mediating immune defects, this will include markers and patterns of exhaustion to further characterize PD-L1/PD-1 mediated T-cell impairment in CLL.

2. *To investigate the effect of in vivo immune modulation on CLL/T-cell interactions*

As outlined in Chapters 1.1.3 and 1.3.2, several novel treatments have been shown to produce anti-tumour immune responses in preclinical and early clinical studies. Among those, lenalidomide probably provides the best evidence in CLL patients of functional immune enhancement, introducing the distinct possibility of reactivating the immune system to eliminate tumour cells. Although not yet explored clinically in CLL, PD-L1/PD-1 blockade also holds the promise of restoring anti-tumour immunity. Despite the differences in these two strategies, immune modulation may in fact constitute the only safe route to long-term disease control or cure. Thus, investigating the *in vivo* potential of lenalidomide and PD-L1/PD-1 blockade using the TCL1 mouse model validated in Aim 1, and conducting detailed studies of their impact on effector T-cell responses, will be the second aim of this PhD project.

### 3 Materials and Methods

#### 3.1 Mice and animal procedures

##### 3.1.1 Ethical considerations relating to animal work

To ensure the most ethical use of animals, to safeguard animal welfare, and to improve scientific quality, *in vivo* research is guided by the principle of the “Three Rs” (3Rs) – *replacement, reduction and refinement*<sup>368</sup>. *Replacement* refers to the preferred use of non-animal over animal methods whenever this is equivalent in achieving selected scientific aims. *Reduction* refers to the reduction of numbers of animals used in scientific experiments while producing statistically valid results to answer a scientific question. *Refinement* refers to all methods that alleviate or minimize animal pain, suffering and distress, and ensure animal welfare during experimental procedures. In EU countries and the US, these principles are now officially embraced in legislations and guidelines governing animal use<sup>369, 370</sup>.

The research conducted in this project was also guided by the principles of the 3Rs. First, the lack of suitable CLL cell lines or *in vitro* model systems that mimic the complex dimensions of the natural CLL microenvironment justifies the use of an animal model to investigate the role of host immunity in the context of long-term cancer development (*replacement*). The number of animals was reduced by limiting experiments and procedures to interventions and repair strategies that have been demonstrated to be effective *ex vivo*. In addition, rigorous statistical calculations were performed for each experiment to determine the numbers of mice needed to obtain at least 80% power to detect significant changes in a Fisher exact test performed at the one-sided 0.05 significance level (*reduction*). The lymphocytosis, hepatosplenomegaly and lymphadenopathy associated with CLL development in mice are, just as in the majority of patients, generally painless. Adverse signs, which might present as impeded movement or dyspnoea, are generally rare. The interventions tested in this project were based on substances and application routes that are generally well-tolerated or cause only minimal and transient discomfort. In addition, mice were inspected daily and underwent regular physical examinations and monitoring of disease status or impaired health (e.g. piloerection, sunken eyes, hunched posture, inactivity, reduced grip strength, weight loss). The combination of these follow-up procedures with the rigorous definition of disease endpoints minimised the probability of suffering from the disease or an intervention (*refinement*).

### 3.1.2 Breeding and standard maintenance of mice

All animal work was carried out under Project Licence PPL 70/7531, in accordance to the Animals (Scientific Procedures) Act 1986. This licence was renewed in November 2012 and amended in August 2013 to include treatment with additional novel substances that had demonstrated great efficacy in early clinical trials. Four TCL1 breeding pairs on the B6C3H-F1 (abbreviated to C3H hereafter) and the backcrossed C57BL/6 (hereafter abbreviated to B6) background were provided by Dr. Carlo Croce, The Ohio State University, Columbus Ohio, who is one of our main collaborators within the CLL Research Consortium (CRC). Wild-type (WT) mice for breeding and experimental procedures were purchased from Charles River laboratories, UK, Harlan laboratories, UK, and Cancer Research UK laboratories. Mice were kept in suitable barrier systems in the Biological Services Unit (BSU) at Charterhouse Square, and all regulated *in vivo* procedures were carried out under sterile conditions in designated procedure rooms in the BSU.

The colony was maintained and extended by breeding TCL1 transgenic males with a harem of WT syngeneic females. Breeders were paired at the age of 6 to 8 weeks and kept for a maximum of 10 months or until no new litters were produced for more than 2 months. Litters were weaned at 3 to 4 weeks of age, ear-marked and genotyped and kept with a maximum of 5 littermates.

Animals were observed daily for general signs of ill health, such as hunched posture, ruffled fur, separation from littermates, inactivity or weight loss. Disease status was monitored by physical examination of spleens and lymph nodes, and by haematology testing using blood smears and if necessary immunophenotyping. Mice were euthanized when they showed signs of ill health, or fulfilled one of the following criteria: white blood cell (WBC) count in blood smear >100 WBC/high power field (hpf, 40x objective), >90% of lymphocytes CD19+CD5+ CLL cells and/or spleen size >3cm in diameter compressing other organs. Endpoint definitions for experimental animals were in part adapted to the specific research question and are described in the respective materials and methods sections. Animals were euthanized using cardiac puncture under terminal anaesthesia and/or cervical dislocation.

### 3.1.3 Haematology testing

The standard method of haematology testing was by blood smears, which routinely began at the age of 6 months in transgenic mice. Experimental animals, for which larger blood volumes were required, were subjected to repeated tail bleeding. For flow cytometry-based analyses, blood was stained in a total volume of 100µl FACS buffer [PBS with 2% fetal calf serum (FCS)] with fluorochrome-labelled antibodies at a ratio of 1:100. Specific antibodies, clones and suppliers are listed in the respective chapters. Erythrocytes were then lysed in 5ml 1X ammonium-chloride-based RBC lysis buffer (NH<sub>4</sub>CL 8.3g/l, KHCO<sub>3</sub> 1g/l, EDTA 0.037g/l). After 10 minutes incubation, 2x volume PBS was added, cells were centrifuged at 300 x g for 10 minutes at 4°C and resuspended in 350µl FACS buffer. 300µl was transferred to polypropylene flow-cytometry tubes. Cells were then recorded at a LSRII Fortessa cytometer (BD Biosciences, UK) and analysed using FlowJo and FACS Diva Software. Where appropriate, the remaining 50µl of cell suspension were analysed at a ViCell counter (Beckman-Coulter, UK) in a 1:10 dilution to obtain an automated estimate of total WBC count.

### 3.1.4 Processing of mouse organs into single cell suspension

Organectomy was performed under sterile conditions in the BSU immediately after the death of the animal by cervical dislocation and/or exsanguination. Lymphoid organs were kept in ice-cold PBS with 20% FCS and bones in ice-cold RPMI 160 medium supplemented with 10% FCS and 1% Penicillin/Streptomycin, and processed quickly under a class II biosafety cabinet. Spleen single cell suspensions were prepared using an automated tissue dissociator (Miltenyi, UK) following the manufacturer's recommendations for mouse spleen without enzymatic treatment. Lymph nodes were dissociated by mashing through a 70µm strainer (Fisher Scientific, UK) with the rubber plunger of a 1ml tuberculin syringe (BD, UK). Bones were crushed with a sterile mortar and pestle, of flushed with ice-cold FACS buffer. Erythrocytes were lysed using an ammonium-chloride-based RBC lysis buffer (NH<sub>4</sub>CL 8.3g/l, KHCO<sub>3</sub> 1g/l, EDTA 0.037g/l), and the reaction was stopped using 1.5-2x volume PBS. All centrifugation steps for mouse organs were performed at 300 x g for 10 minutes at 4°C. Cells were then either frozen at a maximum density of 200x10<sup>6</sup>cells/ml in FCS/10% DMSO (Fisher Scientific, UK) and kept in liquid nitrogen for long-term storage without any further manipulation before the freezing process, or used directly in experiments and downstream applications.

### 3.1.5 Adoptive transfer of syngeneic mouse cells

Based on available data in the literature<sup>214-216, 220</sup> and previous experiences of the group, we adoptively transferred  $4 \times 10^7$  previously frozen syngeneic mouse CLL cells from spleen by tail vein injection following standard protocols for mice<sup>371</sup>. Before the adoptive transfer, the percentage of CD19+CD5+ CLL cells of viable lymphocytes (CLL content) in donor cells was assessed by flow-cytometry. Control mice received an equal concentration of healthy mouse B cells from pooled WT donors by tail vein injection. Maximum volumes for all i.v. injections were 5ml/kg. Recipient mice were between 3 and 5 months of age, and both WT and TCL1 transgenic recipients were used. After adoptive transfer, mice were closely monitored, and haematology testing using blood smears and flow cytometry was conducted in regular intervals. Mice were euthanized when they showed signs of ill health, or fulfilled one of the following criteria: WBC count in blood smear  $>100$  WBC/hpf (40x objective),  $>90\%$  of lymphocytes CD19+CD5+ cells and/ or spleen size  $>3$ cm in diameter compressing other organs. Endpoint definitions for experimental animals were partly adapted to specific research questions and are described in the respective materials and methods sections. Animals were euthanized using cardiac puncture under terminal anaesthesia and/or cervical dislocation.

### 3.1.6 Application of experimental substances

Experimental substances tested for their potential to prevent or reverse T-cell defects were applied by i.p. injection or by oral gavage. Doses, application routes and treatment schedules were selected based on available data in the literature, or followed advice of our CRC collaborators who have conducted toxicity studies in WT and TCL1 mice. Maximum volumes for all i.p. injections were 10ml/kg, and 20ml/kg for oral administration. Drugs were dissolved in sterile PBS, and a single stock was prepared under sterile conditions at the beginning of the experiment and used to treat all animals within one experiment. When indicated, the stability of the drug was confirmed by mass spectrometry. Control mice received equal concentrations or amounts of drug vehicle or isotype antibodies, and were kept under identical conditions. During treatment, mice were monitored daily and sacrificed at predefined endpoints.

### 3.2 Cell thawing procedures

Cells were re-derived from cryopreservation by thawing them in a water bath set to 37°C. Before opening the vials under a class II biosafety cabinet, they were disinfected with 70% IMS (Fisher Scientific, UK). Cells were carefully added into 10ml pre-warmed RPMI 1640 medium supplemented with 10% FCS, 1% Penicillin/Streptomycin (both from Sigma, UK), and 50µM β-mercaptoethanol (Gibco, UK). Cells were centrifuged at 300 x g for 10 minutes at room temperature and resuspended at a volume adequate for the size of the cell pellet. Automated cell counting was performed on a Vi-cell XR haemocytometer (Beckman Coulter) at a 1:10 dilution.

### 3.3 Cell separation procedures

#### 3.3.1 Positive selection of CLL and B cells

Positive selection of murine CLL and B cells from spleen was performed using magnetic activated cell sorting (MACS®, Miltenyi Biotec, UK). Spleens were processed into single cell suspension or re-derived from cryopreservation. After cell counting, cells were centrifuged at 300 x g for 10 minutes at 4°C, and the supernatant was aspirated completely. Cells were resuspended in 90µl ice-cold MACS buffer (PBS, pH 7.2, 0.5% bovine serum albumin, 2mM EDTA) per 10<sup>7</sup> total cells, and 10µl of murine CD19 conjugated MicroBeads per 10<sup>7</sup> total cells were added. The cell suspension was mixed and incubated for 15 minutes at 4°C, with repeated gentle shaking every 2 to 3 minutes. Cells were then washed by adding 2ml MACS buffer, centrifuged as above, and resuspended in MACS buffer at a concentration of up to 10<sup>8</sup> cells in 500µl. MACS LS columns with a maximum capacity of 2x10<sup>9</sup> total cells were placed in a QuadroMACS magnet (both from Miltenyi) and rinsed with 3ml MACS buffer. The CD19 labelled cell suspension was applied to the column and washed through with 3 x 3ml MACS buffer. The effluent representing the unlabelled cell fraction was collected in a 15ml Falcon tube and prepared for negative isolation or cell sorting as described below. To obtain the CD19 labelled cell fraction, LS columns were removed from the magnetic field and flushed through with 5ml MACS buffer and a provided plunger. Eluted cells were collected in a separate 15ml Falcon tube, and cells in both the positive and negative fraction were counted. During the whole isolation protocol, cells, buffers and reagents were kept on ice to prevent capping of antibodies on the cell surface and non-specific cell labelling.

### 3.3.2 Negative selection of T cells

Negative selection was also performed following protocol developed by Miltenyi Biotec. After purification of CLL and B cells as described above, unlabelled cells in the negative fraction were counted, centrifuged at 300 x g for 10 minutes at 4°C, and the supernatant was aspirated completely. Cells were resuspended in 40µl MACS buffer per 10<sup>7</sup> total cells, and 10µl of biotin antibody cocktail from the murine pan T-cell isolation kit II (Miltenyi, UK) per 10<sup>7</sup> total cells was added. The cell suspension was mixed and incubated for 15 minutes at 4°C, with repeated gentle shaking every 2 to 3 minutes. Subsequently 30µl buffer and 20µl anti-biotin microbeads per 10<sup>7</sup> total cells were added. The cell suspension was mixed and incubated for an additional 20 minutes at 4°C with repeated gentle shaking every 2 to 3 minutes. Cells were then washed by adding 2ml MACS buffer and resuspended at a concentration of up to 1 x 10<sup>8</sup> cells in 500µl buffer after centrifugation. MACS LS columns were placed in a QuadroMACS magnet and rinsed with 3ml MACS buffer. The labelled cell suspension was applied to the column and washed through with 3 x 3ml MACS buffer. The effluent representing the unlabelled T-cell fraction was collected in a 15ml Falcon tube, counted, and prepared for immune synapse assays or CFSE labelling. During the whole isolation protocol, cells, buffers and reagents were kept on ice to prevent capping of antibodies on the cell surface and non-specific cell labelling.

## 3.4 Flow cytometry

### 3.4.1 Surface staining

Staining procedures using single-cell suspensions were generally performed at 2 to 8°C to avoid antibody capping and internalisation. Surface molecules requiring different staining conditions or methods for experiments combining surface staining with intracellular/intranuclear staining are described in the specific methods and materials sections of the respective chapters. After cell counting, cells were transferred to 5ml polystyrene round-bottom tubes (BD, UK) or round-bottom 96-well plates (VWR, UK), washed with PBS/2% FCS, centrifuged at 300 x g for 10 minutes at 4°C and resuspended in 100µl PBS/2% FCS. Antibodies were generally used at a 1:100 dilution and prepared as a master mix to ensure consistency of staining. Cells were incubated for 30 minutes at 4°C in the dark, washed with PBS/2% FCS, centrifuged at 300 x g for 10 minutes at 4°C and resuspended in 200-300µl PBS/2% FCS containing 250ng/ml 4'6-diamidino-2-phenylindole (DAPI) to allow live/dead discrimination of cells. As the integrity of cell membranes is lost during cell death, DAPI enters the nucleus and binds

A-T rich regions of DNA, therefore labelling dead cells as DAPI-positive. All samples were kept on ice and in the dark until flow cytometry was performed.

### **3.4.2 Intracytoplasmic and intranuclear staining**

In experiments using intracytoplasmic and intranuclear staining, fixable viability dyes instead of DAPI were used for live/dead discrimination, as the preparation of cells requires the permeabilisation of the cell membrane. Intracellular and intranuclear staining were performed in both 5ml polystyrene round-bottom tubes (BD, UK) and round-bottom 96-well plates (VWR, UK). After cell stimulation or short-time cell culture, cells were washed twice with 200µl (for 96 well plates) or 2ml (for 5ml tubes) azide-free and serum/protein-free PBS. Fixable Viability Dye 505 or 450 (eBioscience, UK) was prepared as a working stock solution in azide- and serum/protein-free PBS at a concentration of 1µl/ml. Cells were resuspended in 100µl or 1ml PBS/fixable viability dye stock solution, and the antibody cocktail for surface staining was added. Cells were then mixed well, incubated for 30 minutes at 4°C in the dark, and washed twice with 100µl or 1ml PBS/2%FCS. To prepare intracytoplasmic staining, cells were resuspended in 200µl or 2ml 1X fixation buffer (eBioscience, UK) and incubated in the dark at room temperature for 30 minutes. To prepare intranuclear staining, cells were resuspended in 200µl or 2ml Foxp3 fixation/permeabilisation working solution, which was prepared by diluting Foxp3 fixation/permeabilisation concentrate (1 part) with Foxp3 fixation/permeabilisation diluent (3 parts, eBioscience, UK), and incubated in the dark at room temperature for 30 minutes. To cells kept in 5ml tubes, 2ml of 1X permeabilisation buffer (eBioscience), which was prepared by diluting the 10X concentrate with distilled water prior to use, was added directly before centrifugation. Cells kept in 96 well plates were centrifuged first, and then resuspended in 200µl of 1X permeabilisation buffer. All cells were centrifuged again, and the washing step with 200µl or 2ml 1X permeabilisation buffer was repeated. After centrifugation, cells were resuspended in 100µl 1X permeabilisation buffer for intracytoplasmic staining. Antibodies for intracellular cytokines were added as a cocktail at a 1:100 dilution, and cells were incubated for 1h at 4°C in the dark. Cells were washed with 100µl or 1ml 1X permeabilisation buffer, centrifuged, and resuspended in 200-300µl PBS for analysis.

### 3.4.3 Absolute numbers

Absolute numbers of cell populations were enumerated using CountBright™ absolute counting beads (Molecular Probes, UK), which are a calibrated suspension of fluorescent microspheres at a known concentration. A specific volume of the microsphere suspension is added to a specific volume of sample, so that the ratio of sample volume to microsphere volume is known. The volume of sample analysed can then be calculated from the number of microsphere events, and can be used with cell events to determine cell concentrations of population of interest.

To enumerate absolute numbers in blood, the volume of sample available was recorded, and surface staining was performed in a total volume of 100µl FACS buffer. Cells were stained and red blood cells lysed as described in Chapters 3.1.3 and 3.4.1. To enumerate absolute numbers in bones and lymph nodes, organs were processed into single cell suspension in a standardized fashion (see Chapter 3.1.4) and resuspended consistently at a volume of 2ml (for bones) and 200µl (for lymph nodes), of which 100µl each were used for surface staining as described in Chapter 3.4.1. To enumerate absolute numbers in spleen, organs were processed into single cell suspension as described in Chapter 3.1.4, and the total number of cells were counted on a ViCell haemocytometer (Beckman-Coulter, UK). Throughout experiments, a consistent number of cells were used for surface staining as described in Chapter 3.4.1. Specific antibodies, clones and suppliers are listed in the respective chapters.

Counting beads were allowed to adjust to room temperature, gently vortexed for 30 seconds, and 50µl were immediately added to stained and washed cells resuspended at 300µl FACS buffer/DAPI. The sample was then acquired on the flow cytometer, and beads were visualized on a plot depicting side scatter on a log scale *versus* R670/14 on a linear scale. Gating was then performed as necessary for individual experiments. Cell concentrations were calculated by applying the following formula: (number of cell events in population of interest/ number of bead events)\*(assigned bead count of the lot (beads/50µl)/volume of sample (µl)). For blood, this was normalized for the total volume used for staining, and reported as absolute number of population of interest per µl of blood. For lymph nodes and bone marrow, absolute numbers were reported per µl of cell suspension. For spleen, numbers were normalized for spleen weight. As an alternative method without counting beads, percentages of populations were multiplied by the total number of cells per spleen, which yielded very similar results to counting beads and has been reported as the method of choice by other groups<sup>195</sup>.

### 3.4.4 Flow cytometry based functional T-cell assays

#### 3.4.4.1 Cell stimulation for functional assays

All functional assays were performed on fresh cells. For proliferation assays, cells were stimulated with Dynabeads® Mouse T-Activator CD3/CD28 beads (Gibco, UK). Dynabeads (25µl per  $10^6$  T cells) were first washed with full medium (RPMI 1640 with 10% FCS, 1% Penicillin/Streptomycin, and 50µM β-mercaptoethanol), recovered by magnet, and resuspended at the original volume in full medium. T cells were resuspended in full medium at a concentration of  $1 \times 10^6$ /ml, and 200µl aliquots were added to 96 well round-bottom plates. Washed Dynabeads were added at a 1:1 beads:cell ratio, and cells were cultured for 72 hours at 37°C and 5% CO<sub>2</sub>. Beads were removed prior to staining by placing the tube on a magnet and transferring cells to a fresh tube. As controls, unstimulated cells cultured under the same conditions were used. For intracellular staining and the CD107a degranulation assay, cells were stimulated with 500X cell stimulation cocktail containing 40.5µM PMA (Phorbol 12-Myristate 13-Acetate) and 670µM ionomycin (eBioscience, UK) at a 1:500 dilution for 6 hours at 37°C/5%CO<sub>2</sub>. For the last 5 hours of culture, 500X protein transport inhibitor cocktail containing brefeldin A (5.3mM) and monensin (1mM), (eBioscience, UK) was added at a 1:500 dilution. Unstimulated cells and unstimulated cells cultured in the presence of brefeldin/monensin for the last 5 hours were included as controls.

#### 3.4.4.2 Proliferation assays

##### 3.4.4.2.1 CFSE labelling of lymphocyte for *in vitro* proliferation assay

For selected experiments, T cells were labelled with carboxyfluorescein diacetate succinimidyl ester (CFSE) to assess *ex vivo* proliferation upon stimulation with CD3/CD28 following a staining protocol modified for mouse lymphocytes<sup>372</sup>. Up to  $5 \times 10^7$  purified T cells were resuspended in 1ml pre-warmed PBS/5% FCS and transferred to a fresh 15ml Falcon tube wrapped in aluminium foil. The tube was then inverted almost horizontally, 110µl of PBS was pipetted to a non-wetted portion of plastic at the inside top of the tube, and 1.1µl of 5mM CFSE stock (Molecular Probes, UK) was diluted into the drop of PBS to give a final concentration of 5µM in the cell suspension. After capping the tube, it was immediately inverted quickly several times and vortexed at low speed for 20 seconds. Cells were incubated at room temperature in the dark for exactly 5 minutes, and washed three times with 10ml pre-warmed PBS/5% FCS. Unlabelled cells were included as controls.

#### 3.4.4.2.2 Intranuclear ki67

Intranuclear ki67 was assessed to measure T-cell proliferation *ex vivo* in selected experiments. Ki67 is present during all active phases of the cell cycle (*i.e.* G1, S, G2 and M), but is absent from resting cells in G0 phase<sup>373</sup>. It can therefore be used to determine the growth fraction of a given population of cells. Fresh cells were cultured for six hours *ex vivo* alongside cells intended for intracellular cytokine assays, but in the absence of any stimulating agents. Cells were processed and prepared for intranuclear staining as described above.

#### 3.4.4.2.3 EdU incorporation

*In vivo* proliferation was assessed by EdU (5-ethynyl-2'-deoxyuridine) incorporation. This is considered one of the most accurate methods to track DNA synthesis, and provides a good alternative to radioactive nucleoside based assays using <sup>3</sup>H-thymidine<sup>374</sup>. Similar to BrdU (bromo-deoxyuridine), EdU is a nucleoside analogue which is incorporated into DNA during active DNA synthesis. EdU detection is based on a "click" reaction, a copper catalysed, covalent, highly specific and stable reaction between an azide and an alkyne<sup>375, 376</sup>; the alkyne is found in the ethynyl moiety of EdU, while the azide is coupled to a fluorescent dye which can be detected by flow cytometry. The EdU assay can be multiplexed with additional antibodies against surface and intracellular markers, and is considered to be gentler than BrdU assays as it does not require the denaturation of DNA. Mice were injected i.p. with 100µg/g body weight EdU (Life Technologies, UK) 20 hours before they were sacrificed. EdU powder was dissolved in sterile PBS to a concentration of 1mg/100µl and kept at -20°C. Spleen cells ( $2 \times 10^6$ ) in a single cell suspension were fixed in 4% paraformaldehyde (PFA) for 15 minutes, washed once with PBS/1% bovine serum albumin (BSA) and permeabilised in PBS/0.1% Triton X-100 (Sigma, UK) for 30 minutes. After washing, cells were resuspended in 100µl Click-iT reaction cocktail containing 8.75µl 10X Click-iT cell reaction buffer, 2µl CuSO<sub>4</sub>, 0.5µl fluorescent dye Alexa488 azide, 1µl 10X reaction buffer additive and 87.75µl H<sub>2</sub>O per reaction and incubated at room temperature in the dark for 30 minutes (all components from LifeTechnologies, UK). Control cells were incubated with the same cocktail without Alexa488 dye. Cells were then washed, and surface stained with for 20 minutes at room temperature, washed again and resuspended in 300µl FACS buffer.

#### **3.4.4.3 CD107a degranulation assay**

Cell-mediated cytotoxicity was measured by flow-cytometry-based assays assessing effector cell degranulation as a non-radioactive alternative to chromium-release assays<sup>377</sup>. CD107a (LAMP-1) is a component of the lipid bilayer surrounding cytotoxic granules such as Granzyme B and perforin in T cells. Upon cell stimulation, granules are transported towards the immune synapse, their membrane fuses with the cell membrane, and the content of the granules is released into the synapse. As a consequence of the fusion of lysosomal and cellular membranes during the degranulation, CD107a is transiently expressed on the cell surface and can be detected with fluorescently labelled antibodies<sup>378</sup>. In our experiments, 5µg/ml CD107a antibody was added per well, and cells were stimulated as described above. Controls included wells with CD107a and protein transport inhibitor cocktail, but no cell stimulation cocktail.

#### **3.4.5 Flow Sorting**

Flow sorting was performed on a BD Aria II to isolate T-cell populations of interest. Frozen samples were debulked of CLL by magnetic separation and surface stained for flow cytometry as described above. Specific sorting strategies, gating and purities of sorted populations are described in specific methods and materials sections.

#### **3.4.6 Controls**

Unstained controls subjected to the same procedures as described above were included in all experiments to set photomultiplier tube (PMT) voltages on the flow cytometer. Isotype controls were used for surface staining experiments where a significant population of target antigen negative cells was not expected. For intracytoplasmic staining, stimulated and unstimulated cells prepared in the same way as described above but omitting the intracytoplasmic staining step, and unstimulated cells prepared as described above and stained with intracytoplasmic antibodies, were used. For intranuclear staining, unstimulated cells prepared in the same way as described above, but without the intranuclear staining step, were used. Each experiment included multiple internal controls such as healthy samples without aberrant expression of markers and Fluorescence-Minus-One (FMO) controls.

Compensation controls usually consisted of anti-rat immunoglobulin compensation beads (CompBeads; BD, UK). Compensation beads were prepared by adding one drop of negative control beads and anti-rat compensation beads to 80µl PBS/2% FCS in a 5ml polystyrene round-bottom tube for each fluorochrome represented in a panel. 1µl Igk rat anti-mouse fluorochrome-conjugated antibody was added to each tube, and incubated at 4°C for 30 minutes in the dark. The beads were then washed with 2ml PBS/2% FCS and resuspended in 300µl PBS for analysis. However, beads could not be used for fluorescently labelled markers with a hamster isotype and for DAPI. For these, single-stained cells were used.

### 3.4.7 Data acquisition and analysis

Data was acquired on a LSR Fortessa II (BD, UK) equipped with a four-laser optical system, integrated fluidics and the software package BD FACSDiva™. The red laser emits at 640nm wavelength, yellow/green at 561nm, blue at 488nm, and violet at 405nm. Beam shaping lenses and pinholes focus the combined laser light as a single beam into a cuvette, and emitted light is delivered through fibre optics to detector arrays arranged to maximise the signal detection using reflecting mirrors. Bandpass filters (for red lasers 670±14nm, 730±45nm, 780±60nm, for yellow/green 585±15nm, 675±20nm and 780±60nm, for blue 695±40nm and for violet 525±50nm and 450±50nm) and PMTs improve spectral resolution, and are calibrated on a weekly basis using the FACS Comp software and Calibrite Beads (BD, UK) by a specialized technician.

PMT voltages were adjusted for each experiment to ensure maximum signal:noise ratio and minimal spectral overlap in competing PMT detectors. Apart from the wavelength-specific, bandpass-filtered fluorescence intensity arising from each fluorochrome as detected at the PMTs, data on light forward scatter (representing particle size) and side scatter (representing internal complexity of the particle) were collected. PMT voltages required for the amplification of signal from specific fluorescently-labelled antigens were determined in optimization experiments. To preserve experimental samples, compensation beads coated with antibody recognizing the appropriate isotype for each fluorochrome represented in a specific panel in combination with uncoated beads as the internal negative control were used. Compensation plots were produced using FACSDiva software which plotted the appropriate output channel on the x axis, against all other output channels under investigation in turn on the y axis. Compensation was adjusted until the 'positive' stained beads aligned horizontally with the 'negative'

stained beads by eye, and confirmed by calculating their Median Fluorescence Intensity (MFI). The compensation matrix was then applied to all samples and to cytometer setting.

After compensation, cells were gated on the basis of DAPI/fixable viability dye and side scatter (SSC) to exclude dead cells from the analysis. A second gate was applied to viable (*i.e.* DAPI negative) cells, and cells were plotted as SSC-area (SSC-A) and SSC-width (SSC-W) to identify single cells. A third gate showing forward scatter (FSC) and side scatter (SSC) characteristics was then applied to viable single cells to exclude debris from the analysis. Lymphocytes/mononuclear cells (MNC) were identified based on specific FSC/SSC characteristics. Specific cell populations were evaluated based on whether they were expressing or not expressing a target antigen (*i.e.* positive or negative for a marker), expressed as a percentage of a defined parent population, or whether there were degrees to which they expressed an antigen, measured by MFI. However, MFI bears a non-linear relationship to the actual number of molecules expressed on each cell. Stopping gates and number of recorded events used in individual experiments are described in specific methods. Recorded data was exported as .FCS files, and analysed with FlowJo (Tree Star Inc.) software.

### **3.5 Immune synapse formation assay**

#### **3.5.1 Cell conjugation assays**

Up to  $1.5 \times 10^6$  T cells were resuspended in 1ml full medium in 1.5ml Eppendorf tubes and rested in the incubator. Up to  $1.5 \times 10^6$  healthy B or CLL cells were transferred into 1.5ml Eppendorf tubes, washed twice in serum-free medium and resuspended in 500 $\mu$ l serum-free medium. A working stock of serum-free medium containing 2 $\mu$ g/ml 7-amino-4-chloromethylcoumarin (CMAC) CellTracker Blue (LifeTechnologies, UK) was prepared and 500 $\mu$ l were added to the resuspended cells for a final CMAC concentration of 1 $\mu$ g/ml. Cells were incubated for 30 minutes at 37°C, centrifuged at 4000rpm for 1 minute at room temperature in a table-top centrifuge, and resuspended in 1ml full medium containing 2 $\mu$ g/ml of staphylococcal superantigen cocktail (Sigma, UK). After a further 30 minutes incubation at 37°C, both B and T cells were centrifuged and the supernatant was aspirated completely. T cells were then resuspended in 150 $\mu$ l full medium, and transferred into the tube containing the activated B cells in a 1:1 ratio. After centrifugation at 1500rpm for 5 minutes, which allowed a cell pellet to form, resultant B cell/T cell conjugates were incubated at 37°C for 20 minutes, gently

resuspended in 150µl full medium, and transferred onto a Poly-L-lysine coated glass (Fisher Scientific, UK) slides using a 3-well cell concentrator and a cytofuge (Statspin).

### **3.5.2 Staining for confocal microscopy**

While still in the cytofuge, cells transferred to slides were fixed in 150µl 3% methanol-free formaldehyde in PBS (TAAB Laboratories Equipment Ltd., UK) for 15 minutes. After 3 washing steps (150µl PBS each), cells were permeabilised in 150µl 0.3% Triton X-100 (Sigma, UK) in PBS for 5 minutes. After 3 more PBS washing steps, cells were blocked 10 minutes with 0.1% BSA/PBS, again washed 3 times, and stained with rhodamine phalloidin in a goat serum buffer (Invitrogen, UK) 20 minutes at 4°C in the dark. After 3 final washing steps, the cytofuge unit was disassembled. Coverslips were mounted and slides kept at 4°C in the dark until analysis.

### **3.5.3 Confocal microscopy and image analysis**

Confocal images were captured with a Zeiss 510 confocal laser-scanning microscope using a 63x/1.40 oil objective and LSM Version 3.2 SP2 imaging software (Zeiss, UK). A minimum of 10 images were acquired per condition. Images were exported as LSM files and analysed using AxioVision Version 4.8 image analysis software (Zeiss). The AxioVision outline tool was used to draw around each synapse between T cells and B cells, and all available interactions were scored in each condition. The synapse area was reported as the area of T-cell F-actin immune synapses (µm<sup>2</sup>) value, and exported into Prism Version 5 software (GraphPad) for statistical analysis.

### 3.6 Statistical considerations

Data sets were subjected to normality testing using the Shapiro-Wilk normality test. Where all data sets could be accurately modelled by a Gaussian distribution an unpaired t test was used for analysis of differences between groups; where this was not the case the 2-sided Mann Whitney *U* test was used. For survival curves, shown by Kaplan-Meier plot, a log-rank (Mantel-Cox) test was performed and differences were expressed as Hazard Ratio with 95% confidence interval. Statistical dependence between two nonparametric variables was assessed by Spearman's rank correlation coefficient modeling. *P* values of less than .05 were considered statistically significant. Analyses were conducted using Prism Version 5 software (GraphPad). *P* values were visualized with the help of heatmap summaries in selected experiments, with blue colour indicating relative expansion and red colour indicating relative loss of cell subsets. Shades of blue and red were applied to express differences in significance (*i.e.*  $p < .05$ ,  $p < .001$ ,  $p < .0001$ ). Values are reported as median and interquartile range, unless indicated otherwise.

In treatment studies, mouse sample size calculations were based on the required number of mice per group needed to detect a 1.25 standard deviation difference in means of PD-1 expression on CD8<sup>+</sup> T cells between mice without and with intervention (as expected from previous *in vivo* and *in vitro* experiments) in one-sided testing at a significance level  $\alpha = 0.05$  with at least 80% power.

## **4 Breeding and maintenance of TCL1 mice and induction of disease by adoptive transfer**

### **4.1 Specific introduction**

The TCL1 model is a well-established murine model of CLL which closely mirrors the biology and therapeutic responses of aggressive human CLL<sup>212</sup> (see Chapter 1.2.1). In general, mice become fully leukaemic after about 12 to 16 months, which makes the TCL1 model very time-consuming and cost-intensive. Therefore, it is crucial to implement optimized and reproducible standard procedures and protocols for genotyping and follow-up of mice in order to avoid ageing false-positive transgenic animals or to prematurely sacrifice transgenic mice in which the disease has not yet fully developed. We were the first group to demonstrate that this murine CLL is readily transplantable to healthy syngeneic mice by adoptive transfer (hereafter abbreviated to AT) of spleen cells from leukaemic donor mice. This finding has since been confirmed by others<sup>214-216, 220</sup>, and AT is now widely considered to be a reproducible strategy to study the pathomechanistic role of specific molecular targets as well as the efficacy and mechanism of action of novel therapies. However, considerable variability exists in the timing, dose, and application route of donor cells, which hampers the reproducibility of preclinical studies between experiments and different laboratories. It is also unclear whether donor cells should originate from individual mice or whether a pool of cells from several donors should be used. In addition, the biological course of disease after AT in the absence of treatment has not been well characterized. Relevant to this thesis, the generation and validation of standardized conditions for AT is particularly important to be able to rigorously investigate complex disease-related immune and microenvironmental interactions and how these are affected by novel therapeutic approaches.

### **4.2 Goals and objectives**

My first goal for this part of my work was therefore to establish a TCL1 mouse colony in our centre from the breeding pairs we had received as a generous gift from our CRC collaborators. This included setting up protocols and procedures for breeding, genotyping and follow-up of transgenic mice. My second goal was to optimize the conditions for our *in vivo* preclinical studies by validating the AT model and by improving the transplantation conditions and the consistency of disease engraftment and development.

### 4.3 Specific methods

#### 4.3.1 Genotyping

Material for genomic PCR was obtained from ear punches. DNA was extracted using alcohol precipitation after digestion at 55°C overnight with buffer consisting of 50mM TRIS pH 8.0 (Sigma, UK), 25mM EDTA pH 8.0 (Sigma, UK), 100mM NaCl (Fisher Scientific, UK), 1% SDS (Sigma, UK), and Proteinase K 20mg/ml (Roche Diagnostics, UK). DNA content was determined using a NanoDrop™ spectrophotometer (Thermo Scientific, UK). TCL1 primer sequences are: (TCL1 Forward) 5'-GCCGAGTGCCCGACACTC-3'; (TCL1 Reverse) 5'-CATCTGGCAGCAGCTCGA-3'. The expected amplification product is 350 base pairs (bp). PCR products were confirmed by bidirectional sequencing using an ABI 3100 Genetic Analyser (Applied Biosystems, UK). Results were compared to the corresponding sequences for human *TCL1* [accession number TCL1A: NM\_001098725, TCL1B: NM\_004918.3; National Center for Biotechnology Information (NCBI) GenBank database]. The endogenous mouse globin gene was used as an internal positive control. Mouse betaglobin (MBG) primer sequences are: (MBG Forward) 5'-CCAATCTGCTCACACAGGATAGAGAGGGCAGG-3' and (MBG Reverse) 5'-CCTTGAGGCTGTCCAAGTGATTCAGGCCATCG-3'. The expected amplification product is 494 bp. All primers were purchased from Sigma UK. A negative no-template control (NTC) containing master mix and primers but no DNA was used for each primer pair. PCR conditions for TCL1 are activation at 95°C (5 min), then denaturation at 95°C (30 sec), annealing at 58°C (30 sec) and extension at 72°C (30 sec) for 35 cycles, and final extension at 72°C (5 min). PCR conditions for MBG are the same except for an annealing temperature of 70°C. ReddyMix Master Mix (Thermo Scientific, UK) was used for all PCR reactions at a total volume of 10µl. PCR products, controls and a 100bp DNA ladder (Life Technologies, UK) were separated on a 2% agarose gel containing 20µl GelRed nucleic acid gel stain (VWR, UK), and visualized in a Transilluminator.

#### 4.3.2 Follow-up by haematology testing

Mice were pre-warmed under a heat lamp, immobilized in a restrainer, and the lateral tail vein was punctured with a regular 19G needle (BD, UK). Blood smears were prepared, fixed with methanol, and stained with modified Romanowsky stain (Wright stain, Sigma, UK). A WBC count was estimated by counting 5 to 10 high power fields (hpf) using a 40x objective of a bright field microscope (Zeiss, UK) in an appropriate

area. When larger blood volumes were required, lidocaine-containing local anaesthetic ointment was applied to the tip of the tail and mice were warmed for 10 minutes in a heating chamber at 37°C. The tip of the tail was then cut with a sterile scalpel and 50µl of blood was collected in an EDTA-coated 1.5ml Eppendorf tube. To assess the proportion of CD19+CD5+ CLL cells in peripheral blood, whole blood was stained with 1:100 CD45 APC (clone 30-F11), CD19 FITC or PE (clone eBio1D3) and CD5 PE or FITC (clone 53-7.3) (all eBiosciences, UK). CD19+CD5+ cells were gated on CD45+ cells after live/dead and singlet/doublet discrimination, and gates were confirmed by including samples from healthy controls.

### 4.3.3 Adoptive transfer experiments

Procedures for this are described in Section 3.1.5. Initial experiments used  $2 \times 10^7$  cells in two separate injections three days apart, while later experiments used the same total cell number ( $4 \times 10^7$ ) in a single injection.

## 4.4 Results

### 4.4.1 Genomic PCR and TCL1 sequence analysis

All TCL1 mice produced under licence PPL70/7531 were genotyped to confirm the presence of the TCL1 transgene. Copy number status and integration site were not examined. Sequence analysis carried out on genomic DNA from the first litter produced in our colony confirmed that the amplified product was identical with the coding region of human *TCL1* (Figure 4 A). An example of a genomic PCR for four different litters is depicted in Figure 4 B. Bands at 494 bp for MBG as a housekeeping gene confirmed the quality of the extracted genomic DNA, while bands at 350 bp confirmed the TCL1 transgene status of the animal. Breeding a transgenic male with WT females usually resulted in 50% TCL1 transgenic offspring, but some variation occurred, with less than half of some litters being transgenic. As transgene homozygosity is not lethal in TCL1 mice, transgenic animals can also be bred with each other. However, we refrained from pursuing this breeding strategy to minimize the likelihood of the development of a TCL1 sub-strain over time and to maintain better control of TCL1 lines derived from specific index animals, in accordance with good practise guidelines on the maintenance of transgenic mouse strains<sup>379</sup>. In addition, our breeding strategy allowed us to perform

specific experiments in age-matched WT littermates raised and kept in identical conditions as experimental animals.

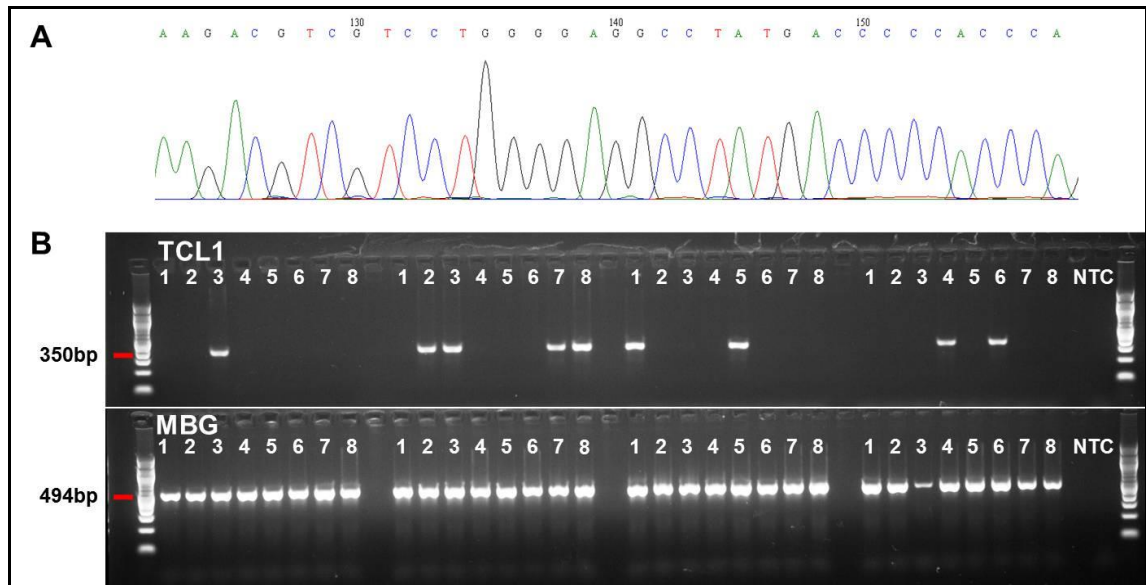


**Figure 4: Validation of genotyping procedure and protocol to maintain the TCL1 colony.** **(A)** TCL1 sequence confirmation was carried out by bidirectional sequencing and compared to the corresponding sequence for human *TCL1* (accession number TCL1A: NM\_001098725, TCL1B: NM\_004918.3), confirming that the amplified product was identical. **(B)** Genomic DNA was amplified with TCL1 and mouse beta globin (MBG) primer pairs. MBG bands at 494bp confirmed the quality of the extracted DNA, while TCL1 bands at 350bp identified transgenic TCL1 offspring. No-template controls (NTC) demonstrate absence of PCR contamination.

#### 4.4.2 Haematology testing and anatomic sites of disease

As seen in human CLL, blood smears from leukaemic mice showed an increase in circulating lymphocytes that were enlarged and displayed condensed nuclear chromatin. Also similar to the human disease, Gumprecht nuclear shadows (also known as smudge cells) as an artefact of the smear preparation were also present (see Figure 5 A). The immunophenotype of circulating lymphocytes also resembled human CLL, as murine leukaemia cells were CD19+CD5+. This population was absent in young transgenic mice and in age-matched WT controls (see Figure 5 B).

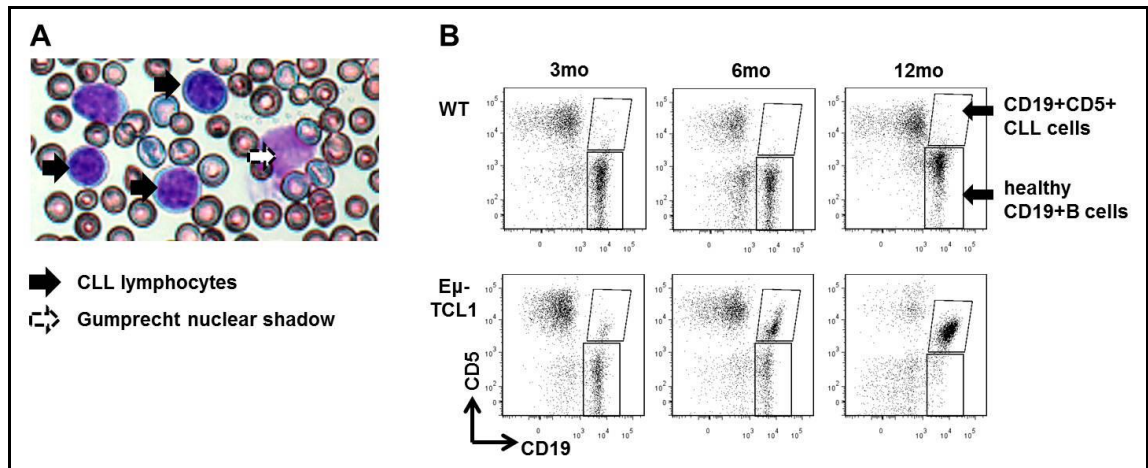


**Figure 5: Results of routine haematology testing in TCL1 and WT mice. (A)** Example of a blood smear of a leukaemic mouse. Smears were stained with a modified Romanowsky stain, and leukocytes were counted in 5-10 hpf using a 40x objective of a bright field microscope in an appropriate area. As in human CLL, mouse leukaemia cells were enlarged and had clumped nuclear chromatin, and Gumprecht nuclear shadows could be found. **(B)** Example of flow cytometry graphs in ageing TCL1 and age-matched WT mice. Whole blood was stained with CD45, CD19 and CD5. Cells were gated on CD45+ lymphocytes after live/dead and singlet/doublet discrimination. While young TCL1 and WT mice were free of CD19+CD5+ CLL cells, this population was found to consistently expand with ageing in transgenic mice.

The morphology of CLL in TCL1 transgenic mice with fully developed disease is depicted in Figure 6 A. Just as is often the case in the human disease, mice with CLL exhibit hepatosplenomegaly and lymphadenopathy, which however are generally painless and cause only moderate impairment to the animals. Spleens are the major organs of disease, and are enlarged up to 5-fold compared to WT spleens (Figure 6 B).

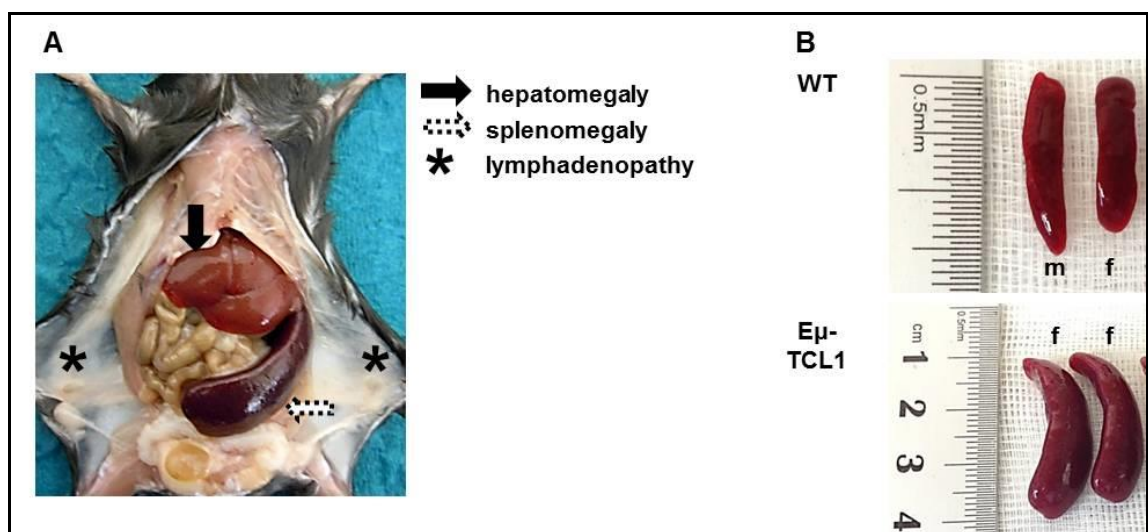


**Figure 6: Anatomic sites of CLL in TCL1 transgenic mice. (A)** Mice with CLL exhibit hepatomegaly (broken arrow), splenomegaly (solid arrow) and lymphadenopathy (\*). **(B)** Differences in spleen sizes in organs taken from WT and TCL1 mice (m – male, f – female). Note differences in scale.

### 4.4.3 Adoptive transfer experiments

A total of 12 consecutive AT experiments were conducted to optimize conditions for our *in vivo* preclinical studies (Table 7). With the exception of experiment 12, where mice were sacrificed at predefined endpoints, a previously determined maximum tolerable degree of splenomegaly assessed by physical examination along with predefined haematological parameters were used as endpoint definitions (see Chapter 3.1).

aim	exp.	date of TPL	no. of inj.	recipients	donors	failed engraftments	weeks with CLL, median (range)	spleen weight, median (range)
<b>testing i.v. TPL procedure</b>	1	17/01/12	2	1 C3H Tg	several, inconsistent		7.86	0.4g
	2	31/01/12	2	1 B6 Tg			11.43	1g
	3	19/03/12	2	2 C3H Tg 4 C3H Tg	several, consistent for individual mice	1 C3H	6.1 (6-20)	2.35g (1.8-5.6)
<b>establishing i.v. TPL procedure using uniform conditions</b>	4	11/05/13	2	2 B6 Tg 4 B6 Tg	single donor		4 (4-5.6)	0.8g (0.6-1.0)
	5	08/06/12	2	5 B6 Tg 4 B6 Tg	single donor		4.43 (3.71-11.44)	1.3g (0.7-2.8)
	6	02/07/12	2	5 C3H Tg 4 C3H Tg	single donor		7.71 (7.71-11.57)	1.8g (1.4-2.5)
	7	12/10/12	2	5 B6 Tg	single donor		9 (no range, same endpoint for all mice)	2.0g (1.6-2.6)
<b>comparing TPL in TCL1 and WT recipients</b>	8	19/04/13	2	5 B6 Tg 5 B6 Tg 5 B6 WT 5 B6 WT	donor pool	1 B6 WT (censored day 60 with lymphocytosis)	WT: 5.8 (5-6.7) Tg: 5 (4.7-5.9)	WT: 1.9g (1.9-2.8) Tg: 1.9g (1.6-2.2)
<b>confirming TPL in WT recipients</b>	9	10/06/13	2	3 B6 WT 4 B6 WT	single donor		8.0 (4.29-10.43)	not assessed
<b>comparing 2x i.v. TPL with 1x i.v. TPL</b>	10	01/10/13	1, 2	10 B6 WT 10 B6 WT	donor pool		1: 7.4 (6.86-10.29) 2: 8.0 (6.86-10.29)	1: 1.75g (1.3-2.2) 2: 1.8g (1.3-2.4)
<b>confirming 1x i.v. TPL</b>	11	11/02/14	1	16 B6 WT	donor pool		5.7 (1.43-9)	1.7g (0.5-2.2)
<b>confirming 1x i.v. TPL, earlier endpoints</b>	12	07/04/14	1	15 B6 WT	donor pool		1.29 (0.43-2.14)	0.2g (0.1-0.5)

**Table 7: Overview of adoptive transfer experiments to validate and optimize the model for preclinical studies.** Abbreviations: TPL – transplantation, i.v. – intravenous, inj. – injection(s), g – gram, C3H – C3HB6 background, B6 – C57Bl/6 background, Tg – transgenic, WT – wild type. Red font represents female recipients and blue font male recipients.

In the first three experiments, the aim of the AT was to test the i.v. transplantation procedure *per se*. Both TCL1 C3H and B6 recipients were used. Due to the limited availability of donors, cell doses and donors were often inconsistent within and between experiments. Therefore, the time between transplantation and culling based on previously defined splenomegaly and haematological parameters was quite variable in the initial experiments, and engraftment was not successful in one recipient. However, as the donor pool was greatly expanded after TCL1 mice in our colony had been successfully aged, we were able to examine the i.v. AT protocol under more uniform conditions. Using young male and female TCL1 recipients on both the C3H and the B6 backgrounds, we injected  $2 \times 10^7$  cells each on d0 and d3 (total of  $4 \times 10^7$  cells per mouse) from single, syngeneic, leukaemic donors in four consecutive experiments (experiments 4 to 7 in Table 7). This led to median survivals of 4 to 9 weeks after AT. Mice were sacrificed once they met previously defined criteria for spleen size and/or lymphocytosis. Examples of the development of lymphocytosis assessed by longitudinal blood smears are depicted in Figure 7. Although disease development appeared to be more aggressive in females, this difference was not statistically significant.

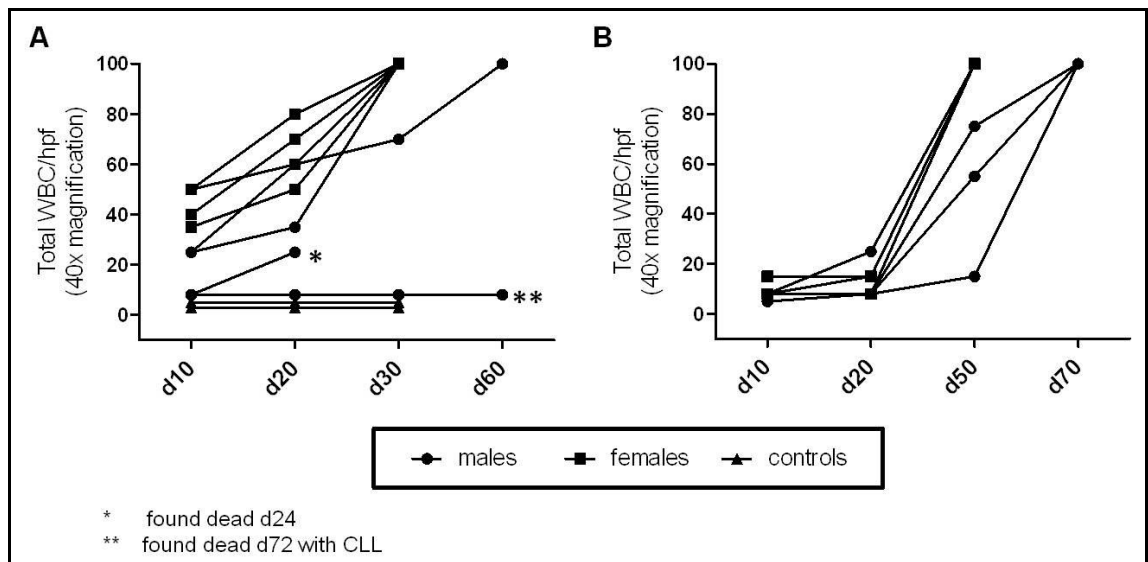


**Figure 7: Longitudinal follow-up of disease development in recipient mice after AT.** Progression of lymphocytosis was assessed by blood smears. **(A)** 3 month old B6 TCL1 transgenic males ( $n=5$ ) and females ( $n=4$ ) were injected with  $4 \times 10^7$  cells from a single aged donor mouse with CLL, and bled every ten days. Non-transplanted transgenic female littermates were bled at the same time intervals as controls. Two males exhibited slower disease progression and were found dead on d24 (\*) and d72 (\*\*). Post-mortem examination showed clear signs of CLL (*i.e.* splenomegaly), indicating that AT was successful in all recipients. **(B)** 4 month old C3H TCL1 transgenic males ( $n=5$ ) and females ( $n=4$ ) were injected with  $4 \times 10^7$  cells from a single aged donor mouse with CLL, and bled in regular time intervals. Longitudinal blood smears demonstrated progressive lymphocytosis, indicating that CLL can be engrafted in both TCL1 backgrounds.

We next wanted to know if AT would lead to similar results in non-leukaemic TCL1 transgenic and WT recipients. We therefore injected cells from a pool of aged, leukaemic B6 TCL1 mice into age- and sex-matched young, non-leukaemic transgenic mice and WT littermates, and followed disease development by blood smears and regular physical examination of spleen sizes. Control transgenic and WT littermates were injected with a pool of normal spleen B cells and sacrificed at identical time points. In mice that received CLL cells, there was no significant difference between WT and TCL1 recipients in the progression rate of lymphocytosis (Figure 8 A), spleen:body weight ratio (Figure 8 C) and percentage of CD19+CD5+ lymphocytes in spleen (Figure 8 D). One WT recipient of CLL cells, in which the i.v. injection had been very challenging and likely led to the application of a lower cell dose, was censored from the study on day 60 with developing lymphocytosis, and sacrificed on day 90. Flow cytometry demonstrated a CLL content of 25% in the spleen, with beginning CLL-typical T-cell phenotypic defects, with the healthy control mouse showing normal B- and T-cell subset distribution. This confirmed that engraftment had been successful, but that the longer latency was most likely related to the application of a suboptimal donor cell dose.

Survival after AT was not statistically different between males and females (data not shown), and there was no difference in survival between WT and TCL1 recipients, although these comparisons are based on limited numbers of mice (Figure 8 B). After we confirmed successful engraftment in a second group of young WT recipients (experiment 9, Table 7), we concluded that WT mice can replace TCL1 mice as recipients in AT experiments. As B6 WT mice are readily available from commercial sources, this eliminates the need to breed and maintain a large stock of younger TCL1 mice in addition to ageing mice.

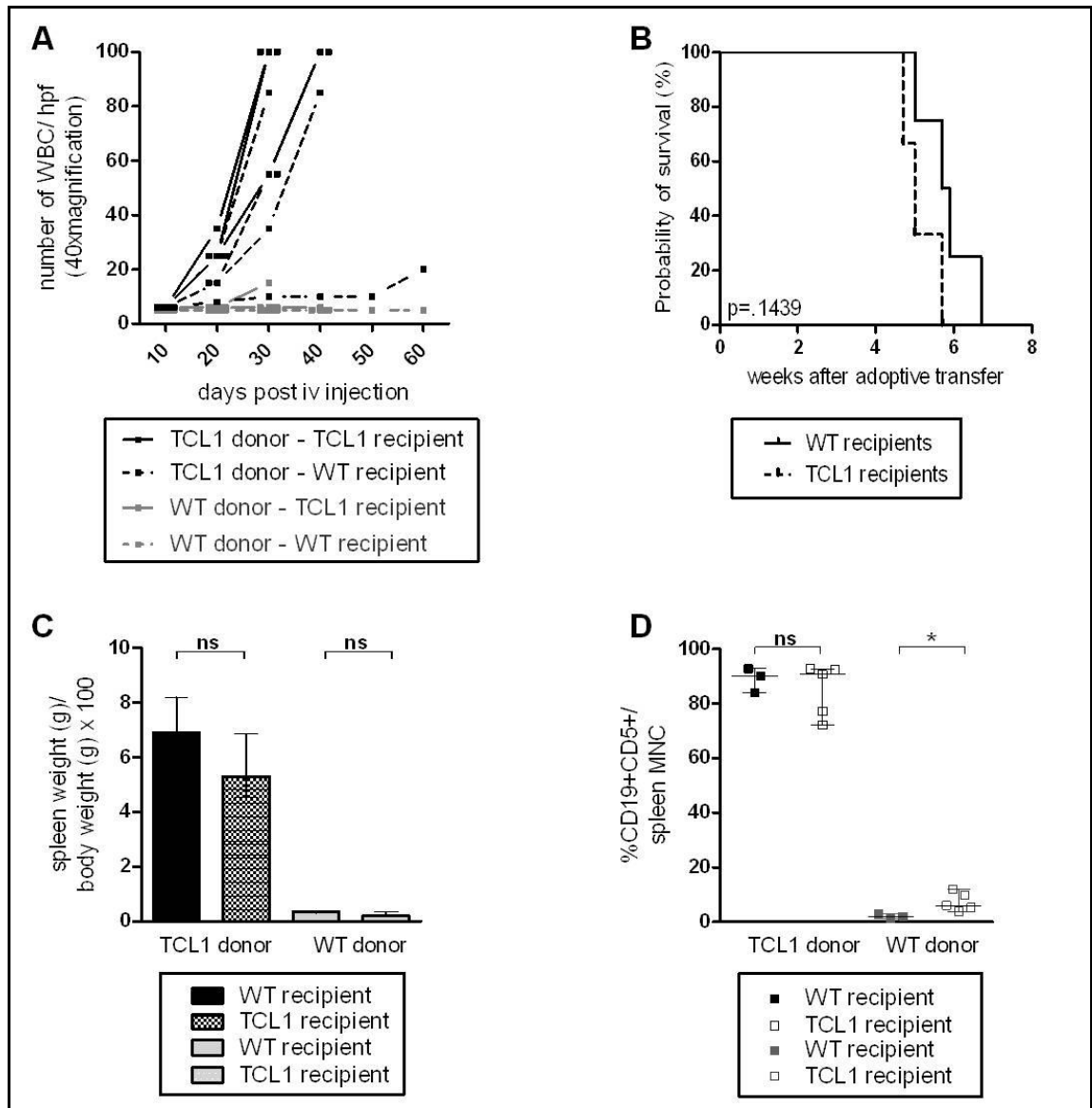


**Figure 8: Comparison of AT into young TCL1 transgenic and WT recipients.** AT into 4 month old transgenic and sex-matched WT littermates reliably induced CLL in all recipients. **(A)** Longitudinal blood smears performed every ten days demonstrated similar progression of lymphocytosis in WT and TCL1 recipients. **(B)** Leukaemic mice were sacrificed after a median time of 5.8 (WT recipients) and 5 (TCL1 recipients) weeks, with no difference between groups (HR .288, 95%CI .05-1.54, p=.1439). At the endpoint, spleen:body weight ratio **(C)** and %CD19+CD5+ lymphocytes in spleen **(D)** were comparable between WT and TCL1 recipients.

We then sought to improve the AT procedure further by reducing the number of i.v. injections to a single injection, while maintaining the total dose of  $4 \times 10^7$  cells. The goals were to reduce animal stress by eliminating a second invasive procedure while also reducing the likelihood of a potentially failed injection leading to the application of a suboptimal dose of cells. Male and female WT recipients were randomized to a single injection of  $4 \times 10^7$  cells (1x), or to two injections of  $2 \times 10^7$  cells each within 3 days of each other (2x), using the same donor pool for all recipients. As observed in previous experiments, females appeared to have a faster progression of lymphocytosis, but this

was not statistically significant. Both 1x and 2x injections produced reliable and similar rates of disease development (Figure 9 A). At the endpoint, there was no difference between 1x and 2x recipients in spleen:body weight ratio ( $p=.9705$ ) and relative percentage of CD19+CD5+ lymphocytes in spleen ( $p=.9517$ ) (Figure 9 B), thus validating the use of a single injection while maintaining a total dose of  $4 \times 10^7$  cells. These findings were confirmed in a second group of young WT recipients (experiment 11, Table 7).

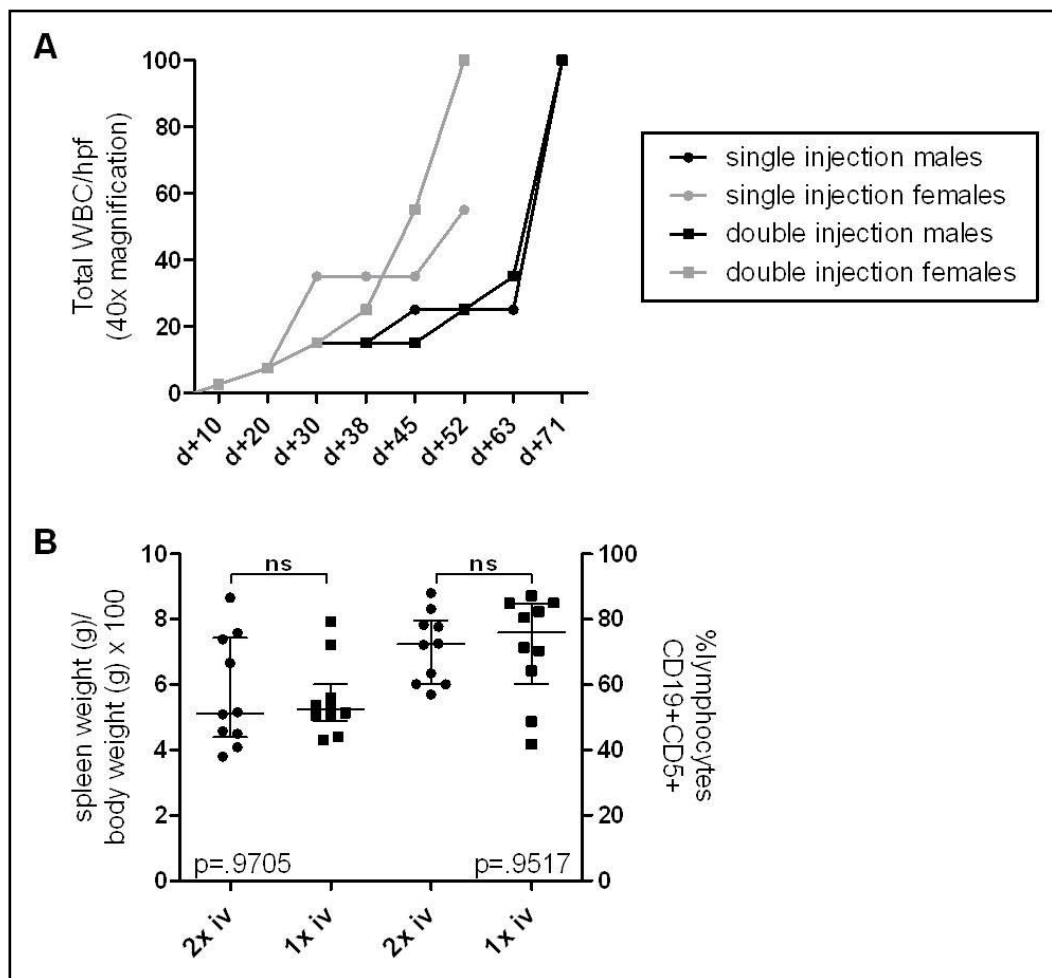


**Figure 9: Improvement of AT model by reducing the number of i.v. injections to a single injection. (A)** Longitudinal blood smears performed in regular intervals demonstrated very similar progression of lymphocytosis in all recipients. Females appeared to have a shorter time to lymphocytosis but this difference did not reach significance. **(B)** At the endpoint, spleen:body weight ratio and spleen CLL load were comparable between 1x and 2x recipients.

CLL was extremely reliably induced across all AT experiments, with only two out of 115 transplanted animals failing engraftment. The median time between AT and fully developed CLL meeting predefined endpoint criteria as described in Chapter 3.1 was 7 weeks (range 3.71-20, Figure 10 A). There were no differences in outcome between mice receiving cells from a single donor (n=36) and those receiving cells from a pool of donors (n=31) (HR .7842, 95% CI .4561-1.348, Figure 10 B). Splenic CLL load, defined as the percentage of CD19+CD5+ lymphocytes among spleen mononuclear cells and measured at the endpoint, was highly significantly correlated with spleen weight, indicating that the estimation of spleen size by palpation is an adequate parameter to determine the disease status of individual mice, with the caveat that inter-examiner heterogeneity might exist due to different levels of experience or interpretations (spearman  $r$  .7936,  $p < .0001$ , Figure 10 C). This can however be limited by setting up and following rigorous previously defined guidelines. In addition, increasing spleen weight and weeks after AT were significantly correlated (spearman  $r$  .7196,  $p < .0001$ , Figure 10 D), indicating that longer time with CLL translates into higher spleen weight as a surrogate for disease load. While some variability exists and is likely dependent on the biology of the transplanted disease as well as the gender of the recipient animal, this correlation allows reasonable estimation of when drug intervention should be initiated (*i.e.* early intervention at an earlier stage of disease *versus* later intervention at fully developed CLL). In sum, these experiments outline a reliable strategy for modelling CLL in mice by AT.

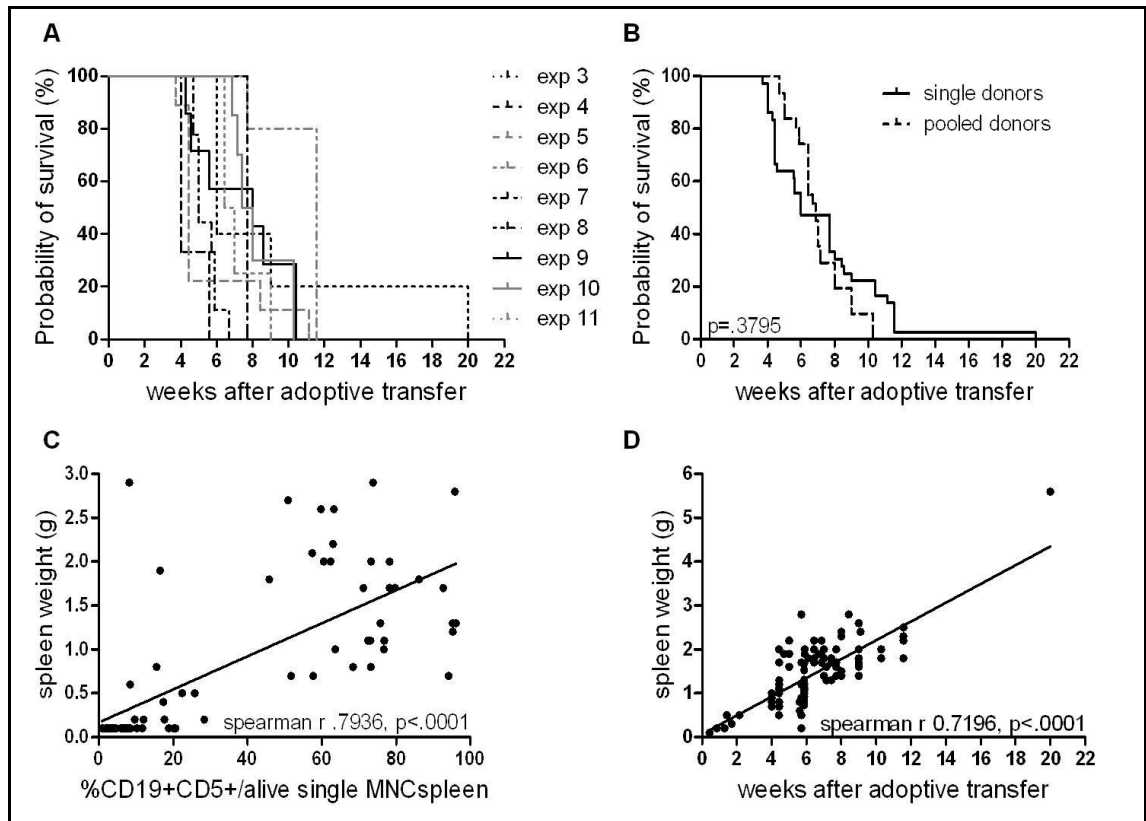


**Figure 10: Reproducibility of and survival after AT:** (A) Across consecutive experiments using different donors, AT led to consistent disease development in recipient mice (median survival 7 weeks, range 3.71-20). (B) Cells from a single donors (n=36 recipients) and cells pooled from several donors (n=31 recipients) produced comparable outcomes (HR .7842, 95% CI .4561-1.348). (C) The relative frequency of spleen CD19+CD5+ lymphocytes was highly significantly correlated with spleen weight. (D) Increasing spleen weight and weeks after AT were significantly correlated with each other.

#### 4.5 Discussion

This fundamental optimization work has led to the establishment of an efficient and well-characterized TCL1 mouse colony and has allowed us to implement the necessary breeding, genotyping and ageing procedures in our centre. It has consolidated i.v. transplantation procedures, which previously were poorly defined, to reliably generate a CLL phenotype in previously disease-free transgenic mice on both the original C3H and the backcrossed B6 background. Furthermore, this work has optimized and standardized AT methodology by validating the use of young WT recipients and by reducing the number of required injections in controlled and randomized experiments. Together, these studies provide a reproducible and far more feasible approach for using the TCL1 mouse model in CLL preclinical research. This work will enormously facilitate the *in vivo* evaluation of novel agents as well as the investigation of immune defects in the context of developing disease, and approaches to repair them.

In contrast to the majority of published studies using AT in immunocompetent recipients, our transplantation strategy consists of higher cell doses and also uses a different application route. In initial reports, up to  $10^6$  and  $10^7$  spleen MNC were applied once by intraperitoneal (i.p.) injection<sup>214, 215</sup>. More recent publications administered 1.5 to  $2 \times 10^7$  MNC in up to 4 i.p. injections<sup>220, 227</sup>. Successful AT in SCID or TCL1 model variations using similar doses and application routes has been demonstrated by several other groups<sup>65, 231, 260, 261</sup>, although the specifics of these experiments vary substantially, and comparison of results between laboratories is therefore challenging. Similar to our strategy, Woyach *et al.* injected XID and B6 mice with  $5 \times 10^6$  to  $5 \times 10^7$  cells i.v.<sup>228</sup>.

In general, higher cell doses led to faster disease development and consequently shorter survival of animals. Animals that received  $10^6$  MNC had a median survival of 166 days, while animals transplanted with  $10^7$  MNC in the same study survived for a median of 121 days<sup>214</sup>. Previous experiments from our group used a total of  $1 \times 10^8$  cells injected i.v., which led to CLL-associated molecular T-cell defects after a latency of just 8 days<sup>216</sup>. To achieve maximal experimental efficiency while being able to study the immune modulating effect of drug treatment, a short latency of disease that still leaves enough time for immune defects to develop is valuable. In view of these results, the dose and administration route selected and validated in this work balance these potentially conflicting experimental requirements and provide a solid basis for preclinical testing of immune modulating mechanisms of actions of novel drugs.

In the current study, we demonstrate that virtually all mice exhibit fully developed CLL after a median of 7 weeks following AT. Although some mice had a later onset of disease (e.g. two males in experiment 6, and one male in experiment 8), all eventually succumbed to disease after showing signs of progressive CLL assessed by spleen size and lymphocytosis following previously defined criteria. This latency can most reasonably be explained by suboptimal injections leading to application of lower donor cell numbers. In general, CLL development was very consistent within single experiments. This was even further improved after reducing the number of injections, thus reducing the likelihood of suboptimal injections. However, variability between different experiments could also be due to the biology of the donor disease. Such differences in disease onset are common even within closely related TCL1 transgenic mice, suggesting that as-yet unidentified variables within individual animals influence the aggressiveness of leukaemia development. These experiments also frequently suggested a faster progression of disease in female mice; however, this difference was not statistically different even when combining data from all experiments.

## 5 Investigation of T-cell dysfunction in E $\mu$ -TCL1 mice on the B6 background

### 5.1 Specific introduction

As described in Section 1.2.1, our group previously demonstrated that development of CLL in TCL1 mice is associated with global T-cell defects similar to those observed in human patients<sup>216</sup>. While expression of the TCL1 transgene in B cells had no effect on T cells before the development of CLL, with non-leukaemic mice exhibiting normal T-cell numbers and function, development of CLL (*i.e.* expansion of CD5+CD19+ B cells) led to various T-cell defects. These included decreased *in vivo* antigen-specific T-cell activation, suppressed T-cell proliferation, and impaired induction of idiotype-specific CD8+ cytotoxic T-cells. T-cell lymphokine production was also dysfunctional and appeared Th2 preponderant. Gene-expression profiling of T cells from TCL1 mice with CLL revealed several differentially expressed genes in both CD4+ and CD8+ cells compared to those from WT or non-leukaemic transgenic mice. These were mostly involved in pathways of cell proliferation, differentiation, effector function, and actin cytoskeleton formation. With increasing tumour burden, these changes became more evident, again correlating with findings in human CLL. The causal relationship between leukaemia and induction of T-cell defects was demonstrated by the finding that AT of CLL cells into young disease-free mice rapidly induced the molecular T-cell changes observed in ageing TCL1 mice with CLL.

In these original experiments, TCL1 mice on the original B6C3H-F1 background were used. B6C3H-F1 mice are hybrids produced by crossing mice of the two inbred strains C57Bl/6 (B6) and C3H [source: <http://research.jax.org/grs/type/hybrid/index.html>, accessed 17.10.11]. Although F1 hybrid mice are genetically and phenotypically uniform and possess great vigour, they are heterozygous at all loci for which their parents have different alleles. When mating F1 mice to produce F2 offspring, litters will therefore all have a unique random mixture of alleles from both parental strains, which will be further mixed in consecutive generations. To obtain a uniform genetic background, TCL1 mice on the B6C3H-F1 background were backcrossed over more than 10 generations to a pure B6 background. More important than eliminating the possibility that such genetic diversity might have an effect on immune responses, mice on a pure B6 background can more easily be crossed with other disease models, for example PD-L1 knockout mice, which will be an integral component of future experiments. Once the backcross was established, only a single study has examined T-cell dysfunction in B6 TCL1 mice by looking at T-cell subset composition changes in lymph nodes and peripheral blood<sup>220</sup>. In this report, TCL1 mice with manifest CLL had increased absolute T-cell numbers and exhibited a shift from naïve to antigen-

experienced CD4+ and CD8+ T cells compared to age-matched WT controls, which was more pronounced in lymph nodes than in peripheral blood. These preclinical observations are largely in line with T-cell subset alterations in peripheral blood in human CLL, as described in Chapter 1.1.4. However, peripheral blood and secondary lymphoid organs and bone marrow have entirely different and distinct microenvironments based on their physiological roles in supporting lymphocyte maturation and differentiation. The importance of these tissue microenvironments for the interaction with CLL cells was recently explored by Mittal *et al.*<sup>380</sup>. The comparison of gene expression profiles of purified CLL cells from peripheral blood, bone marrow and lymph nodes revealed that gene signatures representing pathways critical for survival and activation of B cells were altered in different tissue compartments. Genes associated with the BCR, BAFF/APRIL and NF- $\kappa$ B pathway and immune suppression were enriched in lymph nodes, suggesting that they might be the primary site for tumour growth. In contrast, blood CLL cells overexpressed chemokine receptors, while their cognate ligands were enriched in secondary lymphoid organs and bone marrow. Bone marrow signatures were also enriched with antiapoptotic, cytoskeleton and adhesion molecules, and in TCL1 mice, a high percentage of leukaemic cells from the lymphoid compartment expressed key BCR and NF- $\kappa$ B molecules.

The importance of different microenvironments on T-cell defects is however not well understood, and it is not clear to what extent T-cell defects described in the peripheral blood of CLL patients or TCL1 mice directly mirror the defects in other microenvironments. Moreover, it is possible that T-cell defects might be influenced by differences in CLL load in different compartments, or are subjected to dynamic changes while CLL develops or progresses. These questions have not been fully answered to date; Hofbauer *et al.*<sup>220</sup> focused their characterization of T-cell subsets to peripheral blood and lymph nodes, but excluded spleen. However, the spleen is considered the major organ of disease in this model, and preclinical characterization studies such as the T-cell work from our group<sup>216</sup>, or studies investigating the effect of therapeutic interventions<sup>265</sup>, are generally done using splenocytes from TCL1 mice. In addition, this characterization was only done in a small number of moribund aged TCL1 mice and in mice that became ill after a very long latency of 3 to 6 months after adoptive transfer, resulting in a large biological range of overall CLL disease load which might have biased the exploration of their effect on the T-cell compartment. In addition, a careful and thorough longitudinal investigation of the development of not only phenotypic T-cell subsets, but also functional T-cell defects alongside progressing disease has not been conducted.

## 5.2 Goals and objectives

My next goal was therefore to fully validate the B6 TCL1 model for the investigation of global T-cell defects, to further characterize T-cell subsets in the context of advancing CLL in all CLL affected compartments, and to explore the impact of developing CLL on effector T-cell function. Specifically, I sought to address the following questions:

- Do leukaemic B6 TCL1 mice recapitulate T-cell dysfunction previously observed in leukaemic B6C3H-F1 TCL1 mice?
- Can AT into young TCL1 transgenic and WT B6 mice be used to model the T-cell dysfunction observed in leukaemic TCL1 mice?
- How do T-cell defects develop *in vivo* in relation to CLL development?
- Are T-cell defects observed in spleen representative of T-cell defects in other secondary lymphoid organs and in the peripheral blood?

## 5.3 Specific methods and materials

### 5.3.1 Mice and examined organs

In addition to gene expression profile and effector function, T-cell subset composition appears to be quite similar in human patients and mice with CLL. We therefore used T-cell subsets as a surrogate marker for global T-cell dysfunction to compare ageing TCL1 mice on the B6C3H-F1 background to ageing TCL1 B6 mice, and to validate the AT model to adequately mirror the defects seen in ageing CLL in both backgrounds. Three, 6 and 12 month old TCL1 mice on both backgrounds with confirmed presence of the TCL1 transgene by genomic PCR were selected from our colony. The mice selected were mostly littermates, with males and females being well balanced. To minimize the likelihood of a batch effect, experiments were repeated in a second group of 3, 6, and 12 month old B6 TCL1 mice and in 3 month old B6C3H-F1 TCL1 mice. Additional 6 and 12 month old B6C3H-F1 TCL1 mice were not examined as the breeding of this background was already terminated based on the clear findings of the first cohort. In collaboration with our Animal Technician Service (ATS), we cryopreserved sperm from young B6C3H-F1 TCL1 males before terminating the line. Sperm was confirmed to be viable and fertile after freezing/thawing as demonstrated by the ability to induce a two-cell stage embryo development, which will allow us to quickly recover the line should the need arise. The disease and T-cell phenotype in AT mice was examined using mice from experiments 5, 6, 7 and 11 (as described in Chapter 4).

Age- and sex-matched WT mice were purchased from commercial suppliers. Mice were sacrificed at the required age under protocol 19b2 of PIL 70/7531, and peripheral blood (PB), lymph nodes (LN), bone marrow (BM) and spleens were harvested and processed as described in Chapter 3.1.4.

After optimization of functional T-cell assays, a third round of experiments confirming phenotypic changes, expanding the phenotype panel to include further subsets, and investigating T-cell function in spleen was conducted using 3, 6 and 12 month old B6 TCL1 mice, AT mice, and age- and sex-matched WT controls from commercial suppliers. An overview of all cohorts of mice including numbers, as well as their usage and availability of organs for specific experiments is provided in Table 8.

I. Available mice to assess T-cell phenotype in spleen alongside developing CLL								
	CLL in spleen				T-cell phenotype			
	3mo	6mo	12mo	AT	3mo	6mo	12mo	AT
B6 WT	1 <sub>a</sub> n=6	2 <sub>a</sub> n=6	3 <sub>a</sub> n=4	4 <sub>a</sub> n=6	1 <sub>a</sub> n=6	2 <sub>a</sub> n=6	3 <sub>a</sub> n=4	4 <sub>a</sub> n=6
	1 <sub>b</sub> n=6	2 <sub>b</sub> n=6	3 <sub>b</sub> n=4	not repeated	1 <sub>b</sub> n=6	2 <sub>b</sub> n=6	3 <sub>b</sub> n=4	not repeated
B6 TCL1	5 <sub>a</sub> n=6	6 <sub>a</sub> n=6	7 <sub>a</sub> n=6	8 <sub>a</sub> n=6	5 <sub>a</sub> n=6	6 <sub>a</sub> n=6	7 <sub>a</sub> n=6	8 <sub>a</sub> n=6
	5 <sub>b</sub> n=6	6 <sub>b</sub> n=6	7 <sub>b</sub> n=6	8 <sub>b</sub> n=4	5 <sub>b</sub> n=6	6 <sub>b</sub> n=6	7 <sub>b</sub> n=6	8 <sub>b</sub> n=4
C3H TCL1	9 <sub>a</sub> n=6	10 <sub>a</sub> n=6	11 n=6	12 n=5	9 <sub>a</sub> n=6	10 <sub>a</sub> n=6	11 n=6	12 n=5
	9 <sub>b</sub> n=6	not repeated	not repeated	not repeated	9 <sub>b</sub> n=6	not repeated	not repeated	not repeated
II. Available mice to assess T-cell function in spleen alongside developing CLL								
	CLL in spleen				T-cell function			
	3mo	6mo	12mo	AT	3mo	6mo	12mo	AT
B6 WT	1 <sub>funct</sub> n=6	2 <sub>funct</sub> n=6	3 <sub>funct</sub> n=6	4 <sub>funct</sub> n=10	1 <sub>funct</sub> n=6	2 <sub>funct</sub> n=6	3 <sub>funct</sub> n=6	4 <sub>funct</sub> n=10
B6 TCL1	5 <sub>funct</sub> n=6	6 <sub>funct</sub> n=6	7 <sub>funct</sub> n=6	not done	5 <sub>funct</sub> n=6	6 <sub>funct</sub> n=6	7 <sub>funct</sub> n=6	not done
III. Available mice to assess T-cell phenotype in organs alongside developing CLL								
	CLL in BM, PB, LN				T-cell phenotype			
	3mo	6mo	12mo	AT	3mo	6mo	12mo	AT
B6 WT	1 <sub>a</sub> n=6	2 <sub>a</sub> n=6	3 <sub>a</sub> n=4	4 <sub>a</sub> n=5	1 <sub>a</sub> n=6	2 <sub>a</sub> n=6	3 <sub>a</sub> n=4	4 <sub>a</sub> n=5
	1 <sub>funct</sub> n=6	2 <sub>funct</sub> n=6	3 <sub>funct</sub> n=6	4 <sub>funct</sub> n=10	1 <sub>funct</sub> n=6	2 <sub>funct</sub> n=6	3 <sub>funct</sub> n=6	4 <sub>funct</sub> n=10
B6 TCL1	5 <sub>a</sub> n=6	6 <sub>a</sub> n=6	7 <sub>a</sub> n=6	8 <sub>a</sub> n=6	5 <sub>a</sub> n=6	6 <sub>a</sub> n=6	7 <sub>a</sub> n=6	8 <sub>a</sub> n=6
	5 <sub>funct</sub> n=6	6 <sub>funct</sub> n=6	7 <sub>funct</sub> n=6	not done	5 <sub>funct</sub> n=6	6 <sub>funct</sub> n=6	7 <sub>funct</sub> n=6	not done

**Table 8: Summary of all cohorts of mice used to validate and further characterize T-cell defects in spleen and other organs.** Abbreviations: mo – months, AT – adoptive transfer, B6 – C57Bl6, WT – wild type, C3H – B6C3H-F1, BM – bone marrow, PB – peripheral blood, LN – lymph nodes.

### 5.3.2 Multicolour flow cytometry for cell surface markers

As in humans, murine CD3 $\epsilon$  expression is correlated with T-cell maturation, and the CD8+ and CD4+ molecules are used for identification of helper and cytotoxic T cells<sup>381</sup>. Antigen-experienced T-cell markers include CD44, CD62L, and CD45RB. CD62L (L-selectin) is a peripheral lymph node homing receptor<sup>382</sup>. As a marker of T-cell development it is expressed on naive and memory T cells, while effector cells downregulate CD62L and can also express a diverse set of homing receptors to enable them to pass through non-lymphoid tissues<sup>383, 384</sup>. Murine CD44 and CD45RB correspond to human CD45RO as markers of antigen-experienced T cells, and are highly expressed on memory and effector T cells<sup>385-387</sup>. The concept of CM and EM cells was introduced in in 1999<sup>388</sup>. Both are functional subsets within CD45RO memory cells in humans, but show differences in their anatomical location, expression of cell surface markers and functional responses. Mice contain a comparable CD44+ cell population after clearance of acute viral infection, fitting the description of CM cells, and CD44RB-CD44+CCR7-CD62L- T cells, fitting the description of EM cells<sup>389</sup>. In our experiments, T-cell subsets were characterized based on the surface expression of CD3, CD4, CD8, CD62L, CD44 and CCR7, and CLL by CD19 and CD5. Information on antigens, fluorochromes, clones, concentrations and suppliers is listed in Table 9.

	mouse antigen	fluorochrome	clone	concentration	host/isotype	supplier
<b>T-cell phenotype</b>	CD3e	APCCy7	17A2	0.2 mg/ml	rat IgG2bk	Biolegend
	CD4	PerCPCy5.5	RM4-5	0.2 mg/ml	rat IgG2ak	eBioscience
	CD8a	FITC	53-6.7	0.5 mg/ml	rat IgG2ak	eBioscience
	CD62L	APC	MEL-14	0.2 mg/ml	rat IgG2ak	eBioscience
	CD44	PE	IM7	0.2 mg/ml	rat IgG2bk	eBioscience
<b>extended T-cell phenotype</b>	CD3e	APCCy7	17A2	0.2 mg/ml	rat IgG2bk	Biolegend
	CD4	PerCPCy5.5	RM4-5	0.2 mg/ml	rat IgG2ak	eBioscience
	CD8a	BV605	53-6.7	0.5 mg/ml	rat IgG2ak	Biolegend
	CD62L	FITC	MEL-14	0.2 mg/ml	rat IgG2ak	eBioscience
	CD44	AF700	IM7	0.2 mg/ml	rat IgG2bk	eBioscience
	CCR7	PeCy7	4B12	0.2 mg/ml	rat IgG2ak	eBioscience
<b>CLL</b>	CD5	APC	53-7.3	0.2 mg/ml	rat IgG2ak	eBioscience
	CD19	FITC	eBio1D3	0.5 mg/ml	rat IgG2ak	eBioscience

**Table 9: Summary of antigens, fluorochromes, clones, concentrations and suppliers used to assess T-cell subsets in relation to CLL.**

Cells were prepared for flow cytometry as described in Chapter 3.4, with the exception of CCR7, which required different conditions due to continuous recycling of chemokine receptors: cells were stained at 37°C at 5% CO<sub>2</sub> for 20 minutes, followed by staining with the remaining fluorochrome cocktail for 20 minutes at room temperature. Cells were then washed and processed as described in Chapter 3.4.1. Optimization experiments demonstrated that this resulted in better resolution between positive and negative populations, and that this could be achieved by using a 4:100 dilution (see Figure 11).

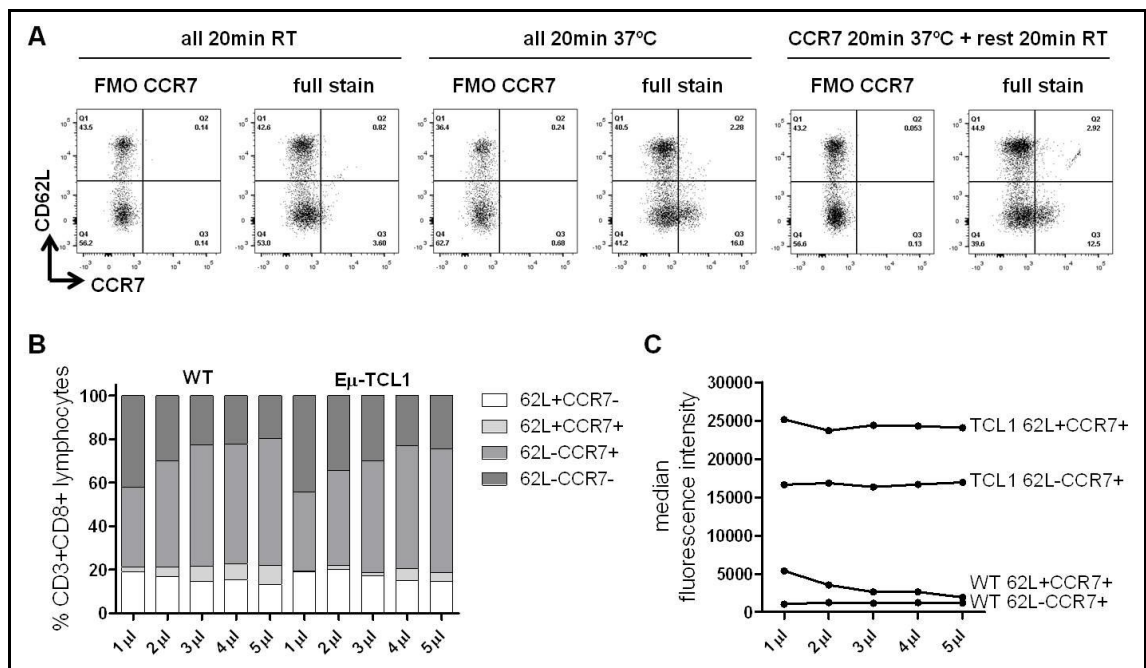


**Figure 11: Optimization of CCR7 4B.12 antibody. (A)** TCL1 spleen cells were stained with a cocktail of anti-CD3, 4, 8, 44, 62L and CCR7 antibodies (full stain) for 20 minutes at room temperature (RT), at 37°C, or with CCR7 for 20 minutes at 37°C followed by 20 minutes staining at RT with the remaining cocktail. Fluorescence-minus-one (FMO) controls for CCR7 were included for all conditions. Incubation at 37°C resulted in better resolution of positive and negative populations, and could be further improved by consecutive 37°C/ RT staining. **(B)** WT and TCL1 spleen cells were then stained at 37°C for 20 minutes followed by 20 minutes RT for the remaining cocktail using decreasing concentrations of CCR7. 3 to 5 μl resulted in comparable resolution of CCR7+ populations, while brightness measured by median fluorescence intensity of CCR7-PeCy7 was not enhanced **(C)**.

Samples were acquired on a BD LSR II. Stopping gates were set to record at least 12,000 CD3+CD8+ events. An example of the gating strategy to identify naïve vs. antigen-experienced effector and memory, as well as CM and EM CD8 T cells, is depicted in Figure 12. Cells were gated on viable (*i.e.* DAPI-negative) single mononuclear cells (MNC) (Figure 12 B). CD4 and CD8 were gated on CD3+ lymphocytes (Figure 12 C), and CD8 subsets were gated on CD3+CD8+ MNC. Naïve

cells were identified as CD44<sup>low</sup>+CD62L<sup>+</sup> and antigen-experienced cells as CD44<sup>+</sup>, with memory cells being CD62L<sup>+</sup>CD44<sup>high</sup>+ and effector cells being CD44<sup>medium/high</sup>+CD62L<sup>low</sup>+. EM and CM cells were characterized based on CD62L/CCR7 expression. FMO controls for CD44 and CCR7 were included in all experiments (Figure 12 D).

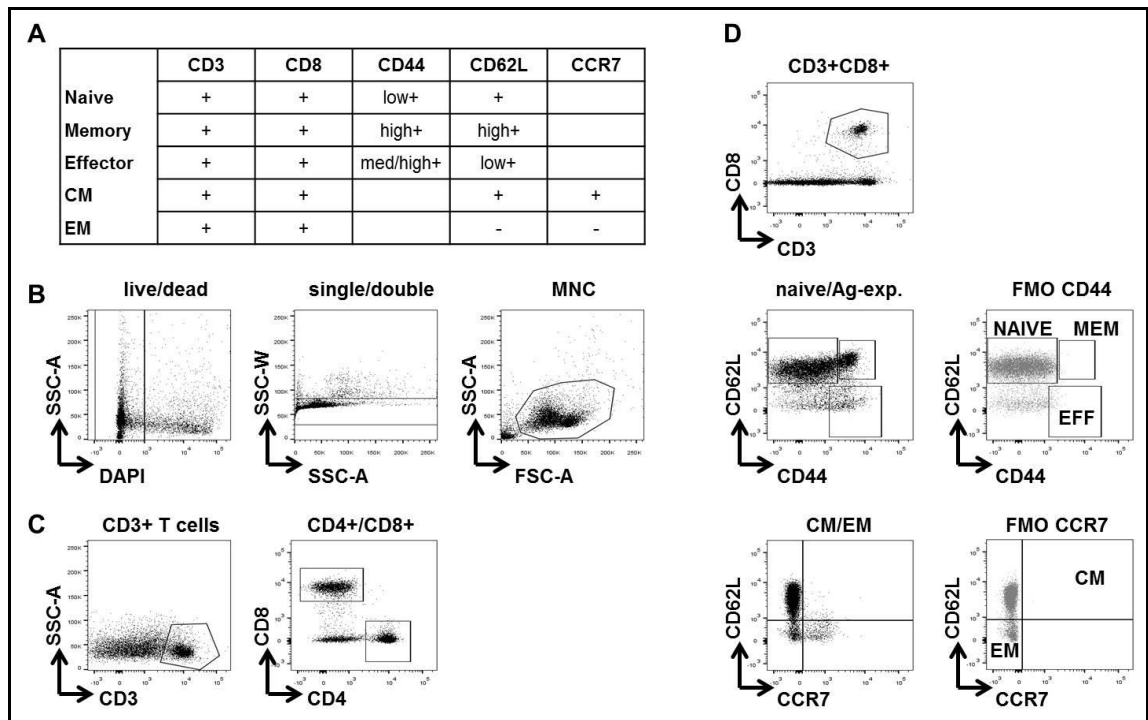


**Figure 12: Gating strategy to identify naive vs. antigen-experienced effector, memory, central memory (CM) and effector memory (EM) CD8 T cells. (A)** Summary of expression patterns and surface antigens to identify cell subsets. **(B)** Cells were gated on DAPI-negative single mononuclear cells (MNC). **(C)** CD4 and CD8 were gated on CD3+ MNC. **(D)** Naive, antigen-experienced (Ag-exp.), EM and CM cells were gated on CD3+CD8+ MNC, and fluorescence-minus-one (FMO) controls for CD44 and CCR7 were included in all experiments.

### 5.3.3 Multicolour flow cytometry for intracellular cytokines and effector function

For these studies, T-cell subsets were characterized based on the surface expression of CD3, CD8 and CD44 to allow a basic discrimination between naïve CD44<sup>-</sup> and antigen-experienced CD44<sup>+</sup> cells. Cytotoxicity was assessed by measuring CD107a effector cell degranulation and intracellular Granzyme B (GrB). Intracellular IFN- $\gamma$ , IL-2 and IL-4 were selected as representative Th1/Th2 cytokines and cytokines that our group has identified to be aberrantly produced by CD8<sup>+</sup> T cells in humans<sup>133</sup>. *Ex vivo* proliferation was measured by intranuclear ki67. Information on antigens,

fluorochromes, clones, concentrations and suppliers is listed in Table 10. Up to  $1 \times 10^6$  fresh spleen cells were kept in 250 $\mu$ l RPMI 1640 with 10% FCS (Sigma), 1% Penicillin/Streptomycin, 1% Glutamine (both LifeTechnologies), and 500mM beta-mercaptoethanol (Gibco) in round-bottom 96-well-plates (VWR). 5 $\mu$ g/ml CD107a was added to each well, and cells were stimulated with 500X PMA/Ionomycin cell stimulation cocktail (eBioscience, UK) for 6 hours at 37°C/5% CO<sub>2</sub>, while 500X brefeldin A/monensin protein transport inhibitor cocktail (eBioscience, UK) was added for the last 5 hours of culture. Controls included wells with CD107a and protein transport inhibitor cocktail, but no cell stimulation cocktail, for each mouse. After the incubation, cells were harvested and processed as described in Chapter 3.4.2. Cells were then washed, and unstimulated wells were split for cytokine and ki67 stains. After fixation and permeabilisation as described in Chapter 3.4.2, cells were stained with intracellular and intranuclear antibodies for 1h at 4°C at a 1:100 dilution. All steps were performed in a 96-well plate.

	mouse antigen	fluorochrome	clone	concentration	host/ isotype	supplier
surface stain	CD3e	APCCy7	17A2	0.2 mg/ml	rat IgG2bk	Biolegend
	CD8a	BV605	53-6.7	0.5 mg/ml	rat IgG2ak	Biolegend
	CD44	AF700	IM7	0.2 mg/ml	rat IgG2bk	eBioscience
cytotoxicity	CD107a	PE	eBio1D4B	0.2 mg/ml	rat IgG2ak	eBioscience
	GrB	e450	NGZB	0.2 mg/ml	rat IgG2ak	eBioscience
intracellular cytokines	IFN- $\gamma$	AF488	XMG1.2	0.5 mg/ml	rat IgG2ak	eBioscience
	IL-2	PeCy7	JES6-5H4	0.2 mg/ml	rat IgG2bk	eBioscience
	IL-4	PerCPeFl 710	11B11	0.2 mg/ml	rat IgG1k	eBioscience
proliferation	ki67	PeCy7	SolA15	0.2 mg/ml	rat IgG2ak	eBioscience

**Table 10: Summary of antigens, fluorochromes, clones, concentrations and suppliers used to assess T-cell function in relation to CLL.**

IFN- $\gamma$ , IL-2 and IL-4 were gated on CD3+ viable single MNC and plotted against CD8 (Figure 13 A). CD107a, GrB and IFN- $\gamma$  were gated on viable single CD3+CD8+ MNC and plotted against CD44 (Figure 13 B). Unstimulated cells were used as internal controls to determine correct gate positions. Ki67 was plotted against CD44 and gated on CD3+CD8+ viable single MNC, with FMO ki67 as control (Figure 13 C). CD44 was included as a marker to discriminate between naïve and antigen-experienced cells. Stopping gates were set to CD3+CD8+ cells to record at least 10,000 events, or until the sample had been fully aspirated, whichever occurred first. Differences in T-cell

function between mice with CLL and age-matched WT mice, and between mice of different age groups, were compared by calculating ratios between CD44<sup>+</sup> antigen-experienced cells positive for a cytokine/CD107a/GrB/ki67 and CD44<sup>+</sup> antigen-experienced cells negative for the same marker. Similar comparisons were made, where applicable, among CD44<sup>-</sup> naïve cells (Figure 13 D). Biologically, this describes differences and changes in cell subsets that maintain the ability to exert effector cell function compared to cells of the same subset that do not have this ability within one experimental group. In the context of shifting overall cell subsets with CLL compared to WT, direct comparisons of e.g. CD44<sup>+</sup>CD107a<sup>+</sup> cells of leukaemic mice to CD44<sup>+</sup>CD107a<sup>+</sup> cells of healthy mice might be less accurate, and are likely to not properly reflect the true biological impact of such changes.

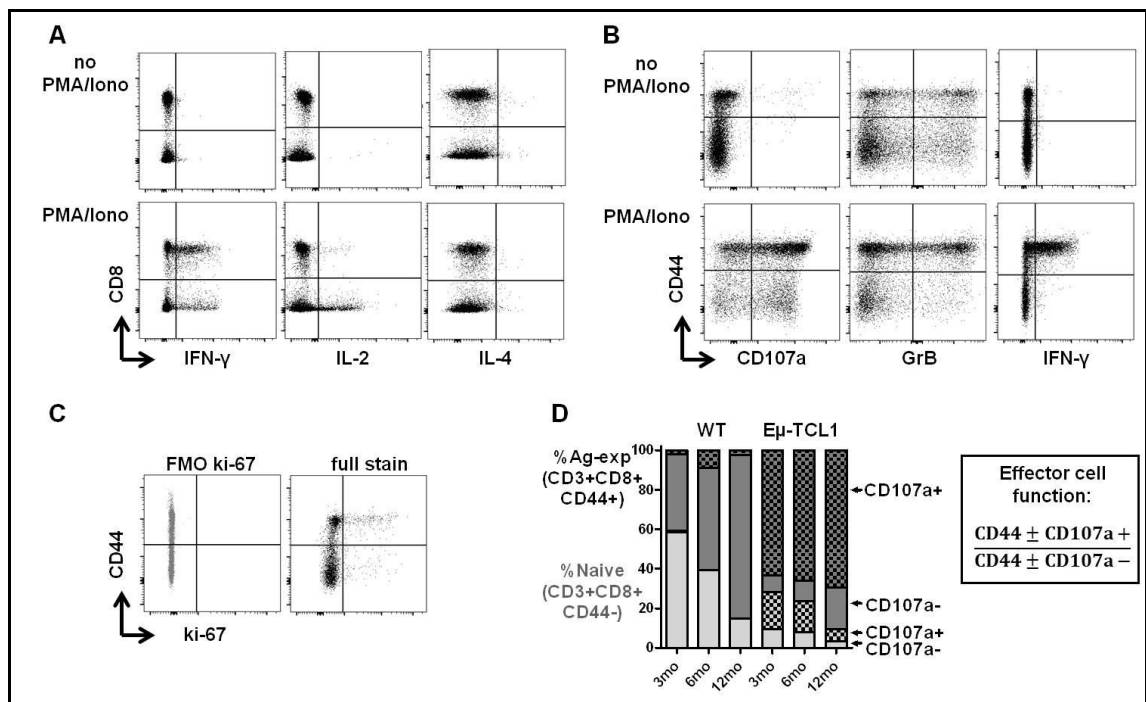


**Figure 13: Gating strategy for functional T-cell assays.** (A) Intracellular cytokines were gated on CD3<sup>+</sup> viable single MNC, plotted against CD8, and compared between unstimulated and mitogen-stimulated cells for each animal. (B) Effector cell cytotoxicity was gated on CD3<sup>+</sup>CD8<sup>+</sup> viable single MNC, plotted against CD44 and compared between unstimulated and mitogen-stimulated cells for each animal. (C) Intranuclear ki67 was gated on CD3<sup>+</sup>CD8<sup>+</sup> viable single MNC and plotted against CD44. (D) Because of overall shifting cell subsets with CLL development and additional dynamics in the context of ageing (as depicted in the graph), changes in T-cell effector function were compared by calculating ratios between cytotoxic cells (CD107a<sup>+</sup>, selected as an example but representative for cytokines, GrB and ki67) and non-cytotoxic cells (CD107a<sup>-</sup>) among CD44<sup>+</sup> or CD44<sup>-</sup> subsets within one experimental group. The ratios of experimental groups were then compared to each other to describe changes in the ability of cells to exert certain effector functions.

### 5.3.4 Multicolour flow cytometry for *in vivo* proliferation

In addition to intranuclear ki67, we measured *in vivo* proliferation by EdU incorporation. Preparation of EdU, injection of mice, and processing of samples and cells are described in Chapter 3.4.4.2.3. Cells were surface stained with CD19 v450 (clone 1D3, BD, UK), CD5 PE (clone 53-7.3, eBioscience, UK), CD8 BV605 (clone 53-6.7, Biolegend, UK) and PD-1 APC (clone RMP11-30, eBioscience, UK) for 20 minutes at room temperature, washed again and resuspended in 300µl FACS buffer. Samples were acquired on a BD LSRII, cells were gated on single MNC, and stopping gates were set to CD5+ cells. CD5 was plotted against CD19 to discriminate between double positive CLL cells, CD19+ B cells, and CD5+ T cells. CD8+ and CD8- cells were then gated on CD5+ cells. An example of the gating strategy is shown in Figure 14. Proliferating cells were identified as Alexa488 positive populations, based on negative internal controls without Alexa488 in the Click-iT cocktail.

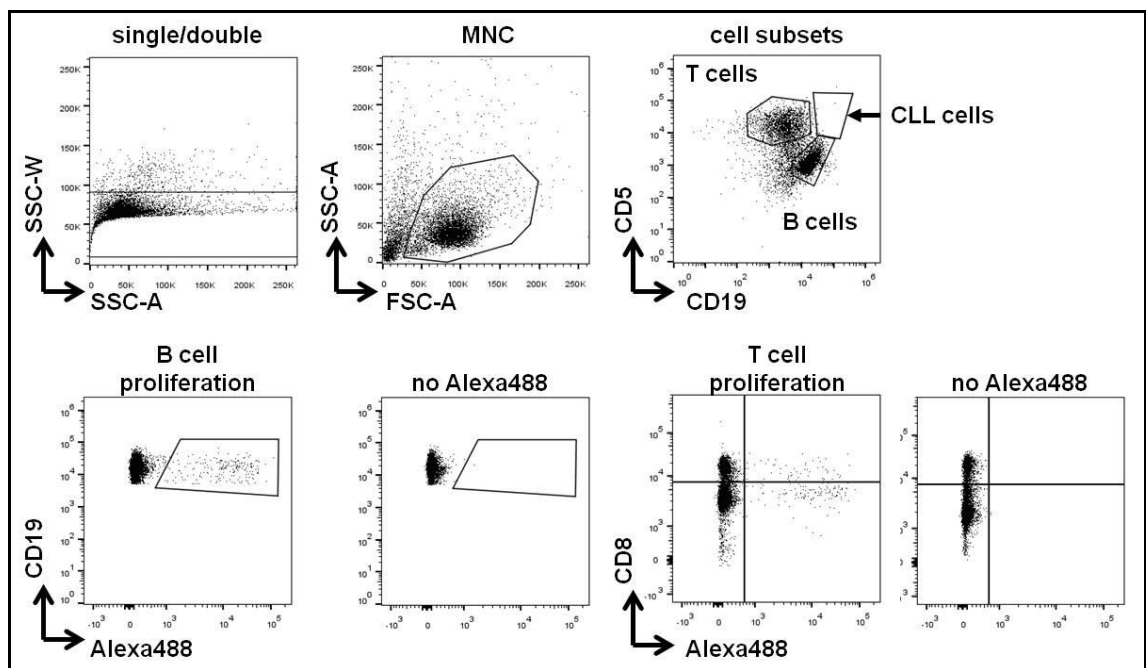


**Figure 14: Gating strategy for EdU *in vivo* proliferation.** Fixed and permeabilised spleen cells were incubated with a Click-iT reaction cocktail with and without Alexa488 azide dye, followed by surface staining for CD5, 19 and 8. Cells were gated on single MNC, and B, T and CLL cells were identified based on CD19 and CD5 expression. B-cell and T-cell proliferation, as well as CLL proliferation (not shown in these plots as example is taken from 3 month old WT mouse without a CLL population) were assessed by Alexa 488 expression. Gates were determined based on samples without Alexa488 staining.

## 5.4 Results

### 5.4.1 CLL progressively develops in transgenic TCL1 mice but shows considerable biological diversity, and can be consistently induced by AT in peripheral blood and secondary lymphoid organs

While young TCL1 mice on both backgrounds were free of CLL, at the age of 6 months, single cell suspensions from spleen, PB, and BM, but not LN started to be enriched for CD19+CD5+ cells. This progressed further with ageing in both the B6 and C3H backgrounds as expected, but considerable biological diversity was observed: among the 12 month old TCL1 cohorts examined, the median CLL load in spleen was 16.5% in group 7<sub>a</sub> (see Table 8), 62.4% in group 7<sub>funct</sub> and 32.3% in group 11, with ranges of 8.4-25.8% (group 7<sub>a</sub>), 8.2-76.8% (group 7<sub>funct</sub>) and 9.8-77.8% (group 11). Similarly wide ranges were detected in other organs, but spleen and PB appeared to be the major compartments/organs of disease, exhibiting the highest median percentages of CD19+CD5+ cells. While these observations validate the backcrossed B6 background, they also underscore the differences in disease behaviour and indicate that even within littermates, some mice can already have late-stage CLL whereas others can still be found to have a relatively low burden of disease. In experiments using aged-matched WT mice, we routinely confirmed the absence of CLL in all examined organs.

As described in Chapter 4, AT resulted in consistent CLL development in virtually all recipient mice. Uniformity of disease load was superior to ageing TCL1 mice, even when combining different AT experiments with different donors into the same analysis. The only exception were LNs, where the relative frequency of CD19+CD5+ lymphocytes was lower than in 12 month old leukaemic TCL1 mice (AT median 2.4%, range 0.3-21.9, *versus* 12 month TCL1 median 7.0%, range 1.6-16.6,  $p=0.0083$ ). However, LNs also appeared to have a longer disease latency and lagged behind other organs in ageing leukaemic TCL1 transgenic mice, as there was no difference in LN disease involvement between 3 month old (median 0.7%, range 0.3-1.8) and 6 month old (median 0.6%, range 0.4-4.8) transgenic mice ( $p=0.4023$ ). Thus, although AT might not mirror the rate of leukaemic development in LNs observed in ageing TCL1 transgenic mice, this model still appears more than adequate to model immune cell interactions with the LN microenvironment.

We conducted all comparisons in individual ageing TCL1 transgenic mice and AT mouse cohorts separately. As the overall trend was found to be very similar within cohorts, making the existence of a batch effect unlikely, we combined cohorts for

statistical analyses to consolidate their statistical power. Figure 15 A depicts a summary of CLL development in combined cohorts of different age groups. Data is depicted as median with interquartile range. Figure 15 B summarizes statistical differences in the relative expansion of the CD19+CD5+ cell subset compared to 3 month old TCL1 mice as baseline.

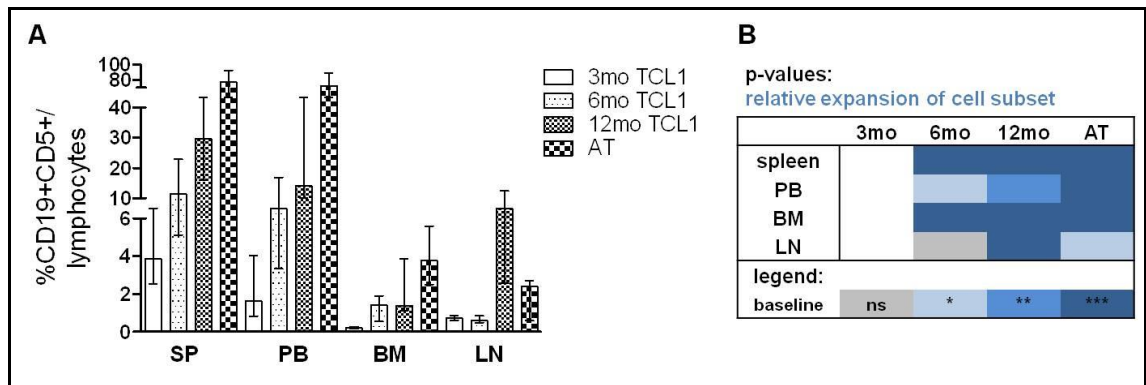


**Figure 15: CLL development in ageing TCL1 mice and after AT in peripheral blood (PB) and secondary lymphoid organs.** PB and single cell suspensions from bone marrow (BM), lymph nodes (LN) and spleen (SP) of 3, 6 and 12 month old TCL1 mice and AT mice were stained for CD19 and 5 to determine disease load. **(A)** CLL progressively developed in TCL1 mice but showed considerable biological diversity. Disease could be more consistently induced by AT, but CLL load in LN was lower than in ageing TCL1 mice. Graph depicts median with interquartile range (IQR). **(B)** Heatmap summary of p-values describing statistical differences in the organ CLL load. Groups were compared to the relative percentage of CD19+CD5+ cells in 3 month old mice. Blue colour indicates relative expansion of cell subsets. ns = not-significant; \* $p < .05$ , \*\* $p < .001$ , \*\*\* $p < .0001$ . Mann-Whitney test was used for non-normally distributed data and unpaired t-test for normally distributed data, as determined by Shapiro-Wilk normality test.

#### 5.4.2 Developing CLL is associated with significant changes in relative and absolute numbers of T-cell subsets in spleen

We next examined changes in T-cell phenotype in organs from ageing TCL1 transgenic and AT mice. Groups of experimental animals are summarized in Table 8 under “I. Available mice to assess T-cell phenotype in spleen alongside developing CLL”. We first focused on the spleen in B6 and C3H TCL1 mice, and then compared B6 TCL1 mice to age- and sex-matched B6 WT mice. C3H WT mice were not examined, as the primary focus of these experiments was to validate the B6 TCL1 by direct comparison of relative patterns to the C3H TCL1 model, and then compare relative and absolute changes between B6 TCL1 to WT mice in a second step. In addition, our colony did not produce sufficient numbers of C3H WT littermates to allow us to easily include them as controls, as we had received C3H TCL1 mice bred to homozygosity from our collaborators. Although we altered the breeding strategy for the B6 background by

breeding TCL1 mice with WT mice, as discussed in the previous chapter, we did not pursue this for the C3H background due to time and cost considerations. For the same reason, we decided against purchasing aged B6C3H-F1 WT mice from commercial suppliers, as we believed this would not have added significant information to further the project.

In ageing transgenic mice of both backgrounds, we observed a loss in the percentage of CD3<sup>+</sup> T cells among all lymphocytes with increasing CLL burden, with the greatest range at the age of 12 months (data not shown), which is in line with the biological diversity of CLL development described in Chapter 5.4.1. Within CD3<sup>+</sup> cells, the CD4<sup>+</sup>/CD8<sup>+</sup> ratio decreased with developing CLL (Figure 16 A) as a result of a combination between an expansion of CD3<sup>+</sup>CD8<sup>+</sup> cells and a reduction of CD3<sup>+</sup>CD4<sup>+</sup> cells (data for percentages of CD3<sup>+</sup>, CD4<sup>+</sup> and CD8<sup>+</sup> cells not shown). This was more clearly recapitulated in ageing B6 TCL1 than in C3H TCL1 mice, and could be induced by AT in young TCL1 mice as well as in young WT mice. In ageing WT mice, the relative frequencies of CD3<sup>+</sup> and CD4<sup>+</sup> cells were constant, but CD8<sup>+</sup> cells were lost. This led to an increase of the CD4<sup>+</sup>/CD8<sup>+</sup> ratio (Figure 16 A), which is in marked contrast to the CLL-driven inversion observed in TCL1 mice. In line with the CLL-associated organomegaly, absolute numbers of CD3<sup>+</sup>, CD4<sup>+</sup> and CD8<sup>+</sup> cells increased in ageing B6 TCL1 and after AT in young WT mice, while remaining largely constant or being reduced in ageing WT mice (note: analysis of absolute numbers was only conducted for B6 TCL1 and WT mice but not for C3H TCL1 mice, Figure 16 B and Table 11).

Within the CD3<sup>+</sup>CD8<sup>+</sup> compartment, naïve T cells were lost (*i.e.* their percentage decreased), and shifted towards antigen-experienced cells (*i.e.* their percentage increased). In 12 month old B6 TCL1 mice, antigen-experienced CD3<sup>+</sup>CD8<sup>+</sup> T cells appeared slightly shifted towards a memory phenotype (memory median 54.22% range 34.16-61.65, effector median 41.56% range 30.88-57.36), but this was not-significant ( $p=.0931$ ), while in 12 month old C3H TCL1 mice and all AT mice these cells were more skewed towards an effector phenotype (C3H memory median 23.87% range 21.22-41.41, effector median 32.49% range 20.75-41.06; AT WT memory median 10.92% range 7.96-15.69, effector median 54.84% range 51.77-70.88; AT B6 TCL1 memory median 30.99% range 23.13-40.98, effector median 51.63% range 29.82=57.94; AT C3H TCL1 memory median 21.99% range 9.08-32.72, effector median 53.5% range 51.87-64.46; Figure 16 C). In AT mice, however, the transgene status of the recipients (*i.e.* WT or TCL1) influenced if the relative number of memory cells was reduced or expanded. WT recipients appeared to lose memory cells

compared to 3 month old WT controls, showing a reduced frequency of CD44<sup>+</sup>CD62L<sup>+</sup>CD3<sup>+</sup>CD8<sup>+</sup> cells; this population, however, was expanded in young TCL1 recipients compared to healthy young TCL1 controls, while 3 month old healthy TCL1 (median 17.56%, range 14.6-35.68) and WT (median 19.58%, range 11.58-32.02) mice showed comparable percentages of memory cells. This observation indicates that the expression of the transgene itself might influence memory distribution in the context of adoptive transfer. Ageing WT mice also had decreased naïve cells and demonstrated a shift towards antigen-experienced cells, with memory and effector CD8<sup>+</sup> cells being equally distributed (memory median 30.04%, range 15.02-28.35 vs. effector median 36.22%, range 27.2-64.66,  $p=.065$ , Figure 16 C).

Similar to absolute numbers of CD3<sup>+</sup>, CD4<sup>+</sup> and CD8<sup>+</sup> cells, the absolute numbers of effector and memory cells increased in ageing B6 TCL1 and after AT in young WT mice, but decreased for naïve CD3<sup>+</sup>CD8<sup>+</sup> T cells in ageing B6 TCL1 mice and increased after AT (Figure 16 D and Table 11). Comparing absolute numbers also demonstrated that although the relative naïve *versus* antigen-experienced shift was to a certain extent also observed in ageing WT mice, there were clear differences in the absolute expansion of effector and memory subsets.

Statistical differences in the relative expansion of T-cell subsets compared to 3 month old mice as baseline are visualized in Figure 16 E.

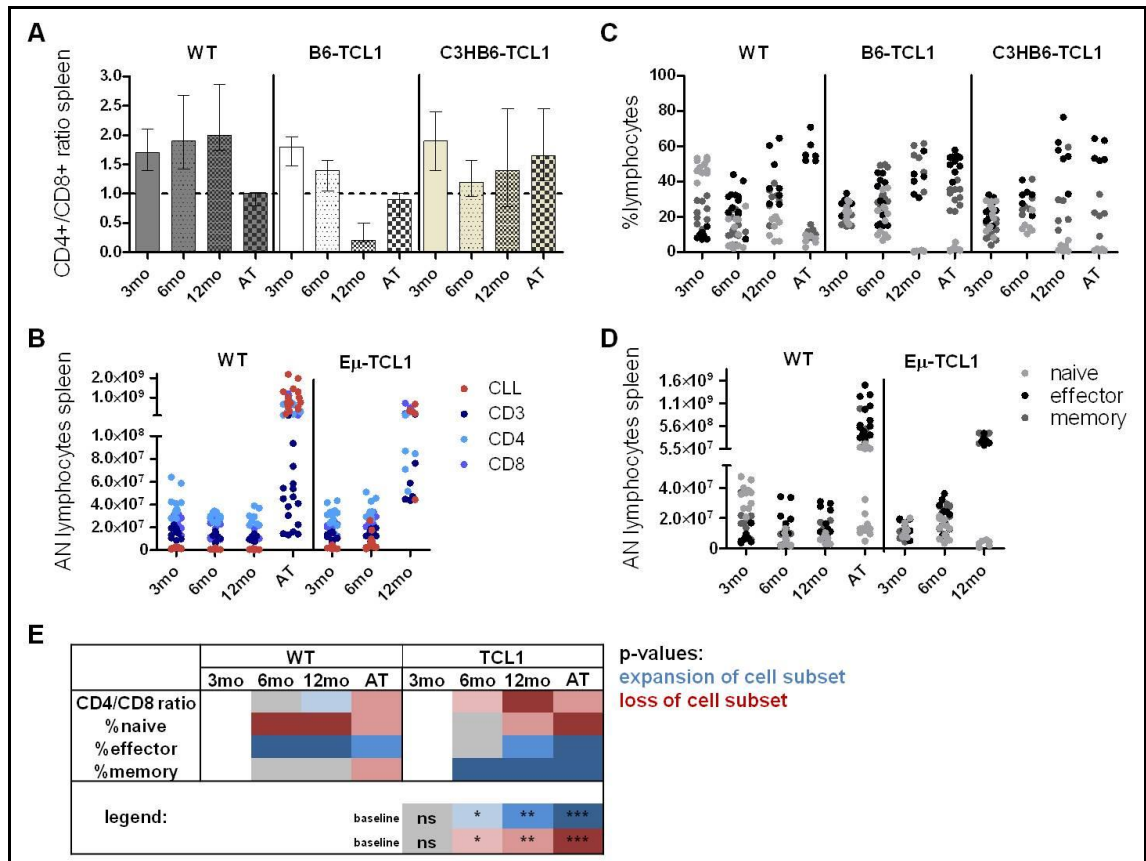


**Figure 16: T-cell subset changes in ageing TCL1 mice and after AT in spleen.** Cohorts of 3, 6 and 12 month old TCL1, WT and AT mice were sacrificed and single cell suspensions of spleen were stained for CD3, 4, 8, 62L and 44. Dead cells were excluded by DAPI. **(A)** With increasing CLL the CD4+/CD8+ ratio decreased, while age-matched WT mice showed an increase of the CD4+/CD8+ ratio. This was more clearly recapitulated in B6 TCL1 than in C3H TCL1 mice, but could be induced by AT in both young TCL1 and WT mice. **(B)** Absolute numbers (AN) increased, in line with CLL-associated organomegaly. **(C)** Within CD3+CD8+ cells, naïve cells were lost and shifted towards antigen-experienced cells. Naïve cells were also reduced and shifted towards antigen-experienced cells in WT mice. **(D)** AN of these subsets were significantly increased in TCL1 mice. **(E)** Heatmap summary of p-values describing statistical differences in T-cell subsets. Groups were compared to 3 month old mice. Blue colour indicates expansion, red colour indicates loss of cell subsets. ns = non-significant, \*p<.05, \*\*p<.001, \*\*\*p<.0001. Mann-Whitney test was used for non-normally distributed data and unpaired t-test for normally distributed data, as determined by Shapiro-Wilk normality test.

absolute numbers of cell subset		B6 WT			B6 TCL1			
		3mo	6mo	12mo	3mo	6mo	12mo	AT
CD3+	med	1.56E+07	1.29E+07	9.34E+06	1.49E+07	1.36E+07	5.30E+07	4.31E+07
	min	1.07E+07	7.59E+06	8.01E+06	1.09E+07	1.09E+07	4.44E+07	1.77E+07
	max	1.91E+07	1.43E+07	1.28E+07	1.56E+07	1.83E+07	9.50E+07	5.74E+07
CD3+ CD4+	med	3.58E+07	2.89E+07	2.75E+07	3.07E+07	3.00E+07	8.59E+07	3.92E+08
	min	3.30E+07	2.49E+07	2.22E+07	2.39E+07	2.66E+07	6.61E+07	2.92E+08
	max	4.25E+07	3.26E+07	3.52E+07	3.44E+07	4.07E+07	1.33E+08	5.83E+08
CD3+ CD8+	med	2.33E+07	1.49E+07	1.29E+07	1.71E+07	2.28E+07	3.17E+08	4.12E+08
	min	1.62E+07	9.56E+06	1.06E+07	1.50E+07	1.91E+07	2.70E+08	3.32E+08
	max	2.88E+07	2.18E+07	1.31E+07	2.14E+07	2.77E+07	5.53E+08	6.86E+08
CD3+ CD8+ effector cells	med	6.97E+06	1.28E+07	2.08E+07	1.45E+07	1.97E+07	2.15E+08	5.37E+08
	min	3.58E+06	3.42E+06	1.09E+07	4.99E+06	8.11E+06	1.32E+08	1.40E+08
	max	1.69E+07	3.42E+07	3.10E+07	1.94E+07	3.63E+07	3.92E+08	1.45E+09
CD3+ CD8+ memory cells	med	1.65E+07	7.09E+06	1.41E+07	1.08E+07	2.23E+07	2.78E+08	1.96E+08
	min	5.69E+06	1.91E+06	7.21E+06	4.21E+06	1.30E+07	1.71E+08	8.09E+07
	max	3.71E+07	1.21E+07	1.85E+07	1.48E+07	2.95E+07	4.01E+08	9.34E+08
CD3+ CD8+ naive	med	1.74E+07	2.43E+07	7.48E+06	2.65E+07	1.89E+07	1.90E+07	1.19E+08
	min	9.67E+06	2.02E+07	1.11E+06	1.44E+07	9.86E+06	9.61E+06	6.42E+07
	max	3.03E+07	3.19E+07	3.18E+07	3.34E+07	3.70E+07	3.43E+07	1.89E+08

**Table 11: Summary of changes in absolute numbers of T-cell subsets in spleen.** med=median, min=minimum, max=maximum.

We confirmed that these patterns were recapitulated in an additional round of experiments (summarized in Table 8 as “III. Available mice to assess T-cell phenotype in organs alongside developing CLL”). As outlined in Chapter 5.3.1, these experiments consisted of a substantially larger multicolour panel for spleen, included CM and EM cells, used different fluorochromes/antigen conjugates, and were restricted to B6 TCL1 and B6 WT mice. These experiments confirmed the previously observed changes, *i.e.* the decrease of the CD4+/CD8+ ratio with developing CLL and after AT in young WT mice, while this was stable and increased slightly in ageing WT mice (Figure 17 A), the increase of absolute numbers of CD3+, CD4+ and CD8+ T cells (Figure 17 B), the shifts in naive and antigen-experienced CD3+CD8+ T cells (Figure 17 C) and their increases in absolute numbers (Figure 17 D) in mice with CLL. In AT mice, which were WT recipients, the previously observed relative loss of CD3+CD8+ memory cells compared to age-matched healthy controls was confirmed.

The most significant output of these experiments, however, was the additional information on CM and EM subsets, which revealed major differences between healthy and leukaemic mice: while both subsets showed relative expansion in ageing WT mice (CM 3 month median 2.89%, 6 month 2.86%, 12 month 7.78%; EM 3 month median

7.21%, 6 month 8.67%, 12 month 36.03%), CM were decreased in ageing TCL1 mice and after AT (3 month median 11.04%, 6 month 11.68%, 12 month 3.36%, AT 1.4%), and cells were shifted towards an expanded EM subset (3 month median 5.42%, 6 month 10.9%, 12 month 14.23%, AT 55.26%; Figure 17 C). Absolute numbers of CM and especially EM CD3+CD8+ cells increased in mice with CLL (Figure 17 D and Table 12).

Statistical differences in the relative expansion of T-cell subsets compared to 3 month old mice as baseline are summarized in Figure 17 E. Absolute numbers of CD3+CD8+ CM and EM cells are summarized in Table 12.

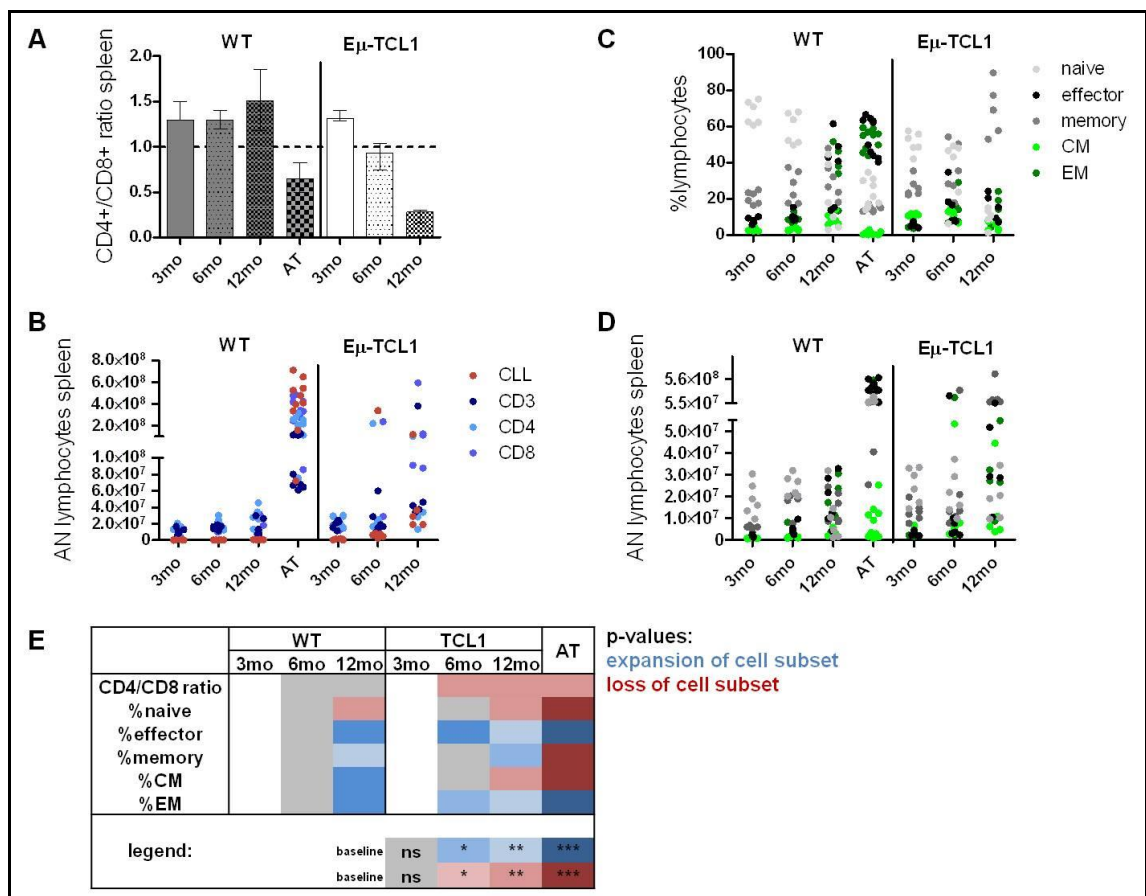


**Figure 17: Confirmation of T-cell subset changes in ageing TCL1 and WT mice and after AT in spleen. (A)** Confirmation of decreased CD4+/CD8+ ratio in mice with CLL and **(B)** increase of absolute CD3+, CD4+ and CD8+ T cells numbers (AN). **(C)** Confirmation of loss of CD3+CD8+ naive cells and shift towards antigen-experienced cells. In WT mice, CM and EM subsets expanded with ageing, while CM were lost in ageing TCL1 mice and after AT and EM expanded. **(D)** AN of these cell subsets were significantly increased in mice with CLL. **(E)** Heatmap summary of p-values describing statistical differences in T-cell subsets. ns = non-significant, \*p<.05, \*\*p<.001, \*\*\*p<.0001.

absolute numbers of cell subset		B6 WT			B6 TCL1			AT
		3mo	6mo	12mo	3mo	6mo	12mo	
CM	med	8.33E+05	1.25E+06	4.22E+06	5.61E+06	5.63E+06	6.20E+06	6.21E+06
	min	6.03E+05	8.68E+05	1.84E+06	2.93E+06	2.76E+06	3.70E+06	7.03E+05
	max	9.05E+05	1.95E+06	5.85E+06	6.73E+06	5.33E+07	4.44E+07	2.52E+07
EM	med	1.95E+06	3.37E+06	1.44E+07	2.37E+06	4.94E+06	2.72E+07	3.49E+08
	min	1.06E+06	2.13E+06	3.56E+06	1.57E+06	2.14E+06	8.66E+06	8.12E+07
	max	2.67E+06	8.04E+06	3.05E+07	3.80E+06	1.71E+08	5.48E+07	5.29E+08

**Table 12: Summary of changes in absolute numbers of T-cell subsets in spleen.** med=median, min=minimum, max=maximum, CM=central memory, EM=effector memory.

Altogether, these experiments suggested that some similarities in T-cell subset changes exist between ageing WT and ageing TCL1 mice. This implies that observations in ageing leukaemic mice might be confounded by the effects of ageing, as might be expected. However, clear patterns regarding T-cell subset shifts (*i.e.* CD4+/CD8+ ratio, effector, memory, CM and EM cells) and differences in absolute numbers appeared to be associated only with CLL and to develop alongside progressing disease. This was not only supported by the AT experiments, but also by the observation that CLL-specific T-cell patterns were recapitulated in a younger mouse in the 6 month old TCL1 cohort that already had advanced-stage CLL (CD19+CD5+ cells in spleen 57.4%). Together, these observations confirm that AT experiments allow the elimination of the confounding factor of ageing.

### 5.4.3 CLL-specific T-cell subset changes are recapitulated in peripheral blood

We next sought to determine if the phenotypic changes in spleen as the major organ of disease were recapitulated in other organs, where T cells are exposed to a different microenvironment. These experiments were repeated twice as described above for spleen, and the graphs depicted in the following chapters contain the combined data of these experiments, unless indicated otherwise. Just as in spleen, the CD4+/CD8+ ratio in PB decreased with increasing CLL tumour load and after AT (Figure 18 A) as a combined result of an expansion of CD3+CD8+ cells and a reduction of CD3+CD4+ cells (data for percentages of CD3+, CD4+ and CD8+ cells not shown). In ageing WT mice, the CD4+/CD8+ ratio also decreased, albeit not the degree observed in mice with CLL (12 month TCL1 median .09 range 0-.2 vs. 12 month WT median .59 range .11-1.1;  $p < .0001$ ). Absolute numbers of CD3+ T cells were largely constant in ageing WT mice (3 month median 2.9/ $\mu$ l blood, 6 month 3.4, 12 month 2.55) and increased in ageing TCL1 mice and moderately after AT (3 month median 3.5, 6 month 4.6, 12

month 17.3, AT 3.9). Absolute numbers of CD4+ were reduced in both ageing WT (3 month median 1.62, 6 month 1.32, 12 month .96) and ageing TCL1 mice and after AT (3 month median 1.46, 6 month 2.08, 12 month .98, AT .70), while CD8+ T cells were largely constant in ageing WT mice (3 month median 1.34, 6 month .64, 12 month 1.26) but increased in TCL1 and AT mice (3 month median 1.71, 6 month 2.14, 12 month 11.87, AT 2.49; note: analysis of absolute numbers was only conducted in the first experiment; Figure 18 B).

In mice with CLL, naïve CD3+CD8+ T cells were shifted towards antigen-experienced cells, which were generally skewed towards a memory phenotype in ageing TCL1 and in TCL1 mice with CLL after AT. In contrast, AT WT recipients were skewed towards an effector phenotype, as previously observed (Figure 18 C). Ageing WT mice also decreased naïve cells, however not to the same degree as ageing TCL1 mice (12 month TCL1 median 4.32% range, 1.15-13.32 vs. 12 month WT median 30.07%, range 1.17-60.09;  $p=.0024$ ).

Absolute numbers of naïve cells were largely stable in ageing WT mice (3 month .67, 6 month .63, 12 month .69) but decreased in ageing TCL1 mice and after AT (3 month median 1.28, 6 month .96, 12 month .62, AT .11; Figure 18 D). Both effector (3 month median .06, 6 month .1, 12 month 1.01, AT .68) and memory (3 month median .29, 6 month .76, 12 month 9.58, AT .94) CD3+CD8+ cells increased in ageing TCL1 mice and after AT.

Statistical differences in the relative expansion of T-cell subsets compared to 3 month old mice as baseline are summarized in Figure 18 E.

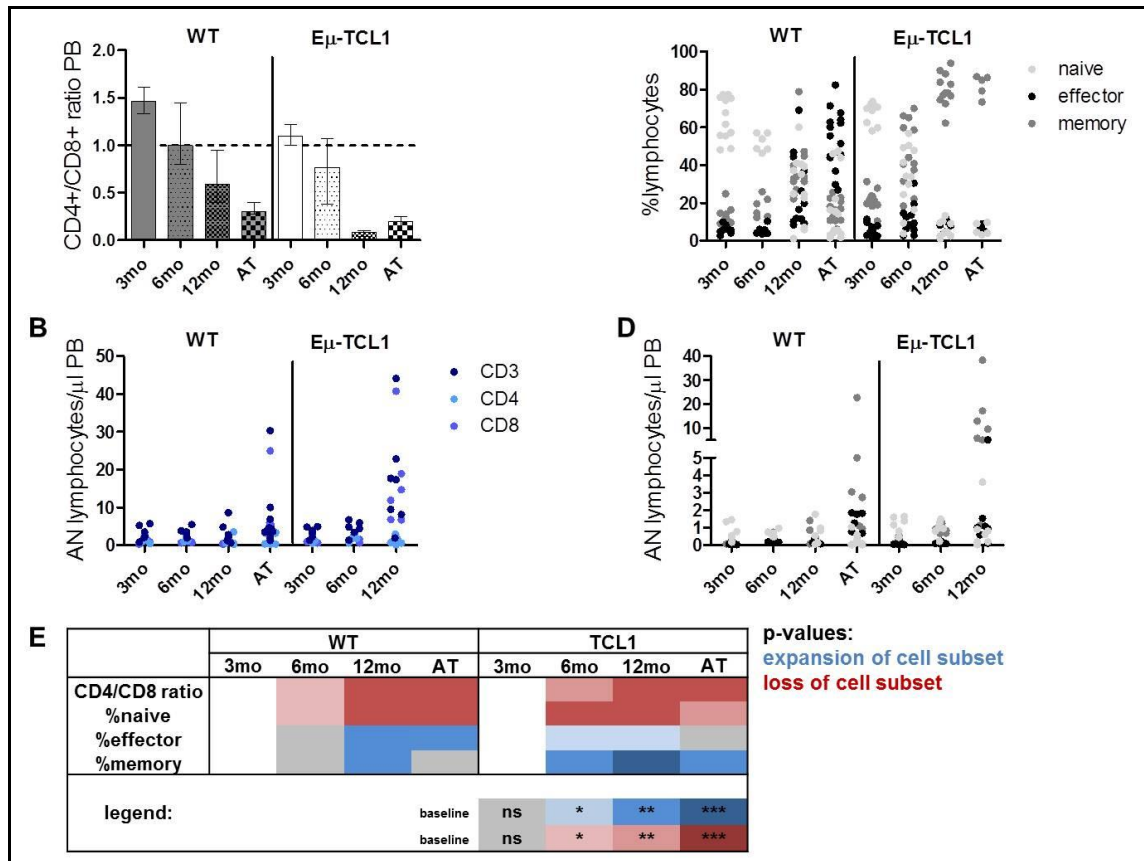


**Figure 18: Confirmation of T-cell subset changes in ageing TCL1 and WT mice and after AT in peripheral blood (PB).** (A) Confirmation of decreased CD4+/CD8+ ratio in mice with CLL and (B) changes of absolute CD3+, CD4+ and CD8+ T cells numbers (AN). (C) Confirmation of loss of CD3+CD8+ naïve cells and shift towards antigen-experienced cells in mice with CLL, and (D) changes in AN. (E) Heatmap summary of p-values describing statistical differences in relative frequencies of T-cell subsets. ns = non-significant, \*p<.05, \*\*p<.001, \*\*\*p<.0001.

#### 5.4.4 CLL-specific T-cell subset changes are recapitulated in bone marrow

Similar to spleen and PB, the CD4+/CD8+ ratio in BM decreased with increasing CLL tumour load and after AT (Figure 19 A), mainly due to an expansion of CD3+CD8+ cells while CD3+CD4+ cells remained largely stable. In WT mice, the CD4+/CD8+ ratio in 3 month old mice was relatively low due to a low percentage of CD4+ cells. This led to an increase of the ratio in ageing WT mice when compared to the 3 month old group, which however was consistent between 6 and 12 month old ageing WT mice. Absolute numbers of CD3+ cells increased in ageing TCL1 mice and after AT (3 month median 2.45/μl cell suspension, 6 month 6.25, 12 month 5.2, AT 6.6), just as CD4+ (3 month median .52, 6 month .75, 12 month 1.12, AT 1.33) and CD8+ cells (3 month median .67, 6 month 2.15, 12 month 2.02, AT 2.85; note: analysis of absolute numbers was only conducted in the first experiment; Figure 19 B).

In mice with CLL, naïve CD3+CD8+ T cells were shifted towards antigen-experienced and especially effector cells (Figure 19 C). The BM of ageing WT mice, in accordance to other organs, decreased naïve cells, again not to the same extent as ageing TCL1 mice with leukaemia (12 month TCL1 median 1.2%, range 0.07-3.74 vs. 12 month WT 7.68%, range 1.17-60.09;  $p=.0197$ ) and gained effector cells. However, the impact of CLL on T-cell subsets became again apparent when comparing absolute numbers in WT and leukaemic mice – absolute numbers of effector cells increased profoundly in mice with CLL (WT: 3 month median .12/ $\mu$ l cell suspension, 6 month .41, 12 month .66; TCL1: 3 month median .11, 6 month .66, 12 month 1.97, AT 2.53), while memory CD3+CD8+ cells only expanded moderately, as already indicated by the comparison of relative frequencies, in leukaemic TCL1 and AT mice compared to WT mice (WT 3 month median .31, 6 month 1.05, 12 month .46; memory TCL1: 3 month .33, 6 month 1.34, 12 month .88, AT .48; Figure 19 D).

Statistical differences in the relative expansion of T-cell subsets compared to 3 month old mice as baseline are summarized in Figure 19 E.

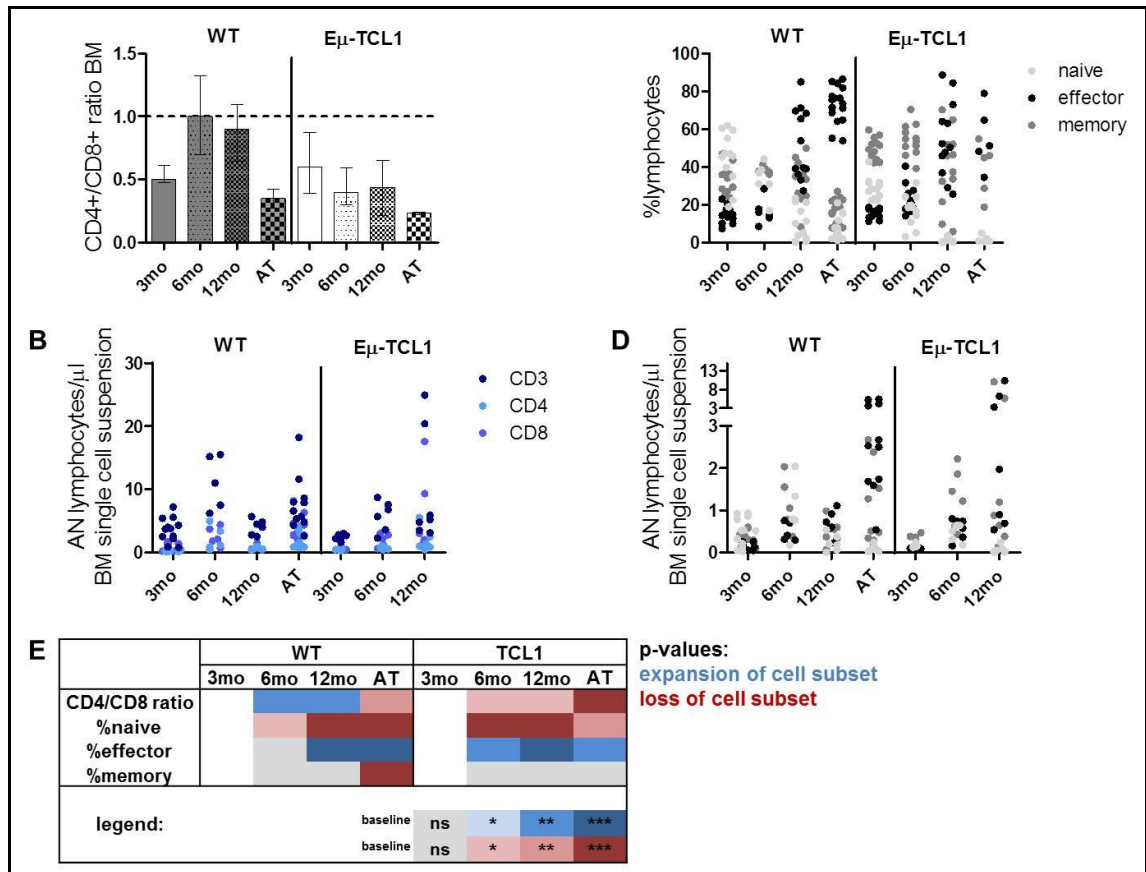


**Figure 19: T-cell subset changes in ageing TCL1 and WT mice and after AT in bone marrow (BM).** (A) Confirmation of decreased CD4+/CD8+ ratio in mice with CLL and (B) changes of absolute CD3+, CD4+ and CD8+ T cell numbers (AN). (C) Confirmation of loss of CD3+CD8+ naïve cells and shift towards antigen-experienced cells in mice with CLL, and (D) changes in AN. (E) Heatmap summary of p-values describing statistical differences in T-cell subsets. ns = non-significant, \*p<.05, \*\*p<.001, \*\*\*p<.0001.

### 5.4.5 T-cell subset changes exhibit particular patterns in lymph nodes

Minor differences in CLL-induced T-cell subset changes were observed in LN. While the CD4+/CD8+ ratio generally decreased in ageing TCL1 mice with developing CLL (Figure 20 A), 3 month old TCL1 mice had a high CD4+/CD8+ ratio (median 1.86, range 1.63-3.78), which was caused by an accumulation of CD4+ T cells in this cohort of mice (data for percentages of CD3+, CD4+, CD8+ cells not shown). In mice with CLL after AT, the CD4+/CD8+ ratio only decreased in TCL1 but not in WT recipients. Absolute numbers of CD3+ (3 month median 15.1/μl cell suspension, 6 month 11.1, 12 month 35.9, AT 51.1) and CD8+ (3 month median 3.68, 6 month 4.56, 12 month 28.81, AT 22.99) increased in leukaemic mice, but decreased in ageing WT mice (3 month CD3 median 20.15, CD8 6.8; 6 month CD3 21.8, CD8 9.35; 12 month CD3 3.5, CD8 1.45). Absolute numbers of CD4+ cells were reduced in both ageing WT (3 month 11.43, 6 month 11.32, 12 month 1.78) and ageing TCL1 mice (3 month 10.47, 6 month

5.74, 12 month 3.78), but not in AT mice (median 20.55, note: analysis of absolute numbers was only conducted in the first experiment; Figure 20 B).

Shifts from CD3+CD8+ naive to antigen-experienced cells were recapitulated in leukaemic mice, with memory cells being the dominant cell type (Figure 20 C). These patterns, however, were less clear in AT mice, with TCL1 but not WT recipients, recapitulating the predominance of memory cells in ageing TCL1 mice. In ageing WT mice, absolute numbers of effector cells were found to be largely stable (3 month median .09/ $\mu$ l cell suspension, 6 month .32, 12 month .1), but increased in ageing TCL1 mice and after AT (3 month median .09, 6 month .21, 12 month 1.01, AT 1.55; Figure 20 D). Similarly, absolute numbers of memory cells increased in ageing leukaemic mice and after AT (3 month median .67, 6 month 1.27, 12 month 21.04, AT 13.91), while being largely stable in WT mice (3 month median .88, 6 month 1.84, 12 month .39). Statistical differences in the relative expansion of T-cell subsets compared to 3 month old mice are summarized in Figure 20 E.

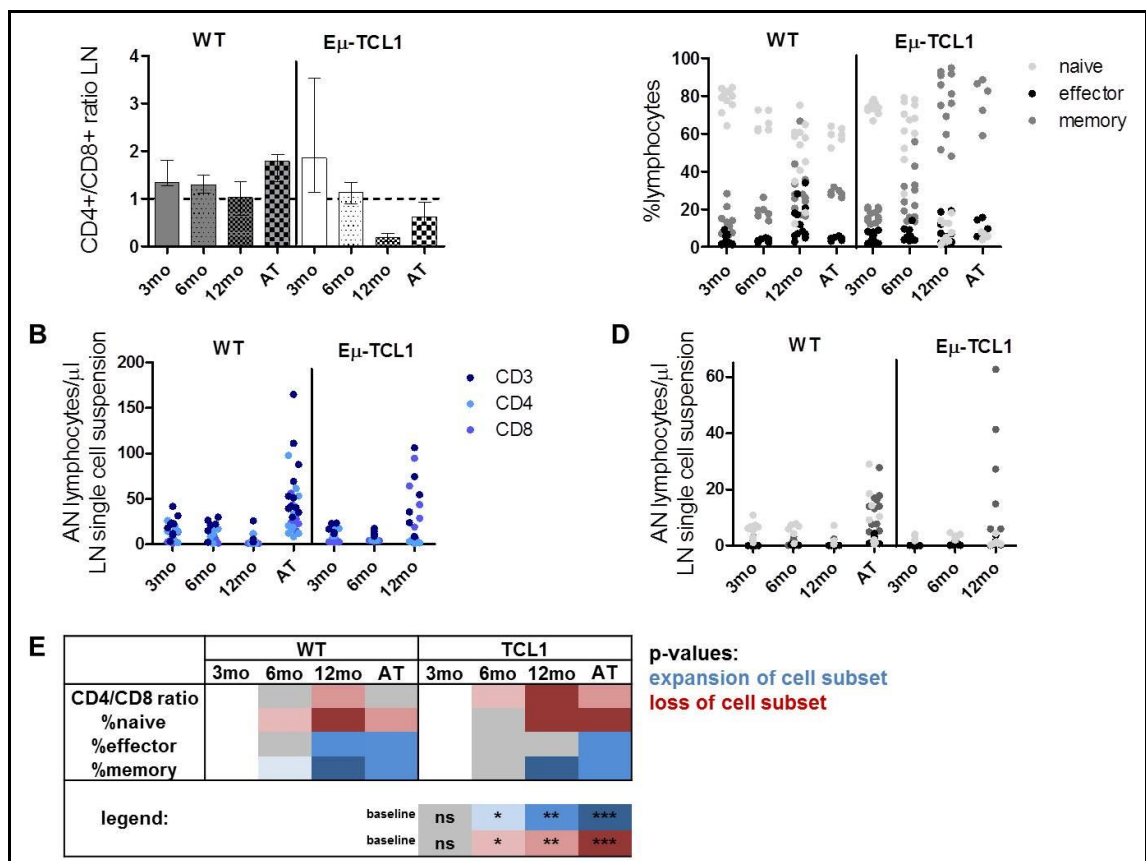


**Figure 20: T-cell subset changes in ageing TCL1 and WT mice and after AT in lymph nodes (LN).** (A) Confirmation of decreased CD4+/CD8+ ratio in ageing mice with CLL, and (B) changes of absolute CD3+, CD4+ and CD8+ cells numbers (AN). (C) Confirmation of loss of CD3+CD8+ naive cells and shift towards antigen-experienced cells in ageing mice with CLL and partly after AT, and (D) increase in AN. (E) Heatmap summary of p-values describing statistical differences in T-cell subsets. ns = non-significant, \*p<.05, \*\*p<.001, \*\*\*p<.0001.

#### 5.4.6 Developing CLL and CD3+, CD4+, CD8+ subset changes are significantly correlated with each other

After characterizing the development of T-cell subset changes over time, we next sought to confirm the direct association between developing disease and T-cell phenotype. We therefore correlated the relative frequencies of CD19+CD5+ and CD3+, CD3+CD4+, and CD3+CD8+ cells, respectively, in all organs from TCL1 and AT mice, using the Spearman's rank correlation coefficient model to determine the statistical dependence between these variables. As indicated by the previous analyses, we found that developing CLL significantly associated with the loss of CD3+ and more importantly, among CD3+ cells, with the loss of CD4+ cells and the increase of CD8+ cells in spleen, PB, BM and LN, suggesting a causal and linear relationship between CLL and those T-cell defects (see Figure 21 A for spleens, B for PB, C for BM and D for LN, and Table 13). LN of AT mice were excluded from this analysis, as disease development is delayed in this compartment.

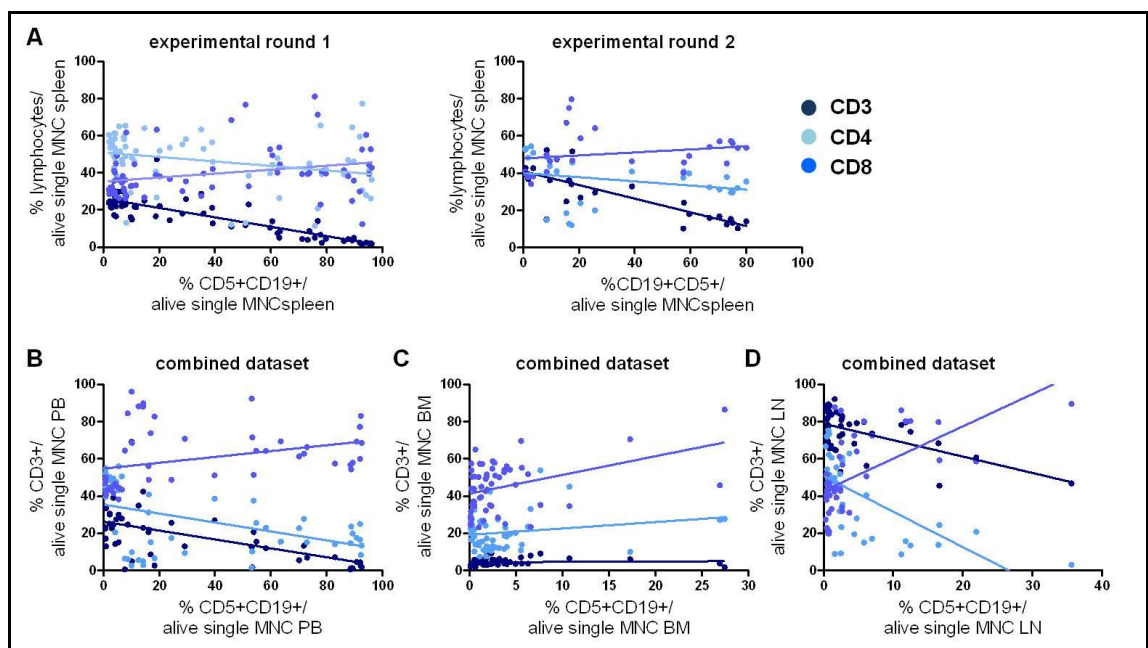


**Figure 21: Statistical correlations between CLL and T-cell subsets.** Using nonparametric Spearman correlation coefficient modelling, the variables “developing CLL in all available TCL1 and AT mice” and “changes in CD3, 4 and 8 subsets” were correlated with each other. Cells were gated on mononuclear cells (MNC). Each data point is representative of a single mouse, correlating the relative frequency of CD3, 4 or 8 (depicted in different shades of blue and plotted on the y-axes) with the corresponding relative frequency of CD19+CD5+ CLL cells (plotted on the x-axes). **(A)** In mice phenotyped in both experimental round 1 and 2, progressing CLL and the loss of CD3+ and CD3+CD4+ cells and the increase of CD3+CD8+ were significantly associated with each other. Associations with CD3+CD4+ and CD3+CD8+ cells were confirmed in **(B)** peripheral blood (PB), **(C)** bone marrow (BM) and **(D)** lymph nodes (LN), excluding the AT mice in LN correlation analyses.

		spleen		PB combined dataset	BM combined dataset	LN combined dataset
		exp. round 1	exp. round 2			
CD3	<i>spearman r</i>	-0.8155	-0.7759	-0.6436	0.4735	-0.3489
	<i>95% CI</i>	-0.8836 to -0.7138	-0.8951 to -0.5533	-0.7852 to -0.4381	0.2354 to 0.6580	-0.5840 to -0.05988
	<i>p value (two-tailed)</i>	< 0.0001	< 0.0001	< 0.0001	0.0002	0.0162
	<i>p value summary</i>	***	***	***	***	*
CD4	<i>spearman r</i>	-0.3901	-0.5330	-0.5614	-0.03445	-0.6358
	<i>95% CI</i>	-0.5786 to -0.1621	-0.7642 to -0.1803	-0.7303 to -0.3279	-0.2996 to 0.2357	-0.7839 to -0.4193
	<i>p value (two-tailed)</i>	0.0009	0.0042	< 0.0001	0.7992	< 0.0001
	<i>p value summary</i>	***	**	***	ns	***
CD8	<i>spearman r</i>	0.3819	0.5061	0.6016	0.3645	0.6252
	<i>95% CI</i>	0.1527 to 0.5722	0.1445 to 0.7485	0.3811 to 0.7574	0.1070 to 0.5762	0.4047 to 0.7770
	<i>p value (two-tailed)</i>	0.0012	0.0071	< 0.0001	0.0053	< 0.0001
	<i>p value summary</i>	**	**	***	**	***

**Table 13: Summary of results of statistical Spearman correlation coefficient analyses for all examined organs according to CD3, 4 and 8 subset.** Abbreviations: BM – bone marrow, PB – peripheral blood, LN – lymph nodes, CI – confidence interval, ns – not-significant.

#### 5.4.7 Developing CLL leads to characteristic functional changes in T-cell intracellular cytokines and effector cytotoxicity function

After confirming the suitability of the B6 TCL1 model in general and the AT model specifically to mirror the T-cell defects previously described in the original C3H TCL1 model, and that the spleen appears to be representative for the examined CLL-affected organs, we investigated changes in T-cell function in the context of developing CLL in splenocytes from 3, 6 and 12 month old ageing TCL1, WT and AT mice.

In WT mice, intracellular IL-2 was predominantly produced by CD4+ cells, and showed a trend towards increased production with ageing, which was however not-significant ( $p=0.09$  for IL-2 levels at 3 vs. 12 months). In contrast, CD4+ cells from TCL1 mice demonstrated a significantly decreased production of IL-2 with developing CLL ( $p=0.0043$  for 3 vs. 12 months), but not after AT ( $p=0.31$  for AT mice vs. healthy, age-matched WT mice, note: AT recipients were WT recipients). Interestingly, CD8+ cells

from TCL1 mice also started to produce more IL-2 with increasing CLL ( $p=.0043$  for 3 vs. 12 months), but not after AT (Figure 22 A).

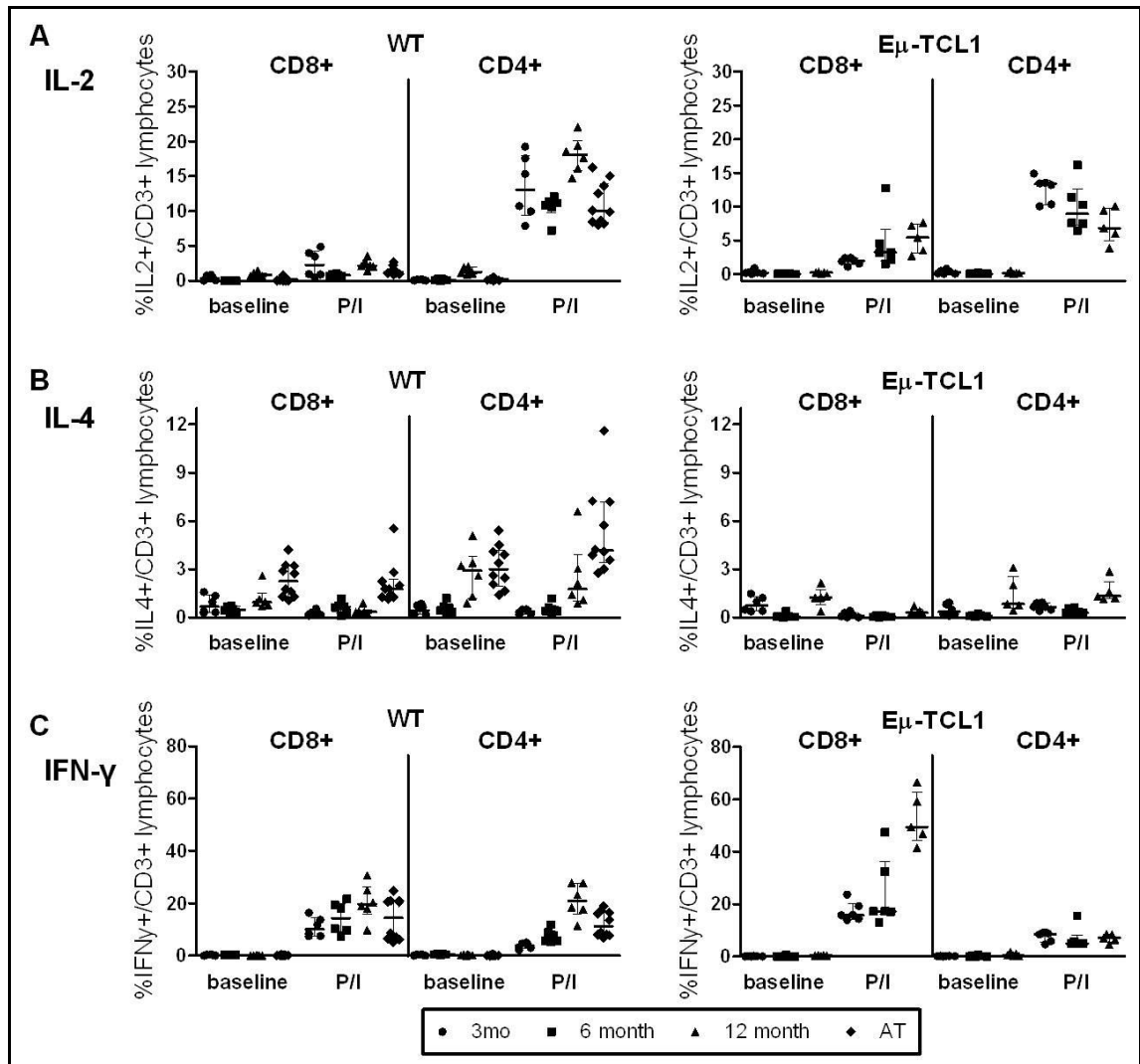


**Figure 22: Intracellular cytokine production by CD4+ and CD8+ cell subsets.** Fresh splenocytes from 3, 6 and 12 month WT and TCL1 mice and from mice with full CLL after AT were stimulated for 6 hours with PMA and ionomycin (P/I) in the presence of brefeldin/monensin for the last 5 hours of culture. Cells were then harvested, surface stained, fixed, permeabilised and stained with antibodies against IL-2, IL-4 and IFN- $\gamma$ . **(A)** Intracellular IL-2 was predominantly a CD4 cytokine, increased in ageing WT mice, but decreased with developing CLL. CD8+ cells increased IL-2 production with ageing CLL, but not after AT. **(B)** Intracellular IL-4 was also predominantly a CD4 cytokine, increased in ageing WT CD4+ cells but was stable in CD8 cells without and with mitogen. CD4+ cells from ageing TCL1 mice required mitogen to maintain production. AT mice had significantly increased IL-4 production. **(C)** CD8+ cells from ageing TCL1 mice had significantly increased IFN- $\gamma$  production, which was not fully recapitulated in AT mice. In CD4+ cells from ageing leukaemic mice, IFN- $\gamma$  production was lost while WT mice exhibited an increase just as in CD8+ cells. CD4+ cells from AT mice maintained increased IFN- $\gamma$  production. All graphs show median with interquartile range (IQR).

Intracellular IL-4 was detected in both CD4<sup>+</sup> and CD8<sup>+</sup> cells, with a predominance in CD4<sup>+</sup> cells (see Figure 22 B). Even without PMA/Ionomycin, CD4<sup>+</sup> cells from ageing WT increasingly produced IL-4 ( $p=.0022$  for CD4<sup>+</sup> cells at 3 vs. 12 month), which was not further increased by mitogen. IL-4 production by WT CD8<sup>+</sup> cells appeared relatively stable without and with mitogen. CD4<sup>+</sup> cells from TCL1 mice showed no significantly altered IL-4 production without mitogen ( $p=.1255$  at 3 vs. 12 months), and this could only be increased by PMA/Ionomycin in mice at 12 months compared to young TCL1 mice ( $p=.008$ ). Interestingly, both CD4<sup>+</sup> and CD8<sup>+</sup> cells from AT mice appeared to have significantly increased IL-4 production (CD4<sup>+</sup> cells:  $p=.0002$  without and with PMA/Ionomycin; CD8<sup>+</sup> cells:  $p=.0079$  without and  $p=.0002$  with PMA/Ionomycin, both compared to age-matched healthy WT mice), indicating that this setting might predispose for IL-4 production.

Both CD4<sup>+</sup> and CD8<sup>+</sup> cells appeared able to produce IFN- $\gamma$ , but baseline production was negligible and mitogenic stimulation was required (see Figure 22 C). Differences were apparent between ageing WT and TCL1 mice: while CD8<sup>+</sup> cells from ageing WT showed slightly increased IFN- $\gamma$  production ( $p=.0152$  at 3 vs. 12 months), this was significantly increased in ageing TCL1 mice ( $p=.0043$ ), and 12 month old leukaemic mice showed almost twice the percentage of IFN- $\gamma$ -producing CD8<sup>+</sup> cells. In AT mice, this was only recapitulated in a few mice, with the overall group having no different CD8<sup>+</sup> IFN- $\gamma$  production compared to age-matched healthy mice. In contrast, IFN- $\gamma$  production by CD4<sup>+</sup> cells appeared lost in leukaemic mice, while WT mice exhibited an increase just as in CD8<sup>+</sup> cells ( $p=.0022$  at 3 vs. 12 months). CD4<sup>+</sup> cells from AT mice, however, maintained increased IFN- $\gamma$  production relative to healthy aged-matched WT controls ( $p=.0002$ ).

In the same experiment, we measured cytotoxicity by CD107a degranulation and intracellular GrB and attributed these effector functions, along with IFN- $\gamma$  production, specifically to the antigen-experienced CD44<sup>+</sup>CD3<sup>+</sup>CD8<sup>+</sup> subset. To describe CLL/ageing-induced changes within antigen experienced CD44<sup>+</sup> cells, we formed a ratio between cells expressing a certain effector marker and cells lacking this expression after stimulation with PMA/Ionomycin. A decreased ratio is therefore indicative of loss of cells able to act as effector cells, and vice versa. In ageing WT mice, CD44<sup>+</sup>CD3<sup>+</sup>CD8<sup>+</sup> cells largely maintained their ability to localise CD107a to their surface and to produce IFN- $\gamma$ . Intracellular GrB ratio also remained relatively constant, indicating that key effector functions were maintained. Some trends were observed over time, but none reached statistical significance (3 vs. 12 month CD107a ratio  $p=.1797$ ; GrB ratio  $p=.2403$ ; IFN- $\gamma$  ratio  $p=.3095$ , Figures 23 A, B and C upper panels).

In contrast, with developing CLL both ageing TCL1 and AT mice showed a decreased CD107a ratio, demonstrating that within the CD44+ subset, cells without the ability to degranulate (*i.e.* functionally deficient cells) became predominant ( $p=.0173$  for TCL1 mice at 3 vs. 12 months;  $p=.0001$  for AT vs. aged-matched healthy controls, Figure 23 A).

Intracellular GrB ratio, however, remained constant, albeit at a generally lower level than in WT mice, and was even increased after AT ( $p=.0261$ ), indicating that the production of lytic granule content is at least maintained to a certain extent in the presence of leukaemic cells (Figure 23 B). Interestingly, developing CLL in TCL1 mice was accompanied by an increase in the ratio of IFN- $\gamma$  producing *versus* non-producing CD44+ cells ( $p=.0087$  for mice at 3 vs. 12 months, Figure 23 C). However, this was not-significant in AT mice compared to age-matched healthy WT mice ( $p=.2119$ ). In accordance to their differentiation status, these effector functions were restricted to antigen-experienced cells, and absent in naïve CD3+CD8+CD44- cells.

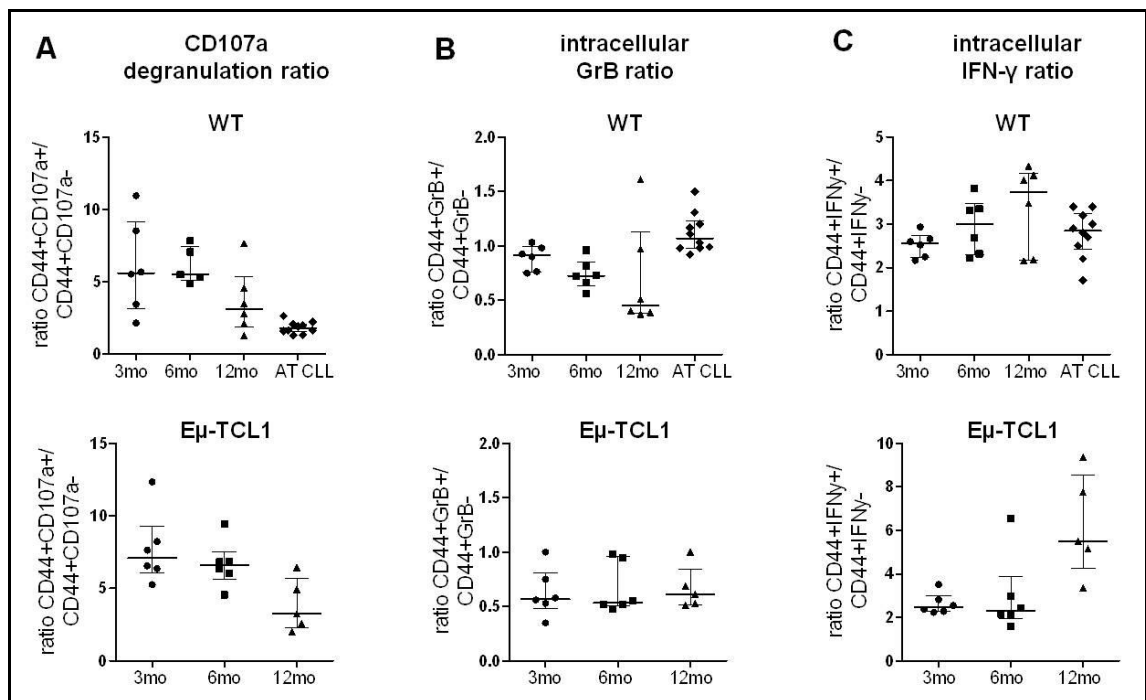


**Figure 23: Effector cell function in CD3+CD8+CD44+ antigen experienced cells.** Key effector cell cytotoxic functions were measured after PMA/Ionomycin stimulation and expressed as a ratio between cells expressing CD107a, GrB and IFN- $\gamma$ . **(A)** In contrast to ageing WT mice, developing CLL (*i.e.* ageing TCL1 mice and AT mice) led to significantly decreased CD107a ratio. **(B)** Intracellular GrB ratio remained constant in ageing TCL1 mice and increased after AT. **(C)** Developing CLL was accompanied by a highly significant increase in IFN- $\gamma$  ratio in ageing TCL1 but not AT mice.

#### 5.4.8 Developing CLL is accompanied by increasing T-cell proliferation

As another marker of T-cell effector function, we determined *ex vivo* and *in vivo* proliferation by ki67 and EdU incorporation, respectively. In ageing WT mice, the proliferation of CD3+CD8+ T-cells, expressed by changes in the ki67 ratio, remained relatively constant but showed a trend towards decreased proliferation ( $p=.0632$  at 3 vs. 12 months; Figure 24 A). In ageing TCL1 mice with developing CLL, however, the ki67 ratio increased significantly, indicating that within the CD44+ subset, cells with the ability to proliferate became predominant ( $p=.0274$  at 3 vs. 6 months;  $p=.0013$  at 3 vs. 12 months; Figure 24 A). This was also recapitulated after AT ( $p=.0016$  for AT vs. age-matched WT). These patterns were confirmed by measuring *in vivo* proliferation (Figure 24 B): T-cell proliferation, indicated by cells positive for AF488-coupled incorporated EdU, remained constant in WT T cells over time, but increased significantly with developing disease ( $p=.0043$  at 3 vs. 6 months and  $p=.0002$  at 3 vs. 12 months for TCL1 mice;  $p=.0007$  for AT vs. age-matched WT mice). This was observed in both CD8+ and non-CD8+ (*i.e.* largely CD4+) cells (CD8+:  $p=.0087$  for 3 vs. 6 months;  $p=.0007$  for 3 vs. 12 months;  $p=.0002$  for AT vs. WT; non-CD8+:  $p=.0173$  for 3 vs. 6 months;  $p=.0002$  for 3 vs. 12 months;  $p=.0002$  for AT vs. WT).

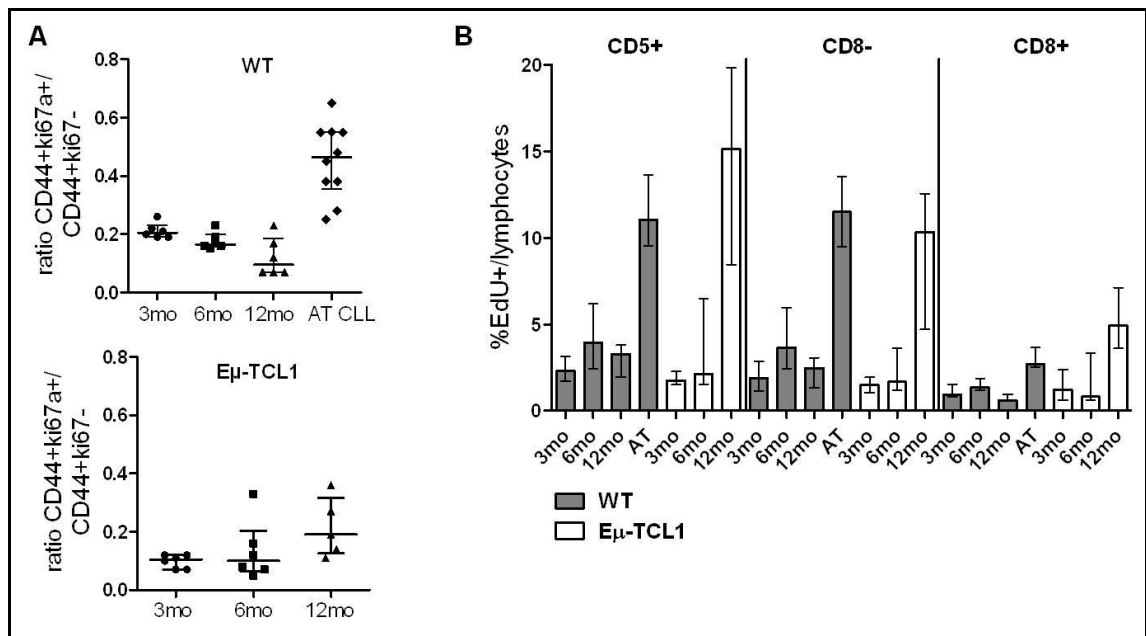


**Figure 24: Proliferation in T-cell subsets.** Proliferation was measured *ex vivo* by intranuclear ki67 in CD3+CD8+ T cells and *in vivo* by EdU incorporation in all CD5+ T cells and CD8+ and CD8- T-cell subsets. **(A)** In contrast to ageing WT mice, developing CLL in TCL1 mice and AT led to significantly increased ki67 ratios in CD3+CD8+CD44+ cells, indicating increasing proliferation in the presence of CLL. **(B)** Confirmation of increased T-cell proliferation *in vivo*, both in CD8+ and in CD8- subsets.

As the EdU technique allows multiplexing with a variety of other markers, we also concurrently assessed B-cell proliferation in both ageing WT and TCL1 mice and after AT (see Figure 25). The proliferation of healthy CD19+CD5- B cells remained constant in ageing WT mice, but increased in CD19+CD5- B cells from 6 month old TCL1 mice and was similar to their CLL cell proliferation (*i.e.* CD19+CD5+ cells). This 6 month age group represents an early stage of CLL, where both a healthy B cell and a malignant CLL cell population exist and can be directly compared. With progressing CLL, the CD19+CD5+ population continued to proliferate, as expected.

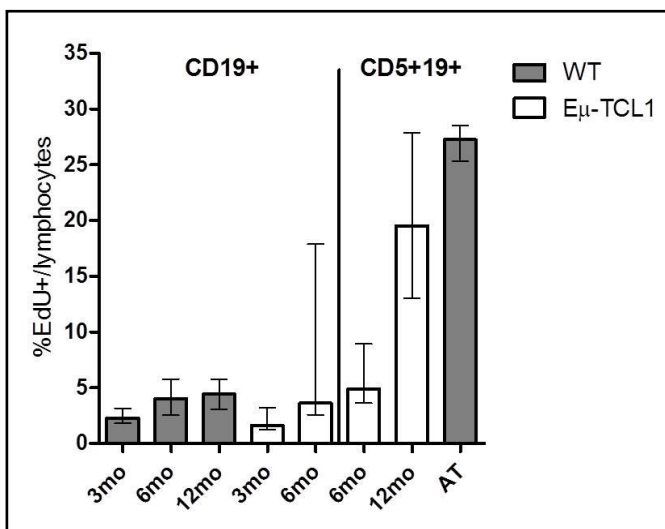


**Figure 25: Proliferation of healthy B and CLL cells *in vivo*:** Proliferation of healthy B cells remained constant in ageing WT mice, but CD5+CD19+ CLL cell proliferation continued to increase with developing disease.

#### 5.4.9 Developing CLL is accompanied by impaired ability of autologous B and T cells to form immunological synapses

Our group has demonstrated that impaired immune synapse formation is an important feature of T-cell dysfunction in both human and murine CLL. To conclude the characterization of how T-cell defects develop alongside progressing CLL, we measured T-cell synapse formation between autologous B/CLL and T-cells in 3, 6 and 12 month old TCL1 mice and in AT mice, and compared this to the synapse formation observed in autologous cells from 3 month old WT mice. While the ability to form immunological synapses was comparable in 3 month old TCL1 and WT mice, this was significantly impaired in 12 month TCL1 mice and after AT ( $p < .0001$ , respectively). Surprisingly, this did not appear to be a linear progressive loss, as 6 month old TCL1 mice, *i.e.* at the early stage of CLL, exhibited superior synapse formation compared to 3 month old TCL1 mice (Figure 26).

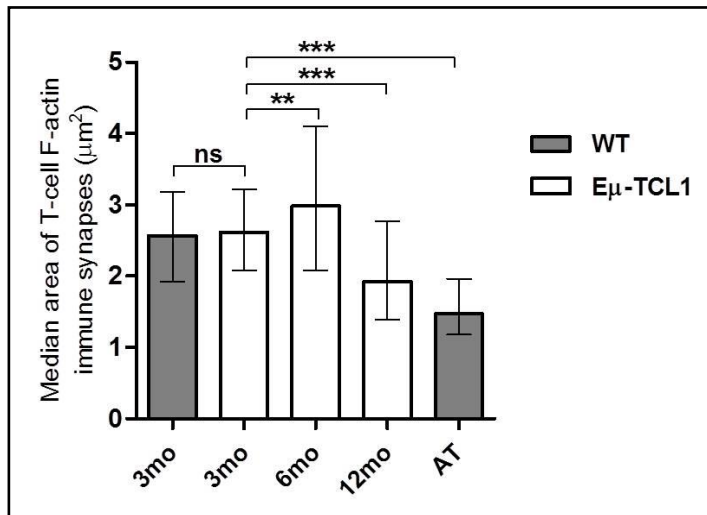


**Figure 26: Development of immune synapse formation:** The ability of autologous B and T cells to form immunological synapses was measured in 3, 6, 12 month old TCL1, 3 month old WT, and AT mice. Compared to young TCL1 mice, this was significantly impaired in aged TCL1 and AT mice, but not 6 month old TCL1 mice with early stage CLL.

### 5.5 Summary of phenotypic and functional T-cell defects developing with progressing CLL

In summary, we were able to demonstrate that developing CLL and phenotypic changes in T cell subsets were highly significantly correlated with each other, and that this is equally modelled in B6 TCL1 and C3H TCL1 mice. This included a decrease in CD4+/CD8+ ratio, which was recapitulated in spleen, PB, BM and LN. Within CD3+CD8+ cells, naïve cells were progressively lost and the population shifted towards antigen-experienced cells. The subset of antigen-experienced cells, however, appeared to be dependent on the microenvironment: effector cells progressively became the dominant cell type in BM, and memory cells in PB and LN. In spleens of B6 TCL1 mice, memory and effector cells were equally expanded, while C3H mice exhibited a more pronounced shift to effector cells. Regardless, the spleen memory pool of B6 TCL1 mice was further characterized by a shift towards EM and loss of CM cells. While some of these phenotypic T-cell changes, such as the progressive decrease of naïve cells and subset shifts among effector and memory cells, were also observed to a certain extent in ageing WT mice, they were considerably more pronounced in the presence of CLL. In addition, the extent of differences between healthy ageing T cells and ageing CLL T cells became apparent when comparing their absolute numbers, which were in general considerably higher in TCL1 mice. This allowed the identification of a CLL-specific T-cell phenotype, which included the CD8+ and EM subset expansions and the massive naïve cell loss. The AT model was confirmed to be a generally adequate tool to mirror the phenotypic T-cell changes of ageing CLL. However, the following differences became apparent: the disease load in

LN did not fully mirror 12 month old TCL1 mice, and as a consequence, the T-cell phenotype was not as clearly confined to CLL-typical changes in this compartment. In addition, minor differences were observed in effector *versus* memory subset distribution depending on whether AT recipients were WT or TCL1 mice. Functionally, typical cytokine T-cell defects that developed alongside CLL were a loss of IL-2 producing CD4+ cells and aberrantly increased percentages of CD8+ cells producing IL-2, the loss of spontaneous IL-4 producing CD4+ cells, and significantly increased IFN- $\gamma$  producing CD4+ and CD8+ cells. Cytokine profiles were only partly mirrored in AT mice, as they seemed to be enriched for IL-4 producing CD4+ and CD8+ cells while lacking a significant increase in IFN- $\gamma$  producing cells. Antigen-experienced CLL T-cells appeared to lose their ability to localise CD107a to their surface progressively, which is indicative of impaired cytotoxicity function, but maintained the ability to produce cytolytic GrB, while increasing their IFN- $\gamma$  production potential. Except for the latter change, this was mirrored in AT mice. Accordingly, immune synapse formation was significantly impaired in ageing TCL1 and AT mice, but this did not appear to be a linear development as 6 month old TCL1 mice exhibited an increased ability to form synapses relative to 3 month old TCL1 mice. Surprisingly, T-cell proliferation was found to increase with developing CLL and after AT. Statistical differences in the relative expansion or loss of functional T cell subsets compared to 3 month old mice as baseline are summarized in Figure 27.

			WT			TCL1			AT
			3mo	6mo	12mo	3mo	6mo	12mo	
proliferation	<i>in vitro</i> <i>in vivo</i>	ki67 (CD3+CD8+ T cells)							
		Edu (CD5+ T cells)							
		EdU (CD8+ T cells)							
		EdU (non-CD8 T cells)							
intracellular cytokines	IL-2	CD3+CD8+ T cells PMA/Ionomycin							
	IL-4	CD3+CD8+ T cells PMA/Ionomycin							
	IFN- $\gamma$	CD3+CD8+ T cells PMA/Ionomycin							
	IL-2	CD3+CD8- T cells PMA/Ionomycin							
	IL-4	CD3+CD8- T cells PMA/Ionomycin							
	IFN- $\gamma$	CD3+CD8- T cells PMA/Ionomycin							
cytotoxicity	degranulation	107a ratio Ag-exp. CD3+CD8+ T cells							
	granzyme B	GrB ratio Ag-exp. CD3+CD8+ T cells							
	IFN- $\gamma$	IFN $\gamma$ ratio Ag-exp. CD3+CD8+ T cells							
immune synapse formation	area of accumulated F-actin								
<i>p-value legend:</i>			relative loss			relative expansion			
			baseline	ns	*	**	***		
			baseline	ns	*	**	***		

**Figure 27: Heatmap summary of p-values describing statistical differences in functional T-cell subsets.** Groups were compared to the relative percentage of functional subsets in 3 month old mice. Blue colour indicates relative expansion, red colour indicates relative loss of cell subsets. ns = non-significant, \*p<.05, \*\*p<.001, \*\*\*p<.0001.

## 5.6 Discussion

The goal of this part of the work was to validate the B6 TCL1 model for the investigation of global T-cell defects, to further characterize T-cell subsets in the context of advancing CLL in different CLL-affected compartments, and to explore the impact of developing CLL on T-cell effector function.

Using T-cell phenotype as an established surrogate marker for global T-cell defects in human CLL and the TCL1 model<sup>118-120, 133, 220</sup>, we demonstrated that this can be adequately modelled in both the original C3H-F1 TCL1 and the backcrossed B6 TCL1 model, therefore validating the latter for further studies on the characterization and repair of T-cell dysfunction. Previous work of our group on T-cell defects in mice has been done using C3H-F1 TCL1 mice, and the backcrossed B6 TCL1 model was been inadequately characterized so far. Therefore, in order to fully understand the underlying changes in the context of developing CLL, and in a second step, the impact of repairing our previously described T-cell defects in backcrossed B6 TCL1 mice, a thorough validation of this model was an essential first step. This comparison between C3H and B6 TCL1 mice was however restricted to splenic T-cell subsets, as the spleen is considered the major organ of disease in this model, but was excluded from the B6 TCL1 characterization work of Hofbauer et al<sup>212, 220</sup>. In addition, preclinical characterization studies such as the T-cell work from our group<sup>216</sup>, or studies investigating the effect of therapeutic interventions<sup>265</sup>, are generally done using splenocytes from TCL1 mice, also in part because sufficient cell numbers are more easily obtained from an enlarged spleen than from LN or blood from a mouse. We were able to confirm that the T-cell phenotype in murine CLL cells from spleen mirrors that of human CLL<sup>121, 122, 133, 390, 391</sup>, and includes the fall in the CD4+/CD8+ ratio, and a shift from naïve to antigen-experienced CD3+CD8+ cells.

However, this CLL-specific T-cell phenotype in human studies is largely based on the characterization of T cells from PB, while the only other murine study using backcrossed B6 TCL1 mice so far describing similar phenotypic alterations used T cells from PB and LN<sup>220</sup>. In contrast, an older study in CLL patients, which characterized T cells from LN and BM, reported increased numbers of CD4+ T cells in these compartments<sup>392</sup>. To directly compare differences in T-cell subsets in different organs from the same animals, we characterized CD3+, CD4+, CD8+ and CD3+CD8+ naïve and effector/memory cells in spleen, PB, LN and BM in ageing B6 TCL1 and age-matched WT mice. We found that the major aspects of the CLL-specific T-cell phenotype were recapitulated in all organs, indicating that the described phenotypic T-cell changes are induced by the presence of CLL regardless of the microenvironment.

It has been suggested that the relative reduction in numbers of PB CD4<sup>+</sup> T cells is due to their increased susceptibility to FasL-mediated apoptosis<sup>126</sup>, and a recently published study using B cell-derived lymphoblastoid cell lines proposed that this could be mediated by constitutively produced MHCII(+)FasL(+) exosomes produced by B-cells<sup>393</sup>. In addition, relatively reduced peripheral CD4<sup>+</sup> cell numbers could also be a result of chemokine/cytokine driven migration into secondary lymphoid organs<sup>129</sup>. Studies in other disease entities associated with chronic inflammatory responses have also demonstrated that T-cell subpopulations differ between lymphoid organs and PB, and that this could be mediated by cytokines such as CCR4, CXCR3<sup>394, 395</sup>. Our findings support an accumulation of CD4<sup>+</sup> T cells in the bone marrow and secondary lymphoid organs, probably as a result of migration, as in leukaemic mice, the CD4<sup>+</sup>/CD8<sup>+</sup> ratio was generally higher in BM, LN and spleen than in PB. In line with previous reports in both human and mouse CLL, we largely found increased numbers of T-cell subsets due to leucocytosis and organomegaly in all examined compartments compared to age-matched WT mice.

In all organs, naïve CD3<sup>+</sup>CD8<sup>+</sup> cells were progressively lost and the population shifted towards antigen-experienced cells. The subset of antigen-experienced cells, however, appeared to be dependent on the microenvironment: effector cells progressively became the dominant cell type in BM, and memory cells in PB and LN. In spleens of B6 TCL1 mice, memory and effector cells were equally expanded, while C3H mice exhibited a more pronounced shift to effector cells. Regardless, the spleen CD8<sup>+</sup> memory pool of leukaemic mice was further characterized by a shift towards EM and loss of CM cells, based on the coexpression of CCR7 and CD62L. A skewing towards CD8<sup>+</sup> and CD4<sup>+</sup> antigen-experienced cells in PB and LN has been previously described in murine CLL<sup>220</sup>. This paper, however, refers to these cells as memory cells and reports statistical values in the text for memory cells, but the corresponding figures and tables are consistently labelled “effector+memory” cells. It is therefore unclear based on the published information, which subset they found to be preferentially expanded. Another study using the original TCL1 C3H mice reported an expansion of CD8<sup>+</sup> effector cells in the peritoneal cavity, but termed this population effector memory cells, although their panel did not include any markers such as CCR7 to allow such a discrimination<sup>135</sup>.

Previous work from our group has found that human CLL CD8<sup>+</sup> T cells in blood differentiate into CCR7<sup>-</sup> EM cells<sup>133</sup>. As this is very similar to our findings in spleen, this shift might be recapitulated regardless of microenvironment. Differences in human CD8<sup>+</sup> lymphocyte subsets were originally thought to be potentially explained by the

presence of CMV<sup>144</sup>, but work from our group later confirmed that impaired T-cell function and altered subset composition were irrespective of CMV serostatus<sup>133</sup>. Based on the observation that CMV-reactivations are uncommon in untreated CLL, suggesting that antiviral responses are uncompromised, a recently published study suggested that CMV-specific CD8+ T cells were indeed functionally intact, while global T-cell defects were still present<sup>148</sup>. Therefore, changes in the T-cell compartment in CLL are likely to be very heterogeneous and potentially influenced by a variety of other factors. Murine studies allow us to at least control for the confounder of any underlying common infection, as mice are generally considered free of infection. This is ensured by the maintenance of mice in specific barrier-systems and rigorous infection screening, which were also conducted regularly and were confirmed negative in our colony.

The AT model was confirmed to be a generally adequate tool to mirror the phenotypic T-cell changes of ageing CLL, while having the advantage of developing CLL more uniformly as a cohort than 12 month old TCL1 mice, where individual animals of the same age usually exhibit a wide range of stages of CLL development. The AT model therefore appears superior to ageing CLL in terms of more consistently modelling the full inhibitory effect of CLL on T-cells; therefore it can be argued that CLL-associated T-cell changes are most adequately modelled in AT mice, while eliminating confounders such as underlying age. However, the TCL1 model *per se* has also been characterized to mirror the biological properties of aggressive human CLL, such as stereotyped B-cell receptors or epigenetic alterations (see Chapter 1.2.1.2). Due to its shorter disease latency, it is therefore possible that the AT model needs to be considered as even more aggressive than CLL that develops in ageing TCL1 mice. In addition, it is not known if serial leukaemia transfer in mice fosters clonal evolution of specific CLL sub-clones or mutations in BCR pathways, which have been described in human CLL. Therefore, our data on ageing TCL1 mice could be used to model the T-cell defects occurring in more indolent CLL, while AT mice mirror aggressive CLL.

As spleen appeared to be representative for CLL-affected secondary lymphoid organs, we investigated changes in T-cell function in the context of developing CLL in splenocytes from TCL1, WT and AT mice. For a complete analysis of function in secondary lymphoid organs compared to blood, it would have been desirable to conduct these investigations in a direct comparison. However, functional assays in blood were not feasible given the very small volumes of blood retrieved by cardiac puncture. Regardless, we were able to identify typical cytokine T-cell defects that developed alongside CLL; these included the loss of IL-2 production in CD4+ cells and aberrantly increased production by CD8+ cells, the loss of spontaneous IL-4 production

by CD4<sup>+</sup> cells, and significantly increased IFN- $\gamma$  production by CD4<sup>+</sup> and CD8<sup>+</sup> cells. Cytokine profiles were only partly mirrored in AT mice, as they seemed to be enriched for IL-4 producing CD4<sup>+</sup> and CD8<sup>+</sup> cells while lacking a significant increase in IFN- $\gamma$  production, which is however very similar to a pattern recently described by Brusa *et al.* in T cells from CLL patients<sup>134</sup>. Early studies in human CLL suggested that CLL was a CD4<sup>+</sup> Th2-mediated disease, with increased numbers of both CD4<sup>+</sup> and CD8<sup>+</sup> T cells producing IL-4<sup>153, 396</sup>. However, a number of other reports have described increased production of IFN- $\gamma$  and TNF- $\alpha$  by T cells from CLL patients, which also correlated with disease stage<sup>164, 397-400</sup>. In addition, IL-2 was shown to increase CLL cell proliferation<sup>401</sup>. Previous work from our group found that CD4<sup>+</sup> T cells from CLL patients showed increased production of IFN- $\gamma$  and IL-2, and no reduction in TNF- $\alpha$ , while CD8<sup>+</sup> T cells had increased production of IFN- $\gamma$  and TNF- $\alpha$  without any reduction in IL-2 when compared with healthy controls<sup>133</sup>. Our previous murine work suggested that T-cell cytokines were Th2 preponderant<sup>216</sup>. Assuming that the ageing TCL1 mouse model is more indolent and the AT models represents more aggressive disease, our present data indicate that CD4<sup>+</sup> cells are IFN- $\gamma$ /Th1 preponderant in more indolent stages, but become IL-4/Th2 preponderant in aggressive CLL. Similarly, indolent CLL would be associated with aberrant IL-2 and IFN- $\gamma$  production by CD8<sup>+</sup> T cells, and aggressive CLL with aberrant IL-4 and loss of IFN- $\gamma$  production. However, these different cytokine secretion patterns between more and less aggressive CLL might also be biased by immune responses associated with the process of ageing. Although we were conducting all comparisons between leukaemic mice and age-matched WT mice (*i.e.* compared ageing TCL1 mice with ageing WT mice, and young AT mice with young age-matched WT), the cytokine-secretion potential of T cells has been demonstrated to undergo fundamental changes with ageing<sup>402</sup>. Therefore, the different cytokine repertoire in AT mice might also be explained by the fact that younger mice simply have a different repertoire of cytokine secretion potential than older mice.

A more consistent picture between ageing TCL1 and AT mice was found regarding CD8 T-cell effector function: developing CLL led to a progressively lost ability of CD107a relocation to the cell surface, which was used as a measurement of cytotoxicity, but cells maintained the ability to produce cytolytic GrB. Accordingly, immune synapse formation was significantly impaired in ageing TCL1 and AT mice, but this did not appear to be a linear development as 6 month old TCL1 mice exhibited an increased ability to form synapses. We have previously described in both murine and human CLL that GrB mRNA levels were not impaired in CLL T cells, but that cells still had an impaired cytotoxicity function and poor immunological synapse formation<sup>77, 171, 216</sup>.

Impaired cytotoxicity was later found to be explained by an impaired ability of human CLL PB T-cells to focus CD107a and GrB polarisation into the immunological synapse, therefore preventing the targeted lysis of antigen-presenting cells<sup>133</sup>. In the present study, we have confirmed that all these functions were affected in T cells from spleen. This indicates that impaired effector function is a hallmark of CLL T cells regardless of the microenvironment, and that the defects are developing progressively alongside CLL from an early stage on.

Somewhat surprisingly, T-cell proliferation was found to increase with developing CLL and after AT. This is a novel finding and is in marked contrast to our previous human work, which found a proliferative defect in PB CLL T cells due to a combination of a reduction in the proportion of cells able to divide upon polyclonal activation, and prolongation of the division time of the proliferating cells<sup>133</sup>. This, however, was measured by CFSE incorporation following 72h *ex vivo* stimulation with anti-CD3/CD28 beads, whereas proliferation of murine T cells was measured both directly *in vivo* and *ex vivo* without any further antigen or mitogen stimulation. This can therefore be considered the most accurate measurement of actual T-cell proliferation *in vivo*. Interestingly, Roth *et al.* described significantly shorter average telomere lengths in naïve and memory T cells from ZAP-70+/CD38+ patients compared to ZAP-70-/CD38- patients and healthy controls, indicating increased proliferation of T cells in CLL patients with poorer risk disease. Therefore, increased proliferation of T cells in TCL1 mice might be another indication of the aggressiveness of the disease.

CLL B-cells themselves have long been viewed as non-proliferating cells; this was challenged by clinical studies using heavy water to label CLL cells *in vivo*, and more recently by murine studies demonstrating that CLL cells had higher proportions of proliferating cells than non-leukaemic lymphocytes, which is in line with our present observations comparing healthy B-cells and CLL cells<sup>260, 403</sup>. The same murine study also found that BrdU incorporation into T cells did not differ between TCL1 and WT mice, indicating that T-cell proliferation was at least maintained. The discrepancy to the increase in T-cell proliferation observed in our current work could be explained by the fact that Enzler *et al.* examined mice with a lower burden of disease, which are probably more similar to the 6 month old TCL1 mice we used in our study, and that increased proliferation might have become apparent had they used older mice with more progressed CLL as well.

In sum, we have extensively validated the backcrossed B6 TCL1 model for the characterization and repair of T-cell defects in CLL, we have demonstrated the strengths and potential shortcomings of the AT model to mirror the T-cell defects seen

in ageing TCL1 mice, and we have shown for the first time how different microenvironments and compartments affect the T-cell phenotype in murine CLL. In addition, we have identified the dynamic alterations of T-cell phenotype and function in the context of developing CLL, and we have described novel mechanisms of T-cell dysfunction. Altogether, this work supports the understanding that, despite a typical CLL-induced T-cell phenotype, CLL T cells are at last partially functional and have developed several mechanisms that try to compensate increasing tumour load and maintain anti-tumour immune responses. The mechanisms of why these anti-tumour immune are not sufficient and do not lead to efficient anti-tumour control, and how the inhibitory effects of CLL cells are mediated, will be further investigated in the next chapter.

## 6 PD-L1/ PD-1 mediated T-cell dysfunction and T-cell exhaustion in TCL1 mice on the B6 background

### 6.1 Specific introduction

Our group has previously identified the molecular signature of human CD4+ and CD8+ T cells in CLL, and confirmed that this is very closely mirrored in leukaemic TCL1 mice<sup>171, 216</sup>. Dysregulated T-cell genes were mostly involved in pathways of cell proliferation, differentiation, effector function, and actin cytoskeleton formation. The functional impact of the latter was modelled in immune synapse formation assays between T cells and antigen presenting cells (APCs). These experiments confirmed that T cells from CLL patients inappropriately respond to APCs due to their inability to regulate actin modelling effectively, and to recruit key cytoskeletal signalling molecules to the immune synapse<sup>77</sup>. These defects could be induced in normal allogeneic T cells by co-culturing them in direct cell-cell contact with CLL cells, and were also recapitulated in synapses between autologous CLL and T cells from leukaemic TCL1 mice. Using functional siRNA screening, aberrant surface expression of CD200, PD-L1, CD270 and CD276 on CLL cells were identified as the major mediators of impaired T-cell actin dynamics, with a dominant role of PD-L1<sup>79</sup>. Blocking these ligands *in vitro* led to a significant improvement of immune synapse formation, with the combined activity of all four molecules having the greatest effect.

The corresponding binding partners of PD-L1 and CD270 - PD-1 and CD160 - have been demonstrated to be aberrantly expressed by CLL T cells, probably as a result of chronic antigenic stimulation<sup>133, 134</sup>. This has been extensively studied in the context of chronic viral infections with high viral replication, such as hepatitis B and C, human immunodeficiency virus (HIV), and simian immunodeficiency virus (SIV), where chronic antigenic stimulation leads to failed immune responses and persistence of viral antigens beyond the effector phase. The continued presence of viral antigen and inflammation drive the on-going replication of virus-specific effector T cells and lead to a number of progressive phenotypic and functional changes that have been termed "T-cell exhaustion". Of note, T-cell exhaustion is not limited to chronic viral infection, but also includes bacterial and parasitic infections. Exhaustion represents a state of functional hypo-responsiveness that occurs as a progressive process over a period of weeks or months, depending on the chronic stimulus, and has been characterized as a hierarchical loss of effector CD8+ T-cell function: first, proliferative capacity and production of IL-2 are lost, followed by the ability to produce TNF- $\alpha$ , and ultimately IFN- $\gamma$ <sup>147</sup>. Loss of function generally coincides with expression of inhibitory surface receptors, including PD-1, LAG-3, CD160, 2B4, TIM-3, BTLA, and CTLA-4<sup>404</sup>. PD-1 has

emerged as a major inhibitory receptor associated with T cell exhaustion<sup>405-407</sup>. Upon binding to its ligands PD-L1 and PD-L2, PD-1/PD-L1/PD-L2 mediated signalling represses T-cell receptor signalling and paralyzes T-cell motility, probably in synergy with other inhibitory receptors<sup>285, 292, 408-410</sup>. In mice, T-cell exhaustion and the associated hierarchical loss of function can be modelled by infections with different strains of lymphocytic choriomeningitis virus (LCMV)<sup>411</sup>. Comparisons of gene expression profiles from naïve, effector, memory and exhausted CD8+ T cells from LCMV models have revealed that exhausted T cells harbour a unique and distinct molecular signature, with alterations in T-cell receptor and cytokine signalling pathways, metabolism, migration and actin-cytoskeleton formation<sup>412, 413</sup>. In addition, a number of transcription factors are differently expressed, such as BLIMP-1, BAT3, NFAT, TBET and EOMES<sup>414, 415</sup>.

However, exhaustion is neither a fixed, irreversible, terminal differentiation state, nor an unresponsive T-cell state, and several studies have demonstrated that exhausted T cells represent a very heterogeneous population containing several subsets of cells that despite PD-1 expression are able to exert certain effector function. For example, T-BET<sup>hi</sup>PD-1<sup>int</sup> cells represent a progenitor T-cell subset, which proliferate in response to persisting antigen, and give rise to EOMES<sup>hi</sup>PD-1<sup>hi</sup> subpopulations. The latter are considered the terminal progeny, express higher levels of other inhibitory receptors and do not replicate, but exhibit high levels of cytotoxic activity. Adoptive transfer experiments have demonstrated that during the early phase of chronic infection, exhausted virus-specific CD8+ T cells can continue their differentiation process and form functional T-cell memory upon transfer into healthy mice, but at the same time maintain an exhausted phenotype, including the surface expression of PD-1<sup>416</sup>. Exhausted T cells from established chronic infections in contrast were unable to differentiate when removed from antigen and did not restore effector functions. The heterogeneity of T-cell populations expressing PD-1 has been underscored by findings on the effect of antibody blockade, which could reverse exhaustion in PD-1<sup>int</sup> cells, but not in terminally differentiated PD-1<sup>hi</sup> T cells<sup>417</sup>.

Several studies have demonstrated that tumour-infiltrating T cells share many phenotypic and functional characteristics of exhausted T cells in chronic infections: these include impaired production of IFN- $\gamma$ , TNF- $\alpha$ , and IL-2, the expression of inhibitory receptors such as PD-1, LAG-3, 2B4, TIM-3, CD160 and CTLA-4, and altered signalling pathways described for exhausted T cells<sup>418-423</sup> were demonstrated to be expressed in a substantial number of CD8+ cells in tumour-bearing mice.

Our group has demonstrated that T cells from CLL patients exhibit features of T-cell exhaustion, such as increased expression of surface exhaustion markers, impaired proliferation, and cytotoxic defects with a reduced ability to lyse target cells, while retaining the capacity to produce cytokines such as IFN- $\gamma$  and TNF- $\alpha$ <sup>133</sup>. Another recently published study found that proliferating CD8 T cells from CLL patients had higher expression of PD-1 than non-proliferating T cells, and that T cells had impaired IFN- $\gamma$  and IL-4 production after direct binding of PD-1 to PD-L1 ligand, with both of those patterns also being observed but at a lower degree after stimulation of T cells from healthy controls<sup>134</sup>, suggesting a somewhat contained physiological reaction in CLL T cells.

Altogether, these observations emphasise the heterogeneity of PD-1 expressing T-cell populations in CLL. Despite the expression of typical exhaustion markers, certain effector functions appear to be maintained, but it is not clear how distinct states of dysfunction develop in the context of advancing CLL and what their functional characteristics are. Findings relating to PD-1 and exhaustion in human CLL are also likely to be biased by age: CLL is predominantly a disease of the elderly, but high PD-1 expression is also found on functional effector memory T cells in healthy older humans<sup>424</sup>. This suggests that PD-1 should not be considered a definitive marker for T-cell exhaustion and dysfunction. In addition, it is likely that factors such as antigen specificity, T-cell receptor affinity, level of tumour antigen, and T-cell differentiation state, as well as non-T-cell factors such as the microenvironment and metabolic conditions contribute to the functional state of not only CLL, but tumour-associated T cells in general.

Understanding the associations between PD-L1 and PD-1 expression and T-cell function is however particularly important for immunotherapeutic interventions, as different subsets might require different strategies to restore cell function: it is possible that blockade of the PD-1/ PD-L1 pathway has distinct effects on T-cell subsets, such as promoting effector T-cell populations with physiological PD-1 expression, restoring impaired effector function of “early exhausted” populations, or rescuing some effector functions in even terminally differentiated T cells. To date, this has only been partly answered in CLL, and studies using human CLL samples are likely to be biased by not only age, but also potentially underlying infections other than CMV, and treatment. In addition, peripheral blood T cells might show different expression patterns than cells in secondary lymphoid organs. The majority of these questions can be answered in the TCL1 model. Our group has demonstrated the suitability of this model to mirror T-cell dysfunction and T-cell directed questions, which was confirmed and extended by

further in-depth work in this project. We therefore hypothesized that TCL1 mice are also an adequate preclinical model to mirror PD-L1/PD-1 mediated immune dysfunction and to further study the concept of exhaustion in the absence of confounders. This is also an essential step to fully understand the effect of *in vivo* antibody blockade of PD-L1/PD-1 interactions.

## 6.2 Goals and objectives

My next goal was therefore to investigate the suitability of the B6 TCL1 model to mirror PD-L1/PD-1 interactions and their inhibitory effect on T-cell function, and to extend this to the second binding partner of PD-1, namely PD-L2. Specifically, I sought to address the following questions:

- Are the inhibitory ligands CD200, CD270, CD274 (PD-L1), CD276 and CD273 (PD-L2) differentially expressed on murine CLL cells?
- Are the previously described corresponding receptors CD160 and PD-1 expressed on murine CD8+ T cells?
- Can T-cell exhaustion be modelled in TCL1 mice, and if yes, what are the functional characteristics?
- How do inhibitory ligands and typical exhaustion markers develop in the context of advancing CLL?
- Can the TCL1 model be used to disentangle functional differences of the heterogeneous “exhausted” T-cell population using PD-1 as a marker?

## 6.3 Specific methods and materials

### 6.3.1 Mice and examined organs

The surface expression of CD200, CD270, CD274 (PD-L1) and CD276 was initially characterized in aged TCL1 mice on both the original C3HB6-F1 and the backcrossed B6 background from our colony, and in AT mice from AT experiments 5 and 6 (see Chapter 4, Table 7). Aged WT mice were retired female breeders from our colony. Mice were sacrificed under protocol 19b2 of PIL 70/7531 once they met the endpoint criteria for established CLL (see general methods), and spleens were harvested and

processed as described in general methods. An overview of mice included in this experiment is depicted in Figure 28.

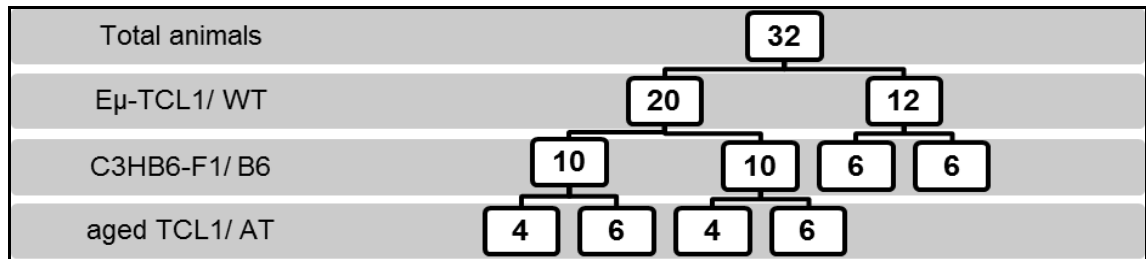


**Figure 28: Overview of mice to initially assess the expression of inhibitory ligands on spleen CLL and normal B cells.** A total of 32 animals were phenotyped (20 TCL1 and 12 age-matched WT mice). Both the original C3H and backcrossed B6 TCL1 mice were used, and leukaemic mice were aged TCL1 mice and young TCL1 mice that developed CLL after adoptive transfer (AT).

The changes in PD-L1 expression in the context of developing CLL were assessed in a second round of experiments, which we conducted alongside the T-cell phenotyping and T-cell functional studies described in the previous chapter using 3, 6 and 12 month old TCL1 and WT and AT mice listed in Table 8 as “II. Available mice to assess T-cell function in spleen alongside developing CLL”. PD-L1 and PD-L2 expression were characterized in spleen, PB, BM and LN from mice listed as 1<sub>func</sub> through 7<sub>func</sub> in “III. Available mice to assess T-cell phenotype in organs alongside developing CLL”.

WT and AT mice, listed as 1<sub>b</sub> through 8<sub>b</sub> in Table 8 as “I. Available mice to assess T-cell phenotype in spleen alongside developing CLL”, were used to characterize the expression and development of typical exhaustion markers in spleen. This was confirmed by a slightly modified panel excluding TIM-3 in spleen from mice listed as 1<sub>func</sub> through 7<sub>func</sub> in “III. Available mice to assess T-cell phenotype in organs alongside developing CLL”. These mice were also used to characterize expression of PD-1 in different organs. In the first experiment, AT recipients were young TCL1 mice, and in the second experiment, young WT recipients were used.

To unmask the effect of ageing and to assess T-cell function, surface T-cell exhaustion markers and functional T-cell assays were conducted in mice from AT experiment 8, Chapter 4. Young TCL1 transgenic mice (n=10) and sex-matched WT littermates (n=10) were randomized to AT with  $2 \times 10^7$  syngeneic CLL cells each, injected i.v. within three days of each other, or a pool of an equivalent number of spleen cells from healthy mice. Further information on AT procedures is provided in Chapter 4. Mice were bled regularly to assess the engraftment and development of CLL, and sacrificed once they

met the criteria for CLL defined in general methods. Matched recipients of normal spleen cells were sacrificed on the same day and served as controls in all experiments.

### 6.3.2 Multicolour flow cytometry for inhibitory ligand expression on normal and malignant B cells

CLL cells and normal B cells were characterized by CD19 and CD5 expression as previously described. Experiments were performed on both frozen and fresh samples. As controls, FMO and isotype controls for CD200, CD270, CD273 (PD-L2), CD274 (PD-L1) and CD276 were prepared. Samples were acquired on a BD LSRII. Stopping gates were set to CD19+CD5+ cells in leukaemic mice and CD19+ in healthy mice to record 15,000 events. Information on antigens, fluorochromes, clones, concentrations and suppliers is listed in Table 14.

	mouse antigen	fluorochrome	clone	concentration	host/isotype	supplier
inhibitory ligands	CD200	PerCPe-fluor 710	OX90	0.2 mg/ml	rat IgG2ak	eBioscience
	CD270	APC	HMHV-1B18	0.2 mg/ml	Armenian hamster IgG	eBioscience
	CD273	PerCPe-fluor 710	122	0.2 mg/ml	rat IgG2ak	eBioscience
	CD274	PeCy7	10F.962	0.2 mg/ml	rat IgG2bk	Biolegend
	CD274	PE	MIH5	0.2 mg/ml	rat IgG2aλ	eBioscience
	CD276	PE	M3.2D7	0.2 mg/ml	rat IgG2ak	eBioscience
CLL	CD5	FITC	53-7.3	0.5 mg/ml	rat IgG2ak	eBioscience
	CD5	APC	53-7.3	0.2 mg/ml	rat IgG2ak	eBioscience
	CD19	APC-Cy7	6D5	0.2 mg/ml	rat IgG2ak	Biolegend
	CD19	FITC	eBio1D3	0.5 mg/ml	rat IgG2ak	eBioscience
isotype controls		PE	RTK2758	0.2 mg/ml	rat IgG2ak	Biolegend
		PeCy7	RTK4530	0.2 mg/ml	rat IgG2bk	Biolegend
		PerCPe-fluor 710	eB149/10H5	0.2 mg/ml	rat IgG2ak	eBioscience
		APC	HTK888	0.2 mg/ml	Armenian hamster IgG	Biolegend

**Table 14: Summary of antigens, fluorochromes, antibody clones, concentrations and suppliers used to assess inhibitory ligand expression.**

An example of the gating strategy to identify cell populations positive and negative for inhibitory ligands is depicted in Figure 29. Cells were gated on viable (*i.e.* DAPI-negative) single MNC. Inhibitory ligands were gated on CD19+ B cells in WT mice and CD19+CD5+ CLL cells in TCL1 and AT mice. Gates were placed based on isotype and

FMO controls for inhibitory ligands and expressed as percentage of cells positive for a specific inhibitory marker (Figure 29 A, example shows gating on CLL cells from a representative TCL1 mouse). In addition, the median fluorescence intensity (MFI) was reported for each ligand, corrected for the MFI of the respective isotype control (specific MFI).

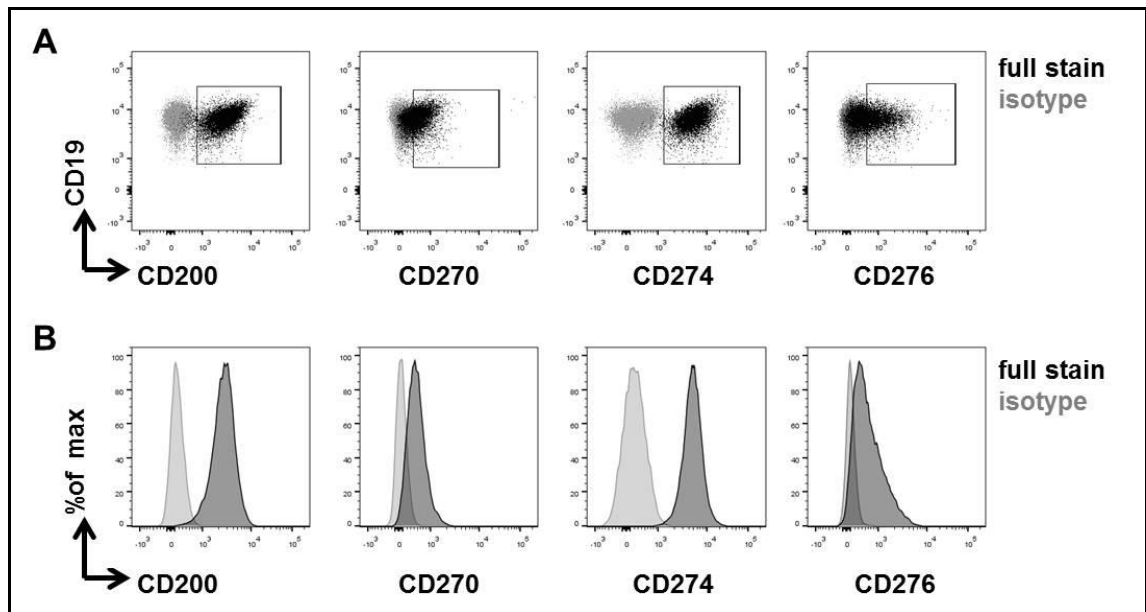


**Figure 29: Gating strategy to assess expression of inhibitory ligands on normal B cells and CLL cells in mice.** Cells were gated on viable single mononuclear cells. CD200, CD270, CD274 and CD276 were gated on CD19+ B cells in WT mice and CD19+CD5+ CLL cells in leukaemic mice. **(A)** Cell populations positive and negative for inhibitory ligand expression were discriminated based on isotype and FMO controls. This graph shows a representative example from a TCL1 mouse, and combines FCS files from the full stain containing all fluorochrome-labelled antibodies (black colour), and the isotype control for the respective marker (grey colour). **(B)** Corresponding histograms depicting the median fluorescence intensity (MFI) for each ligand (dark colour) and the isotype control (grey colour).

### 6.3.3 Comparison of gene-expression profiles from T-cell subsets in deposited data

To investigate the molecular mechanisms of T-cell exhaustion, the gene expression profile (GEP) of CD8+ T cells from leukaemic TCL1 mice published by our group (GEO accession number GSE8836)<sup>216</sup> was compared to previously published GEP data of effector, memory, and exhausted T cells (GSM235537)<sup>412</sup>. The latter was a landmark publication characterizing differences in the molecular signature of exhausted, effector and memory CD8+ T cells from murine LCMV infection models compared to naïve CD8+ cells. This paper used infection with Armstrong strain of LCMV, which is usually cleared by day 10, followed by contraction and differentiation, to model acute infection

and the generation of functional effector and memory CD8<sup>+</sup> T cells. Infection with clone 13 of LCMV leading to chronic infection, accompanied by loss of effector function and ineffective viral control, was used to model T-cell exhaustion. The CLL T-cell dataset was reanalysed with Partek software, and following the criteria of the LCMV analysis, TCL1 genes that were at least 2-fold up- or downregulated were selected as aberrantly expressed and exported to Microsoft Excel for further analysis. This gene list was then manually compared to reported dysregulated genes in effector, memory and exhausted CD8<sup>+</sup> T cells both by gene ID, alternative names, and accession number. Genes that were represented in both the TCL1 and any of the LCMV signatures were considered as overlapping genes, and attributed to specific LCMV subset signatures regardless of whether they were up- or downregulated.

#### **6.3.4 Multicolour flow cytometry for surface expression of T-cell exhaustion markers**

T-cell subsets were characterized based on the surface expression of CD3, CD4, CD8 and CD44. PD-1, TIM-3, CD160, KLRG-1, 2B4 and LAG-3 were selected as typical exhaustion markers that have also been used to define exhaustion-like phenotypes in other murine cancer models. In experiments unmasking the effect of ageing by AT, the panel was extended by the cytokine receptors CD122 and CD127. CLL was routinely determined by CD19 and CD5 expression. Information on antigens, fluorochromes, clones, concentrations and suppliers is listed in Table 15.

Cells were prepared for flow cytometry as described in Chapter 3.4.1. Stopping gates were set to CD3<sup>+</sup>CD8<sup>+</sup> cells to record at least 12,000 events. Cells were gated on viable single MNC. CD4 and CD8 were gated on CD3<sup>+</sup> lymphocytes. Naïve cells were identified as CD44<sup>low</sup> and antigen-experienced cells as CD44<sup>+</sup> based on FMO controls for CD44. Exhaustion markers were gated on CD3<sup>+</sup>CD8<sup>+</sup> MNC and plotted against CD44. Gates to discriminate cells positive and negative for a certain exhaustion marker were placed based on FMO controls for exhaustion markers and included in all experiments.

	mouse antigen	fluorochrome	clone	concentration	host/ isotype	supplier
T-cell phenotype	CD3e	APCCy7	17A2	0.2 mg/ml	rat IgG2bk	Biolegend
	CD4	PerCPCy5.5	RM4-5	0.2 mg/ml	rat IgG2ak	eBioscience
	CD8a	FITC	53-6.7	0.5 mg/ml	rat IgG2ak	eBioscience
	CD44	PECy7	IM7	0.2 mg/ml	rat IgG2bk	eBioscience
	CD44	PE	IM7	0.2 mg/ml	rat IgG2bk	eBioscience
T-cell surface exhaustion markers	PD-1	APC	RMP1-30	0.2 mg/ml	rat IgG2bk	eBioscience
	TIM3	PE	88.2C12	0.2 mg/ml	rat IgG1k	eBioscience
	CD160	PE	eBioCNX46-3	0.2 mg/ml	rat IgG2ak	eBioscience
	LAG3	PE	eBioC9B7W	0.2 mg/ml	rat IgG1k	eBioscience
	LAG3	PerCP e-fluor710	eBioC9B7W	0.2 mg/ml	rat IgG1k	eBioscience
	2B4	APC	244F4	0.2 mg/ml	rat IgG2ak	eBioscience
	KLRG1	PE	2F1	0.2 mg/ml	golden Syrian hamster IgG	eBioscience
KLRG1	PerCP e-fluor710	2F1	0.2 mg/ml	golden Syrian hamster IgG	eBioscience	
T-cell cytokine receptors	CD122	PE	5H4	0.2 mg/ml	rat IgG2ak	eBioscience
	CD127	APC	A7R34	0.2 mg/ml	rat IgG2ak	eBioscience
CLL	CD5	APC	53-7.3	0.2 mg/ml	rat IgG2ak	eBioscience
	CD19	FITC	eBio1D3	0.5 mg/ml	rat IgG2ak	eBioscience

**Table 15: Summary of antigens, fluorochromes, antibody clones, concentrations and suppliers used to assess T-cell exhaustion markers in relation to CLL.**

### 6.3.5 Multicolour flow cytometry for intracellular cytokines and effector function in AT experiments unmasking the effect of ageing

For these studies, T-cell subsets were characterized based on the surface expression of CD3, CD8 and CD44. PD-1 was included into this panel to allow discrimination of effector function based on PD-1 expression. Cytotoxicity was assessed by measuring CD107a effector cell degranulation. The cytokine panel was extended to include intracellular IFN- $\gamma$ , IL-2, TNF- $\alpha$ , IL-4 and IL-5. *Ex vivo* proliferation was measured using CFSE. Table 16 shows information on antigens, fluorochromes, antibody clones, concentrations and suppliers.  $10 \times 10^6$  fresh spleen cells from mice with CLL and  $5 \times 10^6$  fresh spleen cells from healthy mice were kept in RPMI 1640 with 10% FCS, 1% Penicillin/Streptomycin, 1% Glutamine, and 500mM beta-mercaptoethanol in a flat bottom 12 well-plate. 5 $\mu$ g/ml CD107a was added to each well, and cells were stimulated and processed as described in Chapter 5.3.3. Controls included wells with CD107a antibody and protein transport inhibitor cocktail, but no cell stimulation

cocktail. After the incubation, cells were harvested, washed with PBS and prepared for flow cytometry as described before.

For intracellular cytokine production, cells were set up using identical conditions in a separate 12 well plate, with the exception that  $20 \times 10^6$  fresh spleen cells from mice with CLL were used. After the incubation, cells were harvested into Falcon tubes (BD, UK), stained with fixable viability dye 450 (eBioscience, UK) and surface stained 30 minutes on ice. Cells were washed, fixed and permeabilised as described before. Before intracellular staining, both stimulated and unstimulated wells were split equally to Th1 and Th2 cytokine tubes, and cells were stained with intracellular antibody cocktails for 30 minutes at room temperature.

	mouse antigen	fluorochrome	clone	concentration	host/ isotype	supplier
surface stain	CD3e	PerCPeFl 710	17A2	0.2 mg/ml	rat IgG2bk	eBioscience
	CD8a	BV605	53-6.7	0.5 mg/ml	rat IgG2ak	Biolegend
	CD44	AF700	IM7	0.2 mg/ml	rat IgG2bk	eBioscience
	PD-1	APC	RMP1-30	0.2 mg/ml	rat IgG2bk	eBioscience
	PD-1	PerCPeFl 710	RMP1-30	0.2 mg/ml	rat IgG2bk	eBioscience
cytotoxicity	CD107a	PE	eBio1D4B	0.2 mg/ml	rat IgG2ak	eBioscience
intracellular cytokines	IFN- $\gamma$	PE	XMG1.2	0.2 mg/ml	rat IgG1k	eBioscience
	IL-2	PeCy7	JES6-5H4	0.2 mg/ml	rat IgG2bk	eBioscience
	TNF- $\alpha$	APC	MP6-XT22	0.2 mg/ml	rat IgG1k	eBioscience
	IL-4	APC	11B11	0.2 mg/ml	rat IgG1k	eBioscience
	IL-5	PE	TRFK5	0.2 mg/ml	rat IgG1k	eBioscience

**Table 16: Summary of antigens, fluorochromes, antibody clones, concentrations and suppliers used to assess T-cell function in relation to CLL.**

CD107a and intracellular cytokines were gated as described before. In addition, cytokine production was plotted against CD44. Stopping gates were set to CD3+CD8+CD44+ cells to record at least 15,000 events, or until the sample had been fully aspirated, whichever occurred first. Differences in T-cell function between mice with CLL and healthy WT mice, and between PD-1<sup>high</sup> and PD-1<sup>low</sup> subsets were compared by calculating ratios between CD44+ antigen-experienced cells positive or negative for a cytokine or CD107a. This ratio was interpreted as cells with the ability to exert effector cell function compared to cells of the same subset that lack this ability. Changes of this ratio were interpreted as loss or gain of cells with effector cell function.

### **6.3.6 Flow sorting of PD-1 subsets for immune synapse formation assays**

To assess differences of PD-1 subsets in the ability to form immunological synapses with normal mouse B cells as APCs, spleens from 6 available mice with CLL after AT were flow-sorted based on PD-1 expression. A pool of normal frozen mouse splenocytes was used as controls and subjected to the same procedures, including flow sorting. Frozen splenocytes were thawed and debulked of CLL cells by positive magnetic selection as described in Chapter 3.3.1. Positive labelled normal B cells were used as APC and rested in the incubator until needed. Cells in the CD19<sup>-</sup> fractions were stained with CD8 FITC, CD44 PE and PD-1 APC. An example of the sorting strategy is shown in Figure 30 A. CLL T cells were sorted for PD-1<sup>high</sup>, PD-1<sup>low</sup>, and CD8<sup>+</sup> T cells. Normal T cells were sorted for CD8<sup>+</sup> only. Purities were confirmed to be >95% (Figure 30 B), and stopping gates were set to obtain a minimum of 500,000 T cells per subset for each condition in the synapse assay, which was performed as described in Chapter 3.5.

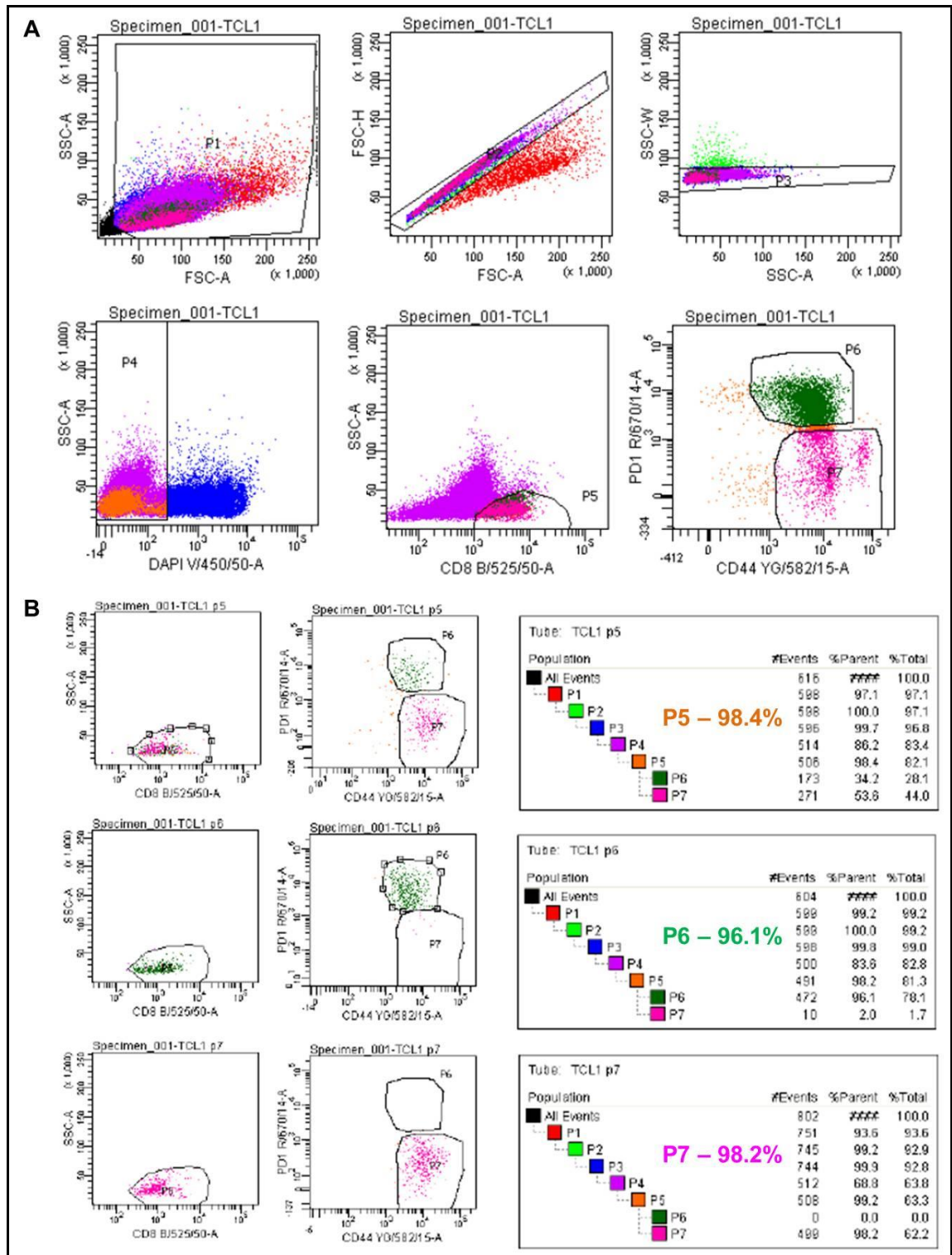


**Figure 30: Flow sorting of CD8+ T cells according to PD-1 expression.** Frozen splenocytes from WT mice and mice with CLL after AT were debulked of B cells by positive selection, and the remaining cells were stained with CD8, CD44 and PD-1. **(A)** Example of gating and sorting strategy. **(B)** Purities were confirmed to be >95% for all sorted populations.

## 6.4 Results

### 6.4.1 Inhibitory ligands CD200, CD270, CD274 (PD-L1) and CD276 are expressed on murine CLL cells but only CD274 and CD276 are significantly upregulated compared to normal B cells

To investigate if the TCL1 model is a suitable tool to mirror PD-L1/PD-1 interactions, we first compared the expression of the previously identified inhibitory ligands CD200, CD270, CD274 (PD-L1), and CD276 on spleen CLL cells from TCL1 and AT mice and compared this to the expression on CD19+ B cells from age-matched healthy WT mice. This first experiment was performed on frozen cells as mice had reached their individual CLL-defined endpoint at different times. To minimize the likelihood of a batch effect, samples were cryopreserved until a sufficient number of mice had been collected, and the phenotyping panel was performed on all previously frozen cells samples at the same time.

The CLL load in spleen was very high, defined as the proportion of CD19+CD5+ cells after gating on viable single MNC in this cohort of leukaemic animals, with a median of 92%, and a minimum of 64% in two animals. WT mice were confirmed to be free of CLL. PD-L1 was uniformly expressed on virtually all spleen CLL cells (median 99.2%, range 95.6-100). CD200 and CD270 were in general highly expressed but the percentage of expression on CD19+CD5+ spleen cells varied among animals (CD200 median 84.8%, range 42.8-99.9; CD270 median 72.3%, range 46.7-96.7). In contrast, CD276 expression levels varied widely among leukaemic animals (median 51.9%, range 7.7-94.7)

However, the comparison to normal spleen B cells from healthy WT mice revealed that in contrast to our human data, the percentage of CD200+ and CD270+ cells was significantly lower in TCL1 mice than in WT mice (CD200  $p=.0216$ , CD270  $p<.0001$ ). Just as in human CLL, the percentages of PD-L1+ and CD276+ cells were higher in TCL1 than in WT mice (PD-L1  $p=.0002$ ; CD276  $p=.0226$ , Figure 31 A). This pattern was also recapitulated when comparing the specific MFI (MFI corrected for the MFI of the FMO/isotype control: CD200  $p<.0001$ ; CD270  $p=.0004$ ; CD274  $p<.0001$ ; CD276  $p=.0008$ ) (Figure 31 B). Both FMO conditions and isotypes were used as controls, which showed very similar results. In general, the expression of all ligands was relatively uniform on normal B cells from WT animals. Consistent with the organomegaly associated with CLL, the absolute numbers of spleen cells positive for CD200, CD270, PD-L1 and CD276 were all significantly increased in leukaemic mice (Figure 31 C).

In leukaemic mice, background (*i.e.* B6 TCL1 vs. C3H TCL1) appeared to have only a minor effect on expression of inhibitory ligands: similar patterns regarding CD270, PD-L1 and CD276 were observed in B6 and C3H TCL1 mice, whereas CLL cells from C3H TCL1 mice showed a borderline significantly higher percentage of CD200 expression (Figure 31 D). This was also confirmed by comparing specific MFIs. No differences were found between aged TCL1 mice with CLL and AT mice, both in terms of relative expression and specific MFI (Figure 31 E).

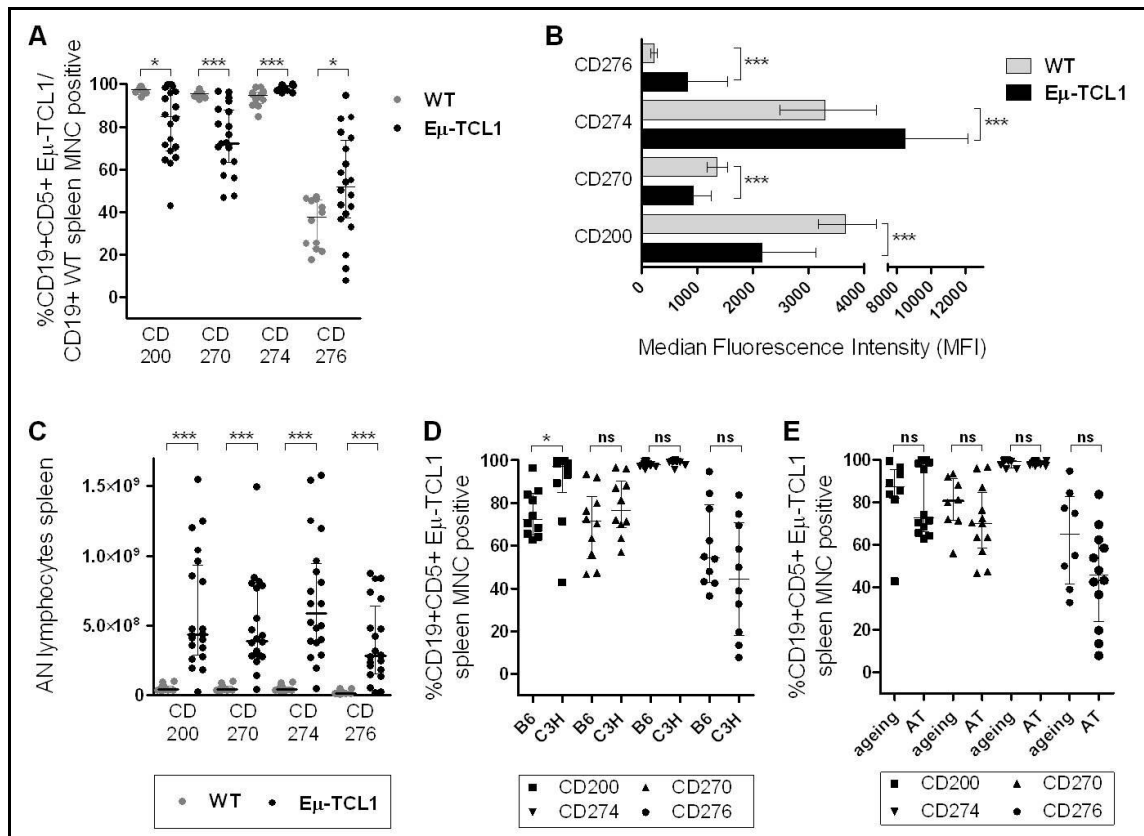


**Figure 31: Expression of CD200, CD270, CD274 (PD-L1) and CD276 on CLL and normal B cells.** Absolute number (AN) of cells positive for a marker, defined by gating on FMO and isotype controls, and specific MFI (Median Fluorescence Intensity, MFI corrected for the MFI of the FMO/ isotype control) were compared. **(A)** Percentage of CD200+ and CD270+ CLL/B cells was lower in TCL1 mice than in WT mice, while percentage of CD274+ and CD276+ cells was higher in TCL1 than in WT mice. **(B)** Similar patterns were found when comparing specific MFIs. **(C)** Consistent with the organomegaly associated with CLL, AN of spleen cells positive for CD200, CD270, CD274 and CD276 were significantly increased in leukaemic mice. **(D)** Similar expression patterns were found in TCL1 mice on both backgrounds (B6 TCL1 vs. C3H TCL1), with the exception of CD200. **(E)** No differences were found between aged TCL1 mice with CLL and AT mice. All graphs depict median with interquartile range (IQR). ns = non-significant, \* $p < .05$ , \*\* $p < .001$ , \*\*\* $p < .0001$ .

#### **6.4.2 Highly aberrant PD-L1 and PD-L2 expression are exclusive to malignant CLL cells and develop in the context of advancing disease regardless of microenvironment**

After we confirmed that aberrant PD-L1 expression on spleen CLL cells can be modelled in TCL1 mice and that it closely mirrors the expression of PD-L1 in human CLL, we sought to examine how this develops in the context of progressing CLL. In addition, characterization of PD-L1 expression in human CLL had been limited to flow cytometry in PB and immunohistochemistry in LN, while the mouse data described in Chapter 6.4.1 was derived from spleen single cell suspensions. Therefore, we sought to extend the mouse phenotyping panel to PB, BM and LN, and to also assess the expression of PD-L2 in 3, 6, and 12 month old TCL1 and WT mice and AT mice (WT recipients). As our first experiment demonstrated that percent positive cells and specific MFI provide effectively the same information, we restricted this analysis to comparison of MFIs.

We routinely confirmed that WT and young TCL1 mice were free of CLL. As before, in mice without a detectable CLL population PD-L1/PD-L2 expression was assessed on CD19+ B cells, while in mice with CLL this was assessed on CD19+CD5+ CLL cells (Figure 32 C). As discussed in the previous chapter, 6 month old TCL1 mice represent an early stage of CLL, where malignant CD19+CD5+ CLL cells exist alongside normal CD19+ B cells, allowing these populations to be directly compared. We therefore assessed expression on both normal and malignant B cells in this age group to gain insight as to whether PD-L1/PD-L2 expression is exclusive to CLL cells.

PD-L1 expression on normal spleen B-cells was relatively constant in healthy ageing WT mice, but increased in TCL1 mice developing CLL and after AT (Figure 32 A). This was recapitulated in BM and LN. In PB, PD-L1 expression in WT mice was significantly increased at 6 and decreased at 12 months, but this was most likely the result of a single outlier in this group of mice. In PB of TCL1 mice developing CLL and in AT mice, PD-L1 expression increased consistently. The direct comparison of normal and malignant B-cell populations in 6 month old TCL1 mice demonstrated that aberrant PD-L1 expression appeared to be restricted to CLL cells in spleen and BM (for both organs,  $p=.0022$  for MFI of PD-L1 in normal B cells vs. CLL cells). A similar, but not-significant, trend was observed in PB ( $p=.09$ ). Interestingly, PD-L1 expression was comparable ( $p=.2805$ ) in normal and malignant B cells in LN in these 6 month old mice, and only became strongly upregulated at 12 months, and to a certain degree after AT. This is consistent with the longer latency of disease accumulation we observed in LN (see previous chapter). Confirming our previous findings, PD-L1 expression was

significantly upregulated in fully leukaemic mice compared to age-matched WT mice in all organs ( $p=.0043$ ). PD-L2 expression appeared to be strongly dependent on the microenvironment in ageing WT mice, as it showed a slight upregulation in spleen, BM and LN, but not PB (Figure 32 B). In TCL1 mice, highly upregulated PD-L2 was restricted to CLL cells, as demonstrated by the direct comparison between normal and malignant B-cell populations in 6 month old TCL1 mice. In addition, PD-L2 expression was significantly higher on CLL cells from all organs from fully leukaemic mice compared to normal B cells from aged-matched healthy WT mice ( $p=.0043$ ). Statistical differences of MFIs compared to 3 month old mice as baseline are summarized in Figure 32 D.

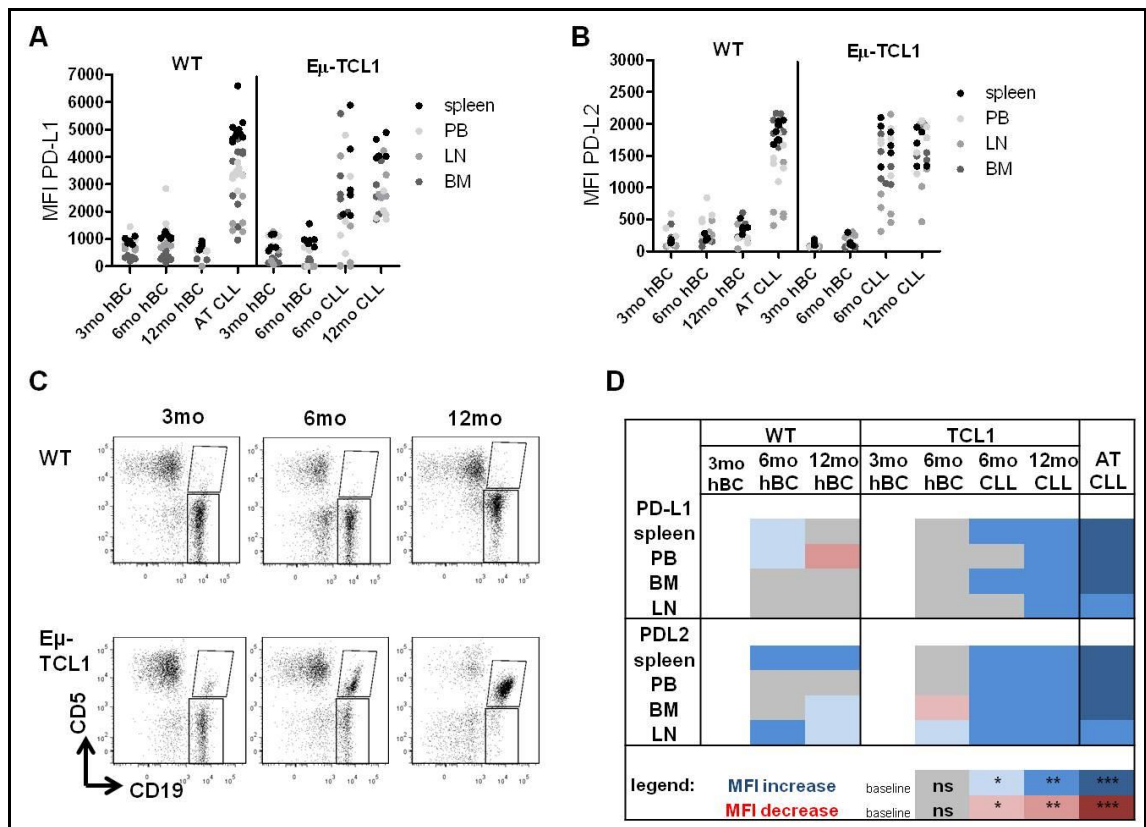


**Figure 32: Development of PD-L1/PD-L2 expression alongside advancing CLL in different organs.** Organs from 3, 6, and 12 month old TCL1 and WT mice and AT mice (WT recipients) were phenotyped by flow cytometry and specific MFIs were compared. **(A)** PD-L1 expression increased progressively in TCL1 mice and after AT in all examined organs. Aberrant expression was restricted to CLL cells as evidenced by direct comparison between normal and malignant B cells in 6 month old TCL1 mice, and was significantly higher in fully leukaemic TCL1 than in healthy WT mice. **(B)** PD-L2 expression appeared to be dependent on the microenvironment in ageing WT mice, and increased progressively in TCL1 mice and after AT in all examined organs. Highly increased expression was exclusive to malignant B cells. **(C)** Examples of representative flow plots from spleen demonstrating the presence/absence/co-existence of normal and malignant B-cell populations. **(D)** Heatmap summary of p-values describing statistical differences in MFI. Groups were compared to specific MFIs in 3 month old mice. Blue colour indicates increase, red colour indicates decrease of MFI. ns = non-significant, \* $p<.05$ , \*\* $p<.001$ , \*\*\* $p<.0001$ .

### **6.4.3 Molecular signature of exhausted T-cells from LCMV infection model is represented in murine CLL T cells but similarities to functional effector cells are maintained**

After confirming the suitability of TCL1 mice to model aberrant PD-L1/PD-L2 expression, we focused on the further characterization of their binding partner PD-1 on CD8+ T cells. Aberrant PD-1 expression has been reported as having implications not only in human CLL, but also in chronic viral infection leading to T-cell exhaustion. In addition, the majority of dysregulated pathways identified in the molecular signature of CLL CD8+ T cells showed resemblance to dysregulated pathways reported in exhausted T cells in chronic viral infection. However, further studies have indicated that T cells in CLL show phenotypic similarities to exhausted T cells but maintain certain effector functions such as cytokine proliferation, indicating that they might not be “truly” exhausted. To investigate the molecular mechanisms of T-cell dysfunction and to determine if dysregulated CLL T cell genes are represented and/ or enriched in the molecular signature of exhausted, effector or memory cells, we compared the gene expression profile of CD8+ T cells from leukaemic TCL1 mice to previously published gene expression profile data of effector, memory, and exhausted T cells<sup>412</sup>.

Between 690 dysregulated genes in the TCL1 and 680 dysregulated genes in the LCMV dataset, 73 genes were overlapping (Figure 33 A). A summary of overlapping genes can be found in Table 28 in the Appendix. Among LCMV genes, Wherry *et al.* confirmed that exhaustion represents a unique state of T-cell gene expression compared to other cell subsets, as it contains a large number of exclusively expressed dysregulated genes (Figure 33 B). In addition, they identified more similarities between exhausted and effector cells than between exhausted and memory cells. A remarkably similar distribution was observed in the overlapping genes from our dataset; over one third of CLL T-cell genes were represented in the exhaustion signature, indicating that this also represents a unique state of gene expression in CLL T cells (Figure 33 C). These genes were mostly involved in the regulation of signalling potential, transcription factors, metabolic/bioenergetic regulation, cytoskeleton regulation and vesicle trafficking. In addition, about 20% of overlapping dysregulated genes from our dataset were also represented in the effector signature, and 16% in the overlapping signature between exhausted and effector cells, which potentially explains the partly maintained effector function of CLL T cells described in the literature.

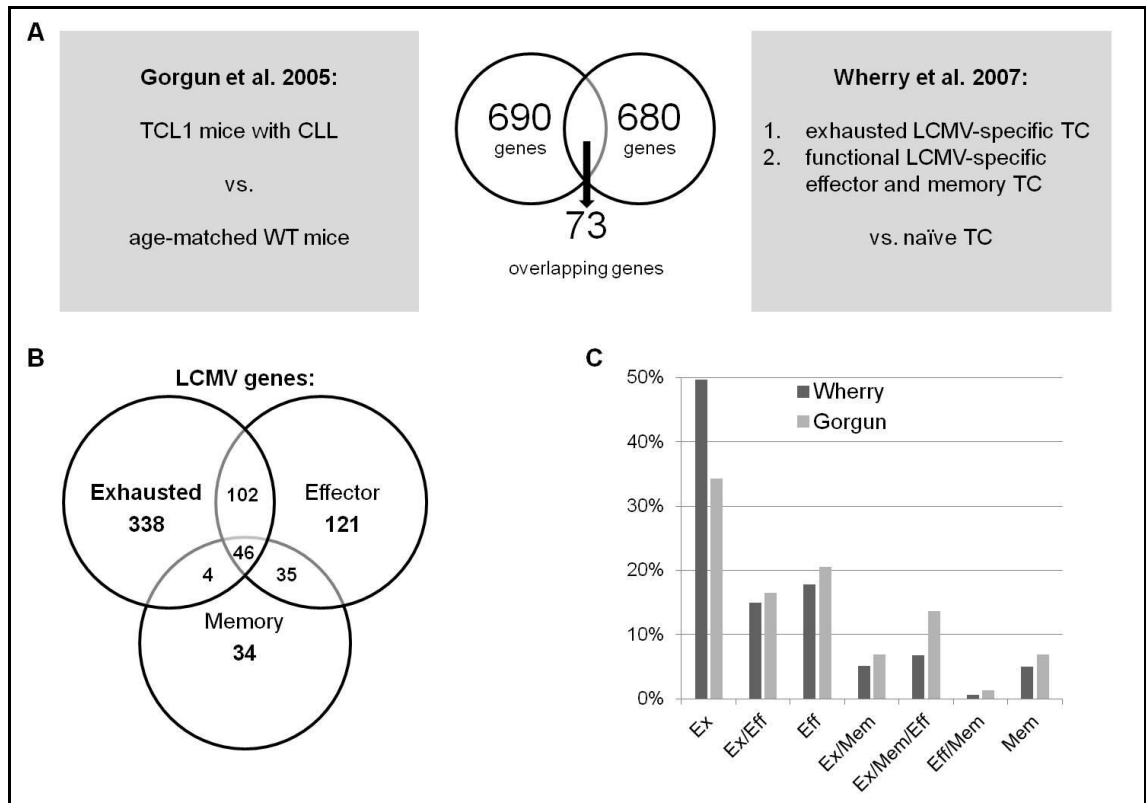


**Figure 33: Comparison of gene expression profiles between deposited data.** The molecular signature of CD8+ T cells from leukaemic TCL1 mice (Gorgun *et al.*<sup>216</sup>, GEO accession number GSE8836) was re-analysed with Partek software applying the criteria of Wherry *et al.*<sup>412</sup> (GSM235537). **(A)** Overlap in gene expression profile for the TCL1 (Gorgun) and the Wherry dataset. **(B)** More similarities exist between exhausted and effector cells than between exhausted and memory cells (graph adapted from Wherry *et al.*, shown here to illustrate the grouping of gene signatures). **(C)** Distributions in the overlapping genes from the TCL1 (Gorgun) and LCMV (Wherry) exhaustion (Ex), effector (Eff) and memory (Mem) signatures.

#### 6.4.4 Typical exhaustion phenotype is modelled in TCL1 mice but is confounded by ageing

After confirming that the molecular signature of CLL CD8<sup>+</sup> T cells resembles that of exhausted T cells, we sought to determine the surface expression of exhaustion markers that had also been described in other murine cancer models. These included PD-1, TIM-3, CD160, KLRG-1, 2B4 and LAG-3. Here, we focused on PD-1 due to the prominent role of its ligands PD-L1 and PD-L2 in both human and murine CLL.

Using CD44 expression to discriminate between naïve (CD44<sup>-</sup>) and antigen-experienced (CD44<sup>+</sup>) CD3<sup>+</sup>CD8<sup>+</sup> cells, we determined changes in the relative and absolute numbers of PD-1<sup>+</sup> and PD-1<sup>-</sup> subsets in 3, 6 and 12 month old TCL1 and WT mice and after AT. Gates were defined based on PD-1 FMO controls (Figure 34 A). An example of how subsets were quantified in the context of the dynamic changes within CD3<sup>+</sup>CD8<sup>+</sup> cells (*i.e.* loss of naïve cells and shift to antigen-experienced cells; see previous chapter) is depicted in Figure 34 B. With developing CLL, PD-1 was step-wise upregulated on antigen-experienced cells, and in line with the organomegaly, absolute numbers increased. This was to a certain extent also observed in ageing WT mice, confirming that the relative PD-1 expression is confounded by the effect of ageing. However, the upregulation of PD-1 could be induced in young mice after AT, suggesting a causal relationship between CLL and PD-1 expression. We confirmed these patterns in two independent experiments using different mice; the relative (left panel) and absolute numbers (right panel) of CD3<sup>+</sup>CD8<sup>+</sup>CD44<sup>+</sup>PD-1<sup>+</sup> cells are shown in Figure 34 C for experiment 1, and in Figure 34 D for experiment 2.

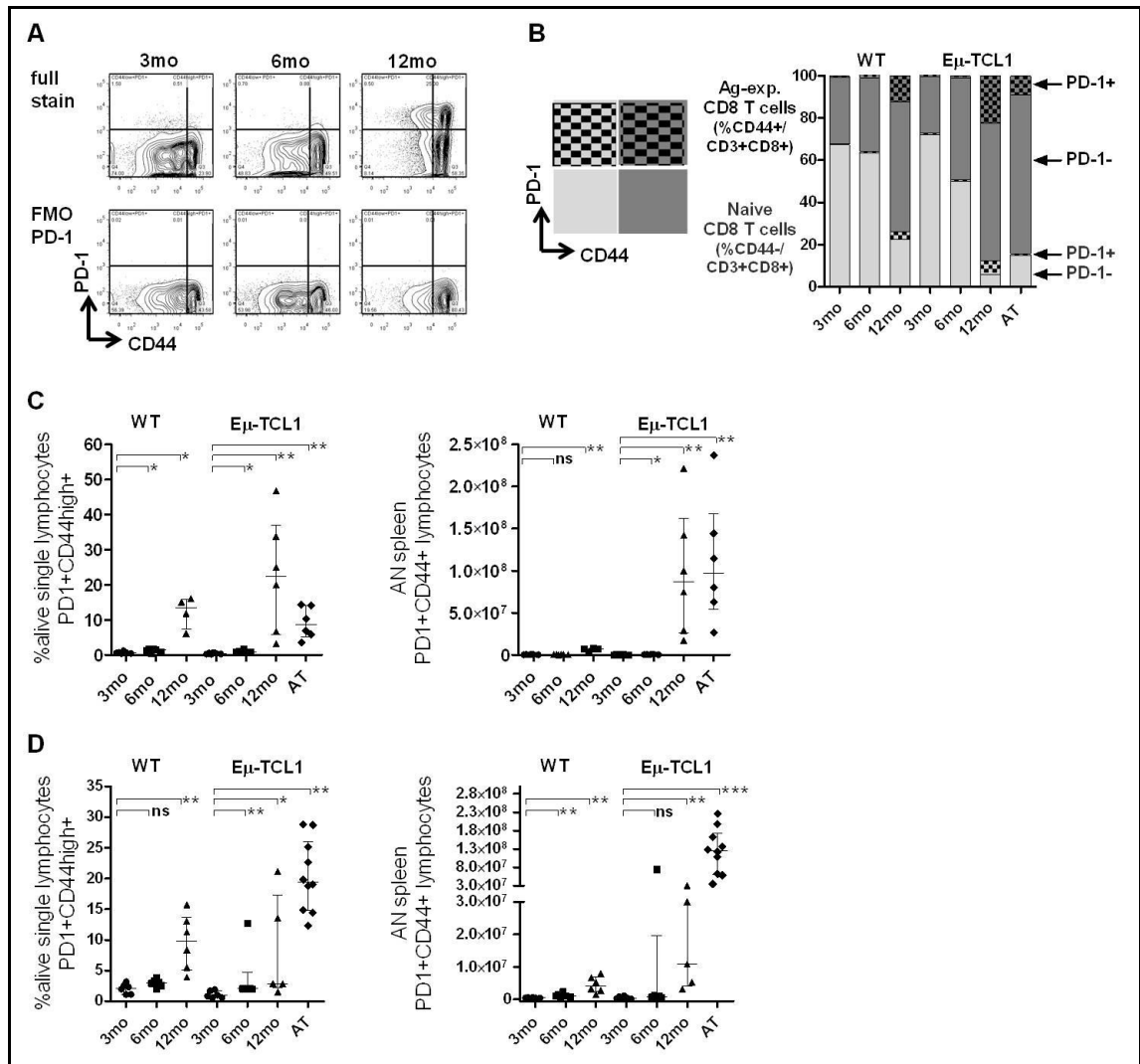


**Figure 34: Surface expression of PD-1 on naïve CD44- and antigen-experienced CD44+CD3+CD8+ cells from spleen.** Changes in relative and absolute numbers (AN) of PD-1+ and PD-1- subsets were compared in 3, 6 and 12 month old TCL1 and WT mice, and after AT. **(A)** Representative flow plots from TCL1 mice at different ages demonstrating the shifts of subsets. FMO controls were used to determine PD-1 gates. **(B)** Quantification of subsets in the context of CLL-induced T-cell subset changes. Stacked bar charts were used to visualize the loss of naïve (light grey) and shift to antigen-experienced cells (dark grey), along with the changing expression of PD-1. **(C)** With developing CLL and after AT, PD-1 expression increased on antigen-experienced cells, and to a certain extent also in WT mice. AN were significantly higher in TCL1 and AT mice. **(D)** Confirmation in second experimental round. All graphs in (C) and (D) show median with interquartile range. ns = non-significant, \*p<.05, \*\*p<.001, \*\*\*p<.0001.

We observed very similar patterns for LAG-3 (Figure 35 A), 2B4 (Figure 35 B) and KLRG-1 (Figure 35 C), which were confirmed by two experimental rounds. TIM-3 expression increased in ageing TCL1 mice but was generally expressed at very low levels (median in all age groups <2% CD3+CD8+CD44+TIM3+), and expression could not be induced by AT (Figure 35 D). As it cannot be assumed that expression changes at such low levels indicate true disease-related aberrations, we excluded this marker from the confirmation experiment.

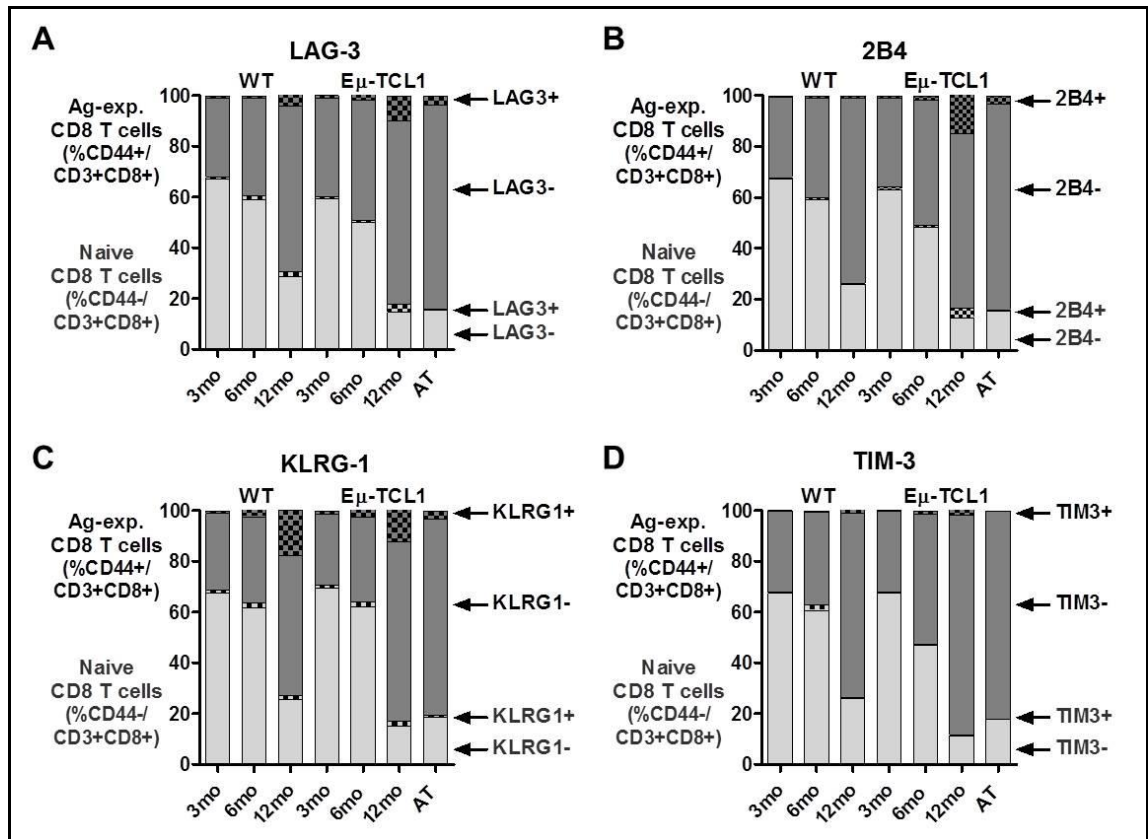


**Figure 35: Surface expression of other exhaustion markers on naive CD44- and antigen-experienced CD44+ CD3+CD8+ cells from spleen.** Confirmation of increased expression of (A) LAG-3, (B) 2B4 and (C) KLRG-1 in ageing TCL1 mice and after AT. (D) TIM-3 was expressed at very low levels and could not be induced by AT. Stacked bar charts provide an overview of data from experiment 1 and are shown as a representative example for both experiments.

A very different pattern was observed for CD160: in the first experiment, expression increased with developing CLL and after AT, in line with the other exhaustion markers. In the second experiment, however, expression was lost in ageing TCL1 mice and after AT, with absolute numbers still being significantly higher than in WT mice, while relative CD160 increased in WT mice (Figure 36 A and B). To rule out that this was caused by slight differences in the gating strategy or a batch effect by mice, data from both experiments was re-gated and re-analysed together, which yielded the same results. In addition, the characteristics of mice used in experiments were compared and no differences were detected (data not shown).

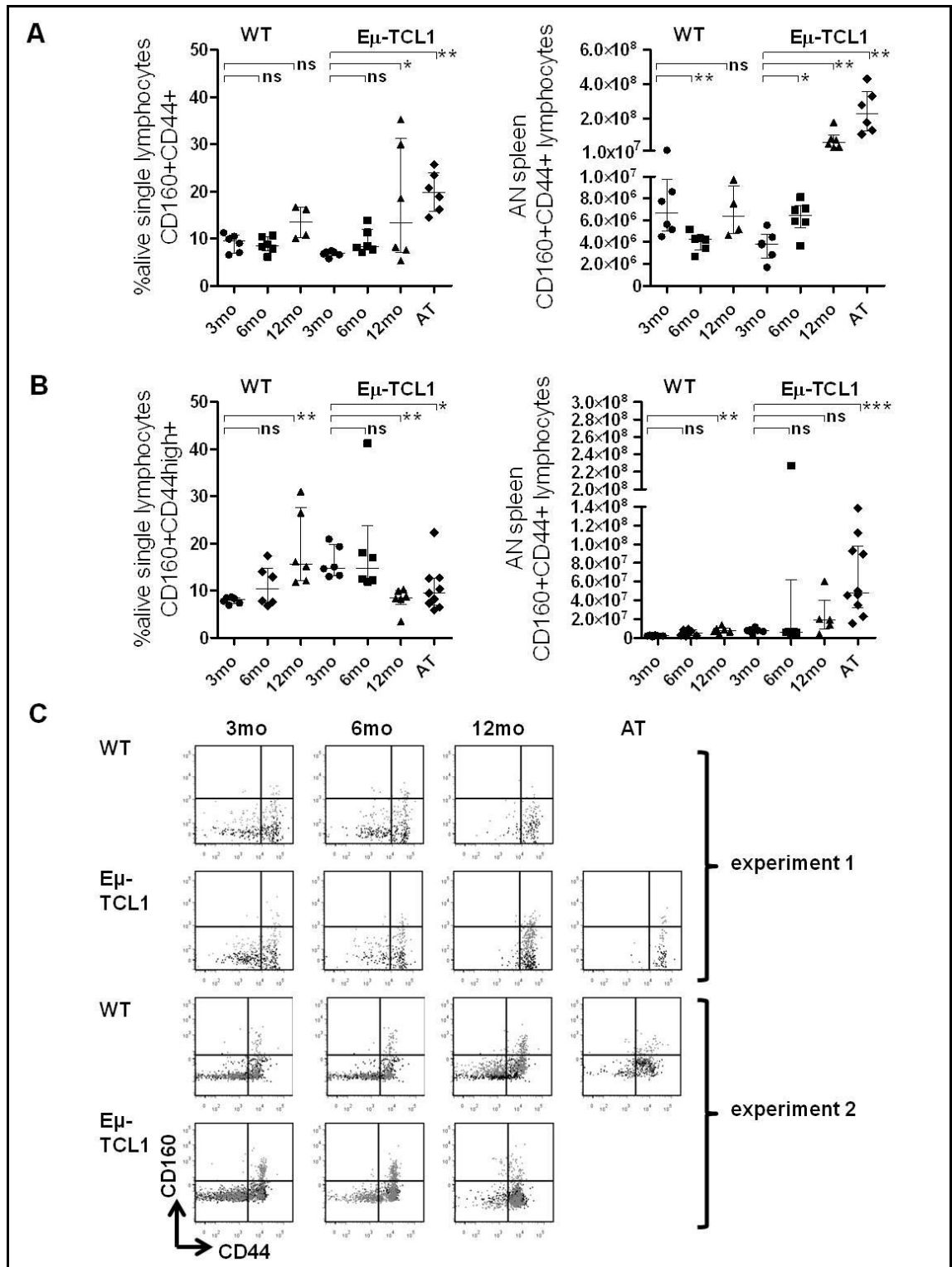


**Figure 36: Surface expression of CD160 on naïve CD44- and antigen-experienced CD44+ CD3+CD8+ cells from spleen.** Conflicting expression patterns were observed in the two experiments conducted. **(A)** The first experiment demonstrated increased expression with developing CLL and after AT and increased absolute numbers (AN). **(B)** In the second experiment, CD160 was lost with developing CLL and after AT, with AN increasing. **(C)** Representative flow plots from WT and TCL1 mice from the two experiments. *Note:* in first experiment, AT recipients were young TCL1 mice, and WT in the second experiment. Plots are overlaid graphs between FMO control for CD160 (black colour) and the full stain (grey colour).

A heatmap summary of relative (panel A) and absolute (panel B) changes of CD3+CD8+CD44+ cells expressing the investigated surface exhaustion markers in all experiments conducted is depicted in Figure 37.

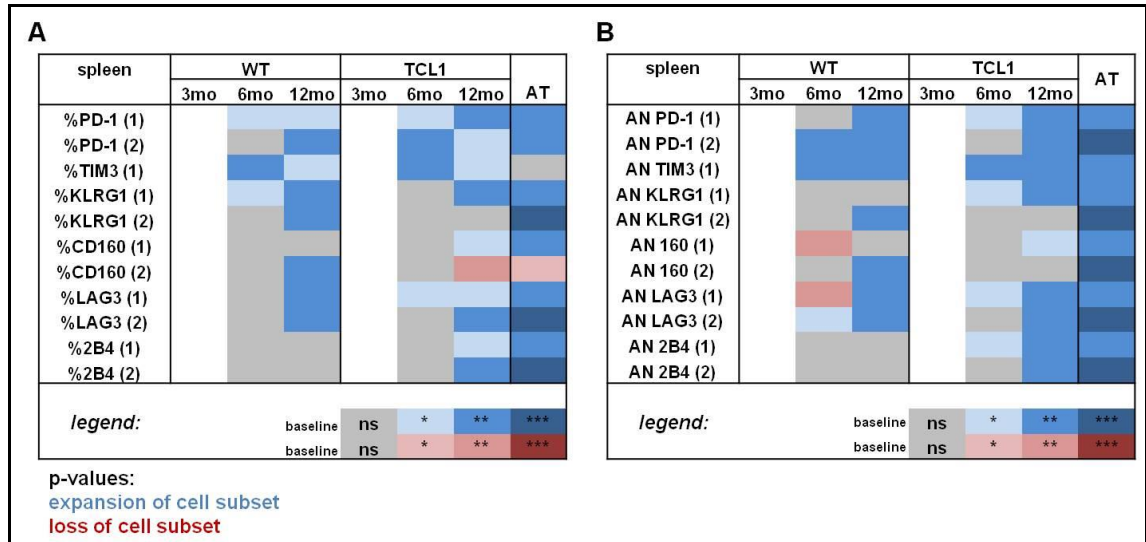


**Figure 37: Heatmap summary of p-values describing statistical differences in relative and absolute changes of cell subsets expressing typical exhaustion markers.** Groups were compared to (A) relative and (B) absolute numbers (AN) in 3 month old mice and experiments were conducted twice using different cohorts of mice. The first experiment is signified as (1), the second one as (2) in these tables. Blue colour indicates expansion, red colour loss of cell subsets. ns=non-significant, \*p<.05, \*\*p<.001, \*\*\*p<.0001.

### 6.4.5 Aberrant PD-1 expression by CD3+CD8+ T cells develops largely regardless of microenvironment

After demonstrating the step-wise upregulation of PD-1 on antigen-experienced CD3+CD8+ T cells from spleen, we compared this to PD-1 expression in PB, LN and BM from 3, 6 and 12 month old TCL1 mice and AT mice. As LNs have been demonstrated to show delayed disease development and model only some aspects of T-cell dysfunction after AT, LN from mice with CLL after AT were excluded from this comparison. With the exception of LN, the step-wise upregulation of PD-1 on antigen-experienced CD3+CD8+ T cells was recapitulated in all organs, and could be induced by AT (Figure 38 A). A heatmap summary of p-values of the statistical comparison with 3 month old mice is depicted in Figure 38 B. Spleen T cells had the highest PD-1 expression (median 19.4%, range 12.3-28.8), followed by BM (median 14.6%, range 10.0-27.9) and PB (median 8.7%, range 5.7-28.8).

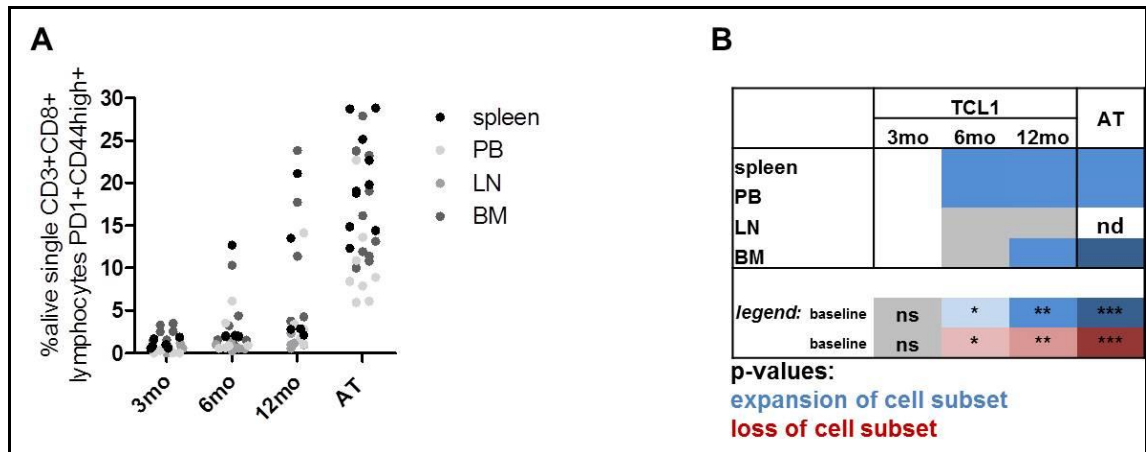


**Figure 38: Development of PD-1 expression on CD3+CD8+ T cells alongside advancing CLL in different organs.** Cells from spleen, PB, BM and LN from 3, 6, and 12 month old TCL1 and AT mice (WT recipients) were phenotyped by flow cytometry and percentages of CD3+CD8+CD44+PD1+ cells were compared. **(A)** PD-1 expression increased in ageing TCL1 mice and after AT in all examined organs, with the highest percentage in spleen, followed by BM and PB. **(B)** Heatmap summary of p-values describing statistical differences. Groups were compared to expression in 3 month old mice. Blue colour indicates expansion, red colour indicates loss of cells expressing PD-1. ns = non-significant, \*p<.05, \*\*p<.001, \*\*\*p<.0001.

#### 6.4.6 Randomized AT experiments unmask the effect of ageing

After we had confirmed that not only PD-L1/PD-L2 but also PD-1 and other exhaustion markers can be adequately modelled in TCL1 mice, but that the underlying mechanisms might be masked by ageing, we next conducted randomized AT experiments. The aim of these experiments was to eliminate ageing as a confounder by using young TCL1 and WT recipients, and to investigate functional differences between PD-1<sup>high</sup> and PD-1<sup>low</sup> T-cell subsets. Complementing other work in this project, additional aims were to directly compare T-cell phenotype changes in TCL1 and WT recipients using donor cells from the same pool. Before the AT, the purity of the donor pool was confirmed by flow cytometry to contain >95% CLL cells, while the WT pool was confirmed to be free of CLL.

##### 6.4.6.1 Confirmation of CLL-induced specific T-cell phenotype in both WT and TCL1 recipients

For this experiment using mice from AT experiment 8 (see Table 7), CLL could be induced in both TCL1 and WT recipients by injecting them with cells from a pool from leukaemic TCL1 donors, without any significant differences in latency or disease characteristics (see Chapter 4.4.3, Figure 8). For mice receiving normal B cells, WT recipients did not develop any leukaemia, but TCL1 recipients had a slightly higher

percentage of CD19+CD5+ CLL cells in spleen (median 6.0%, range 3.9-11.9). This minor increase is in line with very early TCL1 transgene-driven CLL development expected at this age (recipients were 4 months old).

The direct comparison between WT and TCL1 recipients confirmed that AT of CLL cells induced the previously defined disease-specific T-cell phenotype, namely the relative loss of CD3+ cells, the relative increase of CD3+CD8+ cells, the loss of naïve CD3+CD8+ cells, and the shift towards antigen-experienced cells (Figure 39 A and B left panel), and the increase of absolute numbers of all subsets in leukaemic mice (Figure 39 B right panel). This was observed regardless of whether animals were WT or transgenic (all differences for these subsets between WT and TCL1 recipients of CLL cells were not-significant). In line with the very early TCL1-driven CLL development, we observed slight differences in CD3+CD8+ T-cell subsets between WT and TCL1 recipients of normal B cells, namely a beginning loss of naïve and shift to antigen-experienced cells ( $p=.0182$ ).

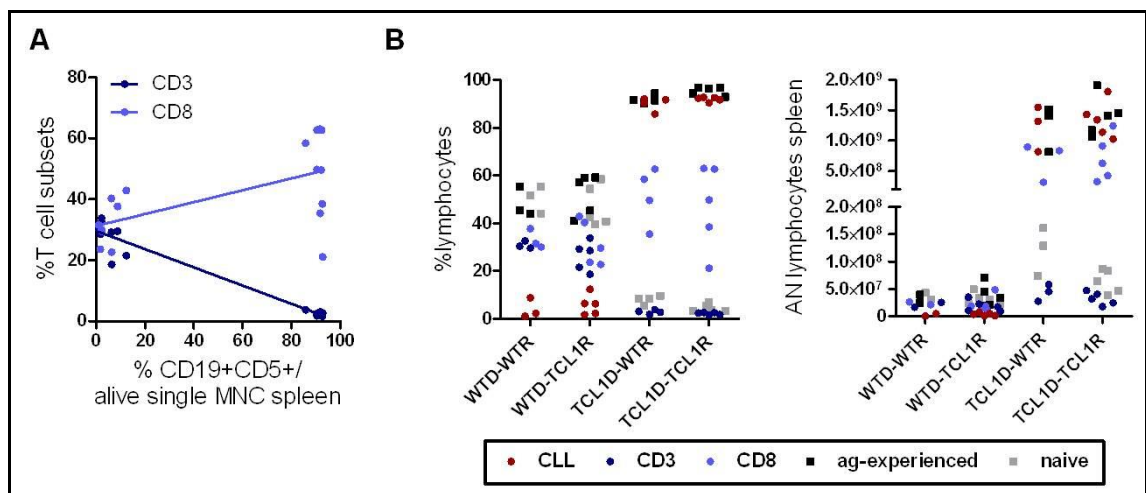


**Figure 39: Confirmation of CLL-specific T-cell phenotype in AT mice.** Mice were injected with donor cells from a leukaemic TCL1 donor or normal B cells. **(A)** Correlation between increasing CLL and relative loss of CD3+ and relative increase of CD3+CD8+ cells were confirmed. Recipients of WT donor cells are clustered on the y-axis, with leukaemic mice exhibiting the CLL-induced phenotypic T-cell defects. **(B)** Confirmation of CLL-specific T-cell phenotype in relative (left panel) and absolute numbers (AN, right panel) of CD3+, CD8+, naïve and antigen-experienced CD3+CD8+ cells. *Abbreviations:* WT=wild-type; D=donor; R=recipient.

### 6.4.6.2 CLL induces aberrant expression of typical surface exhaustion markers

We next compared PD-1 expression between WT and TCL1 recipients of CLL and normal B cells. In recipients of CLL cells, PD-1 was significantly upregulated compared to recipients of normal B cells, regardless of whether recipients were transgenic or not (Figure 40 A, all differences between PD-1+ and PD-1- subsets between WT and TCL1 recipients were not-significant). The very early CLL development in young TCL1 mice did therefore not translate into induction of PD-1, indicating that WT and TCL1 recipients can be analysed together. While eliminating the confounding effect of age, both relative PD-1 expression and absolute numbers (data for absolute numbers not depicted) were significantly higher in both CD44+ (Figure 40 B) and CD44- (Figure 40 C) subsets in mice with CLL. The ratio between PD-1+ and PD-1- cells among CD44+ cells was also significantly higher in recipients of CLL, indicating that the antigen experienced CD3+CD8+ cell population was highly enriched for PD-1+ cells (Figure 40 D, summary of p-values in Table 15).

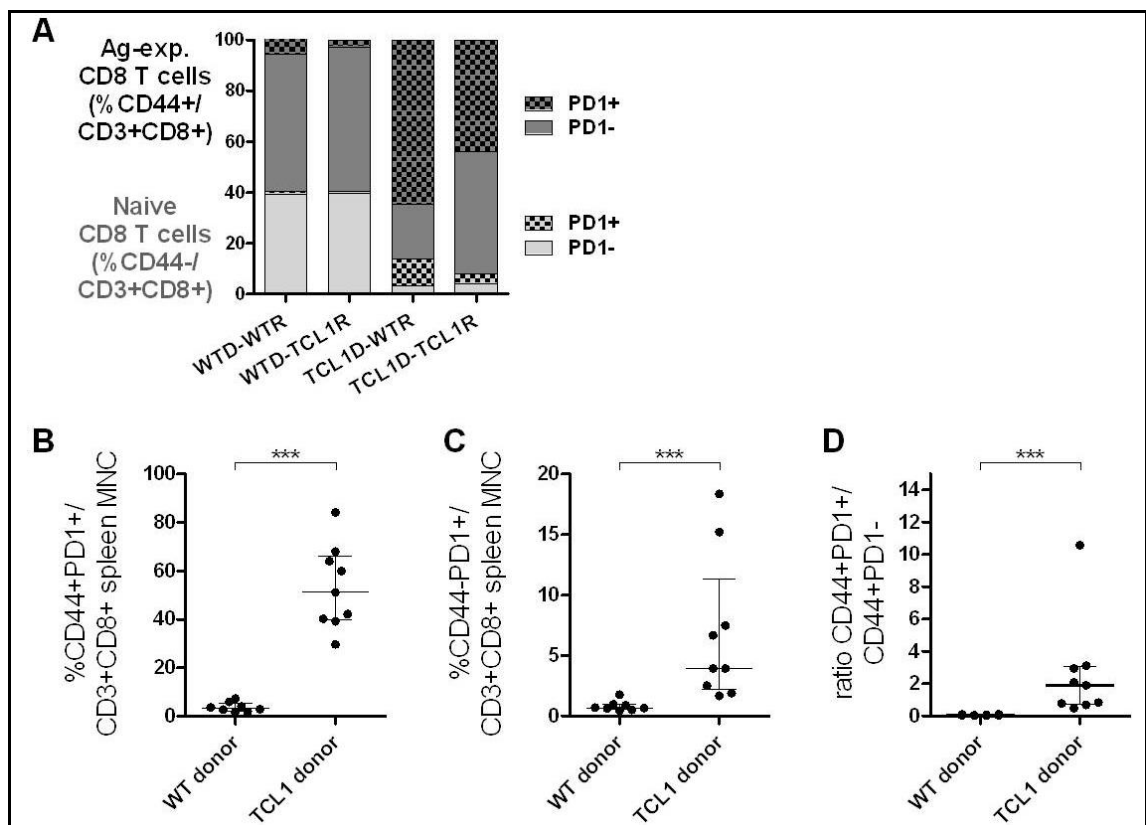


**Figure 40: CLL-induced aberrant expression of PD-1 on CD3+CD8+ cells. (A)** Antigen experienced and naïve CD3+CD8+ cells from mice with CLL showed increased PD-1 expression and expanded numerically irrespective of transgene status of recipient mice. **(B)** Changes of relative PD-1 expression on CD44+ and **(C)** CD44- cells and **(D)** differences in PD-1 subset ratios between mice injected with normal B cells from WT donors compared to mice injected with CLL cells from leukaemic TCL1 donors. WT=wild-type; D=donor; R=recipient. ns = non-significant, \* $p < .05$ , \*\* $p < .001$ , \*\*\* $p < .0001$ .

Virtually identical patterns were observed for KLRG-1, 2B4, and LAG-3, regarding both changes in CD44 subsets and expression of exhaustion markers (summarized in Figure 41 A as stacked bar charts), increase in relative expression, and ratios (Figure 41 B). Absolute numbers of cells expressing these exhaustion markers were also consistently significantly increased in mice with CLL (data not depicted). Representative flow plots are shown in Figure 41 C, and a summary of p-values is available in Table 17.

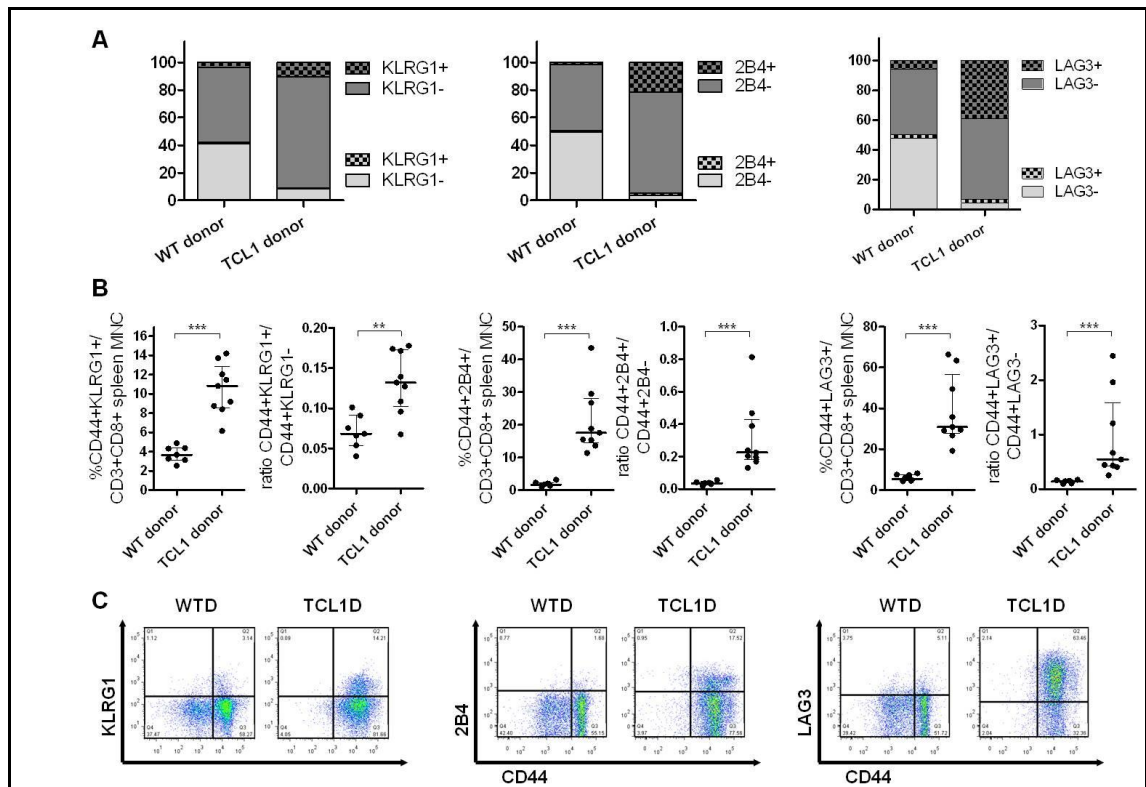


**Figure 41: CLL-induced aberrant expression of KLRG-1, 2B4 and LAG-3 on CD3+CD8+ cells.** (A) Antigen experienced (dark grey) CD3+CD8+ cells from mice with CLL (TCL1 donor) upregulate exhaustion markers compared to normal mice (WT donor). Naïve cells are depicted in light grey. (B) Changes of relative numbers of CD44+ cells expressing exhaustion markers, and differences in ratios between mice injected with normal B cells from WT donors compared to mice injected with CLL cells from leukaemic TCL1 donors. (C) Representative flow plots. ns = non-significant, \*p<.05, \*\*p<.001, \*\*\*p<.0001.

Interestingly, CD160 expression, which had shown conflicting expression patterns in previous experiments, was also increased in mice with CLL (p=.0115, Figure 42 A and B). However, the ratio between CD160+ and CD160- cells among CD44+ cells was not different between leukaemic and healthy mice, indicating that CLL does not lead to an enrichment of CD160+ cells in the antigen-experienced CD3+CD8+ cell population (Figure 42 B right panel). Representative flow plots are depicted in Figure 42 C.

A summary of all p-values of the comparisons between mice injected with normal B cells from WT donors compared to mice injected with CLL cells from leukaemic TCL1 donors is provided in Table 17.

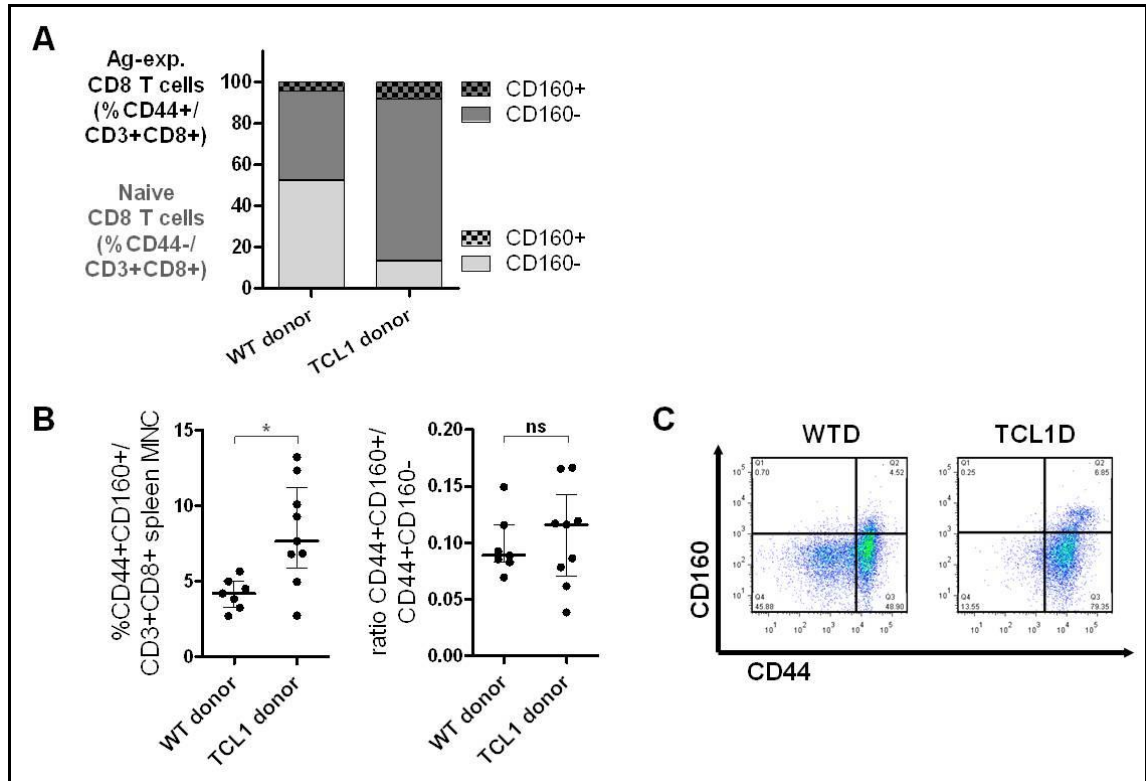


**Figure 42: CLL-induced expression of CD160 on CD3+CD8+ cells. (A)** Antigen experienced CD3+CD8+ cells from mice with CLL (TCL1 donor) upregulate CD160 compared to healthy mice (WT donor). **(B)** Changes of relative numbers of CD160+CD44+ cells and differences in ratios between mice injected with normal B cells from WT donors compared to mice injected with CLL cells from leukaemic TCL1 donors. **(C)** Representative flow plots. ns = non-significant, \*p<.05, \*\*p<.001, \*\*\*p<.0001.

marker	absolute numbers of CD3+CD8+ cells		relative numbers of CD3+CD8+ cells		ratio of positive vs. negative cells in CD44+ subset
	CD44+	CD44-	CD44+	CD44-	
PD-1	<.0001	.0006	<.0001	.0002	.0006
KLRG-1	.0009	.0335	.0002	.02105	.0033
2B4	.0006	.0006	<.0001	.0831	<.0001
LAG-3	.0006	.0006	.0006	.8148	<.0001
CD160	.001	.0047	.0115	.6065	.6806

**Table 17: Summary of p-values of comparisons between mice injected with normal B cells compared to mice injected with CLL cells for expression of exhaustion markers.** For each marker, absolute and relative numbers, as well as ratios of cells positive and negative for exhaustion marker among antigen experienced CD3+CD8+CD44+ cells were compared.

#### **6.4.6.3 CLL induces altered cellular survival cytokine profile indicating switch from IL-7 to IL-2 dependency**

In addition to surface exhaustion markers such as PD-1, KLRG-1, etc., aberrant expression of CD122 and CD127 cytokine receptors has been described as a characteristic of exhausted cells. CD122 is the  $\beta$ -chain of the receptor for IL-2, and CD127 the  $\alpha$ -chain of the receptor for IL-7. CD127 is expressed by naïve and memory cells, and its selective expression in the effector phase identifies CD8<sup>+</sup> T cells that give rise to long-lived memory T cells<sup>425</sup>. TBET has been shown to directly repress expression of the IL7R gene and to downregulate CD127 surface expression, thus promoting effector cell differentiation at the expense of memory cell formation. At the same time, it can upregulate CD122, switching the cellular survival cytokine profile from IL-7 to IL-2, resulting in hypo-responsiveness to homeostatic cytokines and becoming dependant on antigen stimulation for survival<sup>426</sup>.

Antigen experienced CD3<sup>+</sup>CD8<sup>+</sup> T cells from mice with CLL after AT significantly upregulated CD122 ( $p < .0001$ , Figure 43 A and B upper panels) while downregulating CD127 ( $p = .0025$ , Figure 43 A and B lower panels) compared to healthy controls, while expanding both subsets numerically (graphs not depicted, CD122  $p = .0006$ , CD127  $p = .0006$ ). In addition, the ratios between CD122<sup>+</sup> and CD122<sup>-</sup> ( $p = .0002$ , Figure 43 B upper right panel), and CD127<sup>+</sup> and CD127<sup>-</sup> cells ( $p < .0001$ , Figure 43 B lower right panel), respectively, demonstrated that antigen-experienced cells were enriched for CD122<sup>+</sup> and depleted of CD127<sup>+</sup> cells. This result indicates that the pool of cells committed to long-lived memory differentiation was very small. In addition, these patterns potentially reflect an altered dependency from IL-7 to IL-2. Representative flow plots are depicted in Figure 43 C.

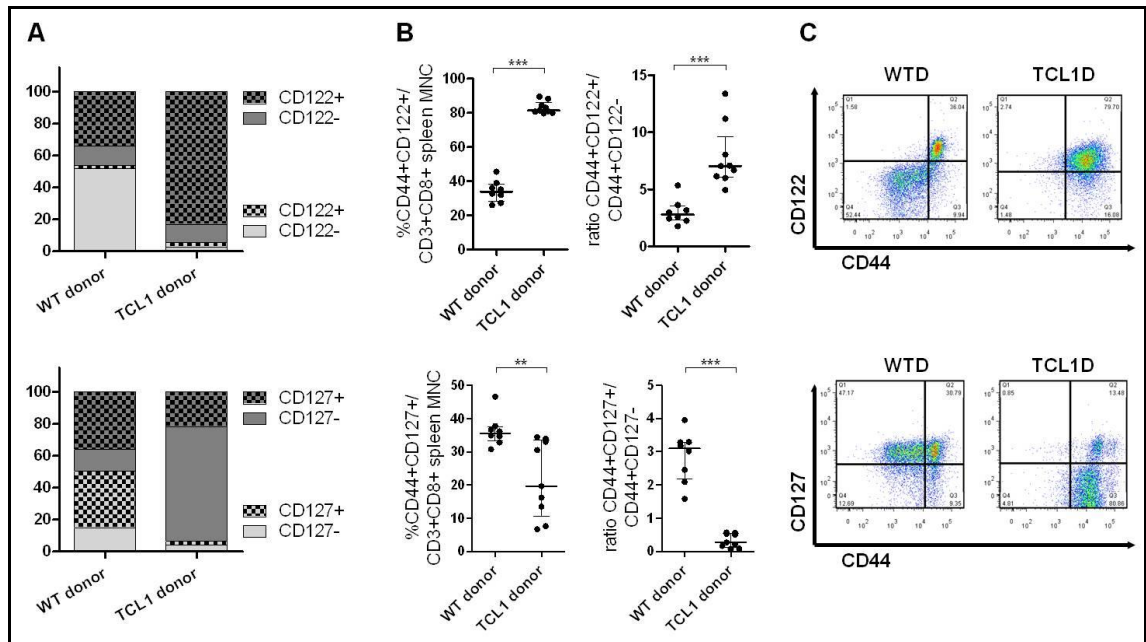


**Figure 43: CLL-induced expression of IL-2 and IL-7 cytokine receptors on CD3+CD8+ cells.** CD122 (IL-2R $\beta$  chain) and CD127 (IL-7R $\alpha$  chain) expression was compared between mice injected with normal B cells compared to mice injected with CLL cells. **(A)** Antigen experienced CD3+CD8+ cells from mice with CLL (TCL1 donor) upregulate CD122 and downregulate CD127 expression compared to healthy mice (WT donor). **(B)** Changes of relative numbers of CD122+ and CD127+CD44+ cells, and differences in ratios. **(C)** Representative flow plots. ns = non-significant, \* $p < .05$ , \*\* $p < .001$ , \*\*\* $p < .0001$ .

#### 6.4.6.4 CLL T-cells maintain certain effector functions such as cytokine production and degranulation despite PD-1 expression

After the phenotypic characterization, we compared key CD3+CD8+ effector functions between mice injected with cells from CLL donors and a pool of WT donors and attributed these to PD-1<sup>high</sup> and PD-1<sup>low</sup> subsets in mice with CLL.

Confirming the findings discussed in the previous chapter, the percentage of CD3+CD8+ cells producing IL-2 was comparable in mice with CLL and healthy mice ( $p = .1605$ , Figure 44 A left panel), while IL-4 ( $p = .0006$ , Figure 44 B left panel) and IFN- $\gamma$  ( $p = .0104$ , Figure 44 C left panel) were significantly increased in mice with CLL. To attribute the ability to produce cytokines to specific cell subsets, we compared the ratios of cytokine producing and non-producing cells within CD44- naïve and CD44+ antigen experienced CD3+CD8+ cells between mice without and with CLL (Figure 44 right panels). While IL-2 ratios were comparable between healthy and CLL mice (Figure 44 A), the increased IL-4 production in CLL T cells was found to be attributed to increased production by CD44- cells, as indicated by the significantly increased ratio in mice with CLL compared to healthy mice ( $p = .0006$ , Figure 44 B). Increased IFN- $\gamma$

production in mice with CLL could be attributed to both naive ( $p=.007$ ) and antigen experienced ( $p=.0148$ , Figure 44 C) cells. Although no differences in the percentage of cells producing TNF- $\alpha$  was found when comparing CD3+CD8+ cells from mice without and with CLL ( $p=.5752$ , Figure 44 D left panel), a significantly reduced TNF- $\alpha$  ratio was found among antigen experienced cells, indicating that they were enriched for cells unable to produce TNF- $\alpha$  ( $p=.0011$ ).

In addition, we largely confirmed the previously observed differences in cytokine production by CD3+CD8- cells (*note*: CD4 antibody was not included in this panel, but as described in the previous chapter, gating CD3 against CD8 allows the identification of a CD3+CD8- population, which we previously found to be mostly CD4+ cells). CD4+ cells from mice with CLL had significantly higher IFN- $\gamma$  ( $p=.0019$ ), but lower TNF- $\alpha$  ( $p=.0002$ ) production compared to healthy mice. In contrast to the previous experiment, IL-2 was not reduced in mice with CLL ( $p=.3823$ ). In addition, there were trends towards increased IL-4 ( $p=.1605$ ) and IL-5 ( $p=.083$ ) production in mice with CLL (Figure 44 E).

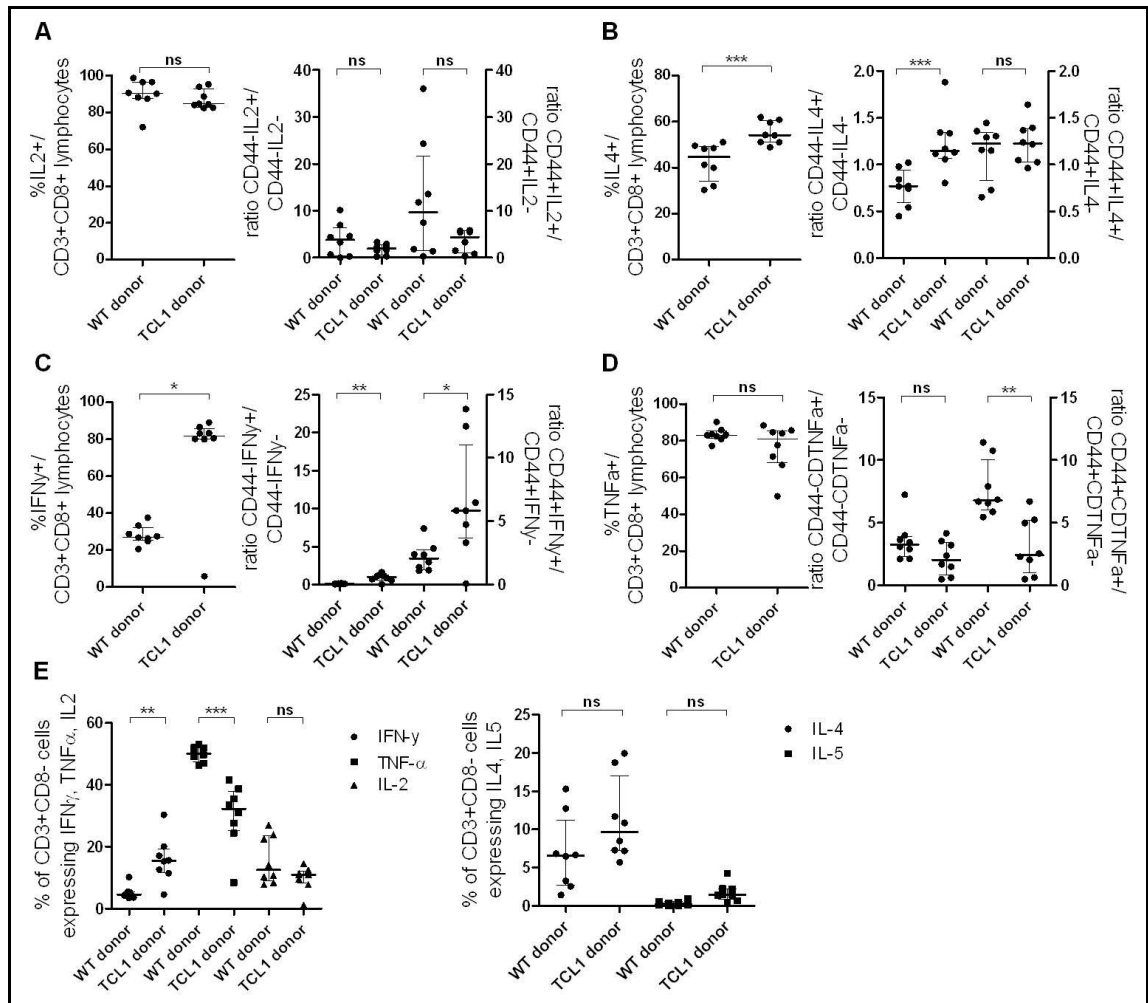


**Figure 44: Intracellular cytokine production by CD4+ and CD8+ subsets.** Intracellular IL-2, IL-4, IFN- $\gamma$  and TNF- $\alpha$  were compared between mice with CLL (TCL1 donor) and healthy mice (WT mice). Cytokines were first gated on CD3+CD8+ cells (left panel (A) to (D)), and then on CD44+ and CD44- subsets, and expressed as ratios (right panel (A) to (D)). **(A)** IL-2 production was not increased, and IL-2 ratios were comparable between healthy and CLL mice. **(B)** Mice with CLL had significantly increased IL-4 production, mostly due to an increased production within CD44- cells. **(C)** IFN- $\gamma$  production was significantly increased in mice with CLL and could be attributed to both CD44- and CD44+ cells. **(D)** No difference in intracellular TNF- $\alpha$  was found when comparing CD3+CD8+ cells, but a significantly reduced TNF- $\alpha$  ratio became apparent in CD44+ cells. **(E)** CD4+ cells from mice with CLL had significantly higher intracellular IFN- $\gamma$ , a trend towards increased IL-4 and IL-5, but lower TNF- $\alpha$  production. In contrast to previous findings, IL-2 was not reduced in CLL T cells.

We next compared cytokine production by CD3+CD8+ cells according to PD-1 expression in mice with CLL. To rule out that mitogen stimulation would have an effect on PD-1 expression, the percentages of CD3+CD8+CD44+ cells positive for PD-1 without and with PMA/Ionomycin treatment were compared, and no general increase of expression was found (Figure 45 E).

In general, intracellular cytokines were detected in both PD-1<sup>high</sup> and PD-1<sup>low</sup> subsets (Figure 45 A). As a higher percentage of cells were PD-1<sup>low</sup>, leading to a substantially different distribution of cells between the PD-1<sup>high</sup> and the PD-1<sup>low</sup> pool, differences in cytokine production were described as ratios within PD-1<sup>high</sup> and PD-1<sup>low</sup> cells, respectively (Figure 45 B). There was no difference between PD-1<sup>high</sup> and PD-1<sup>low</sup> cells in the ratio of CD3+CD8+ cells able to produce IL-2 ( $p=.3939$ ) and IL-4 ( $p=.2345$ ) compared to those not producing any cytokine after PMA/Ionomycin treatment, indicating that despite PD-1 expression, comparable percentages of cells maintained IL-2 and IL-4 production.

Albeit not significant, probably due to the large range between mice, the ratio of IFN- $\gamma$  showed a trend to be increased in PD-1<sup>high</sup> cells ( $p=.38$ ), indicating that those cells were enriched for IFN- $\gamma$  producing cells. In contrast, PD-1<sup>high</sup> cells had a significantly lower TNF- $\alpha$  ratio ( $p=.026$ ), indicating that they were depleted of cells producing TNF- $\alpha$ .

Cytotoxic function, as measured by CD107a relocation to the cell surface after stimulation with PMA/Ionomycin, was maintained in both PD-1<sup>high</sup> and PD-1<sup>low</sup> CD3+CD8+ cells, indicating that cells were able to degranulate (Figure 45 C). When forming the ratio between CD107a+ and CD107a- cells within PD-1 subsets, we found a significantly increased ratio in PD-1<sup>high</sup> cells ( $p=.0104$ ), indicating that cells with the ability to degranulate were enriched compared to the PD-1<sup>low</sup> subset.

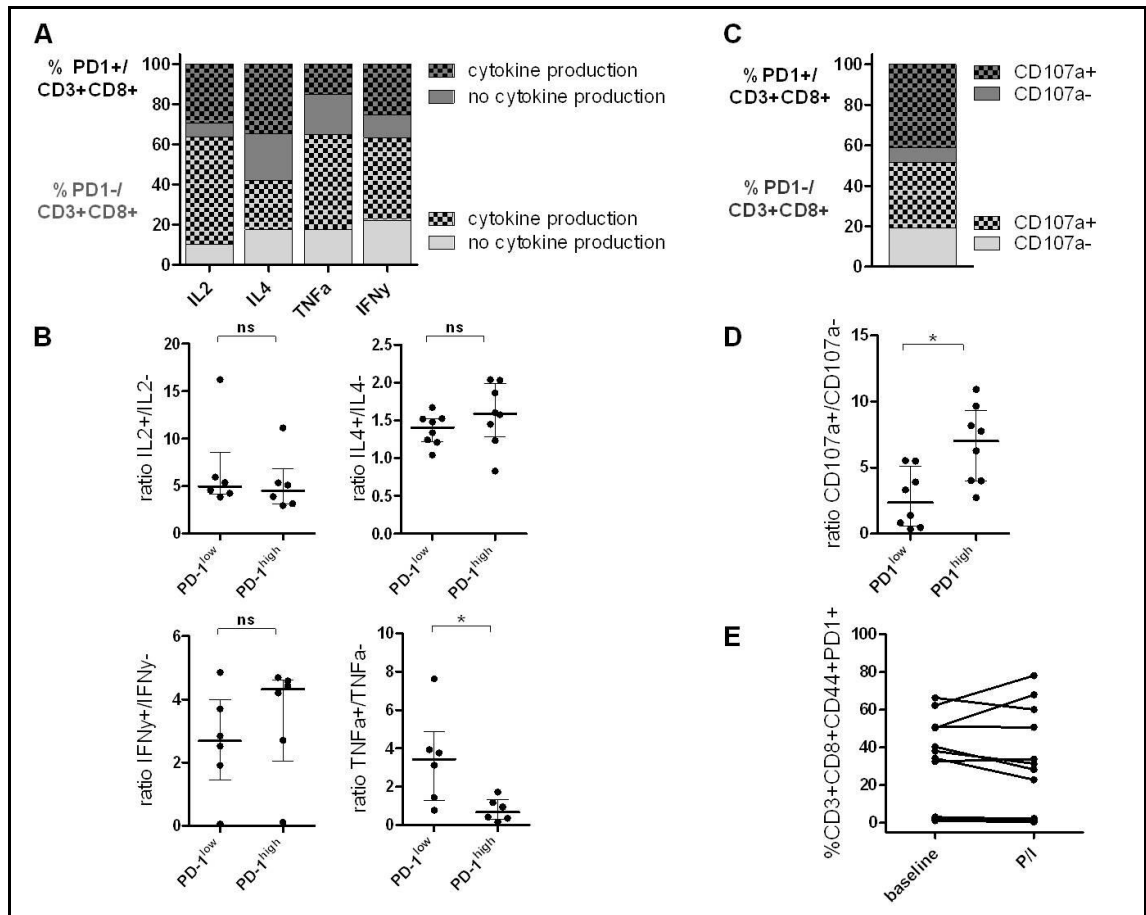


**Figure 45: Intracellular cytokine production and degranulation in PD-1 subsets.** Intracellular IL-2, IL-4, IFN- $\gamma$ , TNF- $\alpha$  and CD107a were gated on PD-1 subsets to compare differences in key effector functions. **(A)** Intracellular cytokines were detected in both PD-1<sup>high</sup> and PD-1<sup>low</sup> subsets. **(B)** Despite PD-1 expression, comparable percentages of cells were able to produce IL-2 and IL-4, while PD-1<sup>high</sup> cells showed a trend to be enriched for IFN- $\gamma$  producing cells but depleted of cells producing TNF- $\alpha$ . **(C)** Both PD-1<sup>high</sup> and PD-1<sup>low</sup> CD3+CD8+ cells were able to degranulate, but cells with the ability to degranulate were enriched in the PD-1<sup>high</sup> subset **(D)**. **(E)** PMA/Ionomycin stimulation had no effect on changes in PD-1 expression.

We had intended to measure T-cell proliferation in this experiment *ex vivo* by CFSE dilution, after optimizing this assay beforehand using normal T cells from WT mice. Optimization included several experiments to determine the optimal number of cells, plates to be used, duration of stimulation and ratio between cells and CD3/CD28 beads. We ultimately established that for mouse T cells, fresh cells needed to be used, that splenocytes had to be depleted of B cells by positive selection of CD19+ B cells with CD19 microbeads, and that  $0.2 \times 10^6$  cells should be stimulated with CD3/CD28 beads at a 1:1 cell:bead ratio and cultured for 72 hours in 96 well round-bottom plates. However, in the AT experiment described here, proliferation measured by CFSE dilution was very inconsistent in mice with CLL, and did not allow comparison of proliferation between CLL and normal T cells using conventional read-outs such as proliferation index. While T-cell proliferation was observed and could be quantified in

normal T cells, CLL T cells had in initial proliferation peak, and then diluted CFSE in “a bulk” instead of in an orderly fashion by cell cycle divisions, probably because CLL T cells were not quiescent at the time of labelling (see Figure 46 A and B). After this had been confirmed in three different mice with CLL, we did not pursue measurement of proliferation *ex vivo* by CFSE, but focused on methods using ki67 and EdU proliferation. Hence, this experiment did not yet yield the desired information on CLL induced proliferation defects and their association to PD-1 expression in T cells from mice with CLL.

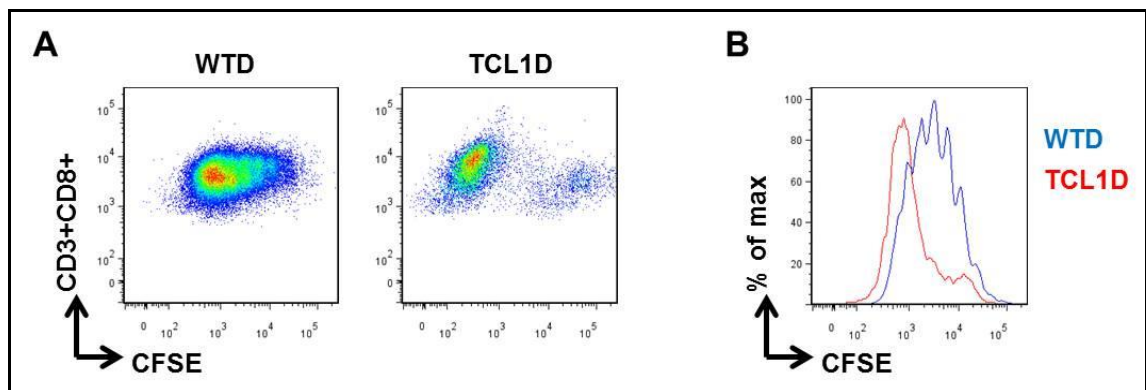


**Figure 46: CD3+CD8+ T-cell proliferation by CFSE dilution.** Fresh splenocytes were debulked of B and CLL cells, labelled with CFSE and cultured for 72h with CD3/CD28 dynabeads. **(A)** Compared to normal T cells from mice injected with B cells from healthy WT donors (WTD), proliferation was not quantifiable using conventional tools such as proliferation index in T cells from mice with CLL after injection with cells from leukaemic TCL1 donors (TCL1D). **(B)** Representative histogram demonstrating proliferation peaks. All graphs show data gated on viable, single, CD3+CD8+ cells.

#### 6.4.6.5 The ability to form immunological synapses is significantly impaired in PD-1<sup>high</sup> compared to PD-1<sup>low</sup> cells

As impaired immune synapse formation has been characterized as one of the major CD8+ effector cell defects, we compared the ability of PD-1<sup>high</sup> and PD-1<sup>low</sup> CD8+ T cells to form synapses with normal mouse B cells as APC. T cells from mice with CLL were flow-sorted for CD8, CD44+PD-1<sup>high</sup> and CD44+PD-1<sup>low</sup>, while normal T cells were flow-sorted for CD8, and their mean areas of T-cell F-actin immune synapses in  $\mu\text{m}^2$  formed with CMAC-labelled normal B cells were compared. Compared to normal CD8+ T cells, the ability of CLL CD8+ T cells to form synapses with normal B cells was significantly impaired ( $p < .0001$ , Figure 47 A). However, PD-1<sup>low</sup> CD8+ T cells formed larger synapses than PD-1<sup>high</sup> CD8+ T cells ( $p < .0001$ ). Compared to all CD8+ T cells, synapses between PD-1<sup>high</sup> T cells and APCs were significantly smaller ( $p < .0001$ ),

while synapses between PD-1<sup>low</sup> T cells and APCs were significantly larger ( $p < .0001$ ), indicating that the impaired ability of CD8+ T cells in general seems to be promoted by the PD-1<sup>high</sup> subset, probably via interference with Lck signalling. Representative confocal images are depicted in Figure 47 B.

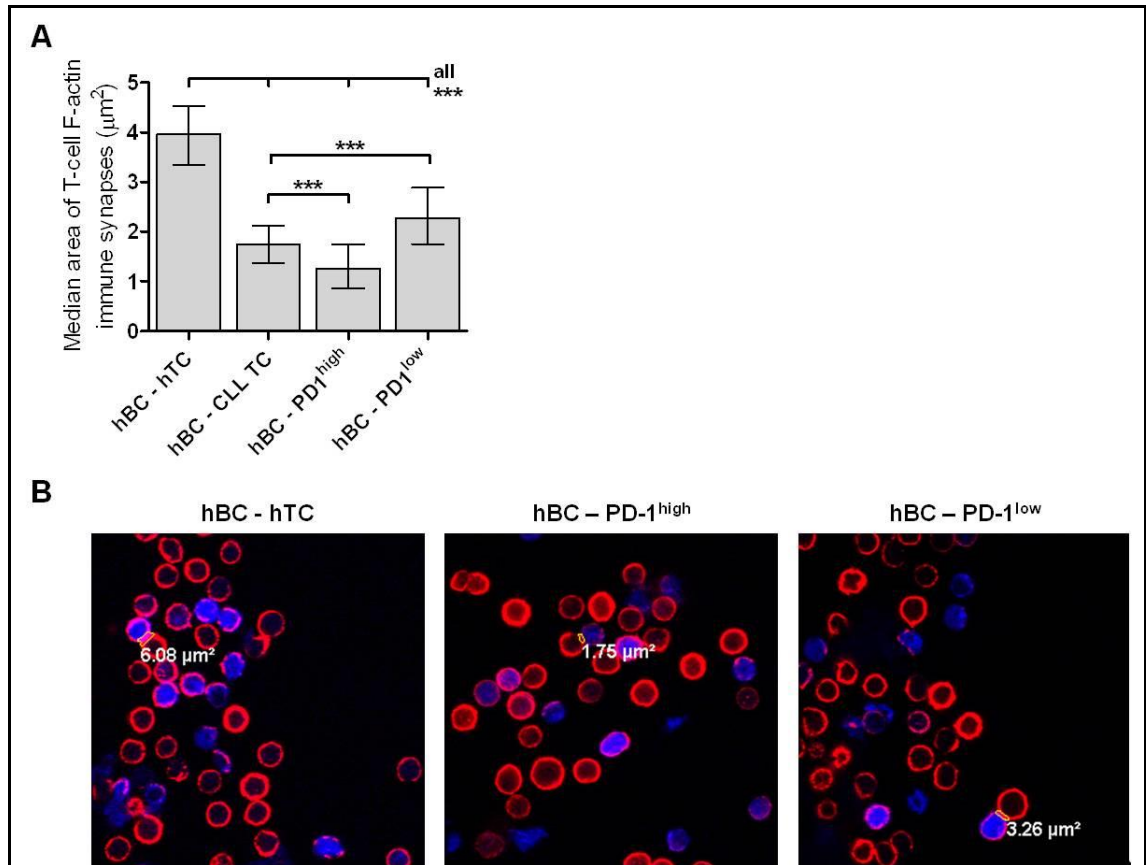


**Figure 47: Immune synapse formation between normal B cells and T cells from healthy mice and mice with CLL. (A)** Compared to normal B and CD8+ T cells (hBC-hTC), the ability of CLL T cells to form synapses with normal B cells as APCs was impaired (hBC-CLL TC), with PD-1<sup>low</sup> CD8+ T cells (hBC-PD-1<sup>low</sup>) forming larger synapses than PD-1<sup>high</sup> CD8+ T cells (hBC-PD-1<sup>high</sup>). **(B)** Representative confocal images of synapses taken with a 63x objective between hBC-hTC, hBC- PD-1<sup>high</sup> and hBC-PD-1<sup>low</sup> cells. Blue = CMAC labelled B cells, red = Rhodamine Phalloidin.

#### 6.4.7 PD-1 expressing normal T cells have markedly different effector functions than PD-1 expressing CLL T cells

After the AT experiments had unmasked the effect of ageing and had demonstrated that effector functions such as cytokine production and degranulation appear to be maintained regardless of PD-1 expression of CLL T cells, we reinvestigated the cohort of ageing TCL1, WT, and AT mice described in Chapter 5.4. We had obtained functional data for these mice to elucidate how T-cell effector functions change in the context of developing CLL, and had also included PD-1 surface stain in these assays. As demonstrated in Chapter 5.4, PD-1 expression by CD3+CD8+CD44+ T cells could be detected in both TCL1 and WT mice from 6 months on. To investigate if PD-1 expression might be associated with different effector functions in healthy mice than in mice with CLL, we attributed CD107a degranulation, intracellular GrB and IFN- $\gamma$ , and EdU proliferation to PD-1<sup>high</sup> and PD-1<sup>low</sup> cells in both WT and TCL1 mice (Figure 48 A-D). Three month old mice had no detectable PD-1 expression and effector function was therefore determined on PD-1<sup>low</sup> cells only.

In ageing WT mice, both PD-1 subsets contributed to the overall patterns associated with ageing described in the previous chapter, *i.e.* maintenance of degranulation and intracellular GrB, reduction of proliferation, and increase of intracellular IFN- $\gamma$  production. The effector ratios for CD107a (Figure 48 A left panel) and EdU proliferation (Figure 48 D left panel) were comparable in PD-1 subsets (PD-1<sup>high</sup> vs. PD-1<sup>low</sup> 6 and 12 month all p-values ns), indicating that both PD-1<sup>high</sup> and PD-1<sup>low</sup> contained comparable proportions of cells able to degranulate and to proliferate. Effector ratios for intracellular GrB (Figure 48 B left panel) and IFN- $\gamma$  (Figure 48 C left panel), however, were 2 to 3 times higher in PD-1<sup>high</sup> than in PD-1<sup>low</sup> cells (GrB 6 month p=.0087, 12 month p=.0931; IFN- $\gamma$  6 month p=.026, 12 month p=.0043). The PD-1<sup>high</sup> subset therefore appeared to be enriched for cells positive for GrB and IFN- $\gamma$  compared to the PD-1<sup>low</sup> subsets, making PD-1 expressing cells the main contributor to exerting these effector functions.

In TCL1 mice developing CLL, effector ratios followed very different patterns: with the onset of CLL at 6 months, the CD107a effector ratios of PD-1<sup>high</sup> and PD-1<sup>low</sup> were very similar to each other (p=.5887), but about 2 fold higher than in age-matched WT mice, indicating that CLL T cells were highly enriched for cells able to degranulate at an early stage of disease (Figure 48 A right panel). With progressing CLL, both subsets lost cells with the ability to degranulate, leading to a significant decrease in ratios. However, no difference between PD-1<sup>high</sup> and PD-1<sup>low</sup> cells was observed (p=.0222), thus demonstrating that effector cells expressing PD-1 maintained the ability to degranulate.

GrB ratios were also found to be higher in mice with CLL compared to age-matched controls: the ratio of PD-1<sup>high</sup> cells was approximately 3 fold higher, and that of PD-1<sup>low</sup> cells was approximately 7 fold higher, than in WT mice (Figure 48 B right panel). These differences led to the predominance of PD-1<sup>high</sup> over PD-1<sup>low</sup> cells in being enriched for GrB-containing cells as it was observed in WT mice being abrogated in the context of developing CLL (GrB ratio PD-1<sup>high</sup> vs. PD-1<sup>low</sup> : 6 month  $p=.8726$ ; 12 month  $p=.2948$ ).

TCL1 mice with CLL at 6 months had IFN- $\gamma$  ratios comparable to age-matched WT mice, but the PD-1 subset ratios were not different in TCL1 mice ( $p=.3095$ ), indicating that the physiological enrichment of PD-1<sup>high</sup> over PD-1<sup>low</sup> cells observed in WT mice was lost with CLL (Figure 48 C right panel). The previously detected CLL-induced significant increase of IFN- $\gamma$  could be attributed to both PD-1<sup>high</sup> and PD-1<sup>low</sup> cells, again with no difference between their ratios ( $p=1.0$ ).

CLL-induced increased T-cell proliferation was found to be attributed to both PD-1<sup>high</sup> and PD-1<sup>low</sup>, but the PD-1<sup>high</sup> ratio was significantly higher than the PD-1<sup>low</sup> ratio (6 month  $p=.0087$ , 12 month  $p=.0317$ , Figure 48 D right panel). Increased T-cell proliferation therefore appears to be predominantly accounted for by PD-1<sup>high</sup> cells.

Table 18 contains an overview of medians and ranges of effector cell ratios for ageing WT and TCL1 mice.

In the AT mice in this cohort, we confirmed that PD-1<sup>high</sup> and PD-1<sup>low</sup> cells maintained comparable effector ratios for CD107a, and that PD-1<sup>high</sup> cells were enriched for IFN- $\gamma$  containing cells compared to PD-1<sup>low</sup> cells. In addition, we added new information regarding GrB and proliferation: just as for IFN- $\gamma$ , PD-1<sup>high</sup> cells were enriched for GrB containing and proliferating cells (graphs not shown, medians and ranges are summarized in Table 18).

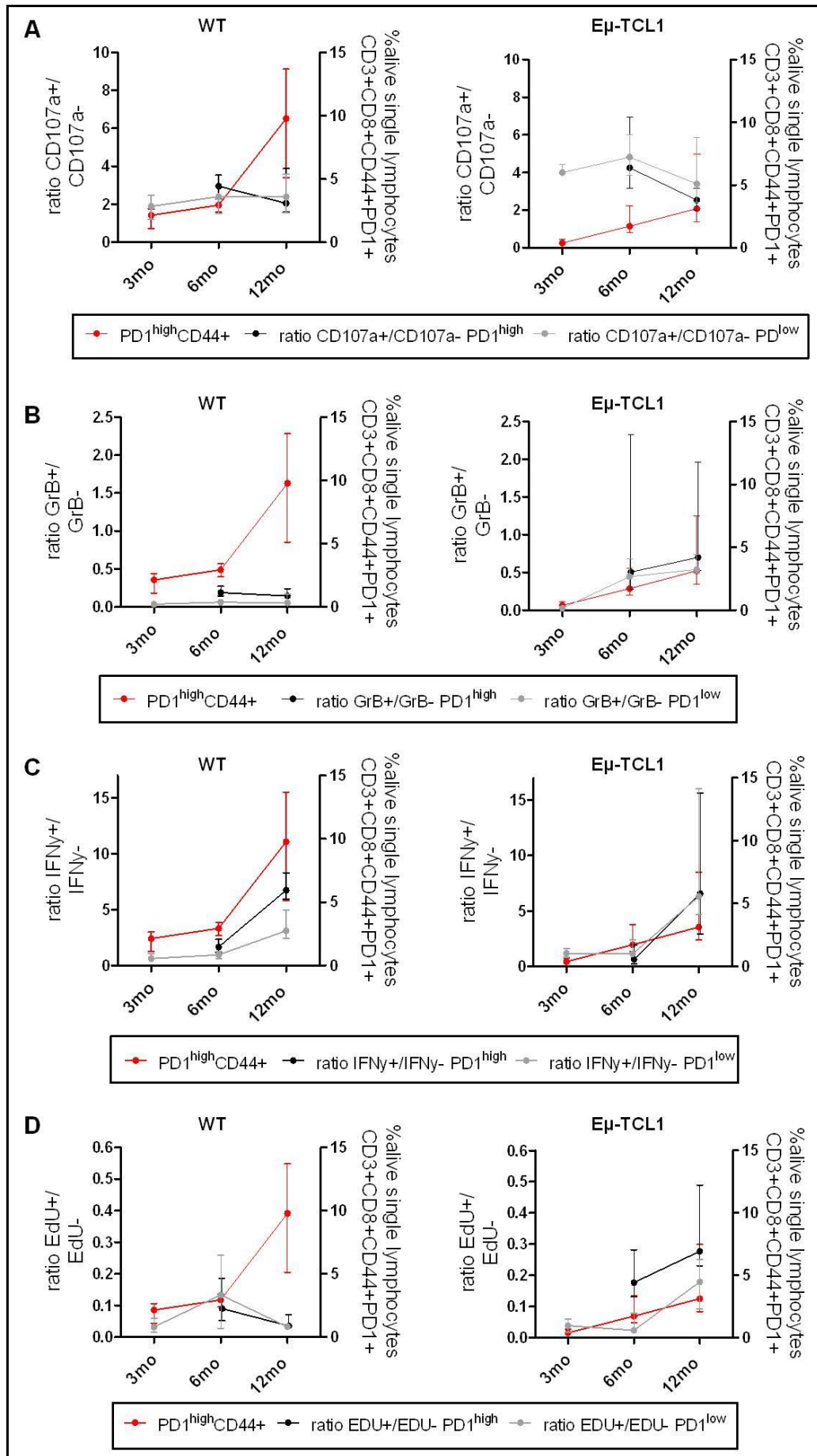


**Figure 48: Associations between PD-1 expression and effector functions in T cells from healthy mice and TCL1 mice with developing CLL.** Ratios for CD107a degranulation, intracellular GrB and IFN- $\gamma$ , and EdU proliferation were compared between PD-1<sup>high</sup> and PD-1<sup>low</sup> cells in WT and TCL1 mice. **(A)** In ageing WT mice, both PD-1<sup>high</sup> and PD-1<sup>low</sup> expressing cells contained comparable proportions of cells able to degranulate. In TCL1 mice with developing CLL, CD107a effector ratios were higher than in age-matched WT mice, but with progressing CLL both subsets similarly lost cells with the ability to degranulate. **(B)** In ageing WT mice, the PD-1<sup>high</sup> subset was enriched for GrB+ cells compared to the PD-1<sup>low</sup> subset. In TCL1 mice, GrB ratios were highly increased, but the predominance of PD-1<sup>high</sup> over PD-1<sup>low</sup> cells in being enriched for GrB+ cells was lost. **(C)** Ageing WT mice also exhibited an enrichment of the PD-1<sup>high</sup> subset for IFN- $\gamma$ + cells, which was lost in TCL1 mice with developing CLL. Both PD-1 subsets contributed to the CLL-induced significant increase of IFN- $\gamma$ . **(D)** In ageing WT mice, both PD-1<sup>high</sup> and PD-1<sup>low</sup> expressing cells contained comparable proportions of proliferating cells. Increased T-cell proliferation in CLL T cells was predominantly driven by PD-1<sup>high</sup> cells. All graphs show median with IQR, and the percentage of PD-1+CD3+CD8+CD44+ cells is depicted for each age cohort on the right x-axis.

			WT			E $\mu$ -TCL1			
			3 mo	6 mo	12 mo	3 mo	6 mo	12 mo	AT
CD107a	PD1 <sup>low</sup>	minimum	1.17	0.02	1.23	3.96	3.66	2.05	1.03
		median	1.89	2.41	2.39	4.00	4.82	3.40	1.27
		maximum	2.68	2.74	5.14	4.42	6.61	6.23	1.79
	PD1 <sup>high</sup>	minimum		0.19	1.52		2.92	1.80	0.90
		median		2.96	2.05		4.26	2.54	1.48
		maximum		4.33	4.63		12.00	3.70	2.50
GrB	PD1 <sup>low</sup>	minimum	0.02	0.03	0.03	0.02	0.41	0.49	0.45
		median	0.04	0.06	0.05	0.03	0.45	0.54	0.59
		maximum	0.08	0.08	0.34	0.06	0.86	0.92	0.68
	PD1 <sup>high</sup>	minimum		0.07	0.07		0.16	0.40	1.68
		median		0.19	0.14		0.47	0.66	2.21
		maximum		0.39	0.25		3.24	2.42	3.22
IFN- $\gamma$	PD1 <sup>low</sup>	minimum	0.34	0.46	2.29	0.78	0.74	3.74	0.70
		median	0.64	0.97	3.13	1.20	1.14	6.31	1.25
		maximum	1.26	1.59	5.30	1.70	4.30	22.27	1.92
	PD1 <sup>high</sup>	minimum		1.07	5.05		0.20	0.49	2.82
		median		1.67	6.74		0.65	6.59	3.65
		maximum		3.92	10.43		3.00	16.67	4.96
EdU	PD1 <sup>low</sup>	minimum	0.00	0.01	0.02	0.02	0.01	0.04	0.12
		median	0.03	0.13	0.03	0.04	0.02	0.18	0.17
		maximum	0.08	0.33	0.05	0.07	0.16	0.27	0.24
	PD1 <sup>high</sup>	minimum		0.01	0.03		0.10	0.23	0.24
		median		0.09	0.04		0.18	0.28	0.30
		maximum		0.27	0.11		0.31	0.58	0.38

**Table 18: Medians and ranges of effector cell ratios for ageing WT, TCL1 and AT mice.**

### **6.5 Summary of PD-L1/PD-1 mediated T-cell dysfunction and T-cell exhaustion in TCL1 mice**

In these experiments, we were able to demonstrate that all inhibitory ligands that have been identified as important mediators of impaired immune synapse formation, namely CD200, CD270, PD-L1 and CD276, were expressed on spleen CLL cells from TCL1 mice with CLL, but that only PD-L1 and CD276 mirrored the aberrant over-expression of human CLL cells compared to normal B cells. This could be modelled in both the original C3H and backcrossed B6 TCL1 strains, as well as in ageing TCL1 mice with fully developed CLL and young mice with CLL after AT. In the context of developing CLL, both highly aberrant PD-L1 and PD-L2 expression were found to be exclusive to malignant CLL cells. This could be detected on CLL cells from PB, BM, LN and spleen, confirming the suitability of TCL1 mice to model aberrant PD-L1/PD-L2 expression of human CLL cells.

The binding partner of PD-L1/PD-L2 on T cells, PD-1, is a major inhibitory receptor associated with T-cell exhaustion in chronic viral infections. As tumour-infiltrating T cells share many phenotypic and functional characteristics of exhausted T cells in chronic infections, we compared the molecular signatures of T cells from murine exhaustion models and murine CLL T cells. CLL CD8<sup>+</sup> T cells genes were enriched in the unique molecular signature of exhausted CD8<sup>+</sup> T cells, but were also represented in the signature of functional effector CD8<sup>+</sup> T cells, indicating that CLL T cells are likely to be very heterogeneous populations with features of both exhaustion and functional effector cells. The surface expression of typical exhaustion markers, namely PD-1, KLRG-1, 2B4 and LAG-3 was found to be step-wise increased on CD44<sup>+</sup> antigen-experienced CD8<sup>+</sup> T cells in mice with developing CLL. This was to a certain extent also observed in ageing WT mice, indicating that surface expression by itself might not be a definitive marker for T-cell exhaustion or dysfunction. PD-1, KLRG-1, 2B4 and LAG-3 expression could however be induced in young mice with CLL after AT, suggesting a causal relationship with disease. With the exception of LN, the step-wise upregulation of PD-1 on antigen-experienced CD3<sup>+</sup>CD8<sup>+</sup> T cells and its induction by AT observed in spleen was recapitulated in cells taken from PB and BM, confirming that PD-1, along with other exhaustion markers, can be adequately modelled in TCL1 mice.

Randomized AT experiments injecting normal B cells and CLL cells into young, previously healthy TCL1 and WT mice confirmed that PD-1, KLRG-1, 2B4 and LAG-3 expression could be induced by AT of CLL cells but not normal B cells. The previously defined disease-specific T-cell phenotype, namely the relative loss of CD3<sup>+</sup> cells, the

relative increase of CD3+CD8+ cells, the loss of naïve CD3+CD8+ cells and the shift towards antigen-experienced cells, and the increase of absolute numbers of all subsets was recapitulated in both TCL1 and WT recipients, validating the use of WT mice for future AT experiments investigating CLL-induced T-cell dysfunction. Functionally, CLL was found to induce altered cellular survival cytokine profiles: antigen experienced CD44+CD3+CD8+ T cells from mice with CLL were enriched for CD122 (IL-2 cytokine receptor) and depleted of CD127 (IL-7 cytokine receptor), indicating altered dependency from IL-7 to IL-2. Confirming findings described in the previous chapter, the percentage of CD3+CD8+ cells expressing intracellular IL-2 was comparable between healthy and leukaemic mice. Similarly, CLL-associated increased IL-4 and IFN- $\gamma$  production were confirmed, and this could be attributed to both CD44- naïve and CD44+ antigen experienced T cells. Although the percentage of CD3+CD8+ T cells positive for intracellular TNF- $\alpha$  appeared similar between normal and CLL T cells, CD44+ T cells from mice with CLL were enriched for cells unable to produce TNF- $\alpha$ . Significantly lower percentages of cells positive for TNF- $\alpha$  were also found in CD4+ T cells in mice with CLL.

Randomized AT experiments also demonstrated that CLL-induced aberrant PD-1 expression on CD3+CD8+ T cells could be associated with different abilities of cells to exert effector functions: in general, intracellular cytokines IL-2, IL-4, IFN- $\gamma$  and TNF- $\alpha$  were detected in both PD-1<sup>high</sup> and PD-1<sup>low</sup> cells, and both PD-1<sup>high</sup> and PD-1<sup>low</sup> cells maintained their ability to degranulate, contrasting the notion that PD-1 expression would lead to a loss of these effector functions. While both PD-1 subsets contained comparable percentages of cells able to produce IL-2 and IL-4 compared to those that were not, PD-1<sup>high</sup> cells appeared to be enriched for IFN- $\gamma$  producing cells but depleted of cells producing TNF- $\alpha$  compared to PD-1<sup>low</sup> cells. In addition, PD-1<sup>high</sup> cells were enriched for cells with the ability to degranulate compared to the PD-1<sup>low</sup> subset, but showed an impaired ability to form immunological synapses with normal B cells.

Linking PD-1 expression with effector function of PD-1<sup>high</sup> cells in ageing WT mice and comparing this to effector function of PD-1<sup>high</sup> cells in ageing TCL1 mice developing CLL revealed the following differences: in ageing WT mice, both PD-1<sup>high</sup> and PD-1<sup>low</sup> cells contributed to the overall patterns associated with ageing described in the previous chapter, *i.e.* maintenance of degranulation and intracellular GrB, reduction of proliferation, and an increase of intracellular IFN- $\gamma$  production. While both PD-1<sup>high</sup> and PD-1<sup>low</sup> subsets contained comparable proportions of cells able to degranulate and to proliferate, cells positive for GrB and IFN- $\gamma$  appeared to be enriched in the PD-1<sup>high</sup> subset compared to the PD-1<sup>low</sup> subset, supporting the understanding that PD-1

expression in normal T cells contributes to the dynamic alterations of how effector functions are maintained in the context of ageing.

CD8<sup>+</sup> T cells from TCL1 mice developing CLL were initially highly enriched for degranulating cells in both the PD-1<sup>high</sup> and PD-1<sup>low</sup> subset, but both subsets lost these cells with progressing CLL, with degranulation being maintained in PD-1<sup>high</sup> cells even at later stages of disease. Similarly, GrB ratios were generally higher in mice with CLL compared to age-matched controls, but the predominance of PD-1<sup>high</sup> over PD-1<sup>low</sup> cells in being enriched for GrB containing cells that was observed in WT mice was abrogated in the context of developing CLL. Although IFN- $\gamma$  ratios at early stages of CLL were roughly comparable to PD-1 subsets from age-matched WT mice, the physiological enrichment of PD-1<sup>high</sup> over PD-1<sup>low</sup> cells observed in WT mice was already lost at this stage. The previously detected CLL-induced significant overall increase of IFN- $\gamma$  at advanced stages of CLL could be attributed to both PD-1<sup>high</sup> and PD-1<sup>low</sup> cells, but the enrichment of PD-1<sup>high</sup> over PD-1<sup>low</sup> cells observed in WT mice was continuously lost. CLL-induced increased T-cell proliferation could be attributed to both PD-1<sup>high</sup> and PD-1<sup>low</sup> cells, but this was predominantly accounted for by PD-1<sup>high</sup> cells. Altogether, these comparisons revealed that despite similar PD-1 expression patterns in healthy and leukaemic TCL1 mice, PD-1 expressing cells are markedly different in their composition of cells able to exert selected effector functions compared to cells that do not demonstrate this ability.

## 6.6 Discussion

The goal of this part of the project was to investigate the suitability of the B6 TCL1 model to mirror PD-L1/PD-L2/PD-1 interactions, to investigate the effect of inhibitory signalling on T-cell exhaustion in the context of developing CLL and in different microenvironments, and to determine if PD-1 expression by CLL T cells can be correlated to specific T-cell effector functions. Using multicolour flow cytometry, we demonstrated that among the inhibitory ligands that have been identified as important mediators of impaired immune synapse formation in human CLL, PD-L1 and CD276 mirrored the aberrant over-expression of CLL cells compared to normal B cells. This was established in single cell suspensions from mouse spleen cells, while previous experiments determining the expression of inhibitory ligands in human CLL patients were done by flow cytometry of peripheral blood cells, and by IHC of lymph nodes, thus representing different compartments where cells might be subjected to different microenvironmental stimuli<sup>79</sup>.

The functional relevance of human PD-L1 and CD276 expression was demonstrated by using *ex vivo* antibody blockade<sup>79</sup>. This augmented immune synapse formation and cytolytic effector function, and prevented the induction of T-cell Rho-GTPase signalling defects, with PD-L1 blockade having the most prominent effect. Aberrant PD-L1 expression by tumour cells and the inhibitory effect on T cells has been shown in a number of other haematological malignancies, as introduced in Chapter 1.3.2, as well as in solid cancers<sup>312-314</sup>. In the current study, PD-L1 was also the most highly differentially upregulated ligand in CLL cells from TCL1 mice compared to B-cells from healthy mice. In contrast, CD200 and CD270 expression were significantly decreased on murine CLL cells compared to normal B cells. This is in marked contrast to human CLL, in which all four ligands were found to be aberrantly over-expressed. It is therefore possible that expression and function of CD200 and CD270 are regulated differentially in mice *versus* humans, and the great diversity of co-stimulatory and co-inhibitory molecules in expression, structure and function, leading to a dual largely context-dependant role, has been described<sup>427</sup>. Therefore, the downregulation of CD200 and CD270 might be an adaptive mechanism by the tumour to counteract a potentially co-stimulatory function. While using *ex vivo* antibody blockade of CD200 and CD276 might have elucidated the associations between expression and effect on T-cell effector function in the TCL1 model, we focused on aberrant PD-L1 expression as a major and clinically relevant mediator of T-cell dysfunction, which can be adequately modelled in TCL1 mice, and indeed our data support this contention.

In addition, all ligands implicated in human CLL were discovered by siRNA screening of the CLL-like Mec-1 cell line, which might not translate to the complexity *in vivo*. Additional ligands or different combinations than those identified *in vitro* might play a role in mediating T-cell dysfunction *in vivo*. This assumption was supported by our findings that not only PD-L1, but also PD-L2 was aberrantly expressed on murine CLL cells, which has not been identified in the previously conducted siRNA screen. PD-L2 is a second ligand for PD-1 and inhibits T-cell activation, T-cell proliferation, cytokine production and cell adhesion, but exhibits a very distinct pattern of expression (see Chapter 1.3.1). Aberrant PD-L2 expression alongside aberrant PD-L1 expression by tumour cells has been described in a number of haematological malignancies<sup>317, 428</sup>. In solid malignancies, in contrast, PD-L1 appears to be the more dominant negative inhibitory molecule, with PD-L2 being expressed in only a minority of patients but still having some prognostic impact<sup>312-314</sup>.

Expression of PD-L2 has not been well studied in CLL. Hence, our findings that murine CLL cells also aberrantly express PD-L2 compared to normal B cells are novel and

indicate that PD-L2 is likely to play a role in mediating T-cell defects in this disease. The use of this model also allowed us to attribute PD-L1 and PD-L2 overexpression specifically to malignant CLL cells by including 6 month old TCL1 mice, which represent an early stage of CLL where malignant CD19+CD5+ CLL cells exist next to normal CD19+ B cells and can be directly compared within the same animal. Interestingly, constitutive expression of PD-L2 was also found on up to 70% of mouse peritoneal CD5+ B1a cells, which share immunophenotypic similarities with CLL cells, with PD-L2 expression not being present on conventional B2-B cells<sup>429</sup>. Although we did not include peritoneal cavity into the current project, we demonstrated that both PD-L1 and PD-L2 expression were also significantly higher on and exclusive to CLL cells from PB, BM and LN compared to normal B cells. This confirmed the suitability of TCL1 mice to model PD-L1/PD-L2 overexpression and provided new insight into the modifying role of the tumour microenvironment

The corresponding binding partner of PD-L1, PD-1, has been demonstrated to be aberrantly expressed by CLL T cells<sup>133, 134</sup> and is also a major inhibitory receptor associated with T-cell exhaustion in chronic viral infections. Exhaustion represents a state of functional hypo-responsiveness that occurs as a progressive process in response to chronic antigenic viral stimulation. It has been characterized as a hierarchical loss of effector CD8<sup>+</sup> T-cell function, which coincides with the expression of inhibitory surface receptors such as PD-1<sup>147,404</sup>. Interestingly, the gene expression profile of exhausted CD8<sup>+</sup> T cells from murine infection models contained alterations in many pathways, including T-cell receptor and cytokine signalling pathways, migration and actin-cytoskeleton formation, that have also been identified in the molecular signature of CLL T cells<sup>216, 412, 413</sup>. Our comparison of deposited data on CLL T cells with exhausted and functional memory and effector CD8<sup>+</sup> T cells demonstrated that CLL T-cell genes that were represented in the comparison dataset were enriched in the molecular signature of exhausted T cells, but were also somewhat represented in the signature of functional effector CD8<sup>+</sup> T cells. This indicated that CLL T cells are likely to be a very heterogeneous population with features of both exhaustion and functional effector cells. Interestingly, this comparison also revealed that CLL T-cell genes enriched in the exhaustion signature appear to be also involved in pathways of T-cell metabolism and bioenergetics defects affecting ribosomal subunits, elongation factors, energy metabolism, citric-acid cycle, solute and ion channels and aquaporins. This is an interesting finding which underlines that defective T cells in CLL are a heterogeneous population, combining cells with many aspects of dysfunction. It also

identifies areas of how T-cell dysfunction in CLL can be further explored using new techniques such as CyTOF mass spectrometry in future studies.

Our findings that the molecular signature of murine CLL T cells contains a mixture of genes that have implications in exhausted cells and in functional effector cells were recently mirrored in functional studies using T cells from CLL patients. Our group demonstrated that CLL T cells exhibit features of T-cell exhaustion, such as increased expression of surface exhaustion markers, including PD-1, impaired proliferation, and cytotoxic defects with a reduced ability to lyse target cells, but retain the capacity to produce cytokines such as IFN- $\gamma$  and TNF- $\alpha$ <sup>133</sup>. In contrast, another recently published study found that proliferating CD8 T cells from CLL patients had higher expression of PD-1 than non-proliferating T cells, and that T cells had impaired IFN- $\gamma$  and IL-4 production after direct binding of PD-1 to PD-L1 ligand, which however was similar to the patterns in healthy controls<sup>134</sup>. These observations emphasise the functional relevance of the heterogeneity of CLL T cells and indicate that PD-1 expression might be linked to function in CLL as a more “physiological” marker than previously assumed, a notion that is clearly supported by our murine data. Several studies in the infection field have demonstrated that subsets of exhausted T cells are able to exert effector function despite PD-1 expression. For example, PD-1 expressing subsets have different abilities to continue their differentiation process and form functional T-cell memory upon transfer into healthy mice, while maintaining an exhausted phenotype, including the surface expression of PD-1<sup>416</sup>. In addition, T-cell populations expressing PD-1 have been demonstrated to react differently to antibody blockade. While this could reverse exhaustion and restore function in PD-1<sup>int</sup> cells, this was not possible in terminally differentiated PD-1<sup>hi</sup> T cells<sup>417</sup>. It is therefore likely that PD-1 expressing T cells in CLL are indeed a very heterogeneous population and probably consist of a larger proportion of functional effector cells despite or with PD-1 expression than previously assumed, while other PD-1 expressing cells might be truly dysfunctional.

Our data demonstrated that the surface expression of typical exhaustion markers, namely PD-1, KLRG-1, 2B4 and LAG-3, was found to be step-wise increased on CD44+ antigen-experienced CD8+ T cells in mice with developing CLL. This was to a certain extent also observed in ageing WT mice, indicating that surface expression by itself cannot be considered a definitive marker for T-cell exhaustion or dysfunction. Indeed, high PD-1 expression is also found on functional effector memory T cells in healthy ageing humans<sup>424</sup>. However, we eliminated the confounding effect of ageing by using AT experiments, which demonstrated that PD-1, KLRG-1, 2B4 and LAG-3 expression could be induced in young mice with CLL after AT, suggesting a causal

relationship with disease. With the exception of LN, the step-wise upregulation of PD-1 on antigen-experienced CD3+CD8+ T cells and its induction by AT was recapitulated in cells taken from PB, BM and spleen, confirming that PD-1, along with other exhaustion markers, can be adequately modelled in TCL1 mice and is, similar to PD-L1/PD-L2 on CLL cells, independent of microenvironment.

Functionally, CLL was found to induce altered cellular survival cytokine profiles that have also been implied in classical exhaustion, namely the enrichment for IL-2R+ and depletion of IL-7R+ CD8+ cells, which indicates an altered dependency from IL-7 to IL-2. IL-7R is expressed by naïve and memory cells, and its selective expression in the effector phase identifies CD8+ T cells that give rise to long-lived memory T cells<sup>425</sup>. TBET has been shown to directly repress expression of the IL7R gene and to downregulate IL7R surface expression, thus promoting effector cell differentiation at the expense of memory cell formation. This is in line with the dominance of CD44+CD62L- effector cells over CD44+CD62L+ memory cells described in the previous chapter, which we have observed in mice with fully developed CLL after AT. At the same time, TBET can upregulate IL-2R, leading to the switch of the cellular survival cytokine profile from IL-7 to IL-2, resulting in hypo-responsiveness to homeostatic cytokines and becoming dependant on antigen stimulation for survival<sup>426</sup>. Although we did not examine transcription factors in this mouse model, increased TBET and EOMES were found in CD8+ T cells from human patients<sup>133</sup>. Interestingly, the percentage of both CD3+CD4+ and CD3+CD8+ cells expressing intracellular IL-2 was comparable between healthy mice and leukaemic mice with CLL after AT, similar to human CLL T cells. IL-2 is predominantly produced by CD4+ T cells, and is important for peripheral T-cell expansion and cell survival<sup>430</sup>. In mice, the major role of IL-2 appears to be to promote the thymic development and peripheral expansion of CD4+CD25+ TRegs which regulate the size of the peripheral T-cell compartment. TRegs are also expanded in human CLL and correlate with progressive disease<sup>176</sup>, and *in vitro* IL-2 induces their expansion<sup>431</sup>. In a recently published *in vivo* study, low dose IL-2 administration enhanced CD8+ T-cell responses in chronically LCMV infected mice, decreased inhibitory receptor levels on virus-specific CD8+ T cells, and increased the expression of IL7R and CD44, shifting cells back to a memory-like phenotype<sup>432</sup>. The combination of IL-2 treatment with blockade of the PD-1 inhibitory pathway had synergistic effects in enhancing virus-specific CD8+ T-cell responses and decreasing viral load, despite increased numbers of TRegs. Increased IL-2R expression by CLL T cells might therefore be a compensation mechanism to account for increased requirement of IL-2 to maintain T-cell function in response to

immunological challenge by CLL cells, which is not met by increased production by T cells. IL-2 has also been indicated in being involved in aberrant PD-L1 and PD-1 expression itself: common gamma-chain cytokines such as IL-2, IL-7, IL-15, and IL-21 were found to up-regulate PD-1 and, with the exception of IL-21, PD-L1 on purified T cells *in vitro*, and to indirectly induce the expression of PD-L1 and PD-L2 on monocytes and macrophages in peripheral blood<sup>433</sup>. As described in the previous chapter, contrary to the AT model, IL-2 production by CD3+CD8+ T cells was found to aberrantly increase in ageing mice with CLL and was detected at early stages of CLL, coinciding with the beginning of aberrant expression of PD-L1/PD-L2 and PD-1. Hence, it could be involved in the induction of PD-L1/PD-L2 and PD-1 expression, or in the promotion of TRegs. If the AT model is interpreted as the aggressive form of CLL with high antigen load, IL-2 production in highly leukaemic mice that is not different to age-matched WT mice might be the end-result of a previous dynamically increased production as indicated by the ageing TCL1 mice, with aberrant IL-2R expression representing the resulting “end-stage” compensation mechanism to maintain functions such as increased proliferation, which we have described in the previous chapter.

Our randomized AT experiments also demonstrated that CLL-induced aberrant PD-1 expression on CD3+CD8+ T cells could be associated with different abilities of cells to exert effector functions: in general, intracellular cytokines IL-2, IL-4, IFN- $\gamma$  and TNF- $\alpha$  were detected in both PD-1<sup>high</sup> and PD-1<sup>low</sup> cells, and both PD-1<sup>high</sup> and PD-1<sup>low</sup> cells maintained their ability to degranulate, contrasting the notion that PD-1 expression would lead to a loss of these effector functions. In addition, we demonstrated that the increase in IFN- $\gamma$  production frequently observed in CLL T cells appeared to be attributed to PD-1<sup>high</sup> cells, while this subset was depleted of cells producing TNF- $\alpha$  compared to PD-1<sup>low</sup> cells and showed an impaired ability to form immunological synapses with normal B cells.

Lastly, the TCL1 model allowed us to better understand the functional difference of expression of PD-1 on CLL CD8+ T cells compared to the physiological expression on normal T cells. Linking PD-1 expression with effector function of PD-1<sup>high</sup> cells in ageing WT mice and comparing this to effector function of PD-1<sup>high</sup> cells in ageing TCL1 mice developing CLL revealed that in ageing WT mice, both PD-1<sup>high</sup> and PD-1<sup>low</sup> cells contributed to the overall patterns associated with ageing described in the previous chapter, *i.e.* maintenance of degranulation and intracellular GrB, reduction of proliferation, and increase of intracellular IFN- $\gamma$  production. While both PD-1<sup>high</sup> and PD-1<sup>low</sup> subsets contained comparable proportions of cells able to degranulate and to proliferate, cells positive for GrB and IFN- $\gamma$  appeared to be enriched in the PD-1<sup>high</sup>

subset compared to the PD-1<sup>low</sup> subset, supporting the understanding that PD-1 expression in normal T cells contributes to the dynamic alterations of how effector functions are maintained in the context of ageing. CD8<sup>+</sup> T cells from TCL1 mice developing CLL were initially highly enriched for degranulating cells in both the PD-1<sup>high</sup> and PD-1<sup>low</sup> subset, probably as a result of beginning immunological challenge by CLL, but both subsets lost these effector cells with progressing CLL. Similarly, GrB ratios were generally higher in mice with CLL compared to age-matched controls, however the predominance of PD-1<sup>high</sup> over PD-1<sup>low</sup> cells in being enriched for GrB containing cells observed in WT mice was abrogated in the context of developing CLL. A similar observation was made for IFN- $\gamma$ , indicating that PD-1 expressing cells indeed are likely to have a GrB and IFN- $\gamma$  deficiency compared to non-PD-1 expressing cells, which however do not render them GrB or IFN- $\gamma$  dysfunctional. In contrast, CLL-induced increased T-cell proliferation was predominantly driven by PD-1<sup>high</sup> cells. In this context, however, PD-1 expression and upregulation might also be a physiological reaction to increased T-cell proliferation in response to tumour antigen. Altogether, these data show that despite similar PD-1 expression patterns in ageing healthy and leukaemic TCL1 mice, PD-1 expressing cells are markedly different in their composition of cells able to exert selected effector functions, but that PD-1 expression in CLL T cells are largely functional T-cell effector cells.

In sum, we have confirmed the suitability of the B6 TCL1 model to mirror PD-L1/PD-1 interactions, we have extended this to the second binding partner of PD-1, PD-L2, and we have demonstrated that aberrant PD-L1/PD-L2/PD-1 expression is utilized by CLL and T cells regardless of their microenvironment. In addition, we have characterised the features of T-cell “exhaustion” in the context of different microenvironments, while unmasking the associations between CLL and ageing. Lastly, we have provided novel data on the associations between PD-1 expression and effector functions of T cells. Altogether, this work highlights the importance of PD-L1/PD-1 mediated inhibitory signalling on T-cell dysfunction in CLL. It supports the hypothesis that T cells in CLL might be rescued and reversed into a functional state able to effectively mount anti-tumour responses by targeting PD-L1 and PD-1, and that the TCL1 model is a very suitable tool to study the effect of such treatment *in vivo*.

## 7 Potential of *in vivo* lenalidomide treatment to restore T-cell function in Eμ-TCL1 mice

### 7.1 Specific introduction

A plethora of preclinical studies have demonstrated that second generation immunomodulatory drugs (IMiDs) such as lenalidomide and pomalidomide modulate the tumour microenvironment through the downregulation of pro-survival and inflammatory cytokines and the activation of immune effector cells. In addition to potently inhibiting TNF- $\alpha$  production *in vitro*<sup>434, 435</sup>, lenalidomide and pomalidomide increase IL-2 and IFN- $\gamma$  production and cytotoxic capacities in T cells<sup>436-439</sup>. The latter most likely is a result of actin cytoskeleton activation. This hypothesis was further consolidated by work from our group showing that T cells from CLL patients exhibit multiple dysregulated genes and pathways involved in cytoskeleton formation and vesicle trafficking. This effect leads to an impaired ability to regulate F-actin polymerization and to polarize the cytoskeleton, therefore offering a unique platform to investigate the effect of IMiD treatment on cytoskeleton modelling<sup>77, 171</sup>. *In vitro* lenalidomide treatment of both APCs and T cells restored the ability of CD4+ and CD8+ T cells to polarize F-actin to the immunological synapse, increased the cytolytic capacity of CD8+ effector cells, and repaired defective integrin LFA-1-directed T-cell adhesion and migration<sup>77, 81</sup>. This was found to be mediated via activation of Rho GTPases RhoA, Cdc42, and Rac1<sup>79</sup>, which have been described as key signal transducer elements in morphological T-cell changes, cytoskeleton polarization and trans-endothelial migration in normal T cells, and also play a role in T-cell activation, thymocyte differentiation and transcription factor regulation<sup>440</sup>. The potential of *in vivo* lenalidomide treatment to restore defective immune synapse formation was recently confirmed in CLL patients treated within a Phase II trial with immunochemotherapy consisting of rituximab, pentostatin and cyclophosphamide (PCR), followed by lenalidomide maintenance<sup>80</sup>. Lenalidomide improved the depth of response in 24% of eligible patients, suggesting that it might prolong the time to re-treatment, and significantly improved immune synapse formation. However, immune synapses were already found to be enhanced after PCR compared to baseline prior to any treatment, indicating that cytoskeleton re-polarization can also partly be achieved by therapy with other substances or by removal of the CLL cells themselves as the patients respond to treatment.

The addition of lenalidomide to co-cultures between CLL and normal allogeneic T cells, as well as treatment of autologous CLL/T-cell co-cultures, was recently demonstrated by our group to overcome the immunosuppressive effect of PD-L1, CD200, CD270 and

CD276 inhibitory signalling, as its effect on restoring the immune synapse and increasing CD8+ T cell cytolytic potential was comparable to the repair achieved by combined antibody blockade of all four inhibitory ligands<sup>79</sup>. In addition, lenalidomide downregulated the expression of PD-L1, CD200, CD270 and CD276 on CLL and tumour-infiltrated DLBCL and follicular lymphoma cells, and prevented the induction of aberrant expression of their receptors, including PD-1, on T cells. Similar effects were seen in a small number of samples from relapsed CLL patients treated with lenalidomide in a clinical trial<sup>79</sup>. Compared to baseline levels of expression prior to lenalidomide exposure, single agent lenalidomide treatment reduced the expression of both inhibitory ligands on CLL cells and the corresponding receptors on T cells, increased T-cell conjugation and synapse function with autologous tumour cells acting as APCs, and increased antigen-induced cytolytic effector activity. The modulation of levels of T cells expressing PD-1, 2B4, and CD57 were recently described in a cohort of 131 CLL patients<sup>441</sup>. Comparing 49 conventionally treated patients to 10 patients who had received a lenalidomide-containing regimen, the authors found that the percentage of CD4+ cells expressing either PD-1, 2B4 or CD57 alone, and all markers in combination, was significantly reduced after lenalidomide treatment, and was comparable to levels observed in healthy controls. Among CD8+ cells, the percentages of all subsets, with the exception of CD8+PD-1+ and CD8+PD-1+2B4+ cells, were similarly reduced in lenalidomide treated patients.

Long term *in vivo* lenalidomide treatment also has the potential to normalize general T-cell subsets in CLL<sup>442, 443</sup>. In 24 patients with untreated CLL enrolled in a Phase II clinical trial of lenalidomide, a significant reduction in percentages and absolute lymphocyte counts were observed after 3 cycles of therapy, with a relative increase of T cells, activated CD8+ T cells producing IFN- $\gamma$ , and TRegs compared to baseline levels before treatment. After 15 cycles of treatment, activated IL-2/IFN- $\gamma$ /TNF- $\alpha$  producing CD4+ T cells, TRegs and activated IFN- $\gamma$  producing CD8+ T cells normalized to the range found in healthy subjects<sup>442</sup>. A long-term analysis of 60 CLL patients treated with lenalidomide (median follow up 4 years) identified a normalisation in the percentage of CD4+ and CD8+ cells and T-cell numbers in 48%, 71% and 99% of long-term responders, respectively<sup>87</sup>. Another immune cell subset that is affected by lenalidomide treatment, either directly or indirectly via T-cell activation, is NK cells<sup>444</sup>. Several preclinical studies demonstrate that IMiDs enhance NK cell mediated cytotoxicity<sup>439, 445</sup>, increase ADCC towards myeloma cells<sup>446</sup>, and reduce the expression of inhibitory ligands such as SOCS1<sup>447</sup>. In CLL, baseline NK cell numbers and activation status could be linked to clinical response to lenalidomide, with higher

numbers of NK cells, a greater capacity for NK cell proliferation *in vitro*, and higher baseline expression of NK cell activating ligands MIC-A/B on CLL cells predicting better outcome in a clinical trial<sup>448</sup>. Further evidence of *in vivo* immune activation stems from the observation of the occurrence of tumour-flare reactions in CLL patients treated with lenalidomide<sup>91</sup>. Tumour-flare reactions clinically manifests as acute and painful swelling of CLL-affected lymph nodes, hepatosplenomegaly, rash, and fever, which usually occur 8-72 hours after initial drug administration but generally respond well to steroid and non-steroid anti-inflammatory treatment. The clinical manifestations are associated with features of immune activation, with upregulation of costimulatory molecules such as CD40, CD80, and CD86 on CLL cells, upregulation of CD69 on T cells, and elevated serum levels of cytokines and chemokines<sup>78, 91, 448</sup>. As lenalidomide is not directly toxic to CLL cells *in vitro*, the anti-tumour effect of lenalidomide therefore appears to be mediated by activating T-cell and NK-cell anti-tumour immune responses rather than inducing direct tumour cell death.

Extensive murine studies on the pharmacokinetics after oral, i.v. and i.p. application of lenalidomide and the resulting tissue distribution revealed that doses of 15 mg/kg i.v., 22.5 mg/kg i.p., and 45 mg/kg orally are well tolerated in mice<sup>449</sup>. The administration of translationally relevant doses of 0.5 and 10 mg/kg led to systemic bioavailability ranges of 90–105% and 60–75% via i.p. and oral routes, respectively, with a dose-dependent tissue distribution. These findings demonstrate that the high oral bioavailability of lenalidomide in mice appears to be consistent with that in humans. Interestingly, studies on the effect of lenalidomide in the TCL1 mouse model are so far limited to *in vitro* studies: our group has demonstrated that the repair of immune synapse formation could be achieved by *ex vivo* treatment of autologous murine B and T cells, recapitulating the effect of lenalidomide in human CLL<sup>216</sup>. Work conducted in this dissertation project has confirmed that PD-L1/PD-1 mediated T-cell dysfunction observed in human CLL is adequately mirrored in TCL1 mice. In addition, we have demonstrated that TCL1 mice can be used to overcome the effect of confounding factors such as age, pre-treatment, or underlying chronic infections, which by themselves can influence the functional effect of PD-L1/PD-1 interactions. Although previous studies using CLL patient samples indicate that both *in vivo* and *ex vivo* lenalidomide treatment has an effect on modulating T-cell subsets and function<sup>442, 443</sup>, as well as PD-L1/PD-1-mediated inhibitory signalling<sup>79, 80, 441</sup>, a comprehensive analysis *in vivo* linking the effect of single agent lenalidomide to aberrant PD-L1/PD-1 expression and functional T-cell defects has not been done.

## 7.2 Goals and objectives

My next goal was therefore to investigate if *in vivo* lenalidomide treatment corrects CLL-induced T-cell dysfunction, with a focus on PD-L1/PD-L2/PD-1, and enhances anti-tumour T-cell responses in mice with CLL. Specifically, I sought to address the following questions:

- Does *in vivo* lenalidomide treatment have the potential to effectively control disease development after adoptive transfer of murine CLL?
- Does *in vivo* lenalidomide treatment prevent the development of the previously described aberrant T-cell phenotype?
- Can *in vivo* lenalidomide treatment restore key T-cell effector functions?
- Can *in vivo* lenalidomide treatment overcome functional T-cell defects relating to aberrant PD-1 expression?

## 7.3 Specific methods and materials

### 7.3.1 Mice and randomization procedure

Three month old female B6 WT mice (n=42) were purchased from commercial suppliers (Charles River, UK), ear marked, and kept in cages containing a maximum of 5 mice each for one week. Sample size was calculated based on the assumption that at least 17 mice per group would be needed to detect a 1.0 standard deviation difference in PD-1 means between treated and untreated mice in two-sided testing at a significance level  $\alpha=0.05$  with at least 80% power. For AT, mice were injected i.v. with  $4 \times 10^7$  syngeneic CLL cells in a single dose from the same pool of aged TCL1 mice. Twenty days after the i.v. injections, 50 $\mu$ l blood was obtained by tail bleeds from each mouse, and the percentage of CD19+CD5+ CLL cells among lymphocytes was determined by flow cytometry. Transplanted mice had a median CLL load of 26% (range 2-36%). Three mice did not show engraftment, and the CLL load could not be assessed in 1; these 4 animals were therefore excluded from the study. The remaining 38 mice were distributed equally between treatment (n=19) and vehicle control (n=19) based on their individual CLL loads. The direct comparison between the intervention groups confirmed that mice with different CLL loads were equally balanced between the intervention groups (p=.6073, Figure 49). Lenalidomide (10mg/kg body weight in 300 $\mu$ l PBS) or vehicle only (300 $\mu$ l PBS) was administered daily by oral gavage. Treatments were initiated on day 21 post AT, and mice were treated for 3 weeks. After

this time (total of 6 weeks after AT), mice were sacrificed under protocol 19b2 of PIL 70/7531. Spleens and PB were processed as described in general methods. Healthy age-matched WT (hWT) mice were not included prospectively into this study. Differences between mice with CLL and healthy mice were depicted by historical comparison with data from hWT used in other experiments.

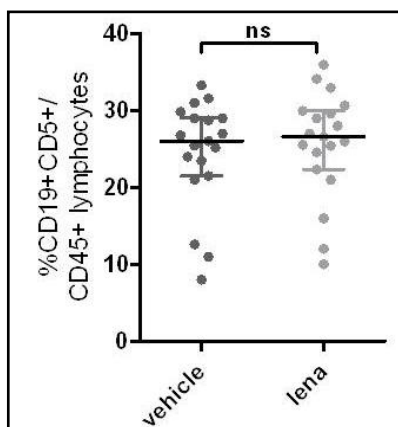


**Figure 49: CLL load in mice assigned to vehicle and lenalidomide treatment.** Three weeks after AT, mice were bled and distributed equally between the vehicle and lenalidomide intervention group based on individual CLL loads, defined as the percentage of CD19+CD5+ lymphocytes. Statistical comparison confirmed that CLL loads were balanced between the intervention groups. Graph shows median with Interquartile Range (IQR). ns = non-significant.

### 7.3.2 Drug preparation and stability

Lenalidomide was received as a kind gift from our collaborators at the Ohio State University (OSU). The drug was extracted from capsules donated by CLL patients no longer on treatment. Upon receipt of the powder, its content was confirmed by mass spectrometric analysis. The powder was diluted at 1:1000 in 30% acetonitrile solution containing 0.1% formic acid in LC-MS grade water (all from Fisher Scientific). Both high resolution Q-TOF MS1 and triple stage quadrupole Vantage mass spectrometry systems (Thermo Scientific, UK) with Agilent Jet Stream technology for electrospray ionization were used. All experiments were carried out in positive ionization mode. Spray voltage was set to 3500 volts, and the sheath gas (nitrogen) flow rate was 20 arbitrary units. Argon was used as collision gas with a pressure of 1.5 mTorr. Data was acquired using Thermo Xcalibur software (version 2.1).

Collecting total ion spectra over a mass range of 210 to 300 m/z, the received powder was confirmed as lenalidomide based on its molecular mass of 259.261 g/mol and published fragmentation patterns (Figure 50 A and B)<sup>450</sup>. Lenalidomide was then dissolved in sterile PBS, and kept in 6ml aliquots at -80°C to allow daily treatment of all mice from the same drug stock. Additional aliquots were kept for further mass spectrometry experiments. After all mice had been treated for 3 weeks, the ion count of the treatment compound was compared to a freshly reconstituted standard to document changes in drug stability. The ion count of the treatment compound was

$1.05 \times 10^7$ , which was lower than the ion count of the freshly reconstituted drug of  $2.03 \times 10^7$ , indicating some degradation of the drug over the treatment period (Figure 50 C).

After the end of the study, 2 additional WT mice were treated with 10mg/kg body weight lenalidomide in 300 $\mu$ l PBS from the treatment compound stock or 300 $\mu$ l PBS vehicle control only. After 5 days of treatment, mice were sacrificed 24 hours after the last dose, and PB, spleen and brain were removed. A leukaemic untreated TCL1 mouse was used as an additional control. Blood was collected in EDTA-coated 1.5ml Eppendorf tubes, centrifuged at 2,000 x g for 10 minutes at 4°C. Supernatant was then centrifuged at 2,000 x g for 15 minutes at 4°C to deplete platelets in the plasma sample. 150 $\mu$ l ice cold methanol containing 50ng/ml of the internal standard carbamazepine was added to the plasma, vortexed for one minute, kept on ice for 30 minutes, and centrifuged at 10,000rpm for 10 minutes at 4°C. The supernatant was transferred to a fresh Eppendorf tube, and methanolic extracts were evaporated to dryness in a Savant Speedvac. Organs were weighed, and 50mg of each sample was homogenised in 1.5 ml of methanol/water (1:1) containing 50ng/ml of carbamazepine, using 5mm steel beads and a tissueLyser-II (Qiagen, UK) at 25 Hz for 5 minutes. Samples were then centrifuged at 16,000 x g for 10 minutes, and supernatants were transferred to fresh Eppendorf tubes and dried in a Savant Speedvac. All dried extracts were reconstituted in 10% acetonitrile, and 10 $\mu$ l of the reconstituted solutions were injected into an ultra-performance liquid chromatography system (Accela UPLC, Thermo Scientific, UK) equipped with an Acquity UPLC BEH C18, 1.7  $\mu$ m, 100 x 2.1 mm column (Waters, UK) and a mobile phase consisting of a mixture of water containing 0.1% formic acid (A), and acetonitrile containing 0.1% formic acid (B). The mobile phase gradient was employed, comprising buffer A = 90% at 0 - 1 min, from 90 to 20% over 2 minutes, held at 20% for 2 minute, from 20 to 90% over 0.1 minutes, ending with 90% for 2.9 minutes, all at a flow rate of 250  $\mu$ l/min. Eluting compounds were detected using the triple stage quadrupole Vantage mass spectrometry system (Thermo Scientific, UK). Samples were analysed in the Multiple Reaction Monitoring (MRM), positive ion modes at a spray voltage of 3500V. Nitrogen was used as sheath and auxiliary gas at a flow rate of 30 and 10 arbitrary units, respectively. Argon was used as collision gas with pressure of 1.5 mTorr. The optimum transitional daughter ions mass and collision energy of each analyt were as follows: Lenalidomide 260.0  $\rightarrow$  149.2 (collision energy 16V) and Carbamazepine 237.1  $\rightarrow$  194.3 (collision energy 20V).

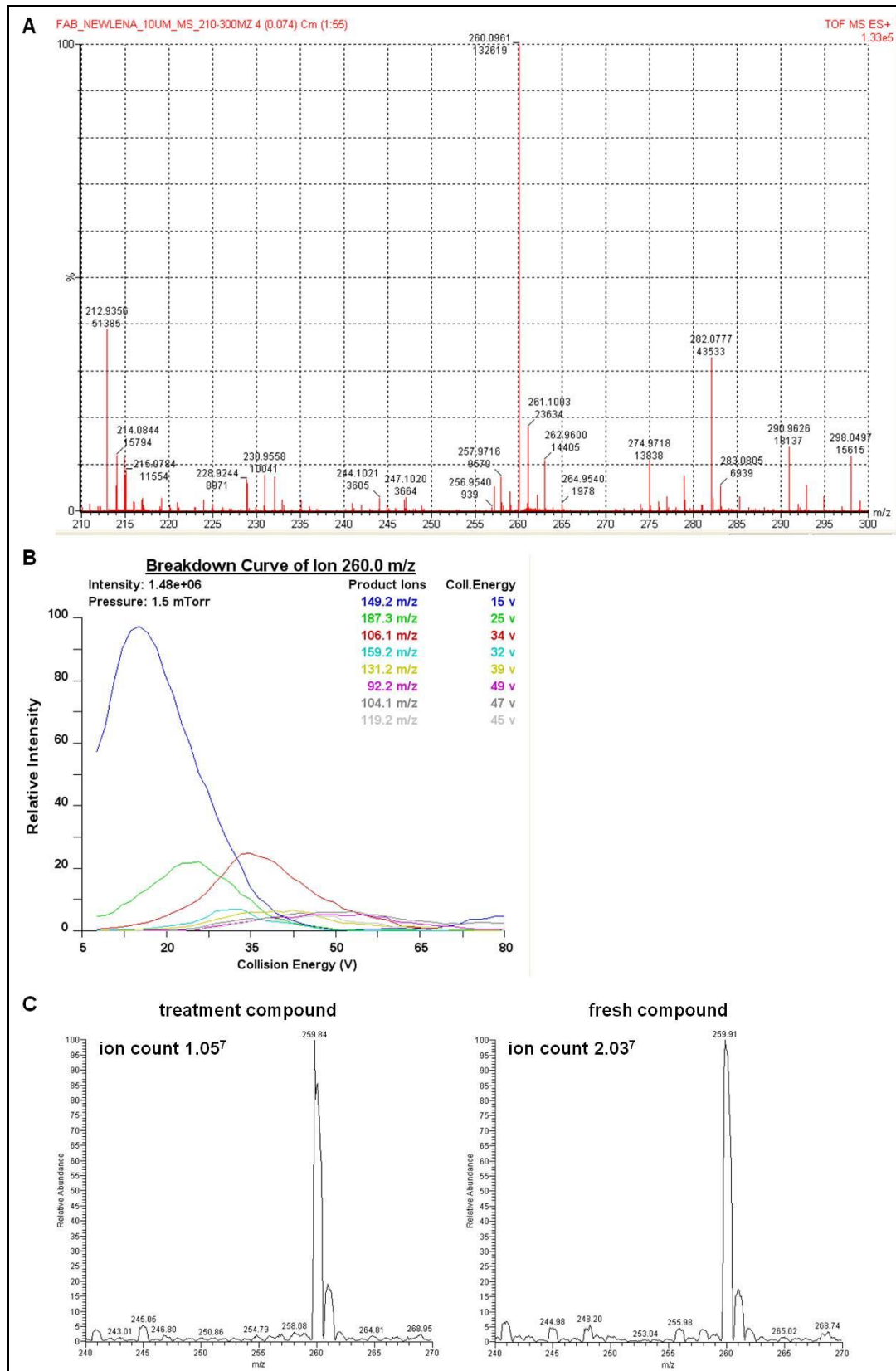


**Figure 50: Mass spectrometric analysis to confirm presence and stability of lenalidomide.** Lenalidomide was extracted from capsules and purified by our collaborators. **(A)** High resolution Q-TOF MS1 confirmed the received compound as lenalidomide based on its molecular mass of 259.261 g/mol and **(B)** principle fragmentation patterns of top 8 fragments. **(C)** After completion of the treatment period, the ion count of the treatment compound was  $1.05 \times 10^7$ , compared to the ion count of  $2.03 \times 10^7$  of the freshly reconstituted drug.

**7.3.3 Multicolour flow cytometry for cell surface markers**

T-cell subsets were characterized based on the surface expression of CD3, CD4, CD8, CD62L, CD44 and CCR7. Exhaustion markers included PD-1, KLRG-1, 2B4, CD160 and LAG-3. Cytokine receptors included CD122 and CD127. CLL was assessed by CD19 and CD5 expression, and PD-L1 and PD-L2 were included into the CLL panel. Antigens, fluorochromes, clones, concentrations and suppliers are described in Chapters 5 and 6. Table 19 contains an overview of the flow panel combinations used in this experiment. Experiments were performed on fresh samples, and FMO controls for CD44, CCR7, exhaustion markers, cytokine receptors, PD-L1 and PD-L2 were included into all experiments. Cells were prepared for flow cytometry as described in the general methods section. The gating strategies have been described in Chapters 5 and 6.

1. spleen							
tube 1		tube 2		tube 3		tube 4	
T-cell subsets/ exhaustion		T-cell exhaustion		cytokine receptors		B cells	
CD4	PerCPCy5.5	CD8	FITC	CD8	FITC	CD5	APC
CD8	BV605	CD3	APCCy7	CD3	APCCy7	CD19	FITC
CD3	APCCy7	CD44	AF700	CD44	AF700	CD45	APCCy7
CD62L	FITC	2B4	APC	CD122	PE	PDL1	PerCPeFl710
CD44	AF700	LAG3	PerCPeFl710	CD127	APC	PDL2	PE
CCR7	PeCy7	CD160	PE	viability dye	DAPI	viability dye	DAPI
KLRG1	PE	viability dye	DAPI				
PD1	APC						
viability dye	DAPI						
2. peripheral blood							
tube 1						tube 2	
T-cell subsets/ exhaustion						B cells	
CD4	PerCPCy5.5					CD5	APC
CD8	BV605					CD19	FITC
CD3	APCCy7					CD45	APCCy7
CD62L	FITC					PDL1	PE
CD44	AF700					PDL2	PerCPeFl710
PD1	APC					viability dye	DAPI
viability dye	DAPI						

**Table 19: Overview of flow panel to phenotype T-cell subsets, exhaustion markers, cytokine receptors, CLL and inhibitory ligands in spleen and peripheral blood.**

### 7.3.4 Multicolour flow cytometry for intracellular cytokines and effector function

Effector function and intracellular cytokines were evaluated as described in Chapter 6 and included CD107a degranulation, intracellular IL-2, IL-4, and IFN- $\gamma$ , and intranuclear ki67. Differences in T-cell function between experimental groups were compared by calculating ratios between CD44+ cells positive for CD107a/IFN- $\gamma$ /ki67, and CD44+ cells negative for these markers, to describe the ratio between effector cells within CD44+ cells compared to non-effector (*i.e.* negative) cells. Differences in ratios were interpreted as an increase of cells able to exert effector functions (increase of ratio), or decrease of cells able to exert effector functions (decrease of ratio), respectively. Similar comparisons were made between PD-1<sup>high</sup> and PD-1<sup>low</sup> ratios.

### 7.3.5 Immune synapse formation assays

CLL and B cells were purified from frozen splenocytes by manual magnetic separation using murine CD19 microbeads (Miltenyi, UK). The column effluent representing the CD19- fraction was further purified by negative selection using murine T-cell isolation kits (Miltenyi, UK). These T cells were used in synapse formation assays with CMAC labelled, sAg-pulsed autologous CLL and B cells as antigen-presenting cells at a 1:1 ratio. Synapse assay, confocal microscopy, and image analysis were conducted as described in Chapter 3.5.

### 7.3.6 *Ex vivo* lenalidomide treatment of autologous murine B and T cells

The effect of *ex vivo* lenalidomide treatment on immune synapse formation between autologous mouse B and T cells was assessed following previously established protocols by our group<sup>77</sup>. After magnetic separation,  $1 \times 10^6$  B and T cells were resuspended separately in 1ml RPMI 1640 with 10% FCS, 1% Penicillin/Streptomycin, 1% Glutamine, and 500mM beta-mercaptoethanol, and transferred into a 24 well plate. Cells were then treated for 24 hours with 0.5 $\mu$ M lenalidomide in acidic PBS vehicle (1% HCl), or vehicle only, washed, and used in immune synapse formation assays as described in general methods. Optimization experiments using autologous B and T cells from three different fully leukaemic TCL1 mice confirmed that *ex vivo* treatment with lenalidomide increased the median area of F-actin immune synapses (Figure 51).

Cells from *in vivo* lenalidomide/vehicle treated mice were treated *ex vivo* following identical procedures.

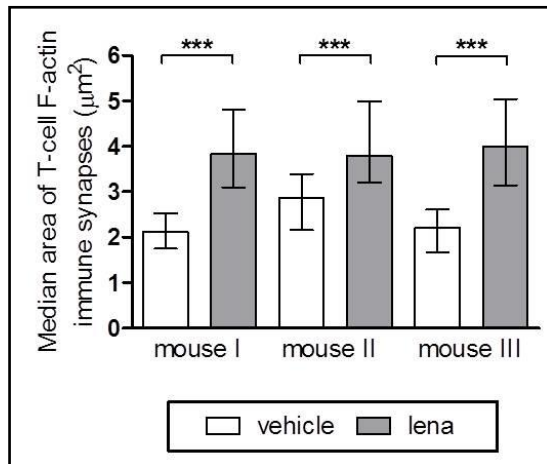


**Figure 51: *Ex vivo* lenalidomide treatment of autologous murine B and T cells:** Purified CLL and T cells from 3 different fully leukaemic TCL1 mice were treated separately for one hour with vehicle (white bars) or 0.5µM lenalidomide (grey bars), washed, and used in immune synapse formation assays. Lenalidomide treatment significantly improved the mean area of immune synapses compared to vehicle treated cells.

### 7.3.7 *Ex vivo* PD-L1 and PD-1 blockade

To assess the effect of additional *ex vivo* PD-L1 and PD-1 blockade, cells from *in vivo* lenalidomide or vehicle treated mice were pre-treated *ex vivo* with purified blocking antibodies against PD-L1 and PD-1, or isotype control blocking antibodies, before immune synapse formation assays. Optimal doses of PD-L1 and PD-1 blocking antibodies were established by flow cytometry based saturation assays. For this, previously frozen spleen cells from fully leukaemic TCL1 mice were thawed, washed, and counted following protocols described in general methods. Cells ( $1 \times 10^6$ ) were then resuspended in 0.1ml FACS buffer and pre-treated with 1, 5, 10, 15, 20, 30, or 40µg/ml purified LEAF™ (“Low Endotoxin, Azide-Free”) anti-mouse PD-L1 antibody (clone 10F.9G2, rat IgG2bk), 1, 5, 10, 15, 20, 30, or 40µg/ml purified anti-mouse PD-1 antibody (clone RMP1-30, rat IgG2bk), equivalent concentrations of purified isotype blocking antibodies, or were left untreated (all antibodies from Biolegend). After 1 hour, cells were washed to remove any unbound antibodies, and stained with PeCy7-labelled anti PD-L1 and APC-labelled PD-1 antibodies on the same clones (*i.e.* 10F.9G2 and RMP1-30, both from eBioscience, UK) at a constant 1:100 dilution. FMO controls for PD-L1 and PD-1 were included into all experiments. MFIs were compared among cells treated with increasing concentrations of blocking antibody, and a decrease in MFI was interpreted as the inability of fluorescently labelled antibody to bind to the PD-L1 or PD-1 epitope because of pre-existing blockade by the purified antibody. Doses at which a plateau was reached, and no further decrease of MFI was observed by using higher concentrations of blocking antibody, were determined as optimal antibody doses to

achieve best possible blockade of PD-L1 and PD-1. For purified PD-L1 antibody, this was determined to be 10 $\mu$ g/ml (Figure 52 A), and for PD-1 20 $\mu$ g/ml (Figure 52 B). Cells from *in vivo* lenalidomide/vehicle treated mice were purified as described above, and treated *ex vivo* for 1 hour with 10 $\mu$ g/ml PD-L1, 20 $\mu$ g/ml PD-1, and blocking antibodies in 0.1ml FACS buffer. Cells were then washed, and used in immune synapse formation assays as described in Chapter 3.5.

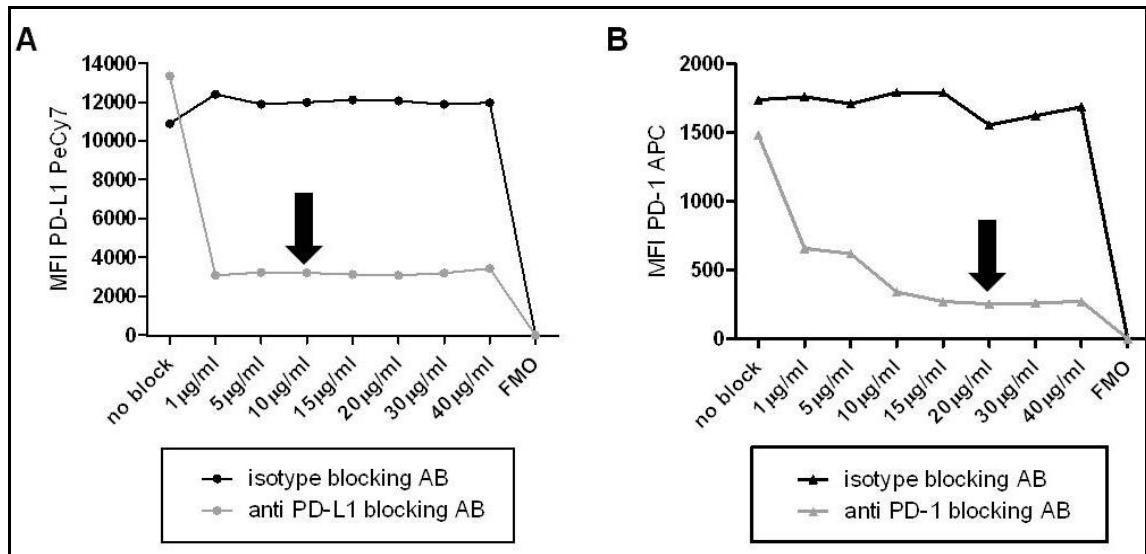


**Figure 52: Saturation curves of blocking PD-L1 and PD-1 antibodies.** To determine optimal doses of PD-L1 and PD-1 blocking antibodies *in vitro*, cells were pretreated for 1h with increasing concentrations of purified blocking PD-L1 (clone 10F.9G2), PD-1 (clone RMP1-30), and isotype blocking antibodies. After washing to remove unbound antibodies, cells were stained with PeCy7-labelled PD-L1 (clone 10F.9G2) and APC-labelled PD-1 (clone RMP1-30). **(A)** Pre-treatment with 10 $\mu$ g/ml anti-PD-L1 was found to sufficiently block the binding of fluorescently labelled PD-L1, determined by a plateau in decrease of Median Fluorescence Intensity (MFI). **(B)** Pre-treatment with 20 $\mu$ g/ml anti-PD-1 sufficiently blocked the binding of fluorescently labelled PD-1. Figure shows representative saturation curves from 3 different experiments. FMO = Fluorescence-Minus-One control.

## 7.4 Results

### 7.4.1 *In vivo* lenalidomide treatment does not result in effective CLL control and has no effect on aberrant PD-L1 and PD-L2 expression

To assess the effect of *in vivo* lenalidomide treatment in mice with CLL after AT of  $4 \times 10^7$  CLL cells from leukaemic E $\mu$ -TCL1 donors, mice received daily lenalidomide or PBS vehicle control. Treatment was started 3 weeks after AT, and mice with different CLL loads were well balanced between intervention groups. After 3 weeks of treatment (a total of 6 weeks after AT), we found that *in vivo* lenalidomide did not result in effective CLL control. This was demonstrated by both spleen weights and CLL load in examined organs; no differences were observed in median spleen weights between lenalidomide (1.05g; range .85-1.24) and vehicle treated mice (1.0g; range .73-1.68,  $p=.7069$ , Figure 53 A), and the median percentages of CD19+CD5+ CLL lymphocytes were comparable in spleen (lenalidomide 71.3%, range 52.2-84.3; vehicle 68.1%, range 56.4-83.8,  $p=.6037$ , Figure 53 B) and PB (lenalidomide 69.7%, range 48.1-86.5; vehicle 70.5%, range 52.9-86.6,  $p=.4335$ , Figure 53 C).

Similarly, *in vivo* lenalidomide had no effect on the surface expression of PD-L1 and PD-L2 on CLL cells from spleen and PB. In spleen, the specific MFI for PD-L1 was 1,052 (range 610.9-1,414) in lenalidomide treated and 1,024 (range 675.2-1,227) in vehicle treated mice ( $p=.3981$ , Figure 53 D left panel). Specific MFIs for PD-L2 were 2,338 (range 1,442-3,870) in lenalidomide treated and 2,463 (range 1,315-3,181) in vehicle treated mice ( $p=.900$ , Figure 53 D right panel). In PB, the specific MFI for PD-L1 was 777.4 (range 508-987.5) in lenalidomide treated and 687.9 (range 511.1-1,087) in vehicle treated mice ( $p=.4389$ , Figure 53 E left panel). Specific MFIs for PD-L2 were 1,826 (range 1,285-2,665) in lenalidomide treated and 1,726 (range 1,376-3,148) in vehicle treated mice ( $p=.8043$ , Figure 53 E right panel).

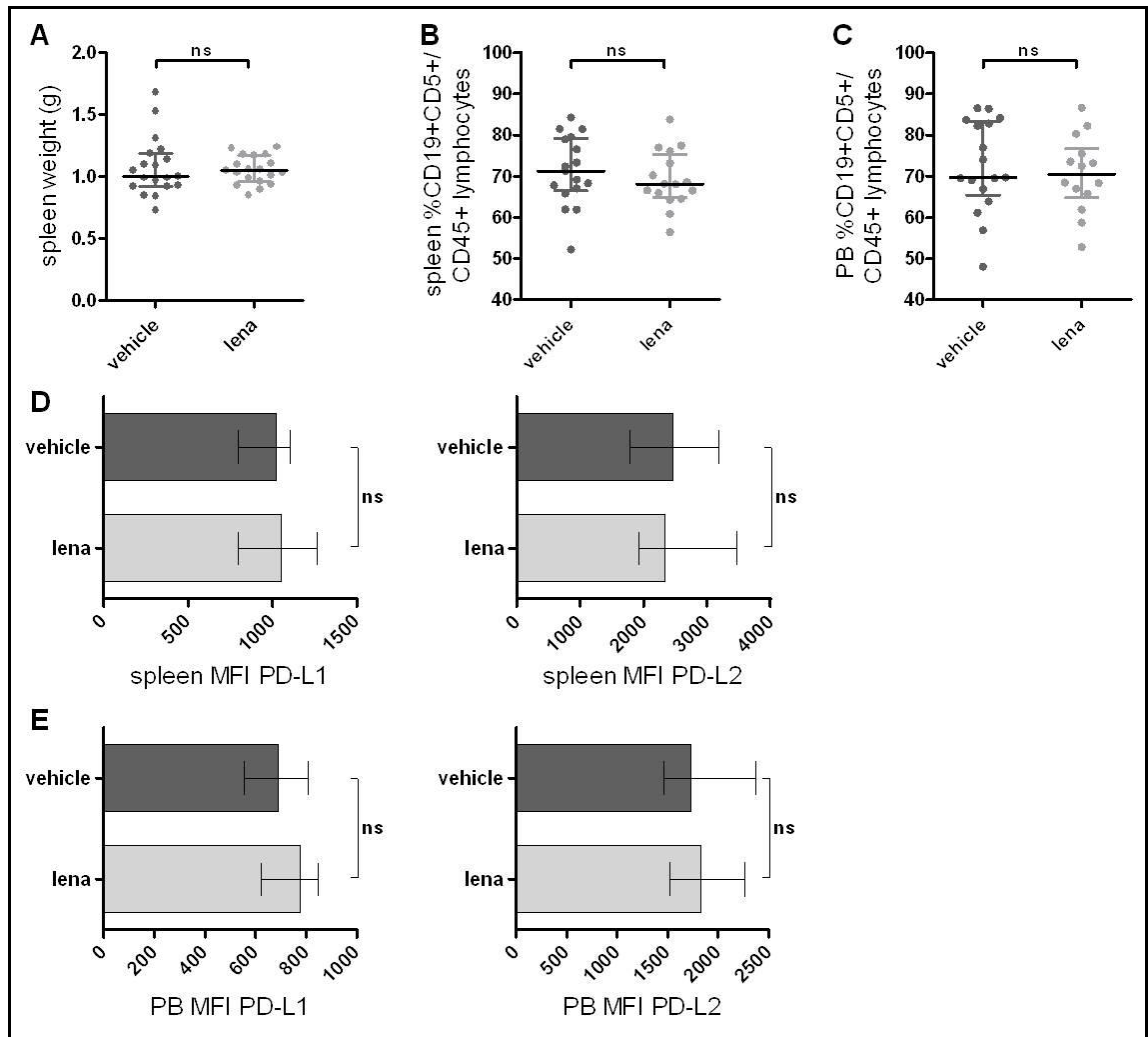


**Figure 53: Effect of *in vivo* lenalidomide treatment on CLL progression and PD-L1 and PD-L2 expression on CLL cells.** Mice were treated with 10mg/kg body weight lenalidomide or vehicle control, started at 3 weeks after AT of  $4 \times 10^7$  splenocytes from leukaemic TCL1 mice, and sacrificed after 3 weeks of treatment. **(A)** median spleen weights; **(B)** percentages of CD19+CD5+ lymphocytes in spleen and **(C)** peripheral blood (PB); **(D)** Median Fluorescence Intensity (MFI) of PD-L1 and PD-L2 in spleen and **(E)** PB CLL cells. All graphs show medians with IQR. ns = non-significant.

#### 7.4.2 Lack of CLL control is reflected by persistence of typical CLL-induced aberrant T-cell phenotype

The ineffective CLL control by *in vivo* lenalidomide treatment was reflected by the persistence of typical CLL-induced T-cell phenotypic alterations. Both lenalidomide and vehicle treated mice exhibited comparable percentages of CD3+, CD3+CD4+ and CD3+CD8+ T cells in spleen (Figure 54 A) and PB (Figure 54 D), leading to non-significantly different CD4+/CD8+ ratios in spleen (Figure 54 B) and PB (Figure 54 E). Among CD3+CD8+ cells, naive cells were lost and shifted towards antigen-

experienced effector and EM cells. This was recapitulated in spleen (Figure 54 C) and PB (Figure 54 F, *note*: CM and EM cell subsets were not assessed in PB).

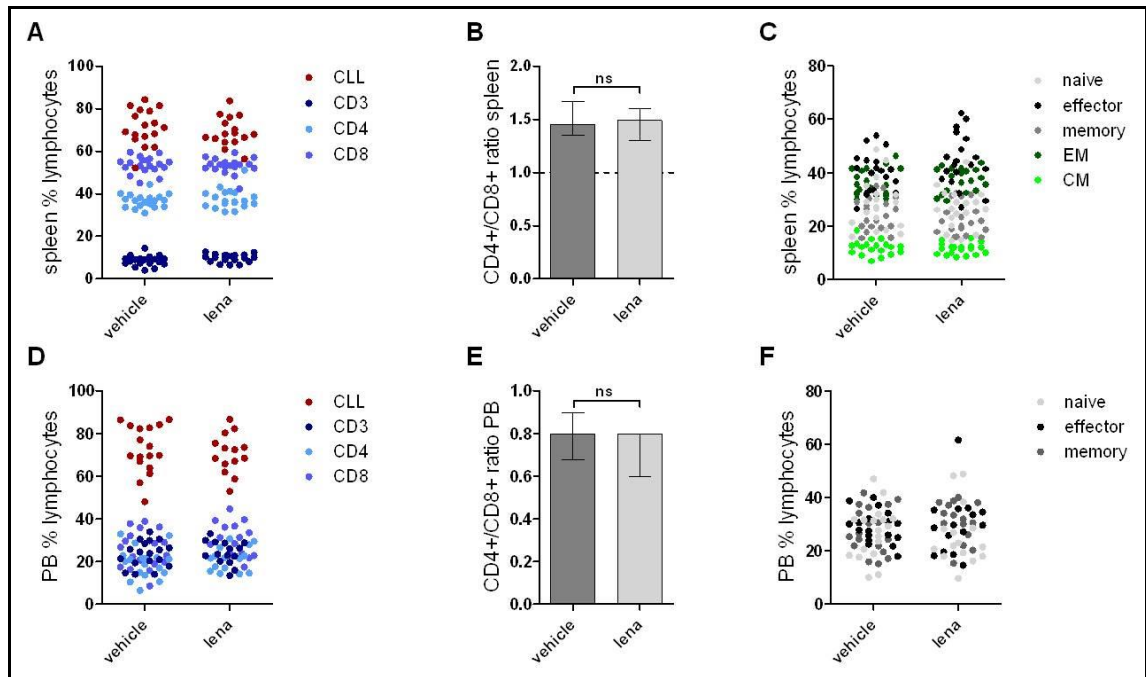


**Figure 54: T-cell phenotype in lenalidomide and vehicle control treated mice.** *In vivo* lenalidomide did not correct the typical CLL-induced aberrant T-cell phenotype. Percentages of CLL cells and CD3+, CD4+, and CD8+ T cells in (A) spleen and (D) peripheral blood (PB), CD4+/CD8+ ratios in (B) spleen and (E) PB, and percentages of CD3+CD8+ T-cell subsets in (C) spleen and (F) PB without and with lenalidomide treatment.

Table 20 summarizes the p-values of statistical comparisons of T-cell subsets between the experimental groups for all examined organs.

T-cell subsets	p-value	
	spleen	peripheral blood
%CD3	.0815	.7156
%CD3+CD4+	.7639	.4459
%CD3+CD8+	.4815	.0927
CD4+/CD8+ ratio	.7149	.1760
%Naïve CD3+CD8+	.5022	.4808
%Effector CD3+CD8+	.3353	.9856
%Memory CD3+CD8+	.1348	.2438
%EM CD3+CD8+	.5727	nd
%CM CD3+CD8+	.5016	nd

**Table 20: Summary of p-values of statistical comparisons of T-cell subsets between lenalidomide and vehicle treated mice for spleen and peripheral blood.** nd – not determined, EM – effector memory, CM – central memory

### 7.4.3 *In vivo* lenalidomide treatment prevents development of typical CLL-induced exhaustion-like T-cell phenotype

Despite the lack of CLL control and persistent T-cell subset alterations, *in vivo* lenalidomide treatment appeared to have an effect on the expression of previously described exhaustion-like markers on CD8+ T cells (Figure 55). Compared to vehicle control treated mice, the surface expression of PD-1 ( $p=.0368$ ), KLRG-1 ( $p=.0039$ ), LAG-3 ( $p=.0011$ ) and 2B4 ( $p=.0157$ ), but not CD160 ( $p=.0977$ ) was significantly reduced on antigen-experienced CD3+CD8+CD44+ T cells from lenalidomide treated mice. The reduction of PD-1 was also observed in CD3+CD8+ T cells in PB ( $p=.0097$ ).

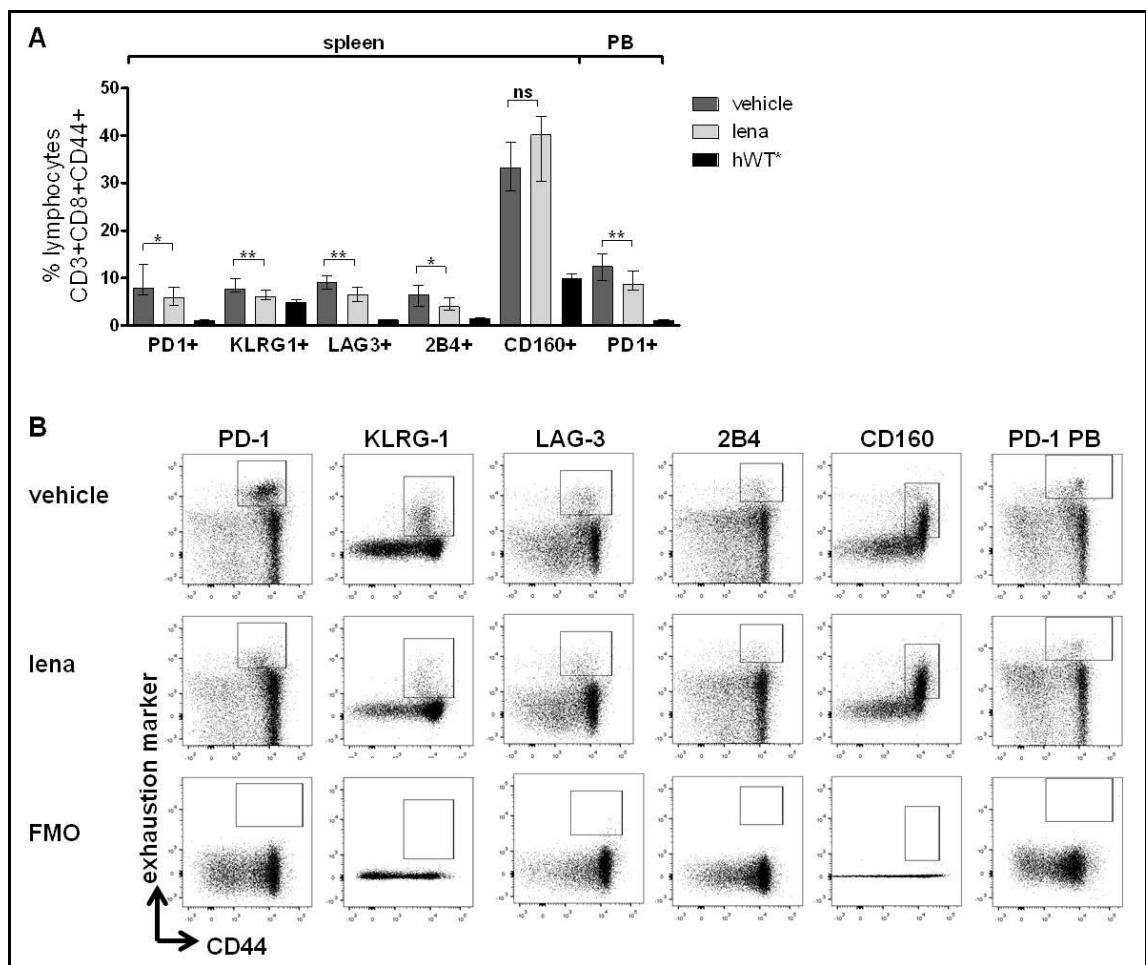


**Figure 55: Exhaustion surface markers in lenalidomide and vehicle control treated mice.** *In vivo* lenalidomide significantly reduced the surface expression of typical exhaustion markers on antigen experienced CD3+CD8+CD44+ cells. **(A)** Surface expression of PD-1, KLRG-1, LAG-3, 2B4 and CD160 in spleen, and PD1 in peripheral blood (PB) on CD3+CD8+CD44+ T cells from lenalidomide treated mice. Samples from healthy WT mice (hWT) analysed with the same panel in a different experiment were retrospectively included to visualize expression levels in normal cells. **(B)** Representative flow plots for all examined markers from vehicle and lenalidomide treated mice, and respective fluorescence-minus-one (FMO) controls. All graphs show median with IQR. hWT are marked with an asterisk to emphasize that they were not prospectively included into the experiment. ns = non-significant.

#### 7.4.4 *In vivo* lenalidomide treatment does not restore key T-cell effector functions

In line with the persistence of CLL-typical aberrant T-cell subsets, effector function was not improved by *in vivo* lenalidomide treatment. There were no differences in the percentages of CD3+CD4+ lymphocytes positive for intracellular IL-4 ( $p=.8492$ ), IFN- $\gamma$  ( $p=.6120$ ) or IL-2 ( $p=.5184$ ) between vehicle and lenalidomide treated mice (Figure 56 A). The retrospective comparison to healthy age-matched WT mice, which had been included into another study, revealed that both lenalidomide and vehicle treated mice maintained aberrantly increased intracellular IL-4 and IFN- $\gamma$ , as well as decreased IL-2 production.

Among CD3+CD8+ cells, the CD107a ratio was equally impaired in lenalidomide and vehicle treated mice ( $p=.7513$ , Figure 56 B), indicating a maintained cytotoxic defect compared to cells from healthy WT mice, while IFN- $\gamma$  ( $p=.3922$ , Figure 56 C) and ki67 ratios ( $p=.8362$ , Figure 56 D) continued to be equally increased. Similarly, *in vivo* lenalidomide treatment had no effect on reducing aberrant intracellular IL-4 production in CD3+CD8+ T cells ( $p=.6678$ , data not shown). The expression of cytokine receptors CD122 and CD127 on CD3+CD8+ cells was also not different between lenalidomide treated and control mice (CD44- cells CD122  $p=.347$ , CD127  $p=.0643$ ; CD44+ cells CD122  $p=.1633$ , CD127  $p=.1765$ , Figure 56 E).

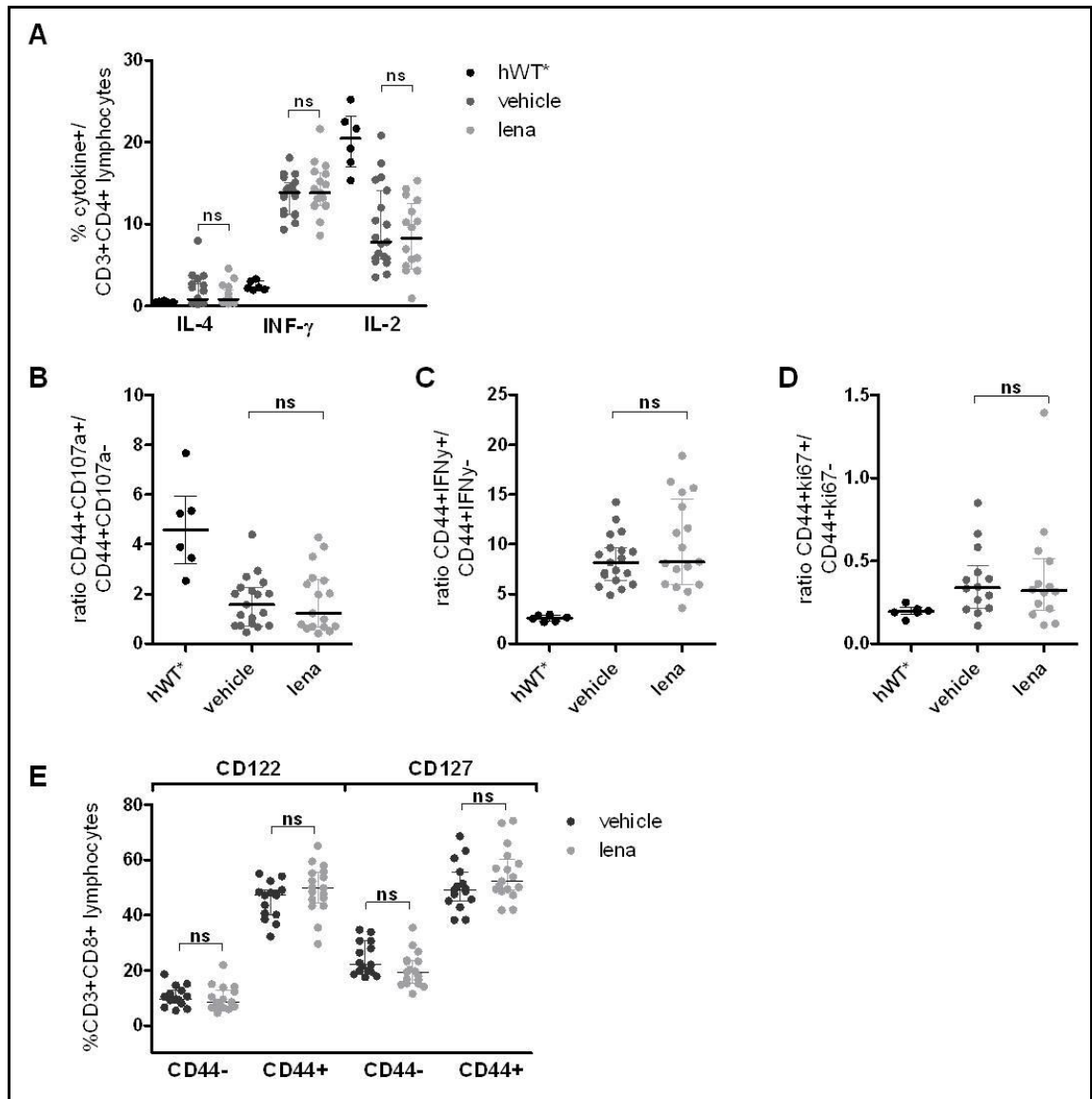


**Figure 56: T-cell effector function in lenalidomide and vehicle control treated mice.** *In vivo* lenalidomide had no effect on key effector functions of CD8+ and CD4+ T cells. **(A)** Percentage of CD3+CD4+ lymphocytes positive for intracellular IL-4, IFN- $\gamma$ , and IL-2 in vehicle and lenalidomide treated mice. **(B)** CD107a; **(C)** IFN- $\gamma$ ; and **(D)** ki67 ratios in CD44+CD3+CD8+ T cells from lenalidomide or vehicle treated mice. **(E)** Expression of cytokine receptors CD122 and CD127 on CD3+CD8+ cells from lenalidomide treated or control mice. All graphs show median with IQR. Healthy WT mice (hWT) are marked with an asterisk to emphasize that they were not prospectively included into the experiment. ns = non-significant.

To assess if differences in PD-1 surface expression would translate into effector function of PD-1<sup>high</sup> and PD-1<sup>low</sup> CD3+CD8+ T cells, we compared CD107a and INF- $\gamma$  ratios between lenalidomide and vehicle treated mice. Both in PD-1<sup>high</sup> and in PD-1<sup>low</sup> CD3+CD8+ T cells, there were no differences in CD107 ratio (PD-1<sup>high</sup> p=.5901, PD-1<sup>low</sup> p=.7274) or INF- $\gamma$  ratio (PD-1<sup>high</sup> p=.2743, PD-1<sup>low</sup> p=.3418), indicating that lenalidomide treatment did not overcome effector defects associated with PD-1 expression (Figure 57 A, B).

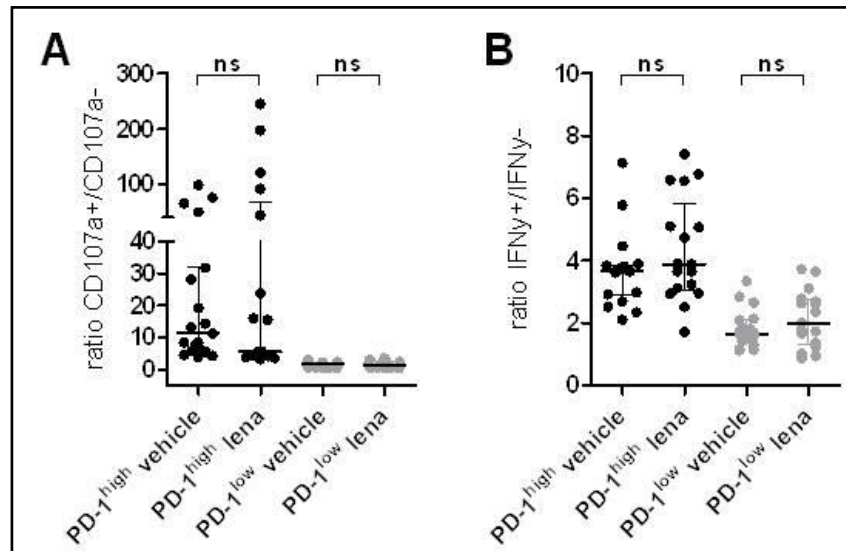


**Figure 57: T-cell effector function in PD-1<sup>high</sup> and PD-1<sup>low</sup> CD8 T cells from lenalidomide and vehicle control treated mice.** *In vivo* lenalidomide had no effect on effector functions in PD-1 cell subsets. **(A)** CD107 ratios and **(B)** INF- $\gamma$  ratios in PD-1<sup>high</sup> and PD-1<sup>low</sup> CD3+CD8+ T cells from lenalidomide or vehicle treated mice. All graphs show median with IQR. ns = non-significant.

#### 7.4.5 *In vivo* lenalidomide treatment improves immune synapse formation which can be further improved by additional *ex vivo* PD-L1 blockade

After we had confirmed previously published findings on the effect of *ex vivo* lenalidomide treatment on murine B and T cells, we compared the abilities of autologous B and T cells to form immunological synapses between lenalidomide and vehicle treated mice. The mean area of T-cell F-actin synapse ( $\mu\text{m}^2$ ) was significantly larger in lenalidomide treated mice compared to vehicle treated mice, but was still impaired compared to normal autologous cells (Figure 58 A; p values are summarized in Table 19). Interestingly, additional lenalidomide treatment *ex vivo* restored the synapse area regardless of previous *in vivo* treatment, even above levels of normal cells, indicating that the repair of cytoskeletal defects is a very rapid and prominent *ex vivo* mechanism of action of this drug.

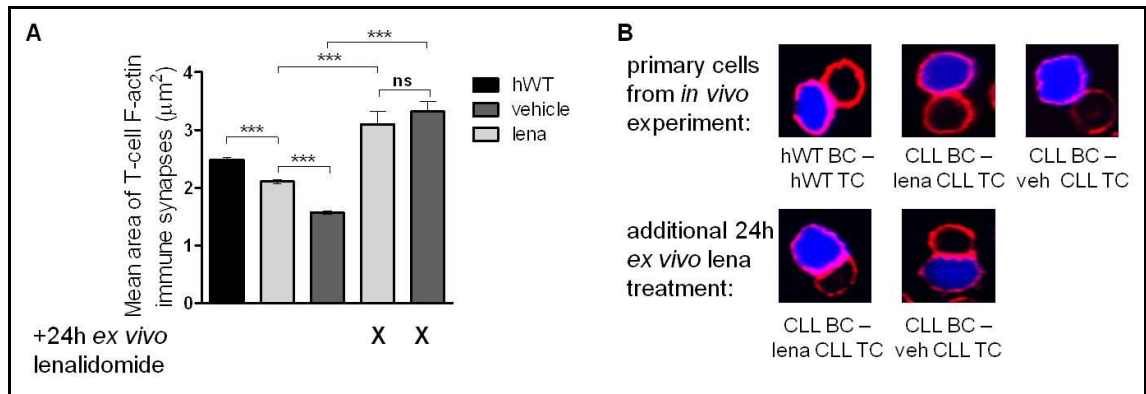


**Figure 58: Immune synapse formation between autologous T and CLL/B cells.** CLL and B cells and autologous T cells were purified from frozen splenocytes and used in immune synapse formation assays. **(A)** Effects of *in vivo* lenalidomide treatment on the ability of CLL T cells to form immunological synapses compared to cells from vehicle treated animals. Additional *ex vivo* lenalidomide treatment for 24hr restored the synapse area regardless of previous *in vivo* treatment. Graph shows mean with standard error of means (SEM). **(B)** Representative confocal images of synapses taken with a 63x objective between autologous WT B cells (hWT BC) and T cells (hWT TC), autologous CLL (CLL BC) and T cells (lena CLL TC) from *in vivo* lenalidomide treated mice, autologous CLL (CLL BC) and T cells from vehicle treated mice (veh CLL TC – all first row), and between autologous CLL (CLL BC) and lena CLL TC and veh CLL TC after additional *ex vivo* treatment with lenalidomide for 24h (second row). Blue = CMAC labelled B cells, red = Rhodamine Phalloidin.

To establish the role of aberrant PD-L1 expression on CLL cells in mediating immune synapse formation defects in this experiment, CLL cells were pre-treated with PD-L1 or isotype blocking antibodies before immune synapse formation assays. While isotype had no effect, with the area of T-cell F-actin immune synapse being comparable to the levels of *in vivo* treated mice (*in vivo* lenalidomide treated mice  $p=.4482$ , *in vivo* vehicle treated mice  $p=.5916$ ), additional *ex vivo* PD-L1 blockade significantly improved the area of immune synapses in both lenalidomide and vehicle treated mice (both  $p<.0001$ ) and even restored immune synapses to normal levels (Figure 59 A).

To quantify the effect of aberrant PD-1 expression on T cells on immune synapse formation, we next pre-treated T cells with PD-1 or isotype blocking antibodies before immune synapse formation assays. While *ex vivo* PD-1 blockage was unable to further increase the area of immune synapses in lenalidomide treated mice ( $p=.283$ ), leaving synapses in those mice significantly smaller than in healthy mice ( $p<.0001$ ), it significantly improved the area of immune synapses in vehicle treated mice ( $p<.0001$ ) to levels comparable to lenalidomide treated mice ( $p=.977$ , Figure 59 B).

The combined *ex vivo* blockade with both PD-1 and PD-L1 antibodies restored immune synapses in both lenalidomide and vehicle treated mice to normal levels, similar to PD-L1 blockade alone (Figure 59 C). Table 21 summarizes the p-values of statistical comparisons of areas of immune synapses between different conditions.

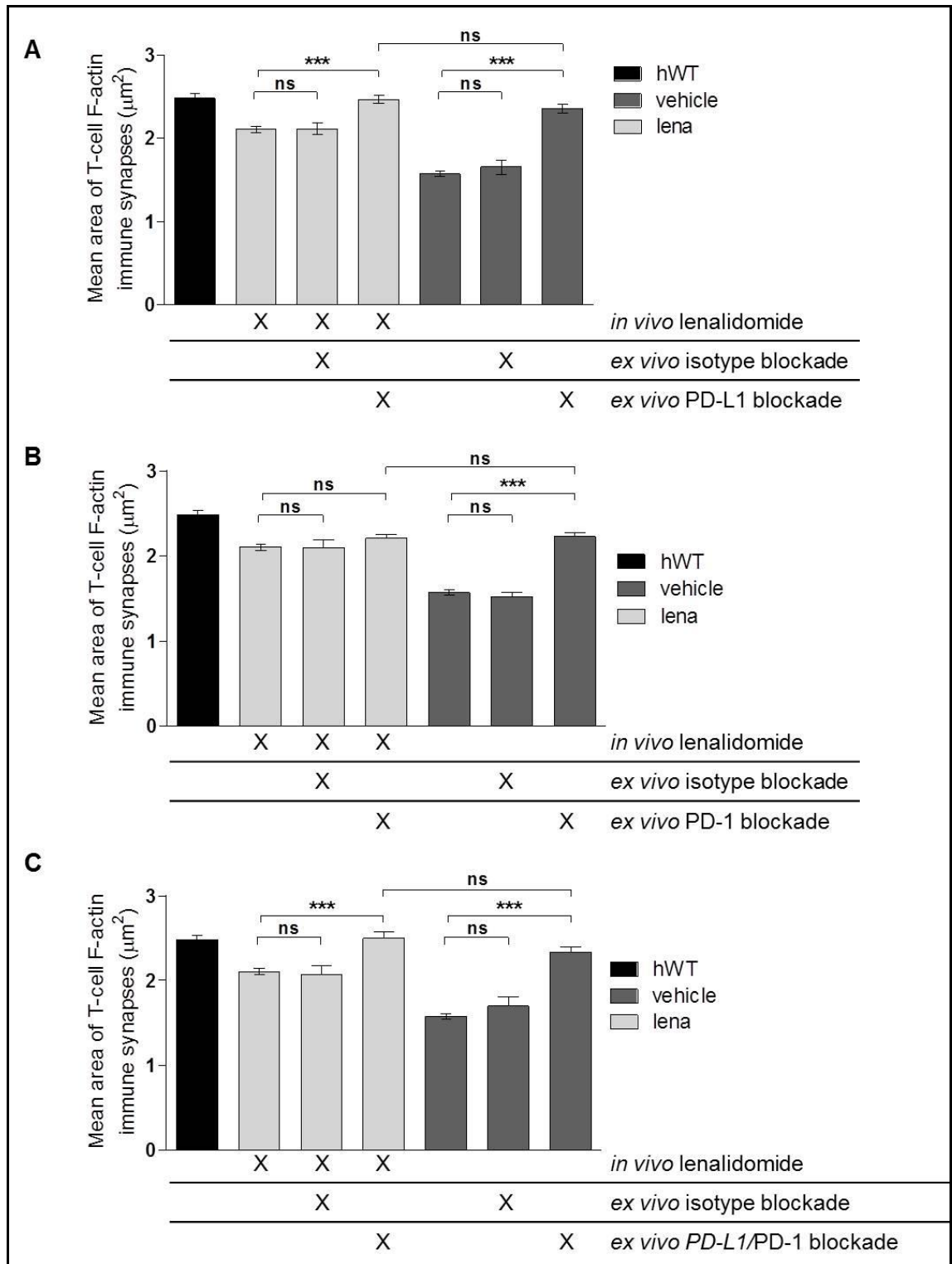


**Figure 59: Effect of ex vivo PD-L1 and PD-1 blockade on immune synapse formation between autologous T and CLL/B cells.** Before synapse assays cells were pre-treated 1 hour with blocking antibodies at previously determined optimal concentrations. **(A)** PD-L1 blockade on CLL cells significantly improved the area of immune synapses in both lenalidomide and vehicle treated mice and restored immune synapses to sizes comparable to healthy WT (hWT) mice. **(B)** PD-1 blockade on T cells significantly improved the area of immune synapses in vehicle treated mice only but did not restore immune synapses to sizes observed in hWT mice. **(C)** Combined PD-L1 blockade on CLL cells and PD-1 blockade on T cells significantly improved the area of immune synapses in both lenalidomide and vehicle treated mice and restored immune synapses to sizes comparable to healthy WT (hWT) mice.

	difference between lenalidomide and vehicle treatment	effect of <i>ex vivo</i> treatment on lenalidomide-treated mice	effect of <i>ex vivo</i> treatment on vehicle-treated mice	difference between healthy and lenalidomide-treated mice	difference between healthy and vehicle-treated mice
<b><i>in vivo</i> treatment only</b>	<b>&lt; .0001</b>	na	na	<b>&lt; .0001</b>	<b>&lt; .0001</b>
<b>24h <i>ex vivo</i> lenalidomide</b>	.2555	<b>&lt; .0001</b>	<b>&lt; .0001</b>	.532	<b>&lt; .0001</b>
<b><i>ex vivo</i> PD-L1 blockade</b>					
PDL-1 blocking AB	.1445	<b>&lt; .0001</b>	<b>&lt; .0001</b>	.9393	.1541
isotype blocking AB	<b>&lt; .0001</b>	.4428	.5916	<b>&lt; .0001</b>	<b>.0009</b>
<b><i>ex vivo</i> PD-1 blockade</b>					
PD-1 blocking AB	.977	.283	<b>&lt; .0001</b>	<b>&lt; .0001</b>	<b>.0001</b>
isotype blocking AB	<b>&lt; .0001</b>	.5476	.4959	<b>.0002</b>	<b>&lt; .0001</b>
<b><i>ex vivo</i> PD-L1/PD-1 blockade</b>					
PD-L1/PD-1 blocking AB	<b>.0176</b>	<b>&lt; .0001</b>	<b>&lt; .0001</b>	.586	.0571
isotype blocking AB	.0293	.9278	.1683	<b>.0037</b>	<b>&lt; .0001</b>

**Table 21: Summary of p-values of statistical comparisons between lenalidomide and vehicle treated mice and healthy WT mice with and without additional *ex vivo* lenalidomide treatment, *ex vivo* PD-L1/PD-1 antibody blockade, and isotype blocking antibodies (AB). na = not applicable. Statistically significant p-values are highlighted in bold.**

#### 7.4.6 Lenalidomide is detectable in tissues and plasma of treated mice

To confirm that the oral application of the selected dose of lenalidomide was sufficient to lead to detectable drug levels in plasma and CLL affected tissues, we treated WT mice with lenalidomide leftover from the stock administered to mice after AT, using identical doses and application routes. Mice received 5 days of oral application of 10mg/kg lenalidomide in 300µl PBS or vehicle (PBS) only, were sacrificed 24 hours after the last dose, and tissues were collected. Lenalidomide concentrations in plasma as well as intracellular concentrations in spleen and brain (non-lymphoid tissue control) were measured by high-resolution mass spectrometry by an investigator blinded to the treatment of the mice. Tissues from an untreated leukaemic TCL1 mouse sacrificed at the same time as the treated mice were included as negative controls, and freshly constituted lenalidomide was included as a positive control. Lenalidomide could be detected in all tissues and plasma from treated mice, but not in tissues from untreated mice. These findings indicate that the drug concentration and stock used in this experiment was sufficient to lead to detectable drug levels in all tissues (Figure 60).

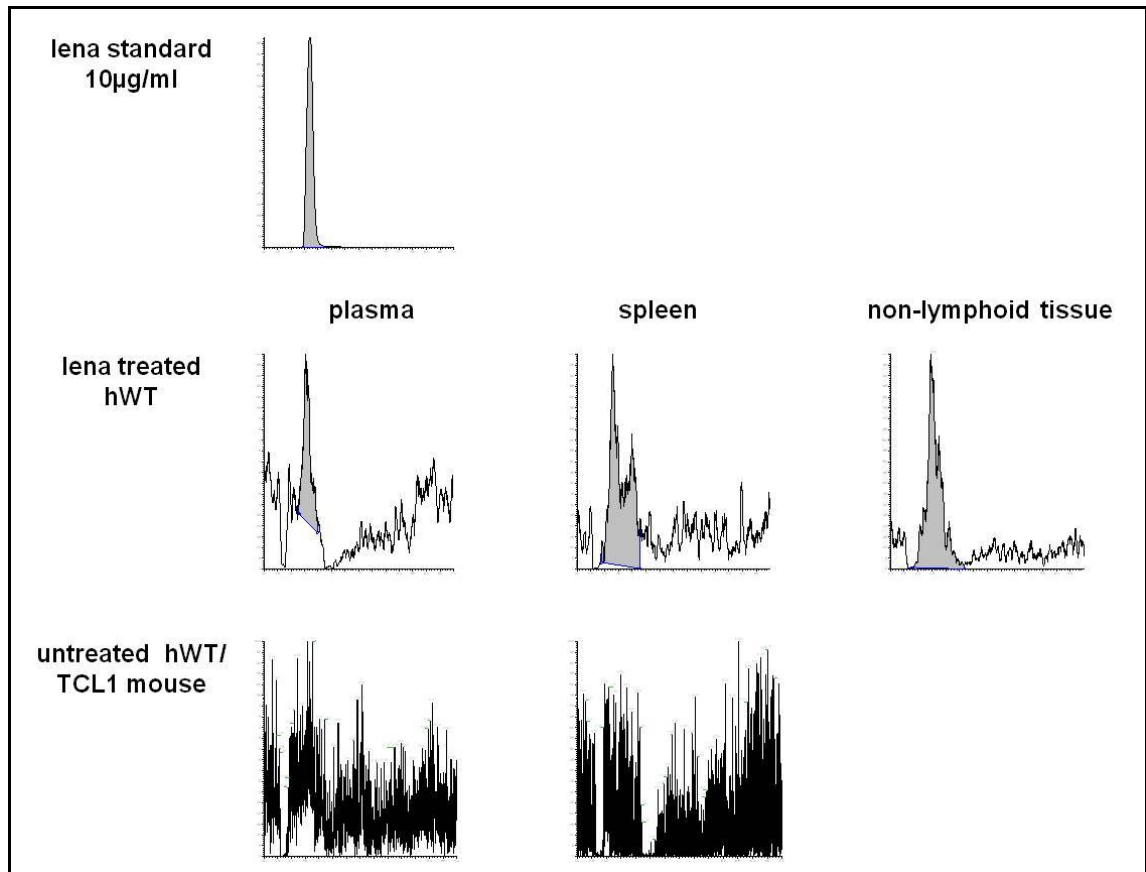


**Figure 60: Confirmation of drug concentrations by mass spectrometry.** High resolution mass spectrometry was used to confirm that treatment for 5 days with 10mg/kg body weight of the lenalidomide stock used in the *in vivo* study was sufficient to lead to detectable intracellular drug concentrations in lymphoid and non-lymphoid tissues, as well as in plasma. The drug could not be detected in tissues from healthy WT mice (hWT) or a leukaemic untreated TCL1 mouse.

### 7.5 Summary of effect of *in vivo* lenalidomide treatment on T-cell dysfunction and T-cell exhaustion in TCL1 mice

In summary, we found that *in vivo* lenalidomide did not result in effective CLL control if administered daily by oral gavage from three weeks after AT of  $4 \times 10^7$  splenocytes from leukaemic TCL1 mice. Median spleen weights and the percentages of CD19+CD5+ CLL lymphocytes in spleen and peripheral blood were comparable in lenalidomide and vehicle treated mice. In addition, treatment had no effect on the expression of PD-L1 and PD-L2 on CLL cells. The ineffective CLL control by *in vivo* lenalidomide treatment was reflected by the persistence of typical CLL-induced T-cell phenotypic alterations. Both lenalidomide and vehicle treated mice continued to exhibit a reduced CD4+/CD8+ ratio, and a loss of naive cells and shift towards antigen-experienced CD8+ effector and EM cells. This was recapitulated in spleen and PB. Accordingly, effector function was not improved by *in vivo* lenalidomide treatment. There were no differences in the percentages of CD3+CD4+ lymphocytes from spleen positive for intracellular IL-4, IFN-

$\gamma$  or IL-2 between vehicle and lenalidomide treated mice, and both groups continued to exhibit aberrantly increased intracellular IL-4 and IFN- $\gamma$ , and decreased IL-2 production by CD4<sup>+</sup> T cells compared to healthy WT mice. Among CD3<sup>+</sup>CD8<sup>+</sup> cells, the CD107a ratio was equally impaired in lenalidomide and vehicle treated mice, indicating a maintained cytotoxic defect compared to cells from healthy WT mice, while IFN- $\gamma$  and ki67 ratios continued to be equally increased, indicating persistent cytokine and proliferation defects. Similarly, *in vivo* lenalidomide treatment had no effect on reducing aberrant intracellular IL-4 production in CD3<sup>+</sup>CD8<sup>+</sup> T cells, or on the expression of cytokine receptors CD122 and CD127.

Despite the lack of CLL control and persistent T-cell subset alterations, *in vivo* lenalidomide treatment appeared to have an effect on the expression of previously described exhaustion-like markers, with the surface expression of PD-1, KLRG-1, LAG-3 and 2B4, but not CD160 being significantly reduced on antigen-experienced CD44<sup>+</sup>CD3<sup>+</sup>CD8<sup>+</sup>T cells from lenalidomide treated mice. The reduction of PD-1 was also observed in CD8<sup>+</sup> T cells in peripheral blood. This however did not translate into improved effector function of PD-1<sup>high</sup> and PD-1<sup>low</sup> CD3<sup>+</sup>CD8<sup>+</sup> T cells, with CD107a and IFN- $\gamma$  ratios in PD-1 subsets being comparable between lenalidomide and vehicle treated mice.

In contrast, *in vivo* lenalidomide treatment had a very strong effect on immune synapse formation between autologous T and CLL cells; the ability of CLL T cells to form immunological synapses was significantly improved compared to vehicle treatment, but synapses were not restored to normal levels. However, additional *ex vivo* lenalidomide treatment for 24 hours fully restored the synapse area regardless of previous *in vivo* treatment, underlining the strong *ex vivo* effect of the drug on cytoskeletal regulation. *Ex vivo* PD-L1 blockade on CLL cells significantly improved the area of immune synapses in both lenalidomide and vehicle treated mice and restored immune synapses to sizes comparable to healthy WT mice. Additional *ex vivo* PD-1 blockade on T cells significantly improved the area of immune synapses in vehicle treated mice only, but did not restore immune synapses to levels observed in WT mice. Combined *ex vivo* PD-L1 and PD-1 blockade significantly improved the area of immune synapses in both lenalidomide and vehicle treated mice and restored immune synapses to sizes comparable to healthy WT mice.

## 7.6 Discussion

The goal of this part of the project was to investigate if *in vivo* lenalidomide treatment can correct CLL-induced PD-L1/PD-L2/PD-1 mediated T-cell dysfunction and enhance anti-tumour T-cell responses in mice with CLL after adoptive transfer. Despite promising early clinical trial data from human CLL, indicating that lenalidomide treatment normalizes general T-cell subsets and restores T-cell cytokine production<sup>441-443</sup>, this was not observed in lenalidomide treated mice with CLL. In our experiments, *in vivo* lenalidomide did not result in the normalization of aberrant T-cell subsets and key T-cell effector functions such as CD4+ and CD8+ T-cell cytokine secretion, CD8+ T-cell proliferation, and CD107a degranulation.

The most apparent explanation for our findings is the lack of effective CLL control by lenalidomide treatment in mice, allowing CLL cells to continuously exert their full immunosuppressive effect on immune cells. Several *in vitro* studies have demonstrated that lenalidomide is not directly toxic to CLL cells<sup>448</sup>, in contrast to multiple myeloma and MDS cells where it has a direct cytotoxic effect<sup>451</sup>. Instead, *in vitro* lenalidomide has been shown to increase the expression of costimulatory molecules, and to induce p-ERK signalling in CLL cells<sup>448</sup>. Other studies have implicated a role for the PI3-kinase pathway in lenalidomide-induced CLL cell activation<sup>71</sup>. The combination of PI3-kinase activation and induction of NFκB and NFAT signalling resulted in enhanced transcription and stabilisation of CD154 (CD40L) mRNA, leading to expression of CD154 on CLL cells<sup>452</sup>. CD154 positive CLL cells upregulated BID, DR5 and p73, became sensitised to tumour necrosis factor-related apoptosis-inducing ligand (TRAIL)-mediated apoptosis, and promoted the co-stimulatory activation of normal B cells, resulting in the production of polyclonal antibodies. A recently published study demonstrated that lenalidomide inhibited CLL proliferation via induction of the CDK inhibitor p21 regardless of functional p53<sup>453</sup>.

In contrast, in our *in vivo* experiment the daily administration of lenalidomide (10mg/kg body weight by oral gavage) from three weeks after AT did not prevent CLL progression in treated mice, as evidenced by comparable spleen weights and CLL load in spleen and peripheral blood in lenalidomide and vehicle treated mice. This lack of CLL control could potentially be explained by insufficient drug application, such as inadequate doses or timing of treatment. According to current FDA guidelines<sup>454</sup>, human equivalent doses (HEDs) are calculated using the following formula:  $HED = \text{animal dose in mg/kg} \times (\text{animal weight in kg} / \text{human weight in kg})$ . Assuming a 60kg human, the mouse dose of 10mg/kg selected in our studies corresponds to 48.8mg in a patient. This is considerably higher than the doses currently used in CLL patients; the

initial clinical study used a starting dose of 25mg/day in the majority of patients, which is the standard target dose for the treatment of multiple myeloma<sup>82</sup>. As this was associated with unacceptable toxicities in CLL patients, especially tumour flare reactions<sup>78, 91</sup>, reduced starting doses as low as 2.5mg were used in further clinical trials, and escalated to a maximum of 25mg<sup>80, 83-86, 90, 455</sup>. Therefore, the dose selected in our study clearly is translationally relevant. In addition, pharmacokinetics and pharmacodynamics studies in mice have demonstrated a high systemic bioavailability of 75% via oral routes and a dose-dependent tissue distribution, which is consistent with the high oral bioavailability in humans<sup>449</sup>. Moreover, we performed repeated mass spectrometry studies to rule out that the lack of CLL control was attributed to degradation of the dissolved drug stock over the treatment period of 3 weeks, as several studies have indicated that IMiDs are unstable in aqueous solutions<sup>456, 457</sup>. Indeed, comparing the PBS diluted treatment compound after three weeks storage at minus 80°C to a freshly reconstituted standard demonstrated a two-fold lower ion count in the treatment compound, indicating some degradation of the drug over the duration of the treatment period. To assess if intracellular and plasma drug concentrations could still be achieved with this degraded compound, we treated additional healthy WT mice for 5 days with 10mg/kg per day, or PBS vehicle control, and sacrificed them 24 hours after the last dose. Despite the lower ion count and the 24 hour latency until the animals were sacrificed, lenalidomide could be detected in spleen, plasma, and non-lymphoid tissues. It is therefore unlikely that the lack of disease control, either by direct or indirect mechanisms, can be attributed to insufficient dosing or degradation of the drug.

It is possible that better CLL control could have been achieved by earlier initiation or longer duration of treatment. In our study, the median CLL load in peripheral blood, defined as the percentage of CD19+CD5+ lymphocytes, was 26% and therefore representative of an earlier stage of CLL. In addition, mice were well balanced between the intervention groups, ruling out that groups might have been enriched for mice with more or less advanced CLL. Initiation of treatment shortly after adoptive transfer might have resulted in the prevention of CLL-induced phenotypic and functional T-cell defects, as the drug would have been administered at a stage of low tumour volume. This hypothesis is supported by earlier findings from our groups, which demonstrated that T-cell defects are rapidly induced *ex vivo* by direct cell-cell contact with malignant cells after just 48 hours of co-culture<sup>77</sup>. However, this would have only insufficiently mirrored published studies using cells from human CLL patients, where a repair of T-

cell phenotype and subsets was observed in patients with manifest disease and indication for treatment<sup>80, 441-443</sup>.

More effective disease control in mice might have also been achieved by prolongation of the treatment period or by the combination with other substances. This hypothesis is supported by data from clinical trials in human CLL. Using lenalidomide monotherapy, ORR of up to 65% for first-line therapy and up to 47% for relapsed/refractory patients were reported, with most patients exhibiting PR<sup>82-85, 90</sup>. However, in these studies the median times to best response were 3 to 18 months in previously untreated and 6 to 9 months in relapsed/refractory patients, with late responses being observed in some patients after more than one year. Combination therapy with monoclonal antibodies such as rituximab or ofatumumab increased ORR to up to 95% in previously untreated and up to 66% in relapsed/refractory patients, while largely increasing the proportion of patients with complete responses<sup>86, 88</sup>. Other studies have demonstrated an association between longer duration of treatment and normalization of T-cell subsets: in 24 patients with untreated CLL enrolled in a Phase II clinical trial of lenalidomide, a relative increase of T cells, activated CD8+ T cells producing IFN- $\gamma$ , and TRegs compared to baseline levels before treatment were observed after 3 cycles of treatment. Only after 15 cycles of treatment, activated IL-2/IFN- $\gamma$ /TNF- $\alpha$  producing CD4+ T cells, TRegs and activated IFN- $\gamma$  producing CD8+ T cells normalized to the range of healthy subjects<sup>442</sup>. Another long-term analysis of 60 CLL patients treated with lenalidomide with a median follow up 4 years showed normalization in the percentages of CD4+ and CD8+ cells and T-cell numbers respectively in 48%, 71% and 99% of long-term responders<sup>87</sup>. Therefore, the treatment duration of 3 weeks in our *in vivo* study might have been too short, and/or the single-agent application too weak to allow for effective disease control and modulation of T-cell subsets. Longer treatments, however, are not feasible in the AT model, as mice usually succumb to their disease after a median of 7 weeks (range 3.7-20, see Figure 10 Chapter 4.4.3). Therefore, lenalidomide treatment of ageing TCL1 mice might be a more beneficial experimental model to study the long-term effect of lenalidomide on CLL and T cells in mice.

There is reasonable concern that the lack of activity of lenalidomide in mice might be caused by species differences of molecular targets, as the first generation IMiD thalidomide has been found to have teratogenic activity in humans, rabbits, chicks, and zebrafish, but not in mice and rats. The molecular target of both thalidomide and second generation IMiDs essential for their activity is cereblon (CRBN), a 442 amino-acid protein and a component of the E3 ubiquitin ligase complex that also contains DNA damage binding protein 1 (DDB1), regulator of cullins (Roc)-1 and Cullin 4

(Cul4)<sup>76, 458-460</sup>. CRBN was found to be largely evolutionarily conserved, and thalidomide was confirmed to bind to CRBN from humans, mice, chick, and zebrafish<sup>458</sup>. However, selected spots in the mouse ortholog of the human thalidomide binding domain (TBD) showed inter-species variability, raising the possibility that this might translate into functional differences. This was further explored by a recently published study describing the crystal structure of human and murine CRBN bound to DDB1 and different IMiDs<sup>461</sup>. The same conformations were found in both human and mouse TBDs, suggesting that any structural changes observed are not likely to be a consequence of species differences. In addition, CRBN orthologs were compared across different animal and plant kingdoms, and found to exhibit 100% sequence conservation in the essential tri-Trp binding pocket. However, due to two rodent polymorphisms proximal to the lenalidomide-binding site, mouse CRBN was unable to rescue the antiproliferative effects of pomalidomide in CRBN deficient DF15R cells and did not exhibit the pomalidomide-dependent degradation of transcription factors. These findings suggest that despite identical molecular targets and binding sites, it is likely that rodents do not respond to IMiD agents in the same way that humans do, which potentially explains the weak modulation of T-cell effector functions we observed.

Two key substrates of the CRBN CRL4 E3 ligase are Aiolos (IKZF3) and Ikaros (IKZF1), which are members of a family of zinc finger transcription factors. It has been demonstrated that binding of lenalidomide and pomalidomide to CRBN in myeloma cells or T cells increased IKZF1 and IKZF3 binding to CRBN, inducing their ubiquitination and subsequent proteasomal degradation<sup>76, 462, 463</sup>. The resulting IKZF depletion led to loss of viability of IKZF-dependent myeloma cells, while simultaneously enhancing the production of IL-2 in T cells. Aiolos has also been described as playing a major role in promoting TH17 differentiation by directly silencing IL-2 expression<sup>464</sup>. In CLL, it was demonstrated by knockdown experiments using *in vitro* CD40L/IL-4/IL10 stimulated CLL cells that p21-mediated reduction of CLL proliferation and degradation of IKZF 1 and 3 after lenalidomide treatment is dependent on CRBN<sup>453</sup>. Congruently, CLL cells from patients treated with lenalidomide within a clinical trial showed induced expression of p21 following lenalidomide therapy. Interestingly, Aiolos expression, but not Ikaros expression, was found to be upregulated in CLL cells<sup>465</sup>. This was later linked to being the result of NF- $\kappa$ B signalling, with enriched active chromatin marks of Aiolos having an effect on Bcl-2 family members<sup>466</sup>. The effect of lenalidomide on CRBN complex-mediated IKZF degradation in CLL T cells is not known. However, previous work from our group demonstrated that knockdown of CRBN significantly

reduced the ability of lenalidomide to modulate Rho GTPase-dependent T cell migration on CD54-coated slides<sup>81</sup>.

Interestingly, despite the lack of disease control and the persistence of CLL-typical phenotypic and functional defects, we observed a reduction of the surface expression of typical exhaustion markers, namely PD-1, on CD8+ cells from lenalidomide treated mice. This is in line with observations in CLL patients treated with lenalidomide. The percentage of CD4+ cells expressing either PD-1, 2B4 or CD57 alone, and all markers in combination, was observed to be significantly reduced after lenalidomide treatment, and was comparable to levels observed in healthy controls<sup>441</sup>. Among CD8+ cells, the percentages of all subsets, with the exception of CD8+PD-1+ and CD8+PD-1+2B4+ cells, were similarly reduced in lenalidomide treated patients. This study, however, did not contain any information on the treatment duration. Our group has demonstrated on a small number of lenalidomide treated patients that aberrant expression of PD-1 was significantly reduced after 3 weeks of treatment<sup>79</sup>. During the same time, however, lenalidomide treatment also resulted in the reduced expression of PD-L1 on CLL cells, increased T-cell conjugation and synapse function with autologous tumour cells, and increased antigen-induced cytolytic effector activity. While the reduction of PD-1 expression on mouse CD8+ T cells did not translate into improved effector function in PD-1 subsets, measured by cytokine secretion and CD107a degranulation, we were able to confirm previous findings on the restoration of the immune synapse; treatment of mice with lenalidomide significantly improved the ability of T cells to form immunological synapses with autologous CLL cells. However, it did not lead to a full restoration of synapses to levels observed in autologous cells from healthy mice. Interestingly, this was achieved by additional *ex vivo* lenalidomide treatment for 24 hours, both in cells from mice treated with lenalidomide and vehicle. These findings underline the strong direct *ex vivo* effect of the drug on cytoskeletal regulation and demonstrate that cells from these animals are capable of synapse formation. Furthermore, these results support the hypothesis that our *in vivo* treatment did not attain sufficiently high lenalidomide levels for an adequate period and/or that the effects are readily reversible *in vivo*, rather than that lenalidomide solely fails to bind murine cereblon.

The addition of lenalidomide to co-cultures between human CLL and normal allogeneic T cells, as well as treatment of autologous CLL/T-cell co-cultures, was able to overcome the immunosuppressive effect of PD-L1 inhibitory signalling, as its effect on restoring the immune synapse and increasing CD8+ T cell cytolytic potential was comparable to the repair achieved by antibody blockade of PD-L1<sup>79</sup>. To assess the role

of PD-L1/PD-1 in inhibiting effective immune synapse formation in the context of *in vivo* lenalidomide treatment of mice, we added *ex vivo* blocking antibodies against PD-L1/PD-1 before immune synapse assays. We found that additional *ex vivo* PD-L1 blockade on CLL cells significantly improved the area of immune synapses in both lenalidomide and vehicle treated mice and restored immune synapses to sizes comparable to healthy WT mice. Interestingly, additional *ex vivo* PD-1 blockade on T cells only improved the area of immune synapses in vehicle treated mice and restored it to levels observed in lenalidomide treated mice. Combined *ex vivo* PD-L1 and PD-1 blockade significantly improved the area of immune synapses in both lenalidomide and vehicle treated mice and restored immune synapses to sizes comparable to healthy WT mice. These findings highlight the importance of aberrant PD-L1 expression on CLL cells to mediate immune synapse formation defects of T cells. As immune synapse formation is an essential step to activate T cells upon the encounter of MHC-presented antigen, it can be hypothesized that the repair of immune synapses by PD-L1 blockade leads to a restoration of T-cell effector functions and overcomes the functional defects associated with aberrant T-cell phenotypes.

In sum, our *in vivo* experiments using single agent and short term lenalidomide treatment have confirmed that the repair of cytoskeleton defects is a prominent mechanism of action that is recapitulated in mice with CLL, even though different therapeutic responses exist in mice with CLL *versus* human CLL patients. In addition, they have highlighted the role of aberrant PD-L1 expression by CLL cells in impairing T-cell function, and provided a strong rationale that this could be overcome using *in vivo* PD-L1 blockade. Therefore, the potential of *in vivo* PD-L1 blockage to correct CLL-induced T-cell dysfunction and enhance anti-tumour T-cell responses in mice with CLL will be explored in the next chapter.

## 8 Potential of *in vivo* PD-L1 blockade to restore T-cell dysfunction

### 8.1 Specific introduction

In physiological settings, co-receptors essential for the activation of immune effector cells (so-called immune checkpoints) tightly regulate the amplitudes and qualities of T-cell responses and thereby maintain self-tolerance, prevent autoimmunity, and protect healthy tissues from being damaged by limiting normal immune responses<sup>332</sup>. Many tumours utilize these checkpoints to their advantage to escape anti-tumour immune responses<sup>338</sup>. PD-L1 and PD-1 have emerged as one of the most prominent immune checkpoint ligand/receptor axes that contribute to maintaining an immunosuppressive tumour microenvironment, and several studies have demonstrated that aberrant PD-L1 expression by tumour cells has an inhibitory effect on T cells, both in haematological malignancies (see Chapter 1.3.2) and in solid cancers<sup>312-314</sup>. Encouraging results from early clinical trials using PD-1/PD-L1 antibodies showed significant response rates, even in heavily pre-treated patients with solid tumours, thus validating PD-L1/PD-1 as key targets for immunotherapy approaches aiming to shift the balance back from a pro-tumour to an anti-tumour microenvironment (see Chapter 1.4.2).

One of the earliest clinical Phase I dose-escalation studies in patients with haematological malignancies using the PD-1 antibody pidilizumab showed a favourable safety profile and evidence of clinical activity in 6 of 18 patients, with no maximum tolerated dose defined<sup>362</sup>. In this cohort of patients, an increase of absolute numbers of peripheral blood CD4<sup>+</sup> T cells was observed that was maintained up to 21 days after treatment. More recently, pidilizumab was administered to patients with DLBCL 30–60 days after autologous haematopoietic stem-cell transplantation (auto-HSCT) at a dosing schedule of 1.5 mg/kg once every 6 weeks for three cycles<sup>359</sup>. The 16-month PFS from first treatment was 72%, and overall survival was 85%. Among 35 patients with measurable disease after auto-HSCT, the ORR after pidilizumab treatment was 51%. Pidilizumab was well tolerated with the most common adverse events noted to be grade one to four neutropenia, fatigue, and diarrhoea. Notably, pidilizumab administration was associated with several changes in the absolute number of circulating lymphocyte subsets, and led to a sustained increase of PD-L1+CD25+CD4+ T cells, CD4+ CM T cells, CD8+ CM T cells, and PD-L1+ monocytes. In addition, the authors found an increase in CD127+ CM CD4+ and CD8+ T cells. In a recently published study, pidilizumab was combined with the anti-CD20 antibody rituximab in patients with relapsed follicular lymphoma<sup>360</sup>. This Phase II trial demonstrated that this combination was well-tolerated and produced overall and CRR of 66% and 52%, respectively, with tumour regression in 86% of patients. Within this trial, a number of

correlative studies were performed to assess the immunological effects of pidilizumab. The authors found that expression of PD-L1 (but not PD-1 or PD-L2) was significantly higher in peripheral blood CD4+, CD8+, and CD14+ cells of responders than non-responders, but was not associated with PFS. The comparison of PB samples taken 14 days after the first pidilizumab infusion with baseline samples demonstrated an increase in absolute lymphocyte count, CD3+ T cells and CD4+ T cells, but not in CD8+ T cells. Naive, EM, and CM CD4+ T cells were significantly increased after treatment. Among CD8+ T cells, terminally differentiated cells were decreased, but other subsets were not-significantly different. The comparison of gene expression profile data of paired core-needle biopsies demonstrated that the change in expression after treatment was correlated with outcome and tumour shrinkage, with increased expression of T-cell activation signatures after pidilizumab being associated with longer PFS. This however was not confirmed by flow cytometry or immunohistochemistry, and paired tissue and peripheral blood samples at diagnosis (*i.e.* from the same patient) could not be correlated with each other. In addition, it is possible that the co-administered anti-CD20 antibody rituximab might have had a confounding effect on the amplitude and quality of T-cell responses; rituximab induces B-cell depletion and modulates immune-mediated cell killing via various degrees of complement-dependent cytotoxicity (CDC), ADCC and phagocytosis<sup>467</sup>, which might have had an effect on the T-cell signatures and phenotypes observed in this study. Ongoing Phase II studies are evaluating the safety and clinical efficacy of pidilizumab in patients with AML and multiple myeloma in combination with cell-based vaccines<sup>468, 469</sup>, and in patients with multiple myeloma in combination with lenalidomide<sup>470</sup>. Another PD-1 antibody currently under clinical evaluation in patients with MDS, multiple myeloma, HL, mediastinal large B cell lymphoma, and NHL is MK-3475 (pembrolizumab)<sup>471</sup>.

Clinical data on anti-PD-L1 antibodies in patients with leukaemias and lymphomas is notably absent. The anti-PD-L1 antibody MPDL3280A is currently being tested in a Phase I dose escalation study in patients with solid and haematological malignancies<sup>472</sup>, but another study evaluating the anti-PD-L1 antibody BMS-936559 in patients with relapsed or refractory haematological malignancies was withdrawn prior to any patient enrolment<sup>473</sup>. Similarly, studies of the immunological effect of *in vivo* PD-L1 blockade are rare, and information is currently limited to preclinical models. Data from murine solid cancer models indicate that *in vivo* PD-L1 blockade in combination with IL-15 administration, CTLA-4 blockade or IDO pathway blockade restores CD8+ T cell IL-2 production and proliferation within the tumour microenvironment<sup>474</sup>, increases the numbers and lytic activity of tumour antigen-specific CD8+ T cells, augments

antigen-specific IFN- $\gamma$  release, and inhibits suppressive functions of regulatory T cells<sup>475, 476</sup>. However, it is becoming clear that PD-L1 is not only aberrantly expressed by tumour cells, but also by cells in the tumour microenvironment such as MDSCs, tumour-associated macrophages, and dendritic cells, which also has an effect on modulating T-cell function<sup>199, 298, 477, 478</sup>.

Despite the increasing pre-clinical evidence pointing towards the importance of PD-1/PD-L1 inhibitory signalling in CLL, neither PD-L1 nor PD-1 blockade has been clinically explored minimally in this disease. The study by Berger *et al.*<sup>362</sup> included only 3 patients with CLL/SLL, of which two showed stable disease with pidilizumab treatment. Future clinical trials on PD-1/PD-L1 blockade in CLL, however, could be supported by preclinical data from the TCL1 model. In-depth work performed in this project confirms that TCL1 mice are a valuable preclinical tool to mirror PD-L1/PD-1 mediated T-cell defects. In addition, our results highlight the significance of the PD-1/PD-L1 axis in suppressing specific T-cell effector functions in CLL, and identify T-cell subsets that are suitable candidates to be promoted to fully functional effector cells by blocking PD-1/PD-L1 inhibitory signalling, as demonstrated in Chapter 7.3.7. TCL1 mice are therefore an ideal model to study if *in vivo* PD-1/PD-L1 blockade has the potential to add to effective disease control by restoring anti-tumour immune responses. Due to the similarity of our model to human CLL, output of these experiments is likely to provide a strong rationale for further clinical assessment of PD-L1/PD-1 immune checkpoint blockade.

## 8.2 Goals and objectives

Based on the data we generated thus far, my next goal was to investigate if *in vivo* PD-L1 blockage corrects CLL-induced T-cell dysfunction and enhances anti-tumour T-cell responses in mice with CLL. Specifically, I sought to address the following questions:

- Does early *in vivo* PD-L1 blockade have the potential to effectively control disease development after adoptive transfer (AT) of murine CLL?
- Can early *in vivo* PD-L1 blockade prevent the development of the previously described aberrant T-cell phenotype?
- Can early *in vivo* anti-PD-L1 treatment restore key T-cell effector functions?
- Can early *in vivo* anti-PD-L1 treatment overcome functional T-cell defects relating to aberrant PD-1 expression?

### 8.3 Specific methods and materials

#### 8.3.1 Mice and *in vivo* treatment

Three month old female B6 WT mice were purchased from Charles River, UK, randomized to “treatment” (n=15), “isotype” (n=10) or “no intervention” (n=6) groups, ear-tagged, and kept in cages containing 5 mice each (6 for “no intervention”) for one week without any further procedures. Sample size was calculated based on the assumption that at least 9 mice per group would be needed to detect a 1.25 standard deviation difference in PD-1 means between treated and untreated mice in one-sided testing at a significance level  $\alpha=0.05$  with at least 80% power. Mice randomized to “treatment” and “isotype” were then injected i.v. with  $4 \times 10^7$  syngeneic CLL cells in a single dose from the same pool of aged TCL1 mice, followed by i.p. injection of 10mg/kg anti-murine-PD-L1 *in vivo* monoclonal antibody (aPD-L1, clone 10F.9G2, rat IgG2b) or *in vivo* isotype monoclonal antibody (clone LTF-2, rat IgG2bk, both BioXcell, USA) on day +1. Administrations of aPD-L1 or isotype antibodies were repeated every 3 days, and mice were sacrificed 31 days later after having received a total of 11 doses, along with the “no intervention” mice, under protocol 19b2 of PIL 70/7531. Spleens, PB, LN and BM were harvested and processed as described before.

#### 8.3.2 Multicolour flow cytometry for cell surface markers

T-cell subsets were characterized based on the surface expression of CD3, CD4, CD8, CD62L, CD44 and CCR7. Exhaustion markers included PD-1, KLRG-1, 2B4, CD160 and LAG-3. CLL was assessed by concurrent CD19 and CD5 expression, and PD-L1 and PD-L2 were included into the CLL panel. Antigens, fluorochromes, clones, concentrations and suppliers are described in the previous chapters. For PD-L1, clone MIH5 was used, as the PD-L1 monoclonal antibody administered *in vivo* was clone 10F.9G2. As demonstrated in the saturation experiments in the previous chapter, pre-incubation with 10F.9G2 reduced consecutive binding of fluorochrome-labelled 10F.9G2. To determine if 10F.9G2 would also block binding of fluorochrome-labelled MIH5, we incubated fresh MNC from the spleen of a leukaemic TCL1 mouse for 1 hour with the previously determined optimal dose of 10mg/ml LEAF™ purified 10F.9G2 antibody, or LEAF™ isotype blocking antibody rat IgG2bk (both Biolegend, UK). Cells were then washed and stained with fluorochrome-conjugated PD-L1 antibodies [clones 10F.9G2 (PECy7) or MIH5 (PerCPeFluor710)] for flow cytometry. Fluorochrome-conjugated isotype controls were also included. This experiment demonstrated that

pre-incubation with 10F.9G2 reduced the MFI of both PEcy7 labelled 10F.9G2 and PerCPeFluor710 labelled MIH5, indicating that the *in vivo* antibody 10F.9G2 partially blocks the binding of MIH5, thereby influencing the correct assessment of PD-L1 expression (Figure 61).

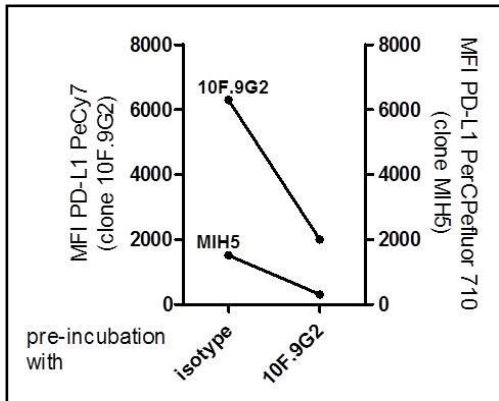


**Figure 61: *In vitro* blockade with PD-L1 clone 10F.9G2 affects binding of PD-L1 clone MIH5:** Fresh mouse spleen MNC were pre-incubated for 1h with 10mg/ml purified anti-PD-L1 antibody clone 10G.9G2 or isotype blocking antibody, and stained with PerCPeFluor710 labelled PD-L1 antibody against clone MIH5. Cells stained with PeCy7 10F.9G2 were used as positive control.

Table 22 contains an overview of the flow panel combinations used in this experiment. Experiments were performed on fresh samples, and FMO controls for CD44, CCR7, exhaustion markers, PD-L1 and PD-L2 were included into all experiments. Cells were prepared for flow cytometry as described before. The gating strategies have been described in Chapters 5 and 6.

1. spleen					
tube 1		tube 2		tube 3	
T-cell subsets/exhaustion		T-cell exhaustion		B cells	
CD4	PerCPCy5.5	CD8	BV605	CD5	APC
CD8	BV605	CD3	APCCy7	CD19	FITC
CD3	APCCy7	CD44	AF700	CD45	APCCy7
CD62L	FITC	2B4	APC	PDL1	PE
CD44	AF700	LAG3	PerCPeFl710	PDL2	PerCPeFl710
CCR7	PeCy7	CD160	PE	viability dye	DAPI
KLRG1	PE	viability dye	DAPI		
PD1	APC				
viability dye	DAPI				
2. peripheral blood					
tube 1		tube 2			
T-cell subsets/exhaustion		B cells			
CD4	PerCPCy5.5	CD5	APC	CD19	FITC
CD8	BV605	CD45	APCCy7	PDL1	PE
CD3	APCCy7	PDL2	PerCPeFl710	viability dye	DAPI
CD62L	FITC				
CD44	AF700				
PD1	APC				
viability dye	DAPI				
3. bone marrow					
same as peripheral blood		same as peripheral blood			
4. lymph nodes					
same as peripheral blood		same as peripheral blood			

**Table 22: Overview of flow panel used in this experiment to phenotype T-cell subsets, exhaustion markers, CLL and inhibitory ligands in mouse tissues.**

### 8.3.3 Multicolour flow cytometry for intracellular cytokines and effector function

Effector function and intracellular cytokines were determined as described in Chapter 5 and included CD107a degranulation, intracellular GrB, IL-2, IL-4, and IFN- $\gamma$ , intranuclear ki67, and *in vivo* EdU incorporation. Differences in T-cell function between experimental groups were compared by calculating ratios between CD44+ cells positive for CD107a/IFN- $\gamma$ /ki67, and CD44+ cells negative for these markers, to describe the ratio between effector cells within CD44+ cells compared to non-effector (*i.e.* negative) cells. Differences in ratios were interpreted as an increase of cells able to exert effector functions (increase of ratio), or decrease of cells able to exert effector functions (decrease of ratio), respectively. Similar comparisons were made between ratios within PD-1<sup>high</sup> and PD-1<sup>low</sup> subsets.

### 8.3.4 Immune synapse formation assays

Frozen splenocytes were debulked of CLL and B cells by manual magnetic separation using murine CD19 microbeads, and the column effluent representing the CD19-fraction was further purified by negative selection using murine T-cell isolation kits as described in Chapter 3.3. These T cells were used in synapse formation assays with CMAC-labelled, sAg-pulsed healthy syngeneic B cells as antigen-presenting cells at a 1:1 ratio. Synapse assays, confocal microscopy, and image analysis were conducted as described in Chapter 3.5.

## 8.4 Results

### 8.4.1 *In vivo* anti-PD-L1 treatment effectively controls CLL and prevents PD-L2 expression on normal B cells

Following AT of  $4 \times 10^7$  CLL cells from leukaemic TCL1 donors, mice treated with 11 doses of murine aPD-L1 showed effective control of CLL relative to mice receiving isotype antibody. Spleen sizes in aPD-L1 treated mice were remarkably reduced (Figure 62 A) and spleen weights were significantly lower compared to the isotype control group (median 0.2g vs. 0.9g,  $p < .0001$ , Figure 62 B). Dark focal pigmentations were apparent in spleens from aPD-L1 treated mice, although these are normal in young B6 mice and are caused by accumulation of melanin<sup>479</sup>. Compared to isotype, aPD-L1 treated mice had a significantly lower relative frequency of CD19+CD5+ CLL lymphocytes in spleens (1.6% vs. 71.7%,  $p < .0001$ ), PB (10.5% vs. 63.5%,  $p = .0019$ ) and BM (.3% vs. 2.7%,  $p < .0001$ ) as determined by flow cytometry of single-cell suspensions (Figure 62 C). In LN, no differences were detected. However, our work previously demonstrated that CLL involvement of LN is not well reflected in the AT model. Together, these results demonstrate very effective tumour control. Interestingly, mice treated with aPD-L1 appeared to have higher CLL loads in blood than in spleen, indicating that PD-L1 might have an effect on homing or migration into secondary lymphoid organs (Figure 62 D).

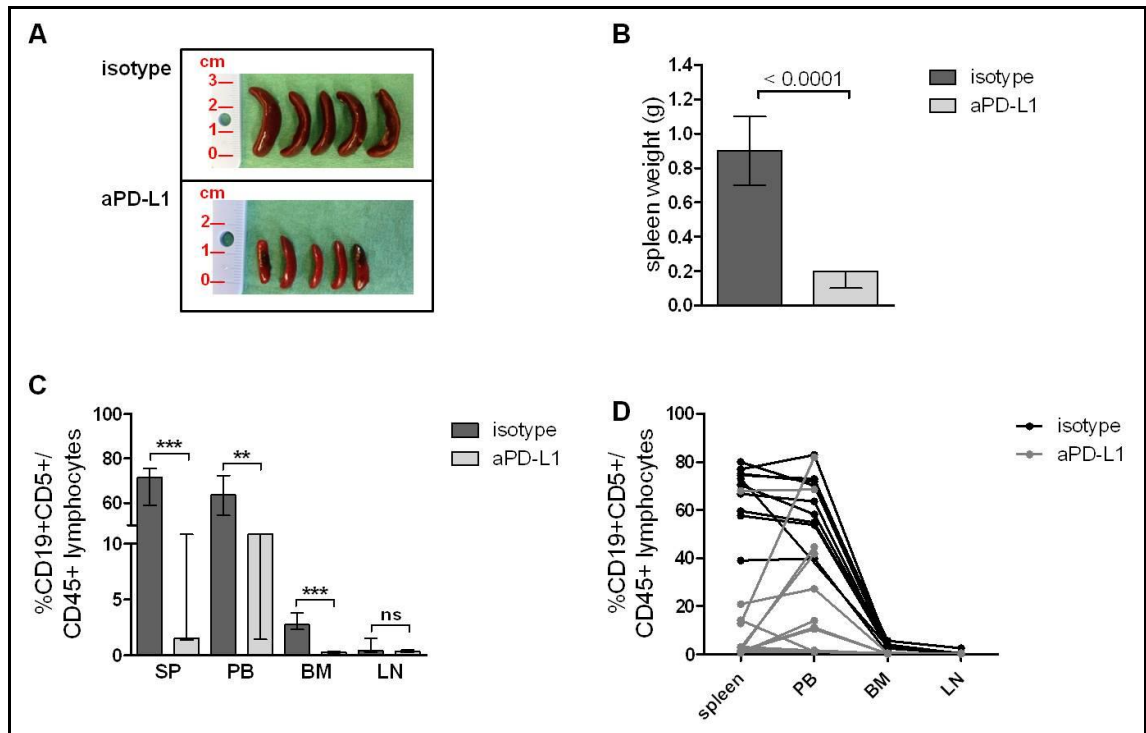


**Figure 62: Effect of *in vivo* aPD-L1 treatment on disease development.** Three month old B6 WT mice transplanted with  $4 \times 10^7$  splenocytes from leukaemic TCL1 mice were randomized to treatment with 10 mg/kg anti-murine-PD-L1 (aPD-L1, n=15) or isotype antibody (n=10), administered i.p. every 3 days starting one day after adoptive transfer, and sacrificed 31 days later. **(A)** Differences in spleen sizes between isotype and aPD-L1 treated mice. **(B)** Spleen weights in aPD-L1 treated and isotype treated mice. **(C)** Relative frequency of CD19+CD5+ CLL lymphocytes in all examined organs. **(D)** CLL loads in different organs in individual mice. All graphs shows median with interquartile range (IQR); (E) shows medians only.

As expected, the specific MFI of PD-L1 was significantly reduced in all examined organs in aPD-L1 treated mice compared to WT mice, reflecting the partial blockade of the binding site of the fluorochrome-labelled PD-L1 antibody used for flow cytometry (clone MIH5) by the *in vivo* PD-L1 antibody (clone 10F.9G2, Figure 63 A). Confirming previous findings, isotype treated mice showed significantly upregulated PD-L1 on CLL cells in all examined organs, as compared to normal B cells from WT mice. As the CLL population was notably absent in aPD-L1 treated mice compared to isotype treated mice (1.6% vs. 71.7% CLL cells), we compared the expression of PD-L2 on normal B cells in aPD-L1 treated mice to expression on CLL cells in isotype treated mice. Although we demonstrated in Chapter 6 that aberrant PD-L2 expression is exclusive to CLL cells, we hypothesized that B cells in aPD-L1 treated mice might still show upregulated PD-L2 as a result of the AT procedure or the immunological challenge by tumour. Interestingly, PD-L2 expression was comparable in aPD-L1 treated and healthy WT mice in all examined organs, and was significantly lower than in isotype treated mice (Figure 63 B).

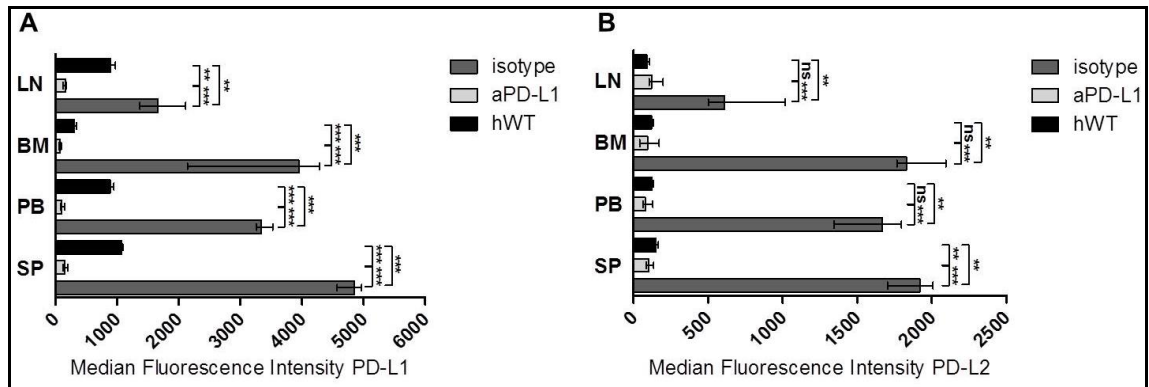


**Figure 63: Effect of *in vivo* aPD-L1 treatment on PD-L1 and PD-L2 expression.** PD-L1 and PD-L2 were gated on CD19+CD5+ CLL cells in isotype treated mice, and on CD19+ B cells in aPD-L1 treated and healthy WT mice (hWT), as treatment had resulted in the significant reduction of the CLL population. **(A)** aPD-L1 treatment partially blocked binding of fluorochrome labelled PD-L1 on a different clone (MIH5), while PD-L1 expression was significantly increased on CLL cells from isotype treated mice compared to B cells from healthy mice. **(B)** PD-L2 expression was comparable in normal B cells from aPD-L1 treated and WT mice, and was significantly increased in isotype treated mice. All graphs show median with IQR. ns = non-significant, \*p<.05, \*\*p<.001, \*\*\*p<.0001.

Table 23 summarizes the p-values of statistical comparisons of specific MFIs for PD-L1 and PD-L2 between the experimental groups for all organs examined.

		aPD-L1 vs. isotype	aPD-L1 vs. hWT	isotype vs. hWT
<b>MFI PD-L1</b>	<i>spleen</i>	<.0001	.0005	.0002
	<i>peripheral blood</i>	<.0001	.0005	.0004
	<i>bone marrow</i>	<.0001	.0005	.0002
	<i>lymph node</i>	.0003	.0095	.0043
<b>MFI PD-L2</b>	<i>spleen</i>	<.0001	.0091	.0002
	<i>peripheral blood</i>	<.0001	.1990	.0004
	<i>bone marrow</i>	<.0001	.9578	.0002
	<i>lymph node</i>	.0009	.1143	.0043

**Table 23: Summary of p-values of statistical comparisons of specific MFIs for PD-L1 and PD-L2 between aPD-L1 and isotype treated mice and healthy WT mice (hWT).** Significant p-values are highlighted in bold.

### 8.4.2 *In vivo* anti-PD-L1 treatment prevents development of the typical CLL-induced aberrant T-cell phenotype

The effective CLL control by *in vivo* aPD-L1 was reflected by significant changes in the T-cell phenotype. Compared to isotype treated mice, the relative frequencies of CD3+, CD3+CD4+ and CD3+CD8+ T cells in all examined organs were comparable in aPD-L1 treated mice and in healthy WT mice (data for percentages of CD3+, CD4+ and CD8+ cells not shown). This was reflected in a normalization of the CD4+/CD8+ ratio in spleen (Figure 64 A), PB (Figure 64 B) and BM (Figure 64 C), indicating that aPD-L1 treatment prevented typical CLL-induced broad phenotypic T-cell defects. Due to the shortcomings of the AT model to mirror LN involvement consistently, T-cell phenotype was not examined in LN.

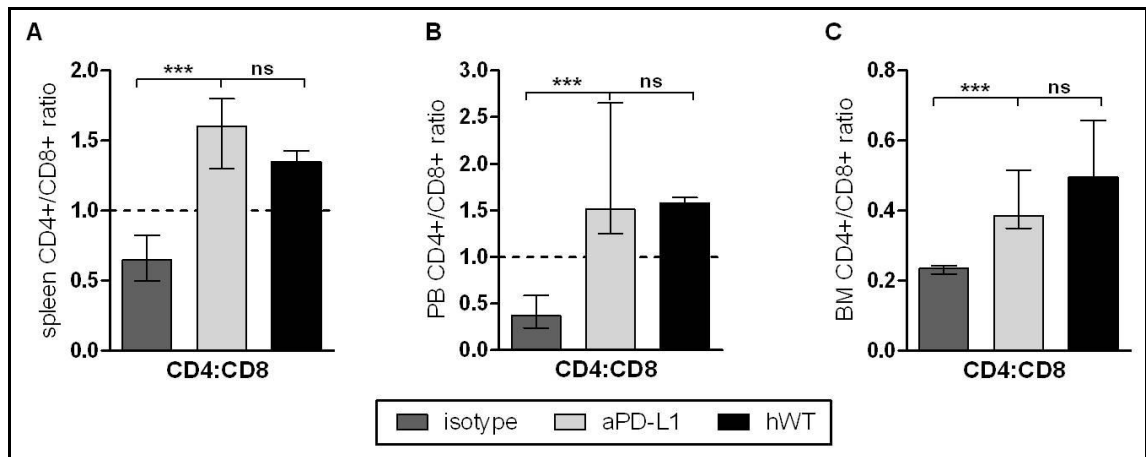


**Figure 64: Prevention of typical CLL-induced aberrant T-cell phenotype in CD3+, CD4+ and CD8+ cells by *in vivo* anti-PD-L1 treatment.** CD4 and CD8 were gated on CD3+ viable single MNC. aPD-L1 treatment led to a normalization of the CD4+/CD8+ ratio in (A) spleen, (B) PB and (C) BM. All graphs show median with IQR. ns = non-significant, \* $p < .05$ , \*\* $p < .001$ , \*\*\* $p < .0001$ . hWT=healthy WT mice.

Similarly, the loss of naïve (CD44-) CD3+CD8+ cells in spleen, and shift to antigen-experienced (CD44+) CD3+CD8+ cells with a relative expansion of effector and EM cells, was prevented by aPD-L1 treatment (Figure 65 A and B). However, aPD-L1 only moderately prevented the loss of CM cells. This was largely recapitulated in PB (Figure 65 C) and BM (Figure 65 D), although the loss of naïve cells was more pronounced in these organs than in spleen (note: phenotyping in PB and BM excluded CM and EM cells). Memory cells appeared to be slightly promoted by aPD-L1 treatment in spleen, but this was not consistently observed in the other organs.

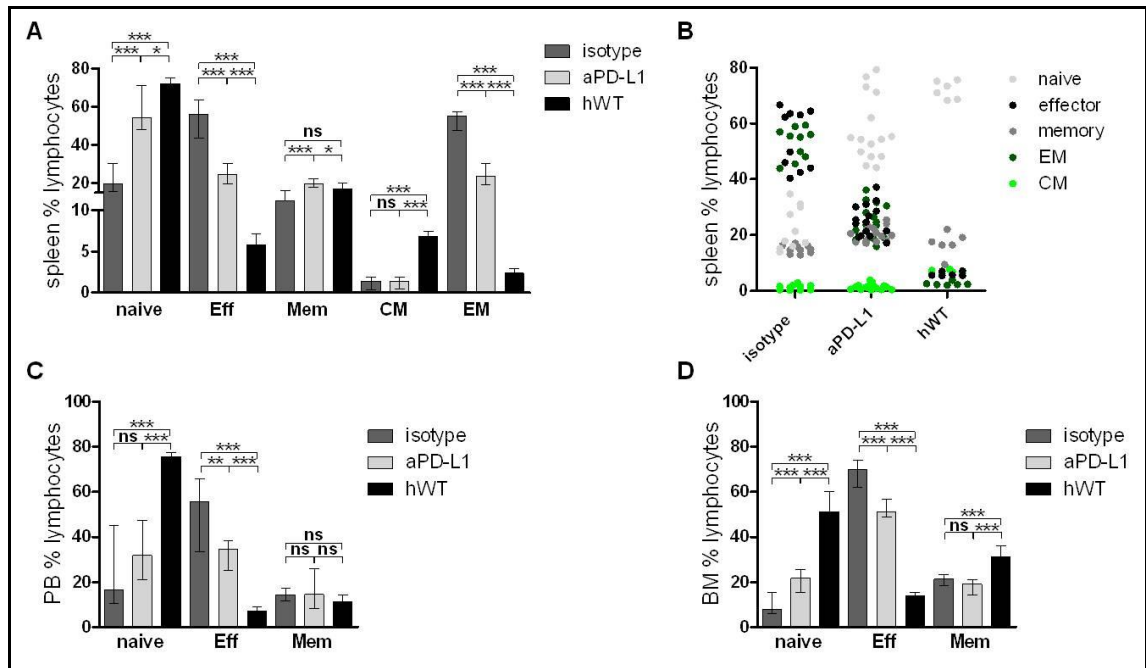


**Figure 65: Prevention of typical CLL-induced aberrant T-cell phenotype in CD3+CD8+ naive and antigen experienced cells by *in vivo* anti-PD-L1 treatment.** Naïve (CD44-CD62L+), effector (CD44+CD62L-), memory (CD44+CD62L+), effector memory (EM) (CD44+CD62L-CCR7-) and central memory (CM) (CD44+CD62L+CCR7+) cells were gated on CD3+CD8+ cells. FMO controls for CCR7 and CD44 were included in all experiments to discriminate positive and negative populations. **(A)** Changes in T-cell subsets in spleen lymphocytes with aPD-L1 treatment. **(B)** Data from (A) shown as stacked graph to depict shifts in cell subsets. **(C)** T-cell subset changes in PB. **(D)** T-cell subset changes in BM. All graphs except (B) show median with IQR. ns = non-significant, \*p<.05, \*\*p<.001, \*\*\*p<.0001. hWT=healthy WT mice.

Table 24 summarizes the p-values of statistical comparisons of T-cell subsets between the experimental groups for all organs examined.

organ	T-cell immunophenotype	aPD-L1 vs. isotype	aPD-L1 vs. hWT	isotype vs. hWT
spleen	% CD3	<b>.0002</b>	<b>.0322</b>	<b>.0002</b>
	% CD3+CD4+	<b>&lt;.0001</b>	.0565	<b>.0002</b>
	% CD3+CD8+	<b>&lt;.0001</b>	.1713	<b>.0002</b>
	CD4+/CD8+ ratio	<b>&lt;.0001</b>	.0683	<b>.0012</b>
	% Naïve CD3+CD8+	<b>&lt;.0001</b>	<b>.0391</b>	<b>.0002</b>
	% Effector CD3+CD8+	<b>&lt;.0001</b>	<b>.0005</b>	<b>.0002</b>
	% Memory CD3+CD8+	<b>&lt;.0001</b>	<b>.0471</b>	.0575
	% EM CD3+CD8+	<b>&lt;.0001</b>	<b>.0005</b>	<b>.0002</b>
	% CM CD3+CD8+	.6492	<b>.0005</b>	<b>.0002</b>
peripheral blood	% CD3	<b>.0244</b>	<b>.0265</b>	<b>.0008</b>
	% CD3+CD4+	<b>&lt;.0001</b>	.9070	<b>.0004</b>
	% CD3+CD8+	<b>&lt;.0001</b>	.7853	<b>.0004</b>
	CD4+/CD8+ ratio	<b>&lt;.0001</b>	.9690	<b>.0004</b>
	% Naïve CD3+CD8+	.0548	<b>.0007</b>	<b>.0004</b>
	% Effector CD3+CD8+	<b>.0018</b>	<b>.0005</b>	<b>.0004</b>
	% Memory CD3+CD8+	.7366	.4137	.0987
bone marrow	% CD3	.6842	1.0	.5622
	% CD3+CD4+	.9118	<b>.0110</b>	<b>.0005</b>
	% CD3+CD8+	<b>&lt;.0001</b>	.8749	<b>.0002</b>
	CD4+/CD8+ ratio	<b>.0002</b>	.0569	<b>.0013</b>
	% Naïve CD3+CD8+	<b>.0006</b>	<b>.0002</b>	<b>.0002</b>
	% Effector CD3+CD8+	<b>.0005</b>	<b>.0002</b>	<b>.0002</b>
	% Memory CD3+CD8+	.1211	<b>.0005</b>	<b>.0010</b>

**Table 24: Summary of p-values for T-cell subset comparisons between aPD-L1 and isotype treated mice and healthy WT mice (hWT).** Significant p-values are in bold.

### 8.4.3 *In vivo* anti-PD-L1 treatment prevents development of typical CLL-induced exhaustion-like T-cell phenotype

After confirming the ability of *in vivo* PD-L1 blockade to prevent the development of aberrant T-cell subset distributions, its effect on the expression of typical exhaustion-like surface markers was determined. This experiment included the exhaustion markers we confirmed in previous experiments of this project to be aberrantly expressed by CD3CD8+CD44+ T cells, namely PD-1, CD160, KLRG-1, 2B4 and LAG-3. Compared to isotype treated mice, aPD-L1 treatment significantly reduced the aberrant expression of PD-1, KLRG-1, 2B4, and LAG-3, but not CD160, in spleen (Figure 66 A). With the exception of PD-1, expression levels were comparable between healthy WT and aPD-L1 treated mice. The prevention of aberrant PD-1 expression was recapitulated in PB and BM, with other exhaustion markers not examined in these organs (Figure 66 B).

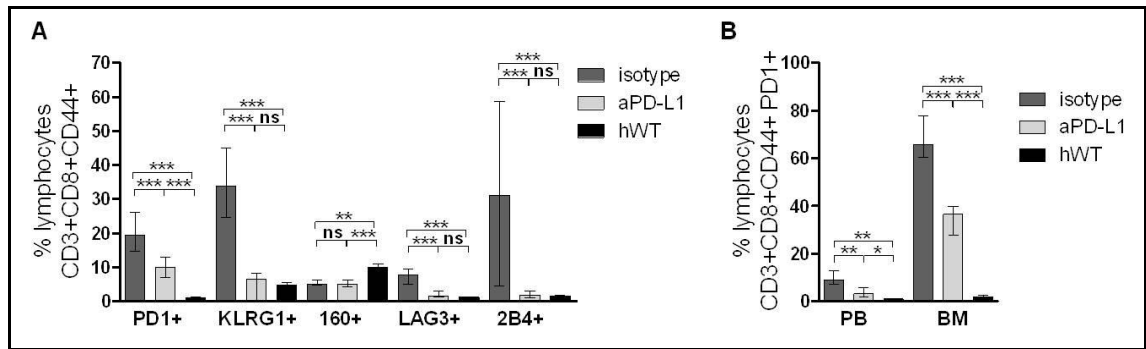


**Figure 66: Prevention of typical CLL-induced exhaustion-like phenotype in CD3+CD8+CD44+ cells by *in vivo* anti-PD-L1 treatment.** Exhaustion markers PD-1, KLRG-1, CD160, LAG-3 and 2B4 were gated on CD3+CD8+CD44+ cells. FMO controls for all exhaustion markers were included in all experiments to discriminate positive and negative populations. **(A)** aPD-L1 treatment prevented the aberrant expression of all exhaustion markers in aPD-L1 treated mice compared to isotype treated mice, with the exception of CD160. **(B)** Similar patterns for PD-1 expression were observed in PB and in BM. All graphs show median with IQR. ns = non-significant, \*p<.05, \*\*p<.001, \*\*\*p<.0001. hWT=healthy WT mice.

Table 25 summarizes the p-values of statistical comparisons of T-cell exhaustion markers between the experimental groups for all organs examined.

organ	T-cell immunophenotype	aPD-L1 vs. isotype	aPD-L1 vs. hWT	isotype vs. hWT
spleen	%PD-1+CD3+CD8+CD44+	<b>&lt;.0001</b>	<b>.0005</b>	<b>.0002</b>
	%KLRG-1+CD3+CD8+CD44+	<b>&lt;.0001</b>	.3705	<b>.0002</b>
	%CD160+CD3+CD8+CD44+	.8185	<b>.0007</b>	<b>.0014</b>
	%2B4+CD3+CD8+CD44+	<b>&lt;.0001</b>	.0565	<b>.0002</b>
	%LAG3+CD3+CD8+CD44+	<b>&lt;.0001</b>	.4137	<b>.0002</b>
peripheral blood	%PD-1+CD3+CD8+CD44+	<b>.0029</b>	<b>.0175</b>	<b>.0018</b>
bone marrow	%PD-1+CD3+CD8+CD44+	<b>&lt;.0001</b>	<b>.0002</b>	<b>.0002</b>

**Table 25: Summary of p-values for comparisons of T-cell surface exhaustion markers between aPD-L1 and isotype treated mice and healthy WT mice (hWT).** Significant p-values are highlighted in bold font.

#### 8.4.4 *In vivo* anti-PD-L1 treatment corrects key T-cell effector functions

After confirming that aPD-L1 treatment prevents the development of typical CLL-induced T-cell phenotypic changes, we examined the effect on T-cell effector functions in spleen. In line with previous experiments in this project, CD107a degranulation, intracellular GrB, IL-2, IL-4 and IFN- $\gamma$  production, *in vivo* and *ex vivo* proliferation and immune synapse formation were determined. In CD3+CD4+ T cells, aPD-L1 treatment reduced the typical CLL-induced loss of IL-2 (Figure 67 A) producing, and the increase of IL-4 (Figure 67 B) and IFN- $\gamma$  (Figure 67 C) producing cells compared to isotype

treated mice. However, this was still markedly different compared to WT mice, probably indicating a cytokine reaction of CD3+CD4+ cells to CLL.

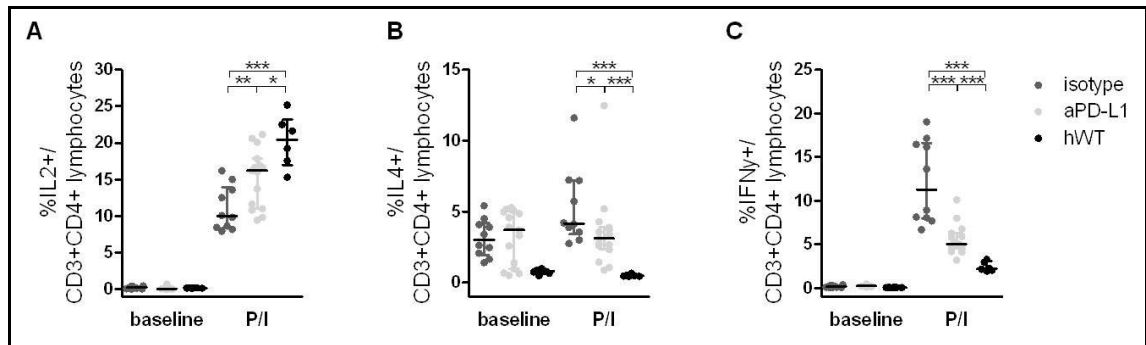


**Figure 67: Prevention of typical CLL-induced CD4+ cytokine production by *in vivo* anti-PD-L1 treatment.** Fresh splenocytes were stimulated for 6 hours with PMA/Ionomycin (P/I), in the presence of Brefeldin/Monensin for the last 5 hours of culture. Cells were then harvested, surface stained, fixed, permeabilised and stained with antibodies against IL-2, IL-4 and IFN- $\gamma$ . Data show the effects of aPD-L1 treatment, compared to isotype treatment or healthy WT mice (hWT), on the percentage of CD3+CD4+ T cells producing (A) IL-2, (B) IL-4, and (C) IFN- $\gamma$ . All graphs show median with IQR. ns = non-significant, \* $p < .05$ , \*\* $p < .001$ , \*\*\* $p < .0001$ .

In CD3+CD8+CD44+ T cells, aPD-L1 treatment prevented the loss of cells able to degranulate, as indicated by comparable CD107a ratios between healthy WT and aPD-L1 treated mice (Figure 68 A). In contrast, no effect on changes in intracellular IFN- $\gamma$  production was observed (Figure 68 B). However, work done in this project (Chapter 5) demonstrates that the CLL-induced increase of IFN- $\gamma$  producing cells observed in ageing TCL1 mice and in CLL patients is inadequately modelled in mice after AT.

aPD-L1 treatment also showed an effect on T-cell proliferation, as it significantly reduced the CLL-induced increased ki67 ratio (Figure 68 C) and the percentages of Alexa488-labelled EdU-positive CD4+ and CD8+ cells (Figure 68 D). In addition, the proliferation of normal CD19+CD5- B cells was comparable between healthy WT and aPD-1 treated mice, while it was significantly increased in CD19+CD5+ CLL cells from isotype treated mice (Figure 68 E). Importantly, aPD-L1 treatment restored the ability of CLL T cells to form immunological synapses with normal syngeneic B cells to the level of autologous cells from healthy WT mice (Figure 68 F).

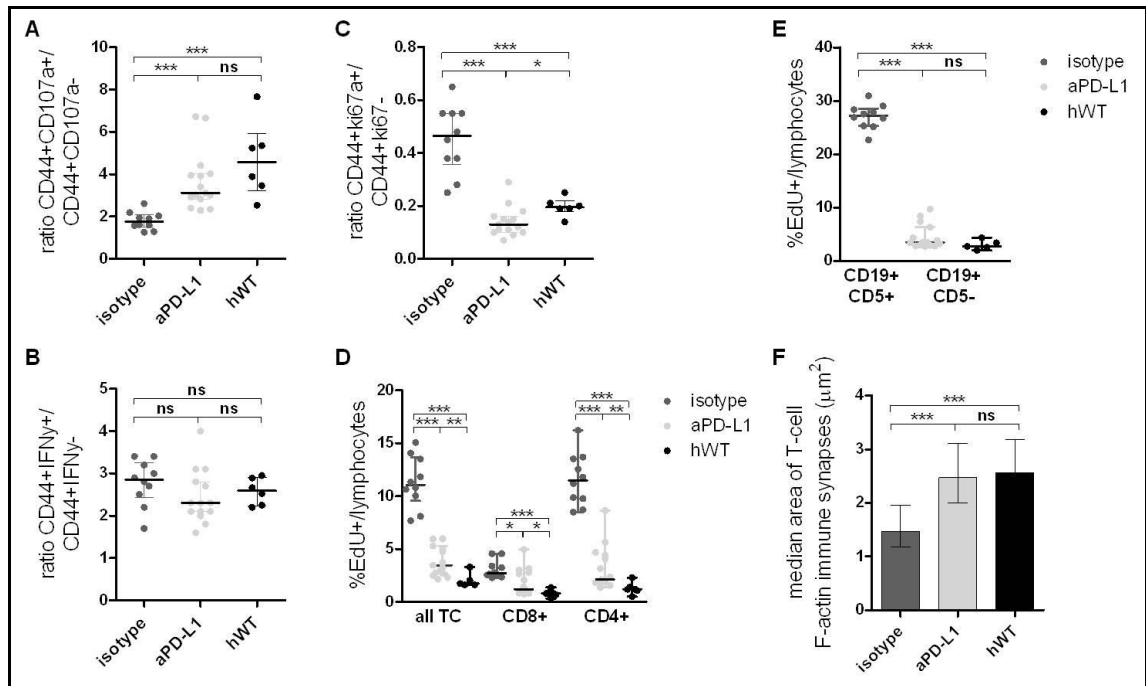


**Figure 68: Prevention of typical CLL-induced effector cell defects by *in vivo* anti-PD-L1 treatment.** Compared to isotype, aPD-L1 treatment corrected key CD3+CD8+CD44+ T-cell effector functions. **(A)** Ratio of CD107a+ to CD107a- cells, reflecting the ability to degranulate; **(B)** Ratio of IFN-γ+ to IFN-γ- cells; **(C)** Ratio ki67+ to ki67-, reflecting proliferation *ex vivo*; **(D)** Percent EdU+ T cells, reflecting *in vivo* proliferation. **(E)** Percent EdU+ CLL and normal B cells. **(F)** Immune synapse formation of CLL T cells with normal syngeneic B cells, as assessed by F-actin area. All graphs show median with IQR. ns = non-significant, \*p<.05, \*\*p<.001, \*\*\*p<.0001.

Table 26 summarizes the p-values of statistical comparisons of key T-cell effector functions between the experimental groups.

T-cell functional markers	aPD-L1 vs. isotype	aPD-L1 vs. hWT	isotype vs. hWT
% CD3+CD4+/IL-2+	<b>.0091</b>	<b>.0265</b>	<b>.0005</b>
% CD3+CD4+/IL-4+	<b>.0305</b>	<b>.0005</b>	<b>.0002</b>
% CD3+CD4+/IFN-γ+	<b>.0002</b>	<b>.0007</b>	<b>.0002</b>
ratio CD107a+:CD107a-CD3+CD8+CD44+	<b>&lt;.0001</b>	.199	<b>.0005</b>
ratio IFN-γ+:IFN-γ- CD3+CD8+CD44+	.1539	.3281	.3283
ratio ki67+:ki67-CD3+CD8+CD44+	<b>&lt;.0001</b>	<b>.0214</b>	<b>.0016</b>
% CD5+EdU+	<b>&lt;.0001</b>	<b>.0088</b>	<b>.0007</b>
% CD5+CD8+EdU+	<b>.0213</b>	<b>.0194</b>	<b>.0002</b>
% CD5+CD8-EdU+	<b>&lt;.0001</b>	<b>.0057</b>	<b>.0002</b>
Immune synapse area	<b>&lt;.0001</b>	.7178	<b>&lt;.0001</b>

**Table 26: Summary of p-values for comparisons of key T-cell effector functions between aPD-L1 and isotype treated mice and healthy WT mice (hWT).** Significant p-values are in bold.

#### 8.4.5 *In vivo* anti-PD-L1 treatment corrects key effector functions attributed to PD-1 expression

Although PD-1 expression was significantly lower in aPD-L1 treated than in isotype control treated mice, they still had a higher percentage of CD3+CD8+CD44+PD-1+ T cells than healthy WT mice (see Chapter 8.4.3). To investigate the associations between PD-1 expression and T-cell effector function, we next compared effector function ratios between PD-1<sup>high</sup> and PD-1<sup>low</sup> cells in isotype *versus* aPD-L1 treated mice. The CD107a ratio was significantly higher in both PD-1<sup>high</sup> and PD-1<sup>low</sup> cells in aPD-L1 treated mice compared to isotype treated mice, indicating that *in vivo* PD-L1 treatment increased the percentage of antigen experienced CD8+ cells with the ability to localize CD107a to their cell surface, also in cells with PD-1 expression (Figure 69 A).

The IFN- $\gamma$  ratio was not different among PD-1<sup>high</sup> cells, but was significantly reduced among PD-1<sup>low</sup> cells in aPD-L1 treated mice compared to isotype (Figure 69 B). aPD-L1 therefore appeared to correct the physiological predominance of the PD-1<sup>high</sup> over the PD-1<sup>low</sup> subset in being enriched for cells containing intracellular IFN- $\gamma$  that we observed in ageing WT mice (see Chapter 6). In isotype treated mice, the median IFN- $\gamma$  ratio in PD-1<sup>high</sup> cells was 3.7 (range 2.8-5.0), and in PD-1<sup>low</sup> cells 1.3 (range .7-1.9), leading to an approximately 3-fold higher ratio in PD-1<sup>high</sup> cells. In aPD-L1 treated mice, the median IFN- $\gamma$  ratio in PD-1<sup>high</sup> cells was 2.9 (range 1.4-7.8) *versus* .6 (range .4-1.8) in PD-1<sup>low</sup> cells, resulting in a 4.6-fold higher ratio in PD-1<sup>high</sup> cells.

GrB ratios were significantly reduced in both PD-1<sup>high</sup> and PD-1<sup>low</sup> cells in aPD-L1 treated mice compared to isotype treated mice (Figure 69 C). In addition, aPD-L1 treatment also corrected the physiological predominance of the PD-1<sup>high</sup> over the PD-1<sup>low</sup> subset in being enriched for cells containing intracellular GrB; in isotype treated mice, the median GrB ratio in PD-1<sup>high</sup> cells was 2.2 (range 1.7-3.2), and in PD-1<sup>low</sup> cells .6 (range .45-.68), leading to a 3.8-fold higher ratio in PD-1<sup>high</sup> cells. In aPD-L1 treated mice, the median GrB ratio in PD-1<sup>high</sup> cells was 1.1 (range .4-2.8) and in PD-1<sup>low</sup> cells .17 (range .09-.37), resulting in a 6-fold higher ratio in PD-1<sup>high</sup> cells.

The EdU ratio was significantly lower in both PD-1<sup>high</sup> and PD-1<sup>low</sup> cells in aPD-L1 treated mice compared to isotype treated mice, indicating that *in vivo* PD-L1 treatment abrogated the enrichment of proliferating cells, also in cells with PD-1 expression (Figure 69 D).

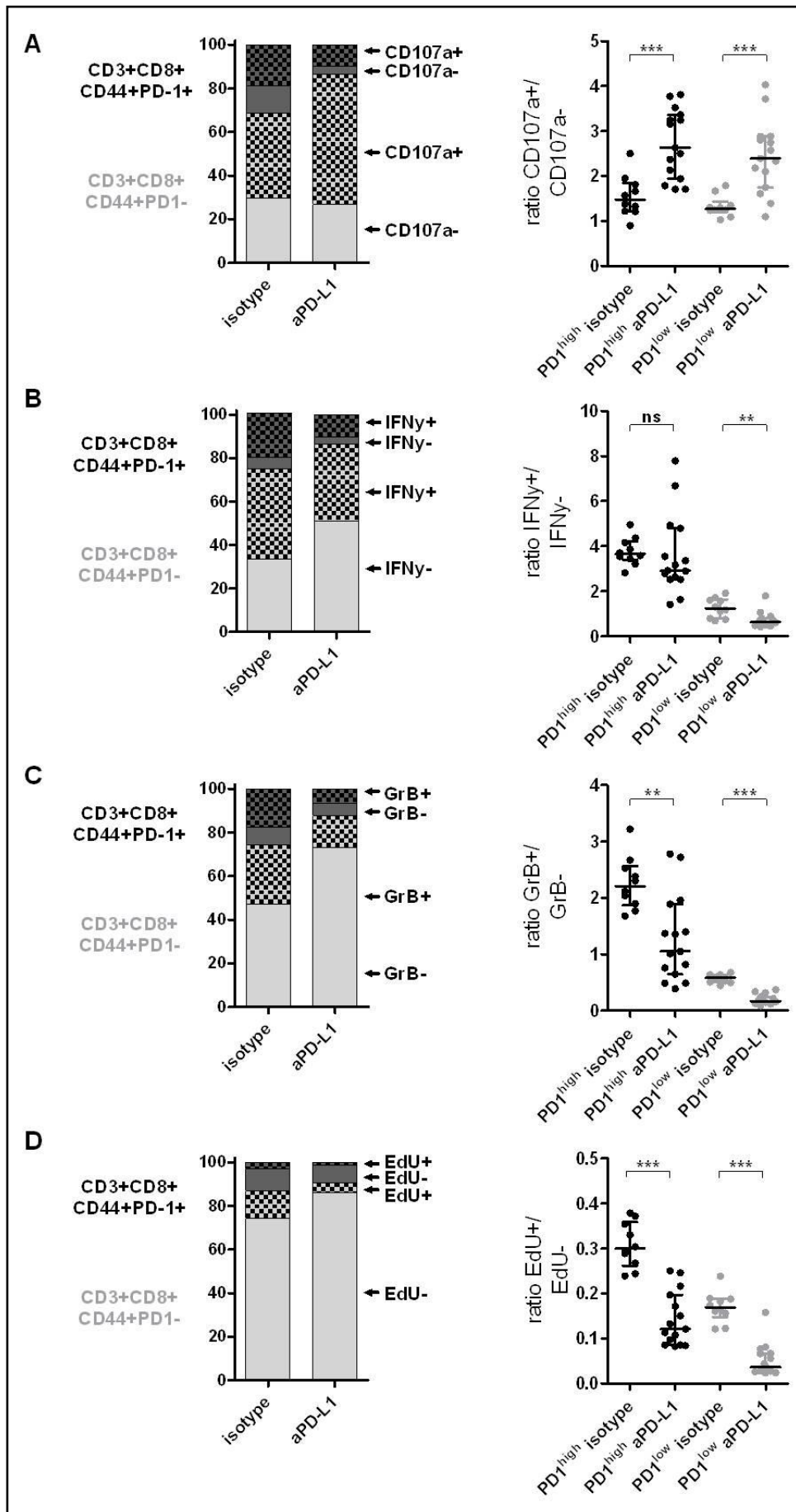


**Figure 69: Differences in effector function between PD-1<sup>high</sup> and PD-1<sup>low</sup> cells in aPD-L1 and isotype treated mice.** To correlate PD-1 expression and T-cell effector function markers, ratios of key effector function markers between PD-1<sup>high</sup> and PD-1<sup>low</sup> cells in aPD-L1 treated *versus* isotype treated mice were compared. Graphs show percentages and ratios of antigen experienced (CD44+) CD8+ T cells expressing: **(A)** cell surface CD107a; **(B)** intracellular IFN- $\gamma$ ; and **(C)** intracellular GrB; as well as **(D)** EdU+ (proliferating) cells, among PD-1<sup>high</sup> and PD-1<sup>low</sup> subsets.

Table 27 summarizes the p-values of statistical comparisons of key T-cell effector functions according to PD-1 expression between aPD-L1 and isotype treated mice.

functional marker (ratio of positive vs. negative)	p-value, aPD-L1 vs. isotype treatment	
	PD-1 <sup>high</sup>	PD-1 <sup>low</sup>
CD107a	<b>.0002</b>	<b>.0003</b>
IFN- $\gamma$	.07437	<b>.0022</b>
GrB	<b>.0014</b>	<b>&lt;.0001</b>
EdU	<b>&lt;.0001</b>	<b>&lt;.0001</b>

**Table 27: Summary of p-values of statistical comparisons of key T-cell effector function markers according to PD-1 expression between aPD-L1 and isotype treated mice.** Significant p-values are highlighted in bold.

### 8.5 Summary of effect of *in vivo* PD-L1 blockade on T-cell dysfunction and T-cell exhaustion in TCL1 mice

In summary, we were able to demonstrate that *in vivo* anti-PD-L1 treatment led to very effective CLL control, while significantly improving the T-cell immune functional phenotype in mice adoptively transferred with CLL. Effective CLL control was demonstrated by remarkably reduced spleen sizes, significantly lower spleen weights, and a significantly lower relative frequency of CD19+CD5+ CLL lymphocytes in spleen, PB and BM in aPD-L1 treated mice compared to isotype control treated mice. PD-L1 expression was significantly increased on CLL cells in isotype treated mice compared to B cells from healthy mice; however, this could not be accurately assessed in aPD-L1 treated mice, as *in vivo* treatment partially blocked the binding of fluorochrome labelled PD-L1 on a different clone. Aberrant PD-L2 expression by normal B cells, however, was prevented in all examined organs by aPD-L1 treatment.

The effective CLL control by *in vivo* aPD-L1 was reflected by remarkable corrections of the CLL-associated T-cell phenotype: aPD-L1 treatment prevented the reduction of the CD4+/CD8+ ratio. Similarly, the loss of naïve CD8+ cells and shift to antigen-experienced cells, with a relative expansion of effector and EM cells, was reduced. This was recapitulated in spleen, PB and BM. Treatment with aPD-L1 also significantly

reduced the aberrant expression of PD-1, KLRG-1, 2B4, and LAG-3, but not CD160, in spleen CD8+ T cells. The effect on reducing aberrant PD-1 expression was also recapitulated in CD8+ T cells in PB and BM.

Functionally, aPD-L1 treatment reduced the CLL-mediated reduction in IL-2 producing, and increase in IL-4 and IFN- $\gamma$  producing, CD4+ T cells. In CD8+ cells, it prevented the loss of cells with the ability to degranulate, but had no effect on intracellular IFN- $\gamma$  production. CLL-mediated increased *ex vivo* and *in vivo* proliferation was reduced both in CD4+ and CD8+ T-cell subsets, and the proliferation of normal CD19+CD5- B cells was comparable between aPD-L1 treated and hWT mice. Lastly, the ability of CLL T cells to form immunological synapses with normal syngeneic B cells was restored to normal levels by aPD-L1 treatment.

The comparison of key effector functions in PD-1<sup>high</sup> and PD-1<sup>low</sup> cells from isotype and aPD-L1 treated mice demonstrated that *in vivo* PD-L1 treatment increased the percentage of antigen experienced CD8+ cells with the ability to localize CD107a to their cell surface even in cells with PD-1 expression, corrected the physiological predominance of the PD-1<sup>high</sup> over the PD-1<sup>low</sup> subset in being enriched for cells containing intracellular IFN- $\gamma$  and GrB, and abrogated the enrichment of proliferating cells in both PD-1<sup>high</sup> and PD-1<sup>low</sup> cells.

## 8.6 Discussion

The goal of this part of the project was to provide a rationale for the clinical evaluation of targeted PD-L1/PD-1 blockade in human CLL by investigating if *in vivo* blockage in mice corrects CLL-induced T-cell dysfunction and enhances anti-tumour T-cell responses. The PD-L1/PD-1 pathway can be targeted from two directions: PD-1 blockade inhibits binding of PD-1 to PD-L1 and PD-L2, but has no effect on binding of PD-L1 to the co-stimulatory molecule CD80, with CD80 having a greater affinity for PD-L1 than for CD28 and about one third the affinity of PD-L1 for PD-1<sup>480</sup>. PD-L1 blockade inhibits binding of PD-L1 to CD80 and PD-1, while having no effect on binding of PD-1 to PD-L2. As the PD-1-mediated inhibition of lymphocyte function is initiated upon binding to its ligands rather than by PD-1 expression *per se*, it is reasonable to counteract the aberrant expression of PD-L1 on tumour cells by blocking PD-L1, especially if it is hypothesized that PD-1 expression by T cells is important to maintain physiological T-cell homeostasis. In addition, several studies have now demonstrated that aberrant PD-L1 expression by MDSCs and TAMs in the tumour microenvironment also has an effect on T-cell effector function<sup>199, 298, 477, 478</sup>. Blocking PD-L1 therefore may

abrogate the inhibitory effects on T cells mediated not just by tumour cells, but also by non-malignant cells in the microenvironment. However, this approach still allows binding of PD-1 to PD-L2, which means that an immunosuppressive effect can be maintained via PD-1/PD-L2 signalling. While PD-L1 blockade has been clinically evaluated in a number of solid tumours<sup>361</sup>, experiences in haematological malignancies and especially CLL are still sparse. PD-1 blockade has recently been demonstrated to be well tolerated and effective in patients with DLBCL and relapsed FL, and correlative studies have provided some insights into the immunological effects of this treatment<sup>359, 360</sup>. Without a randomized trial, however, no conclusive statements can be made regarding the safety and activity of agents targeting PD-1 *versus* those targeting PD-L1.

In the current study, mice were treated with murine anti-PD-L1 antibody from the day after CLL adoptive transfer to assess its ability to control disease and to normalize effector function. PD-L1 rather than PD-1 blockade was selected as we have demonstrated that aberrant PD-L1 expression is utilized by both human<sup>79</sup> and mouse CLL cells (see Chapter 6), leading to impaired T-cell function. In addition, mouse experiments we conducted together with collaborators in Germany have shown that PD-L1 is also aberrantly expressed by myeloid cells and TAMs in this mouse model, and that this has an inhibitory effect on T-cell function *in vitro* [PhD work from B. Hanna, DKFZ Heidelberg, personal communication]. While both *in vitro* PD-L1 and PD-1 blockade were able to restore T-cell effector function<sup>79</sup>, work produced in this project has demonstrated that subsets of CLL T cells are still functional effector cells despite PD-1 expression (see Chapter 6). To investigate the full potential of PD-L1/PD-1 immune checkpoint blockade to repair defects and enhance T-cell subset functions, PD-L1 blockade appears to be a reasonable choice to counteract the inhibitory effect of PD-L1 expression by both tumour and myeloid cells without affecting T-cell receptor signalling itself, therefore allowing the investigation of the full potential of immune checkpoint blockade to influence T-cell function.

The rationale to initiate treatment early after adoptive transfer was based on the hypothesis that this time point represents a state of low-volume disease, during which remodelling and corruption of the immune system are likely to start. Early PD-L1 blockade was therefore hypothesized to protect the immune system from such inhibitory tumour-mediated effects. This assumption is supported by preclinical data from our group, which demonstrated that functional defects observed in T cells from patients with CLL could be induced in previously normal allogeneic T cells after just 48 hours by co-culturing them in direct cell-cell contact with CLL cells<sup>77</sup>. Moreover, T-cell

defects that were very similar to the defects observed in T cells from ageing TCL1 mice with CLL could be induced by adoptive transfer after just 7 days on a molecular level in young previously healthy TCL1 mice<sup>216</sup>.

Here we demonstrate that early PD-L1 blockade effectively controls CLL and prevents aberrant PD-L2 expression of normal B cells even after immunological challenge by CLL. However, we were not able to determine the effect on PD-L1 expression *per se* in aPD-L1 treated mice, as the *in vivo* treatment with 10F.9G2 partially blocked the binding site of fluorochrome labelled MIH5 PD-L1. 10F.9G2 and MIH5 were previously found to prevent binding of PD-L1 to both PD-1 and CD80, while 10F.2H11 prevented binding of PD-L1 to CD80 only<sup>480, 481</sup>. To assess whether these clones bound to overlapping epitopes on PD-L1, Paterson *et al.* pre-incubated 300.19-PD-L1 transfectants with saturating concentrations of purified 10F.9G2, 10F.2H11 or isotype monoclonal antibody and then stained with fluorescently labelled 10F.9G2, 10F.2H11, or MIH5 antibodies<sup>481</sup>. They found that 10F.2H11 was not able to block 10F.9G2 binding to PD-L1 and *vice versa*, suggesting that the 10F.2H11 and 10F.9G2 recognize distinct epitopes on PD-L1, and that pre-incubation with 10F.2H11 had no effect on MIH5 binding. In contrast, 10F.9G2 pre-incubation reduced the level of MIH5 binding, suggesting that the 10F.9G2 and MIH5 dual blockers bind to overlapping epitopes that are distinct from the epitope recognized by 10F.2H11. Based on these data, we attempted to obtain 10F.2H11 for our experiments, either in purified form or fluorescently labelled, to allow us to determine the effect of *in vivo* treatment on PD-L1 expression. However, we were not successful, and this question remains open.

As PD-L1 expression on tumour cells has been demonstrated to be linked with poor prognosis and tumour aggressiveness in a number of malignancies, it might serve as a useful predictive biomarker<sup>332, 482</sup>. Significantly increased PD-L1 expression on CLL cells was found in poor-prognosis patients with a median survival of 38 months compared with good-prognosis patients with a median survival of more than 10 years<sup>79</sup>. More recently, soluble PD-L1 (sPD-L1) has been explored as a biomarker, with elevated sPD-L1 being a predictive biomarker for poorer overall survival in patients with DLBCL<sup>483</sup>. Assessing PD-L1 expression changes might also be beneficial in the context of targeted PD-L1/PD-1 therapy. In a Phase I study of single agent anti-PD-1, tumour PD-L1 expression was found to be a predictive biomarker of response to treatment: while none of the PD-L1 negative patients achieved a tumour response, an overall response rate of 36% was observed in patients with PD-L1 positive tumours<sup>363</sup>.

Although targeted PD-L1 blockade did not prevent binding of PD-1 to PD-L2, our data clearly demonstrate that the effective CLL control by *in vivo* aPD-L1 was reflected by

remarkable corrections of phenotypic and functional T-cell defects: *in vivo* anti-PD-L1 treatment prevented the development of typical aberrant T-cell phenotypes and normalized key T-cell effector functions, even in less functional cells with PD-1 expression. However, this was achieved by initiating treatment at an early stage of disease, and mice were only treated for a total of 31 days, with antibody being administered every three days. It is possible that this improved immune status might not be achieved with less intense or later treatment or be sustained over a longer period of treatment, especially if other immune-escape mechanisms are developed or cells become resistant to PD-L1 blockade and inhibitory signalling shifts towards (for example) PD-L2. Therefore, it is important to consider options for combination therapies. Several preclinical studies have indicated that the combination of PD-L1 antibodies with blockade of other immune checkpoints may increase the quality of T-cell responses<sup>474-476</sup>. This is supported by the observation that PD-1 positive T cells also express other inhibitory receptors such as CTLA-4, TIM-3, LAG-3, BTLA, CD160, and 2B4<sup>404</sup>. It is therefore likely that blocking of PD-L1/PD-1 mediated inhibitory signalling alone might not fully restore the function of anti-tumour T cells. In a mouse model of AML, CD8+ T cells co-expressing PD-1 and TIM-3 were found to be deficient in their ability to produce IFN- $\gamma$ , TNF- $\alpha$ , and IL-2, with blocking the PD-1/PDL1 or Tim-3/galectin-9 pathway alone being insufficient to rescue mice from AML lethality<sup>419</sup>. However, an additive effect was seen in reducing tumour burden and lethality when both pathways were blocked. Similarly, NY-ESO-1-specific CD8+ T cells from patients with epithelial ovarian cancer demonstrated impaired effector function, preferential usage of dominant T-cell receptors, and enriched co-expression of LAG-3 and PD-1<sup>484</sup>. CD8+LAG-3+PD-1+ T cells were more impaired in IFN- $\gamma$ /TNF- $\alpha$  production compared with single positive subsets, and dual blockade of LAG-3 and PD-1 during T-cell priming efficiently augmented proliferation and cytokine production by NY-ESO-1-specific CD8+ T cells. Co-expression of PD-1 and LAG-3 was also demonstrated on tumour-infiltrating CD4+ and CD8+ T cells in different transplantable tumours, with dual LAG-3/PD-1 blockade curing most mice of established tumours that were largely resistant to single antibody treatment<sup>420</sup>. Interestingly, dual PD-L1 and LAG-3 blockade also appears to have implications in other disease. For example, this approach was recently shown to rapidly clear established blood-stage *Plasmodium* infection in mice, to have an effect on the number of follicular helper T cells and germinal-centre B cells and plasmablasts, and to enhance protective antibodies<sup>485</sup>.

CTLA-4 was the first immune checkpoint receptor to be clinically targeted, and CTLA-4 antibodies were the first to achieve FDA approval<sup>486, 487</sup>. In a Phase I dose-escalation

trial of the anti-CTLA-4 antibody ipilimumab in patients with relapsed/refractory B-cell lymphoma, treatment was well tolerated and resulted in clinical response in two of 18 patients, while in 31% of patients, T-cell proliferation to recall antigens was significantly increased<sup>488</sup>. The concept of enhanced efficacy by combination was recently supported by data from a clinical trial in which patients with melanoma were treated with ipilimumab and PD-1 antibody<sup>489</sup>. This combination produced durable tumour regression, with evidence of clinical activity being observed in 65% of patients. In preclinical carcinoma models, blockade of both PD-1 and CTLA-4 resulted in reversal of CD8+ T-cell dysfunction and led to tumour rejection in two thirds of mice. In physiological settings, CTLA-4 is critically required by TRegs to suppress immune responses by affecting the potency of antigen-presenting cells to activate other T cells<sup>181</sup>. The number of TRegs is increased and correlated with aggressive disease in CLL<sup>176</sup>, and could be significantly reduced by *in vitro* CD200 blockade, which also stimulated antigen-specific T cell responses towards the CLL-associated antigen fibromodulin<sup>490</sup>. Therefore, it is possible that the combination of CTLA-4 blockade with antibodies targeting PD-L1/PD-1 or CD200/CD200R might be especially beneficial in CLL.

In DLBCL and FL, PD-L1/PD-1 blockade has been combined with other immunomodulating strategies such as autologous haematopoietic stem cell transplantation and rituximab<sup>359, 360</sup>. Given the potential of novel substances targeting BCR signalling to also overcome CLL-induced immune dysfunction, the combination of PD-L1/PD-1 blockade with agents such as the BTK inhibitor ibrutinib or the PI3k $\delta$  inhibitor idelalisib might represent attractive treatment strategies, especially in older or heavily pre-treated patients unable to tolerate aggressive therapy<sup>168</sup>. In addition, several pre-clinical and clinical studies have demonstrated that lenalidomide can correct typical PD-L1/PD-1 mediated immune deficiencies in CLL<sup>77, 79-81</sup>. Our work supports and extends these findings, confirming that PD-L1 mediated defective immune synapse formation and some T-cell effector dysfunctions can be corrected by *in vivo* lenalidomide treatment. Other combinations could include immune stimulatory agents such as vaccines<sup>491, 492</sup>, cytokines<sup>432</sup>, or even soluble forms of co-stimulatory molecules such as soluble CD80<sup>493</sup>.

In sum, our *in vivo* experiments have provided a strong rationale for the clinical assessment of PD-L1/PD-1 immune checkpoint blockade in CLL, and this could be promoted by further *in vivo* preclinical studies examining the combination of PD-L1 antibodies with additional antibodies or novel agents.

## 9 Overall Discussion

The central hypothesis of this thesis project was that specific T-cell defects result from the interaction of malignant CLL cells with the immune system, and that repairing the defects in T-cell function will be required to activate an effective T-cell mediated anti-tumour immune response. As this was addressed using the *TCL1* mouse model of CLL, it is important to first consider the limitations of this model.

As outlined in Chapter 1.2, the *TCL1* model is a well-established and widely used tool to mirror the biology and therapeutic responses of aggressive human CLL. A variety of alternative models have been created in which specific genes and gene products, transcription factors, or components of signalling pathways that drive CLL development and progression have been manipulated. However, all of these are inferior to *TCL1* mice with regards to disease penetrance and the ability to mirror biological properties of human CLL. Xenograft models of CLL allow the investigation of the direct effect of selected immune cell components and therapeutic interventions on the disease in its natural complexity, but these fall short in their ability to provide the host components of a complete tumour microenvironment. The *TCL1* gene is now recognized as a clinically relevant oncogene in the vast majority of human CLL cases. For example, Herling *et al.* found *TCL1* expression to be correlated with markers of poor prognosis and shorter PFS<sup>494, 495</sup>, while another group indicated that *TCL1* expression serves, in addition to other clinical and genetic factors, as a predictor of OS<sup>496</sup>. Several studies have demonstrated that *TCL1* acts on multiple cellular targets in CLL, such as the serine/threonine kinase AKT pathway<sup>249</sup>, the NF- $\kappa$ B pathway<sup>250, 251</sup>, the transcription factor AP-1<sup>250</sup>, the p53 modulator Atm<sup>497</sup>, and the methyltransferases DNMT3A and 3B<sup>252</sup>.

As CLL is a very heterogeneous and dynamic disease, however, genetically engineered mice driven by selected oncogenes such as *TCL1* might be insufficient to mirror the genetic complexity and clonal evolution that is now recognized as a major hallmark of human CLL<sup>498</sup>. Early experiments demonstrated that transformed *TCL1* murine CLL cells have a wild-type p53 status<sup>215</sup>, which might render the *TCL1* model inadequate to investigate p53-associated resistance mechanisms. The extent to which clonal evolution and novel mutations such as SF3B1 or NOTCH1 can be recapitulated in *TCL1* mice is however not yet known. Despite these apparent limitations, our group pioneered studies highlighting the suitability of this model to mirror T-cell defects of human CLL, both on a molecular and functional level<sup>216</sup>. This was recently expanded to include defects in myeloid cells [PhD work from B. Hanna, DKFZ Heidelberg, personal communication], and several crosses, for example with MIF<sup>-/-</sup><sup>200</sup>, CD44<sup>-/-</sup><sup>261</sup>, rhoH<sup>-/-</sup><sup>263</sup>

or *hs1*<sup>-/-</sup> mice<sup>264</sup>, have emphasized the suitability of TCL1-driven CLL in mice to depict and allow investigation of microenvironmental interactions observed in human CLL.

However, with a disease latency of more than one year, the TCL1 model is very time- and cost-intensive. The fact that disease is readily transplantable and develops in healthy recipient mice is therefore a major benefit and enables the investigation of the pathomechanistic role of specific molecular targets as well as the efficacy and mechanism of action of novel therapies. Although the transplant of TCL1 leukaemia cells is now well-established and is utilized by groups worldwide, considerable variability exists in the timing, dose, and application route of donor cells. These variables impact the reproducibility of preclinical studies between experiments and between laboratories, hampering interpretation and comparison of results. An important contribution from this PhD project was therefore the characterization of adoptive transfer procedures and conditions, along with the biological course of disease after adoptive transfer in the absence of treatment. This work resulted in the generation and validation of standardized conditions that enable the investigation of complex disease-related immune and microenvironmental interactions and how these are affected by therapeutic approaches such as lenalidomide and PD-L1 blockade.

Early work from our group demonstrated the similarities between gene-expression profiles of T cells from leukaemic TCL1 mice and CLL patients, as well as the rapid reproduction of these profiles following adoptive transfer of TCL1 leukaemic cells into young disease-free mice<sup>216</sup>. Among the various defects of T cells in human CLL patients (see Chapter 1.1.4), aberrant subsets and phenotypes, such as a CD4<sup>+</sup>/CD8<sup>+</sup> ratio inversion, a loss of naïve CD3<sup>+</sup>CD8<sup>+</sup> T cells with a shift towards effector cells, and a similarity to exhausted T cells found in chronically infected patients have been described<sup>118-120, 133, 134</sup>. Although aspects of this are already published to be recapitulated in TCL1 mice backcrossed to the genetic B6 background<sup>220</sup>, no studies have been done regarding the effect of different microenvironments (*i.e.* peripheral blood, bone marrow and secondary lymphoid organs) on T-cell subsets and phenotype and how closely adoptive transfer mirrors those defects observed in ageing TCL1 mice. This is particularly interesting, as CLL is now understood as a disease that develops and is maintained due to complex interactions with the microenvironment<sup>499</sup>, indicating that T-cell defects themselves might undergo dynamic alterations depending on their site of contact with the disease. In addition, careful and thorough investigation of the dynamic development of phenotypic T-cell subsets and characterization of functional T-cell defects alongside progressing disease have not been conducted before. This project demonstrated for the first time that the previously documented phenotypic

changes in T-cell subsets are equally modelled in backcrossed B6 TCL1 and C3H TCL1 mice, that the patterns regarding CD4<sup>+</sup> and CD8<sup>+</sup> (naïve and antigen-experienced) T cells are observed regardless of microenvironment, and that this is recapitulated in young mice with CLL after adoptive transfer. Moreover, instead of “snapshot” characterizations of T-cell function in different patients with a certain disease stage, this work has produced for the first time a longitudinal characterization of the dynamic development of T-cell defects in the context of developing disease using a genetically uniform mouse model. This led to novel findings characterizing the stage of B-cell expansion in which T-cell defects emerge, how they evolve over the course of the disease, and how this is influenced by the different microenvironment that peripheral blood, bone marrow and secondary lymphoid organs provide.

Previous work from our group identified PD-L1 as an important mediator of impaired T-cell function in human CLL patients<sup>79</sup>. In addition, circulating T cells from CLL patients were found to exhibit features of T-cell exhaustion, with increased expression of exhaustion markers such as PD-1, a skew towards antigen experienced subsets, an altered transcription factor profile, and functional defects in proliferation and cytotoxicity<sup>133</sup>, highlighting the role of the PD-L1/PD-1 inhibitory signalling axis. However, several studies have indicated that the T-cell compartment in CLL might be very heterogeneous and is potentially influenced by a variety of other factors such as age and/or infection. Although differences in human CD8<sup>+</sup> lymphocyte subsets were previously thought to be explained by the presence of CMV<sup>144</sup>, work from our group confirmed that impaired T-cell function and altered subset composition were irrespective of CMV serostatus<sup>133</sup>. This finding was further supported by a recently published study suggesting that CMV-specific CD8<sup>+</sup> T cells were indeed functionally intact, while CLL-induced global T-cell defects were still present<sup>148</sup>. Moreover, data from “classical” exhaustion models indicated that the T-cell exhaustion state is neither a fixed, irreversible, terminal differentiation state, nor an unresponsive T-cell state, and several studies have demonstrated that exhausted T cells represent a very heterogeneous population containing several subsets of cells that, despite PD-1 expression, are able to exert certain effector functions.

Work from this PhD project highlighted that aberrant PD-L1 over-expression in human CLL is mirrored in the TCL1 model, and identified aberrant PD-L2 expression as an additional inhibitory ligand of potential functional relevance in CLL. The mechanisms of how these molecules are over-expressed require further investigation. Similar to T-cell defects, both ligands were characterized over the course of developing disease, and in the context of different microenvironments. The TCL1 model was further utilized to

identify ageing as a substantial confounding factor for PD-1 associated patterns of T-cell defects, and this was fully unmasked by applying our rigorously characterized adoptive transfer methods. In addition, this project significantly adds to existing knowledge by the comparison of the molecular profiles of CLL T cells with exhausted and functional memory and effector CD8+ T cells. This work clearly demonstrated that CLL T cells are very heterogeneous, with features of both exhaustion and functional effector cells. Interestingly, this comparison also revealed that CLL T-cell genes enriched in the exhaustion signature appear to be also involved in pathways of T-cell metabolism and bioenergetics. These areas of T-cell defects have not been well studied in CLL, and our findings show that these pathways demand further investigation.

Our randomized adoptive transfer experiments also demonstrated that CLL-induced aberrant PD-1 expression on CD3+CD8+ T cells could be associated with different abilities of cells to exert effector functions. In general, intracellular cytokines IL-2, IL-4, IFN- $\gamma$  and TNF- $\alpha$  were detected in both PD-1<sup>high</sup> and PD-1<sup>low</sup> cells, and both PD-1<sup>high</sup> and PD-1<sup>low</sup> cells maintained their ability to degranulate and to proliferate, contradicting the notion that PD-1 expression would lead to a loss of these effector functions. In addition, we demonstrated that the increase in IFN- $\gamma$  production frequently observed in CLL T cells appeared to be attributed to PD-1<sup>high</sup> cells, while this subset was depleted of cells producing TNF- $\alpha$  compared to PD-1<sup>low</sup> cells and showed an impaired ability to form immunological synapses with normal B cells. The TCL1 model also allowed us to better understand the functional impact of the difference in PD-1 expression on CLL CD8+ T cells compared to normal T cells. Linking PD-1 expression with effector function of PD-1<sup>high</sup> cells in ageing WT mice and comparing this to effector function of PD-1<sup>high</sup> cells in ageing TCL1 mice developing CLL demonstrated that despite similar PD-1 expression patterns, PD-1 expressing cells are markedly different in their composition of cells able to exert selected effector functions.

After previous studies using CLL patient samples indicated that both *in vivo* and *ex vivo* lenalidomide treatment can modulate T-cell subsets and function<sup>442, 443</sup>, as well as PD-L1/PD-1-mediated inhibitory signalling<sup>79, 80, 441</sup>, we conducted a comprehensive analysis *in vivo* linking the effect of single agent lenalidomide to aberrant PD-L1/PD-1 expression and functional T-cell defects. Despite a lack of CLL control, resulting in the persistence of typical CLL-induced T-cell phenotypic alterations and T-cell effector dysfunction, we demonstrated that lenalidomide has an effect on the expression of PD-1 and immune synapse formation between autologous T and CLL cells. This important observation highlights that the repair of cytoskeleton defects is a prominent mechanism

of action of lenalidomide that is recapitulated in mice with CLL. Additionally, we demonstrated that *ex vivo* PD-L1 blockade on CLL cells restores immune synapses to sizes comparable to those in cells from healthy WT mice, prompting us to investigate PD-L1 blockade *in vivo*.

Given the lack of clinical studies exploring PD-L1/PD-1 blockade in CLL, our work provides both rationale and preclinical evidence for evaluating targeted PD-L1/PD-1 blockade in patients with this disease. Our findings suggest that blocking PD-L1 in mice with CLL can re-activate the immune system by counteracting CLL-induced changes in T-cell populations and functions, resulting in very effective disease control and significant reduction of tumour load in disease-affected tissues. Consequently, further immune defects induced by chronic antigenic stimulation were resolved. It is tempting to speculate on the advantage of blocking PD-1 *versus* PD-L1, as PD-1 blockade would inhibit the binding of PD-1 both to PD-L1 and PD-L2 expressed by tumours and microenvironmental components. However, no conclusive statements can be made regarding the relative activity of these two approaches on the immune system in the absence of a direct head-to-head comparison. In addition, it is not clear how pronounced the effect of PD-L1/PD-1 blockade on re-activating immune effector cells would be in the context of more established disease. These questions clearly need to be addressed in further pre-clinical studies. Nevertheless, our *in vivo* findings confirm that PD-L1/PD-1 immune checkpoint blockade is a very promising clinical approach in CLL, potentially in combination with agents targeting BCR signaling. Based on experience to date with BCR inhibitory agents such as ibrutinib and idelalisib, these could be used to mobilize and clear tumour bulks, while residual disease could be eradicated and durable remission achieved by the re-activation and restoration of anti-tumour immune responses via PD-1/PD-L1 blockade. Similarly, in patients undergoing HSCT or CAR therapy, PD-1/PD-L1 blockade could be administered in the setting of low tumour volume to re-activate immune responses.

In collaboration with another group, the effect of PD-L1 blockade was also demonstrated in this project to abrogate the CLL-induced differentiation blockade of myeloid cells. This is particularly important in view of very recent findings highlighting that T-cell defects in CLL are not only induced by direct contact with the tumour cells, but that other components of the microenvironment such as TAMs and MDSCs also negatively regulate T-cell function, partly via PD-L1/PD-1 inhibitory signalling<sup>199</sup>. To fully understand the complexity of T-cell defects and their contribution to disease development and progression, it is important to further characterize the interactions between T cells and TAMs and/or MDSCs *in vivo*, to identify the stage(s) during

disease development at which they occur and what the underlying mechanisms are. In fact, we have already conducted preliminary experiments using *in vivo* macrophage depletion with liposomal clodronate after adoptive transfer of murine CLL to address those questions. We observed that in comparison to vehicle-treated mice, clodronate-treated mice had significantly lower spleen weights and a lower percentage of CLL tumour cells in peripheral blood and secondary lymphoid organs, suggesting that macrophages are indeed important, albeit not vital, for disease development. Typical phenotypic and functional T-cell defects were still present in clodronate-treated mice, but were less pronounced than in vehicle-treated mice, confirming that T-cell defects are caused by malignant cells but might be magnified and/or promoted by interactions with macrophages and monocytes. In addition, it is possible that dynamic shifts towards immunosuppressive and tolerogenic phenotypes within myeloid cells determine the point at which CLL cells evade T-cell effector function, as observed in other entities<sup>500</sup>. Further studies will be needed to address the exact contributions of different components of the myeloid compartment, for example by adoptive transfer experiments into myeloid-deficient recipients such as the CX3CR1 mouse model, which is deficient for patrolling monocytes. Complementing our previous gene-expression profiling studies, it would also be attractive to compare the molecular profiles of T cells from mice after adoptive transfer in the absence of macrophages (either from clodronate depletion or by the use CX3CR1 recipients) *versus* those from fully immune competent recipients as used throughout this project.

An important question still to be addressed is the mechanism(s) underlying aberrant PD-L1 expression in CLL. In line with the adaptive immune resistance hypothesis, which is based on the observation that immune and bystander cells produce cytokines as a result of activation by a tumour, prompting the upregulation of PD-L1 by both the tumour and the tumour microenvironment, it is possible that additional signals might be involved in this process. Dr. Croce's group recently reported that circulating miRNAs shed from tumours are a novel aspect of miRNA biology and play an important role in the interaction between cancer cells and the microenvironment<sup>501</sup>. Their work demonstrated that due to their structural similarity with natural ligands, circulating miRNAs bind to intracellular TLR7 in macrophages and induce pro-metastatic inflammatory responses. Given the established role of miRNAs in CLL pathogenesis and progression (see Chapter 1.2.2), aberrant TLR expression in CLL<sup>502</sup>, and published findings linking TLR stimulation in B cells to expression of PD-L1 in patients with seasonal allergic rhinitis<sup>503</sup>, it is tempting to speculate that aberrant PD-L1 expression

in CLL is the result of continuous TLR7 signalling mediated by specific circulating miRNAs shed by tumour cells at an early stage of disease.

We tested this hypothesis using cells from young TCL1, age-matched WT and TLR7<sup>-/-</sup> mice, as well as primary human CLL and normal B cells, and DOTAP liposomal formulations of synthetic miRNAs reported to have an effect on immune cells and to be released by CLL cells. Indeed, we demonstrated that PD-L1 surface expression on murine and human B cells was strongly induced by miRs -21 and -29, and moderately by -150 and -155. The degree of PD-L1 upregulation by miRs -21 and -29 was comparable to that observed with direct TLR7 and TLR9 binding by specific agonists. Similar patterns were seen for CD69 and CD86 expression, and across treatment conditions, PD-L1 expression was highly correlated with the expression of CD69 and CD86. This observation strongly suggests that PD-L1 expression after TLR engagement is a marker of activation/costimulation, and therefore a physiological adaptive immune response to TLR binding in healthy B cells. Functionally, miRNA treatments resulted in increased IL-6, IL-10 and TNF- $\alpha$ . To elucidate when in the course of CLL development PD-L1 expression becomes aberrant and if it ceases to be inducible by miRNA treatment, we sacrificed mice at regular intervals following adoptive transfer to simulate tumour development. With increasing CLL the magnitude of the change of PD-L1 expression following miRNA treatment decreased substantially, and the baseline expression of PD-L1 in miRNA-untreated B cells increased consistently, until a median tumour load of about 70%. Importantly, miRNA treatment did not result in increased PD-L1, CD69 or CD86 expression in B cells from TLR7<sup>-/-</sup> mice, indicating that the miRNA/PD-L1 interactions are indeed mediated by TLR7. These findings therefore support the hypothesis that PD-L1 expression on B cells can be induced by specific miRNAs known to be produced by CLL cells, and that this effect is mediated via TLR7. Future work will focus on the molecular mechanisms of this effect, and the interactions between chronically active BCR signalling and TLR signalling.

In conclusion, this dissertation project not only meaningfully improves our ability to make further discoveries by extensively characterising and validating the use of adoptive transfer to mimic CLL-induced T-cell defects in mice, but also provides substantial new and translationally relevant information to the field of CLL immunology. It is important to note that in CLL, as in other malignancies, immunotherapy is increasingly being recognised as the most likely route to long-term disease control, which results from our increasing understanding of the specificity and potency that can be achieved with proper immune education and activation.

## 10 Appendix

genes represented in exhaustion signature	genes represented in effector signature	genes represented in memory signature	gene function
Alcam			cell surface receptor/ligand
Anxa2	Anxa2	Anxa2	apoptosis
	Apobec		metabolism
		Aqp9	metabolism
Ccnb1	Ccnb1		cell cycle
Ccnb2	Ccnb2		cell cycle
CD1d1			cell surface receptor/ligand
CD72	CD72		cell surface receptor/ligand
	Cdc6		cell cycle
		Ddit4	DNA repair
Dnajb9			regulating ATPase activity of 70 kDa heat shock proteins
	Dstn		miscellaneous
Egr2			transcription factor
	Emp1	Emp1	miscellaneous
	Fcgr2b	Fcgr2b	cell surface receptor/ligand
Figl1	Figl1		miscellaneous
Gzmb	Gzmb	Gzmb	effector function
		Gzmm	effector function
	H2-Aa	H2-Aa	MHC
H2-D1			histocompatibility antigen
	Hba-a1		metabolism
Hbb-b1	Hbb-b1		metabolism
Hist1h2ac	Hist1h2ac		transcription
Ifrd1			Interferon signalling
IgK-V28		IgK-V28	antigen receptors
IL6st	IL6st	IL6st	cytokine signalling
	Il18rap	Il18rap	cytokine signalling
Irf4			IFN response
	Itga4		cell surface receptor/ligand
	Kctd12		metabolism
		Klf4	transcription
Lgals3	Lgals3		
Mad2l1	Mad2l1		cell cycle
Mox2 = CD200			cell surface receptor/ligand
	Myo1f	Myo1f	cytoskeleton
	Nedd4l		proteases
Nedd4l			transcription
Nfatc1			transcription

Nr1d2			transcription
Nr4a2			transcription
Nrp			cell surface receptor/ligand
Pglyrp1			cell surface receptor/ligand
Psm13			proteasome enzyme
	Racgab1		signalling
	Rpa2		DNA repair
Rrm2			metabolism
S100a6	S100a6	S100a6	signalling
Sema4a = kallikrein			cell surface receptor/ligand
Sesn1	Sesn1	Sesn1	miscellaneous
Slc12a2			ion transporter
	Stard10		miscellaneous
St6gal1	St6gal1	St6gal1	glycosylation
Stk38			signalling
TCRb-J			signalling
Tfdp1			transcription
	Tm4SF13		cell surface receptor/ligand
Smarca2	Smarca2		transcription
Nusap1	Nusap1		cell cycle
	clk1		cell cycle
		kcnj8	metabolism
Slc4a7	Slc4a7		metabolism
	csda		metabolism
cmah			metabolism
ell2	ell2	ell2	translation
	Prpf39		translation
bach=acot7	bach=acot7	bach=acot7	miscellaneous
Cst7			miscellaneous
Mcm3			miscellaneous
	Birc5		miscellaneous
Tacc3	Tacc3		miscellaneous
Cxxc5	Cxxc5	Cxxc5	miscellaneous
Spnb2			miscellaneous
Cnn3	Cnn3	Cnn3	miscellaneous

**Table 28: Gene list of overlapping genes in CLL T cell and exhausted/ effector/ memory T cell signature.**

## 11 References

1. Sant M, Allemani C, Tereanu C, et al. Incidence of hematologic malignancies in Europe by morphologic subtype: results of the HAEMACARE project. *Blood* 2010;116:3724-34.
2. Howlander N, Noone AM, Krapcho M, Neyman N, Aminou R, Altekruse SF, Kosary CL, Ruhl J, Tatalovich Z, Cho H, Mariotto A, Eisner MP, Lewis DR, Chen HS, Feuer EJ, Cronin KA (eds). SEER Cancer Statistics Review, 1975-2009 (Vintage 2009 Populations), National Cancer Institute. Bethesda, MD, [http://seer.cancer.gov/csr/1975\\_2009\\_pops09/](http://seer.cancer.gov/csr/1975_2009_pops09/), based on November 2011 SEER data submission, posted to the SEER web site, April 2012.
3. Hallek M, Cheson BD, Catovsky D, et al. Guidelines for the diagnosis and treatment of chronic lymphocytic leukemia: a report from the International Workshop on Chronic Lymphocytic Leukemia updating the National Cancer Institute Working Group 1996 guidelines. *Blood* 2008;111:5446-56.
4. Bene MC, Nebe T, Bettelheim P, et al. Immunophenotyping of acute leukemia and lymphoproliferative disorders: a consensus proposal of the European LeukemiaNet Work Package 10. *Leukemia* 2011;25:567-74.
5. Müller-Hermelink HK, Montserrat E, Catovsky D, Campo E, Harris NL, Stein H. Chronic lymphocytic leukaemia/ small lymphocytic leukaemia. In: Swerdlow SH, Campo E, Harris NL, et al., eds. WHO Classification of tumours of haematopoietic and lymphoid tissues 4th Edition ed. Lyon: International Agency for Research on Cancer (IARC); 2008.
6. Rawstron AC, Bennett FL, O'Connor SJM, et al. Monoclonal B-Cell Lymphocytosis and Chronic Lymphocytic Leukemia. *New England Journal of Medicine* 2008;359:575-83.
7. Fazi C, Scarfo L, Pecciarini L, et al. General population low-count CLL-like MBL persists over time without clinical progression, although carrying the same cytogenetic abnormalities of CLL. *Blood* 2011;118:6618-25.
8. Rai K, Sawitsky A, Cronkite E, Chanana A, Levy R, Pasternack B. Clinical staging of chronic lymphocytic leukemia. *Blood* 1975;46:219-34.
9. Binet JL, Auquier A, Dighiero G, et al. A new prognostic classification of chronic lymphocytic leukemia derived from a multivariate survival analysis. *Cancer* 1981;48:198-206.
10. Damle RN, Wasil T, Fais F, et al. Ig V gene mutation status and CD38 expression as novel prognostic indicators in chronic lymphocytic leukemia. *Blood* 1999;94:1840-7.
11. Hamblin TJ, Davis Z, Gardiner A, Oscier DG, Stevenson FK. Unmutated Ig V(H) genes are associated with a more aggressive form of chronic lymphocytic leukemia. *Blood* 1999;94:1848-54.
12. Crespo M, Bosch F, Villamor N, et al. ZAP-70 expression as a surrogate for immunoglobulin-variable-region mutations in chronic lymphocytic leukemia. *N Engl J Med* 2003;348:1764-75.
13. Döhner H, Stilgenbauer S, Benner A, et al. Genomic Aberrations and Survival in Chronic Lymphocytic Leukemia. *New England Journal of Medicine* 2000;343:1910-6.
14. Tam CS, Shanafelt TD, Wierda WG, et al. De novo deletion 17p13.1 chronic lymphocytic leukemia shows significant clinical heterogeneity: the M. D. Anderson and Mayo Clinic experience. *Blood* 2009;114:957-64.
15. Isobe M, Emanuel BS, Givol D, Oren M, Croce CM. Localization of gene for human p53 tumour antigen to band 17p13. *Nature* 1986;320:84-5.
16. Zenz T, Kröber A, Scherer K, et al. Monoallelic TP53 inactivation is associated with poor prognosis in chronic lymphocytic leukemia: results from a detailed genetic characterization with long-term follow-up; 2008.
17. Dicker F, Herholz H, Schnittger S, et al. The detection of TP53 mutations in chronic lymphocytic leukemia independently predicts rapid disease progression and is highly correlated with a complex aberrant karyotype. *Leukemia* 2008;23:117-24.
18. Calin GA, Dumitru CD, Shimizu M, et al. Frequent deletions and down-regulation of micro- RNA genes miR15 and miR16 at 13q14 in chronic lymphocytic leukemia. *Proceedings of the National Academy of Sciences* 2002;99:15524-9.
19. Balatti V, Bottoni A, Palamarchuk A, et al. NOTCH1 mutations in CLL associated with trisomy 12. *Blood* 2012;119:329-31.
20. Stilgenbauer S, Liebisch P, James MR, et al. Molecular cytogenetic delineation of a novel critical genomic region in chromosome bands 11q22.3-923.1 in lymphoproliferative disorders. *Proc Natl Acad Sci U S A* 1996;93:11837-41.
21. Wang L, Lawrence MS, Wan Y, et al. SF3B1 and Other Novel Cancer Genes in Chronic Lymphocytic Leukemia. *New England Journal of Medicine* 2011;365:2497-506.
22. Quesada V, Conde L, Villamor N, et al. Exome sequencing identifies recurrent mutations of the splicing factor SF3B1 gene in chronic lymphocytic leukemia. *Nat Genet* 2012;44:47-52.
23. Baliakas P, Hadzidimitriou A, Sutton LA, et al. Recurrent mutations refine prognosis in chronic lymphocytic leukemia. *Leukemia* 2014;doi: 10.1038/leu.2014.196.
24. Dreger P, Schnaiter A, Zenz T, et al. TP53, SF3B1, and NOTCH1 mutations and outcome of allotransplantation for chronic lymphocytic leukemia: six-year follow-up of the GCLLSG CLL3X trial. *Blood* 2013;121:3284-8.

25. Schnaiter A, Paschka P, Rossi M, et al. NOTCH1, SF3B1, and TP53 mutations in fludarabine-refractory CLL patients treated with alemtuzumab: results from the CLL2H trial of the GCLLSG. *Blood* 2013;122:1266-70.
26. Stilgenbauer S, Schnaiter A, Paschka P, et al. Gene mutations and treatment outcome in chronic lymphocytic leukemia: results from the CLL8 trial. *Blood* 2014;123:3247-54.
27. Rossi D, Rasi S, Spina V, et al. Integrated mutational and cytogenetic analysis identifies new prognostic subgroups in chronic lymphocytic leukemia. *Blood* 2013;121:1403-12.
28. Pflug N, Bahlo J, Shanafelt TD, et al. Development of a comprehensive prognostic index for patients with chronic lymphocytic leukemia. *Blood* 2014;124:49-62.
29. Gribben JG, O'Brien S. Update on Therapy of Chronic Lymphocytic Leukemia. *Journal of Clinical Oncology* 2011;29:544-50.
30. Oscier D, Dearden C, Erem E, et al. Guidelines on the diagnosis, investigation and management of chronic lymphocytic leukaemia. *British Journal of Haematology* 2012;159:541-64.
31. Tam CS, O'Brien S, Wierda W, et al. Long-term results of the fludarabine, cyclophosphamide, and rituximab regimen as initial therapy of chronic lymphocytic leukemia. *Blood* 2008;112:975-80.
32. Hallek M, Fischer K, Fingerle-Rowson G, et al. Addition of rituximab to fludarabine and cyclophosphamide in patients with chronic lymphocytic leukaemia: a randomised, open-label, phase 3 trial. *Lancet* 2010;376:1164-74.
33. Zenz T, Eichhorst B, Busch R, et al. TP53 Mutation and Survival in Chronic Lymphocytic Leukemia. *Journal of Clinical Oncology* 2010;28:4473-9.
34. Fink AM, Bottcher S, Ritgen M, et al. Prediction of poor outcome in CLL patients following first-line treatment with fludarabine, cyclophosphamide and rituximab. *Leukemia* 2013;27:1949-52.
35. Shanafelt T. Treatment of older patients with chronic lymphocytic leukemia: key questions and current answers. *ASH Education Program Book* 2014;2013:158-67.
36. Hillmen P, Gribben JG, Follows GA, et al. Rituximab Plus Chlorambucil As First-Line Treatment for Chronic Lymphocytic Leukemia: Final Analysis of an Open-Label Phase II Study. *Journal of Clinical Oncology* 2014;32:1236-41.
37. Foà R, Del Giudice I, Cuneo A, et al. Chlorambucil plus rituximab with or without maintenance rituximab as first-line treatment for elderly chronic lymphocytic leukemia patients. *American Journal of Hematology* 2014;89:480-6.
38. Fischer K, Cramer P, Busch R, et al. Bendamustine in Combination With Rituximab for Previously Untreated Patients With Chronic Lymphocytic Leukemia: A Multicenter Phase II Trial of the German Chronic Lymphocytic Leukemia Study Group. *Journal of Clinical Oncology* 2012;30:3209-16.
39. Goede V, Fischer K, Busch R, et al. Obinutuzumab plus chlorambucil in patients with CLL and coexisting conditions. *N Engl J Med* 2014;370:1101-10.
40. Wierda WG, Kipps TJ, Mayer J, et al. Ofatumumab as single-agent CD20 immunotherapy in fludarabine-refractory chronic lymphocytic leukemia. *J Clin Oncol* 2010;28:1749-55.
41. Wierda WG, Kipps TJ, Durig J, et al. Chemoimmunotherapy with O-FC in previously untreated patients with chronic lymphocytic leukemia. *Blood* 2011;117:6450-8.
42. Wierda WG, Padmanabhan S, Chan GW, et al. Ofatumumab is active in patients with fludarabine-refractory CLL irrespective of prior rituximab: results from the phase 2 international study. *Blood* 2011;118:5126-9.
43. Herter S, Herting F, Mundigl O, et al. Preclinical Activity of the Type II CD20 Antibody GA101 (Obinutuzumab) Compared with Rituximab and Ofatumumab In Vitro and in Xenograft Models. *Molecular Cancer Therapeutics* 2013;12:2031-42.
44. Daneshmanesh AH, Hojjat-Farsangi M, Khan AS, et al. Monoclonal antibodies against ROR1 induce apoptosis of chronic lymphocytic leukemia (CLL) cells. *Leukemia* 2012;26:1348-55.
45. Zhang S, Wu CCN, Fecteau J-F, et al. Targeting chronic lymphocytic leukemia cells with a humanized monoclonal antibody specific for CD44. *Proceedings of the National Academy of Sciences* 2013;110:6127-32.
46. Hillmen P, Skotnicki AB, Robak T, et al. Alemtuzumab Compared With Chlorambucil As First-Line Therapy for Chronic Lymphocytic Leukemia. *Journal of Clinical Oncology* 2007;25:5616-23.
47. Zent CS, Call TG, Shanafelt TD, et al. Early treatment of high-risk chronic lymphocytic leukemia with alemtuzumab and rituximab. *Cancer* 2008;113:2110-8.
48. Parikh SA, Keating MJ, O'Brien S, et al. Frontline chemoimmunotherapy with fludarabine, cyclophosphamide, alemtuzumab, and rituximab for high-risk chronic lymphocytic leukemia. *Blood* 2011;118:2062-8.
49. Pettitt AR, Jackson R, Carruthers S, et al. Alemtuzumab in Combination With Methylprednisolone Is a Highly Effective Induction Regimen for Patients With Chronic Lymphocytic Leukemia and Deletion of TP53: Final Results of the National Cancer Research Institute CLL206 Trial. *Journal of Clinical Oncology* 2012;30:1647-55.
50. Bowen DA, Call TG, Jenkins GD, et al. Methylprednisolone-rituximab is an effective salvage therapy for patients with relapsed chronic lymphocytic leukemia including those with unfavorable cytogenetic features. *Leukemia & Lymphoma* 2007;48:2412-7.
51. Badoux XC, Keating MJ, Wang X, et al. Cyclophosphamide, fludarabine, alemtuzumab, and rituximab as salvage therapy for heavily pretreated patients with chronic lymphocytic leukemia. *Blood* 2011;118:2085-93.

52. Badoux XC, Keating MJ, Wang X, et al. Fludarabine, cyclophosphamide, and rituximab chemoimmunotherapy is highly effective treatment for relapsed patients with CLL. *Blood* 2011;117:3016-24.
53. Keating MJ, Flinn I, Jain V, et al. Therapeutic role of alemtuzumab (Campath-1H) in patients who have failed fludarabine: results of a large international study. *Blood* 2002;99:3554-61.
54. Tsimberidou AM, Wierda WG, Plunkett W, et al. Phase I-II Study of Oxaliplatin, Fludarabine, Cytarabine, and Rituximab Combination Therapy in Patients With Richter's Syndrome or Fludarabine-Refractory Chronic Lymphocytic Leukemia. *Journal of Clinical Oncology* 2008;26:196-203.
55. Brown JR, Messmer B, Werner L, et al. A phase I study of escalated dose subcutaneous alemtuzumab given weekly with rituximab in relapsed chronic lymphocytic leukemia/small lymphocytic lymphoma. *Haematologica* 2013;98:964-70.
56. Zent CS, Taylor RP, Lindorfer MA, et al. Chemoimmunotherapy for relapsed/refractory and progressive 17p13-deleted chronic lymphocytic leukemia (CLL) combining pentostatin, alemtuzumab, and low-dose rituximab is effective and tolerable and limits loss of CD20 expression by circulating CLL cells. *American Journal of Hematology* 2014;89:757-65.
57. Byrd JC, Lin TS, Dalton JT, et al. Flavopiridol administered using a pharmacologically derived schedule is associated with marked clinical efficacy in refractory, genetically high-risk chronic lymphocytic leukemia. *Blood* 2007;109:399-404.
58. Lin TS, Ruppert AS, Johnson AJ, et al. Phase II Study of Flavopiridol in Relapsed Chronic Lymphocytic Leukemia Demonstrating High Response Rates in Genetically High-Risk Disease. *Journal of Clinical Oncology* 2009;27:6012-8.
59. Stephens DM, Ruppert AS, Maddocks K, et al. Cyclophosphamide, alvocidib (flavopiridol), and rituximab, a novel feasible chemoimmunotherapy regimen for patients with high-risk chronic lymphocytic leukemia. *Leukemia Research* 2013;37:1195-9.
60. Woyach JA, Lozanski G, Ruppert AS, et al. Outcome of patients with relapsed or refractory chronic lymphocytic leukemia treated with flavopiridol: impact of genetic features. *Leukemia* 2012;26:1442-4.
61. Stevenson FK, Forconi F, Packham G. The Meaning and Relevance of B-Cell Receptor Structure and Function in Chronic Lymphocytic Leukemia. *Seminars in Hematology* 2014;51:158-67.
62. Zhong Y, Byrd JC, Dubovsky JA. The B-Cell Receptor Pathway: A Critical Component of Healthy and Malignant Immune Biology. *Seminars in Hematology* 2014;51:206-18.
63. Hallek M. Signaling the end of chronic lymphocytic leukemia: new frontline treatment strategies. *Blood* 2013;122:3723-34.
64. Herman SEM, Gordon AL, Hertlein E, et al. Bruton tyrosine kinase represents a promising therapeutic target for treatment of chronic lymphocytic leukemia and is effectively targeted by PCI-32765. *Blood* 2011;117:6287-96.
65. Ponader S, Chen S-S, Buggy JJ, et al. The Bruton tyrosine kinase inhibitor PCI-32765 thwarts chronic lymphocytic leukemia cell survival and tissue homing in vitro and in vivo. *Blood* 2012;119:1182-9.
66. de Rooij MF, Kuil A, Geest CR, et al. The clinically active BTK inhibitor PCI-32765 targets B-cell receptor- and chemokine-controlled adhesion and migration in chronic lymphocytic leukemia. *Blood* 2012;119:2590-4.
67. Byrd JC, Furman RR, Coutre SE, et al. Targeting BTK with ibrutinib in relapsed chronic lymphocytic leukemia. *The New England journal of medicine* 2013;369:32-42.
68. O'Brien S, Furman RR, Coutre SE, et al. Ibrutinib as initial therapy for elderly patients with chronic lymphocytic leukaemia or small lymphocytic lymphoma: an open-label, multicentre, phase 1b/2 trial. *Lancet Oncol* 2014;15:48-58.
69. Byrd JC, Brown JR, O'Brien S, et al. Ibrutinib versus Ofatumumab in Previously Treated Chronic Lymphoid Leukemia. *New England Journal of Medicine* 2014;371:213-23.
70. Hoellenriegel J, Meadows SA, Sivina M, et al. The phosphoinositide 3'-kinase delta inhibitor, CAL-101, inhibits B-cell receptor signaling and chemokine networks in chronic lymphocytic leukemia. *Blood* 2011;118:3603-12.
71. Herman SE, Lapalombella R, Gordon AL, et al. The role of phosphatidylinositol 3-kinase-delta in the immunomodulatory effects of lenalidomide in chronic lymphocytic leukemia. *Blood* 2011;117:4323-7.
72. Brown JR, Byrd JC, Coutre SE, et al. Idelalisib, an inhibitor of phosphatidylinositol 3-kinase p110delta, for relapsed/refractory chronic lymphocytic leukemia. *Blood* 2014;123:3390-7.
73. Furman RR, Sharman JP, Coutre SE, et al. Idelalisib and rituximab in relapsed chronic lymphocytic leukemia. *N Engl J Med* 2014;370:997-1007.
74. Roberts AW, Seymour JF, Brown JR, et al. Substantial Susceptibility of Chronic Lymphocytic Leukemia to BCL2 Inhibition: Results of a Phase I Study of Navitoclax in Patients With Relapsed or Refractory Disease. *Journal of Clinical Oncology* 2012;30:488-96.
75. Kater AP, Tonino SH, Egle A, Ramsay AG. How does lenalidomide target the chronic lymphocytic leukemia microenvironment? *Blood* 2014;124:2184-9.
76. Krönke J, Udeshi ND, Narla A, et al. Lenalidomide Causes Selective Degradation of IKZF1 and IKZF3 in Multiple Myeloma Cells. *Science* 2014;343:301-5.
77. Ramsay AG, Johnson AJ, Lee AM, et al. Chronic lymphocytic leukemia T cells show impaired immunological synapse formation that can be reversed with an immunomodulating drug. *J Clin Invest* 2008;118:2427-37.

78. Aue G, Njuguna N, Tian X, et al. Lenalidomide-induced upregulation of CD80 on tumor cells correlates with T-cell activation, the rapid onset of a cytokine release syndrome and leukemic cell clearance in chronic lymphocytic leukemia. *Haematologica* 2009;94:1266-73.
79. Ramsay AG, Clear AJ, Fatah R, Gribben JG. Multiple inhibitory ligands induce impaired T-cell immunologic synapse function in chronic lymphocytic leukemia that can be blocked with lenalidomide: establishing a reversible immune evasion mechanism in human cancer. *Blood* 2012;120:1412-21.
80. Shanafelt TD, Ramsay AG, Zent CS, et al. Long-term repair of T-cell synapse activity in a phase II trial of chemoimmunotherapy followed by lenalidomide consolidation in previously untreated chronic lymphocytic leukemia (CLL). *Blood* 2013;121:4137-41.
81. Ramsay AG, Evans R, Kiaii S, Svensson L, Hogg N, Gribben JG. Chronic lymphocytic leukemia cells induce defective LFA-1-directed T-cell motility by altering Rho GTPase signaling that is reversible with lenalidomide. *Blood* 2013;121:2704-14.
82. Chanan-Khan A, Miller KC, Musial L, et al. Clinical efficacy of lenalidomide in patients with relapsed or refractory chronic lymphocytic leukemia: results of a phase II study. *J Clin Oncol* 2006;24:5343-9.
83. Ferrajoli A, Lee BN, Schlette EJ, et al. Lenalidomide induces complete and partial remissions in patients with relapsed and refractory chronic lymphocytic leukemia. *Blood* 2008;111:5291-7.
84. Badoux XC, Keating MJ, Wen S, et al. Lenalidomide as initial therapy of elderly patients with chronic lymphocytic leukemia. *Blood* 2011;118:3489-98.
85. Wendtner CM, Hillmen P, Mahadevan D, et al. Final results of a multicenter phase 1 study of lenalidomide in patients with relapsed or refractory chronic lymphocytic leukemia. *Leuk Lymphoma* 2012;53:417-23.
86. Badoux XC, Keating MJ, Wen S, et al. Phase II study of lenalidomide and rituximab as salvage therapy for patients with relapsed or refractory chronic lymphocytic leukemia. *J Clin Oncol* 2013;31:584-91.
87. Strati P, Keating MJ, Wierda WG, et al. Lenalidomide induces long-lasting responses in elderly patients with chronic lymphocytic leukemia. *Blood* 2013;122:734-7.
88. James DF, Werner L, Brown JR, et al. Lenalidomide and rituximab for the initial treatment of patients with chronic lymphocytic leukemia: a multicenter clinical-translational study from the chronic lymphocytic leukemia research consortium. *J Clin Oncol* 2014;32:2067-73.
89. Andritsos LA, Johnson AJ, Lozanski G, et al. Higher doses of lenalidomide are associated with unacceptable toxicity including life-threatening tumor flare in patients with chronic lymphocytic leukemia. *J Clin Oncol* 2008;26:2519-25.
90. Chen CI, Bergsagel PL, Paul H, et al. Single-Agent Lenalidomide in the Treatment of Previously Untreated Chronic Lymphocytic Leukemia. *Journal of Clinical Oncology* 2011;29:1175-81.
91. Andritsos LA, Johnson AJ, Lozanski G, et al. Higher Doses of Lenalidomide Are Associated With Unacceptable Toxicity Including Life-Threatening Tumor Flare in Patients With Chronic Lymphocytic Leukemia. *Journal of Clinical Oncology* 2008;26:2519-25.
92. Woyach JA, Furman RR, Liu T-M, et al. Resistance Mechanisms for the Bruton's Tyrosine Kinase Inhibitor Ibrutinib. *New England Journal of Medicine* 2014;370:2286-94.
93. Kolb H-J. Graft-versus-leukemia effects of transplantation and donor lymphocytes. *Blood* 2008;112:4371-83.
94. Gribben JG, Zahrieh D, Stephans K, et al. Autologous and allogeneic stem cell transplantations for poor-risk chronic lymphocytic leukemia. *Blood* 2005;106:4389-96.
95. Baron F, Maris MB, Sandmaier BM, et al. Graft-Versus-Tumor Effects After Allogeneic Hematopoietic Cell Transplantation With Nonmyeloablative Conditioning. *Journal of Clinical Oncology* 2005;23:1993-2003.
96. Dreger P, Brand R, Hansz J, et al. Treatment-related mortality and graft-versus-leukemia activity after allogeneic stem cell transplantation for chronic lymphocytic leukemia using intensity-reduced conditioning. *Leukemia* 2003;17:841-8.
97. Sorror ML, Storer BE, Sandmaier BM, et al. Five-year follow-up of patients with advanced chronic lymphocytic leukemia treated with allogeneic hematopoietic cell transplantation after nonmyeloablative conditioning. *Journal of Clinical Oncology* 2008;26:4912-20.
98. Khouri IF, Bassett R, Poindexter N, et al. Nonmyeloablative allogeneic stem cell transplantation in relapsed/refractory chronic lymphocytic leukemia: long-term follow-up, prognostic factors, and effect of human leukocyte histocompatibility antigen subtype on outcome. *Cancer* 2011;117:4679-88.
99. Brown JR, Kim HT, Armand P, et al. Long-term follow-up of reduced-intensity allogeneic stem cell transplantation for chronic lymphocytic leukemia: prognostic model to predict outcome. *Leukemia* 2013;27:362-9.
100. Dreger P, Corradini P, Kimby E, et al. Indications for allogeneic stem cell transplantation in chronic lymphocytic leukemia: the EBMT transplant consensus. *Leukemia* 2007;21:12-7.
101. Dreger P, Schetelig J, Andersen N, et al. Managing high-risk chronic lymphocytic leukemia during transition to a new treatment era: stem cell transplantation or novel agents? *Blood* 2014;blood-2014-07-586826. [Epub ahead of print].
102. Nosari A. Infectious complications in chronic lymphocytic leukemia. *Mediterranean journal of hematology and infectious diseases* 2012;4:e2012070.
103. Molica S, Levato D, Levato L. Infections in chronic lymphocytic leukemia. Analysis of incidence as a function of length of follow-up. *Haematologica* 1993;78:374-7.

104. Itala M, Helenius H, Nikoskelainen J, Remes K. Infections and serum IgG levels in patients with chronic lymphocytic leukemia. *Eur J Haematol* 1992;48:266-70.
105. Francis S, Karanth M, Pratt G, et al. The effect of immunoglobulin VH gene mutation status and other prognostic factors on the incidence of major infections in patients with chronic lymphocytic leukemia. *Cancer* 2006;107:1023-33.
106. Hensel M, Kornacker M, Yammeni S, Egerer G, Ho AD. Disease activity and pretreatment, rather than hypogammaglobulinaemia, are major risk factors for infectious complications in patients with chronic lymphocytic leukaemia. *Br J Haematol* 2003;122:600-6.
107. Molteni A, Nosari A, Montillo M, Cafro A, Klersy C, Morra E. Multiple lines of chemotherapy are the main risk factor for severe infections in patients with chronic lymphocytic leukemia with febrile episodes. *Haematologica* 2005;90:1145-7.
108. Heath ME, Cheson BD. Defective complement activity in chronic lymphocytic leukemia. *Am J Hematol* 1985;19:63-73.
109. Varga L, Czink E, Miszlai Z, et al. Low activity of the classical complement pathway predicts short survival of patients with chronic lymphocytic leukaemia. *Clin Exp Immunol* 1995;99:112-6.
110. Freeman JA, Crassini KR, Best OG, et al. Immunoglobulin G subclass deficiency and infection risk in 150 patients with chronic lymphocytic leukemia. *Leuk Lymphoma* 2013;54:99-104.
111. Svensson T, Hoglund M, Cherif H. Clinical significance of serum immunoglobulin G subclass deficiency in patients with chronic lymphocytic leukemia. *Scandinavian journal of infectious diseases* 2013;45:537-42.
112. Shvidel L, Tadmor T, Braester A, et al. Serum immunoglobulin levels at diagnosis have no prognostic significance in stage A chronic lymphocytic leukemia: a study of 1113 cases from the Israeli CLL Study Group. *Eur J Haematol* 2014;93:29-33.
113. Cerutti A, Kim EC, Shah S, et al. Dysregulation of CD30+ T cells by leukemia impairs isotype switching in normal B cells. *Nat Immunol* 2001;2:150-6.
114. Wolos JA, Davey FR. B lymphocyte function in B cell chronic lymphocytic leukaemia. *British Journal of Haematology* 1981;49:395-403.
115. Han T, Bloom M, Dadey B, et al. Lack of autologous mixed lymphocyte reaction in patients with chronic lymphocytic leukemia: evidence for autoreactive T-cell dysfunction not correlated with phenotype, karyotype, or clinical status. *Blood* 1982;60:1075-81.
116. Cantwell M, Hua T, Pappas J, Kipps TJ. Acquired CD40-ligand deficiency in chronic lymphocytic leukemia. *Nat Med* 1997;3:984-9.
117. Ranheim EA, Kipps TJ. Activated T cells induce expression of B7/BB1 on normal or leukemic B cells through a CD40-dependent signal. *The Journal of Experimental Medicine* 1993;177:925-35.
118. Catovsky D, Miliani E, Okos A, Galton DA. Clinical significance of T-cells in chronic lymphocytic leukaemia. *Lancet* 1974;2:751-2.
119. Foa R, Catovsky D, Brozovic M, et al. Clinical staging and immunological findings in chronic lymphocytic leukemia. *Cancer* 1979;44:483-7.
120. Vuillier F, Tortevoe P, Binet JL, Dighiero G. CD4, CD8 and NK subsets in B-CLL. *Nouv Rev Fr Hematol* 1988;30:331-4.
121. Herrmann F, Lochner A, Philippen H, Jauer B, Ruhl H. Imbalance of T cell subpopulations in patients with chronic lymphocytic leukaemia of the B cell type. *Clin Exp Immunol* 1982;49:157-62.
122. Platsoucas CD, Galinski M, Kempin S, Reich L, Clarkson B, Good RA. Abnormal T lymphocyte subpopulations in patients with B cell chronic lymphocytic leukemia: an analysis by monoclonal antibodies. *J Immunol* 1982;129:2305-12.
123. Totterman T, Carlsson M, Simonsson B, Bengtsson M, Nilsson K. T-cell activation and subset patterns are altered in B-CLL and correlate with the stage of the disease. *Blood* 1989;74:786-92.
124. Nunes C, Wong R, Mason M, Fegan C, Man S, Pepper C. Expansion of a CD8+PD-1+ Replicative Senescence Phenotype in Early Stage CLL Patients Is Associated with Inverted CD4:CD8 Ratios and Disease Progression. *Clinical Cancer Research* 2012;18:678-87.
125. Scrivener S, Kaminski ER, Demaine A, Prentice AG. Analysis of the expression of critical activation/interaction markers on peripheral blood T cells in B-cell chronic lymphocytic leukaemia: evidence of immune dysregulation. *British Journal of Haematology* 2001;112:959-64.
126. Tinhofer I, Marschitz I, Kos M, et al. Differential Sensitivity of CD4+ and CD8+ T Lymphocytes to the Killing Efficacy of Fas (Apo-1/CD95) Ligand+ Tumor Cells in B Chronic Lymphocytic Leukemia. *Blood* 1998;91:4273-81.
127. Pizzolo G, Chilosi M, Ambrosetti A, Semenzato G, Fiore-Donati L, Perona G. Immunohistologic study of bone marrow involvement in B-chronic lymphocytic leukemia. *Blood* 1983;62:1289-96.
128. Stein H, Bonk A, Tolksdorf G, Lennert K, Rodt H, Gerdes J. Immunohistologic analysis of the organization of normal lymphoid tissue and non-Hodgkin's lymphomas. *Journal of Histochemistry and Cytochemistry* 1980;28:746-60.
129. Ghia P, Strola G, Granziero L, et al. Chronic lymphocytic leukemia B cells are endowed with the capacity to attract CD4+, CD40L+ T cells by producing CCL22. *Eur J Immunol* 2002;32:1403-13.
130. Patten PEM, Buggins AGS, Richards J, et al. CD38 expression in chronic lymphocytic leukemia is regulated by the tumor microenvironment. *Blood* 2008;111:5173-81.

131. Tinhofer I, Weiss L, Gassner F, Rubenzer G, Holler C, Greil R. Difference in the relative distribution of CD4+ T-cell subsets in B-CLL with mutated and unmutated immunoglobulin (Ig) VH genes: implication for the course of disease. *J Immunother* 2009;32:302-9.
132. Tonino SH, van de Berg PJ, Yong SL, et al. Expansion of effector T cells associated with decreased PD-1 expression in patients with indolent B cell lymphomas and chronic lymphocytic leukemia. *Leukemia & Lymphoma* 2012;53:1785-94.
133. Riches JC, Davies JK, McClanahan F, et al. T cells from CLL patients exhibit features of T-cell exhaustion but retain capacity for cytokine production. *Blood* 2013;121:1612-21.
134. Brusa D, Serra S, Coscia M, et al. The PD-1/PD-L1 axis contributes to T-cell dysfunction in chronic lymphocytic leukemia. *Haematologica* 2013;98:953-63.
135. Goethert J, Eisele L, Klein-Hitpass L, et al. Expanded CD8+ T cells of murine and human CLL are driven into a senescent KLRG1+ effector memory phenotype. *Cancer Immunology, Immunotherapy* 2013;62:1697-709.
136. Rissiek A, Schulze C, Bacher U, et al. Multidimensional scaling analysis identifies pathological and prognostically relevant profiles of circulating T-cells in chronic lymphocytic leukemia. *International journal of cancer Journal international du cancer* 2014;135:2370-9.
137. Serrano D, Monteiro J, Allen SL, et al. Clonal expansion within the CD4+CD57+ and CD8+CD57+ T cell subsets in chronic lymphocytic leukemia. *The Journal of Immunology* 1997;158:1482-9.
138. Van den Hove LE, Van Gool SW, Vandenberghe P, Boogaerts MA, Ceuppens JL. CD57+/CD28- T cells in untreated hemato-oncological patients are expanded and display a Th1-type cytokine secretion profile, ex vivo cytolytic activity and enhanced tendency to apoptosis. *Leukemia* 1998;12:1573-82.
139. Junevik K, Werlenius O, Hasselblom S, Jacobsson S, Nilsson-Ehle H, Andersson P-O. The expression of NK cell inhibitory receptors on cytotoxic T cells in B-cell chronic lymphocytic leukaemia (B-CLL). *Annals of Hematology* 2007;86:89-94.
140. Farace F, Orlanducci F, Dietrich PY, et al. T cell repertoire in patients with B chronic lymphocytic leukemia. Evidence for multiple in vivo T cell clonal expansions. *J Immunol* 1994;153:4281-90.
141. Lanasa MC, Allgood SD, Bond KM, Gockerman JP, Levesque MC, Weinberg JB. Oligoclonal TRBV gene usage among CD8+ T cells in monoclonal B lymphocytosis and CLL. *British Journal of Haematology* 2009;145:535-7.
142. Rezvany MR, Jeddi-Tehrani M, Wigzell H, Osterborg A, Mellstedt H. Leukemia-associated monoclonal and oligoclonal TCR-BV use in patients with B-cell chronic lymphocytic leukemia. *Blood* 2003;101:1063-70.
143. Chidrawar S, Khan N, Wei W, et al. Cytomegalovirus-seropositivity has a profound influence on the magnitude of major lymphoid subsets within healthy individuals. *Clin Exp Immunol* 2009;155:423-32.
144. Mackus WJM, Frakking FNJ, Grummels A, et al. Expansion of CMV-specific CD8+CD45RA+CD27- T cells in B-cell chronic lymphocytic leukemia. *Blood* 2003;102:1057-63.
145. Walton JA, Lydyard PM, Nathwani A, et al. Patients with B cell chronic lymphocytic leukaemia have an expanded population of CD4+ perforin expressing T cells enriched for human cytomegalovirus specificity and an effector-memory phenotype. *British Journal of Haematology* 2010;148:274-84.
146. Pourghesari B, Bruton R, Parry H, et al. The number of cytomegalovirus-specific CD4+ T cells is markedly expanded in patients with B-cell chronic lymphocytic leukemia and determines the total CD4+ T-cell repertoire. *Blood* 2010;116:2968-74.
147. Wherry EJ. T cell exhaustion. *Nature Immunology* 2011;12:492-9.
148. te Raa GD, Pascutti MF, García-Vallejo JJ, et al. CMV-specific CD8+ T-cell function is not impaired in chronic lymphocytic leukemia. *Blood* 2014;123:717-24.
149. Fayad L, Keating MJ, Reuben JM, et al. Interleukin-6 and interleukin-10 levels in chronic lymphocytic leukemia: correlation with phenotypic characteristics and outcome. *Blood* 2001;97:256-63.
150. Ferrajoli A, Keating MJ, Manshour T, et al. The clinical significance of tumor necrosis factor alpha plasma level in patients having chronic lymphocytic leukemia. *Blood* 2002;100:1215-9.
151. Lai R, O'Brien S, Maushour T, et al. Prognostic value of plasma interleukin-6 levels in patients with chronic lymphocytic leukemia. *Cancer* 2002;95:1071-5.
152. Mainou-Fowler T, Miller S, Proctor SJ, Dickinson AM. The levels of TNF $\alpha$ , IL4 and IL10 production by T-cells in B-cell chronic lymphocytic leukaemia (B-CLL). *Leukemia Research* 2001;25:157-63.
153. Mainou-Fowler T, Proctor SJ, Miller S, Dickinson AM. Expression and Production of Interleukin 4 in B-Cell Chronic Lymphocytic Leukaemia. *Leukemia & Lymphoma* 2001;42:689-98.
154. Levesque MC, Chen Y, Beasley BE, et al. Chronic lymphocytic leukemia cell CD38 expression and inducible nitric oxide synthase expression are associated with serum IL-4 levels. *Leukemia Research* 2006;30:24-8.
155. Buggins AGS, Patten PEM, Richards J, Thomas NSB, Mufti GJ, Devereux S. Tumor-derived IL-6 may contribute to the immunological defect in CLL. *Leukemia* 2007;22:1084-7.
156. Dancescu M, Rubio-Trujillo M, Biron G, Bron D, Delespesse G, Sarfati M. Interleukin 4 protects chronic lymphocytic leukemic B cells from death by apoptosis and upregulates Bcl-2 expression. *The Journal of Experimental Medicine* 1992;176:1319-26.
157. Bhattacharya N, Reichenzeller M, Caudron-Herger M, et al. Loss of cooperativity of secreted CD40L and increased dose-response to IL4 on CLL cell viability correlates with enhanced activation of NF- $\kappa$ B and STAT6. *International Journal of Cancer* 2014:n/a/n/a.

158. Kitabayashi A, Hirokawa M, Miura A. The role of interleukin-10 (IL-10) in chronic B-lymphocytic leukemia: IL-10 prevents leukemic cells from apoptotic cell death. *Int J Hematol* 1995;62:99.
159. Zaki M, Douglas R, Patten N, et al. Disruption of the IFN- $\gamma$  cytokine network in chronic lymphocytic leukemia contributes to resistance of leukemic B cells to apoptosis. *Leukemia Research* 2000;24:611-21.
160. Podhorecka M, Dmoszynska A, Rolinski J, Wasik-Szczepanek E. Intracellular interleukin-2 expression by T-cell subsets in B-cell chronic lymphocytic leukemia. *Haematologica* 2001;86:549-50.
161. Bojarska-Junak A, Rolinski J, Wasik-Szczepaneko E, Kaluzny Z, Dmoszynska A. Intracellular tumor necrosis factor production by T- and B-cells in B-cell chronic lymphocytic leukemia; 2002.
162. Gallego A, Vargas JA, Castejón R, et al. Production of intracellular IL-2, TNF- $\alpha$ , and IFN- $\gamma$  by T cells in B-CLL. *Cytometry Part B: Clinical Cytometry* 2003;56B:23-9.
163. Podhorecka M, Dmoszynska A, Rolinski J. Intracellular IFN- $\gamma$  expression by CD3+/CD8+ cell subset in B-CLL patients correlates with stage of the disease. *European Journal of Haematology* 2004;73:29-35.
164. Kiaii S, Choudhury A, Mozaffari F, Kimby E, Osterborg A, Mellstedt H. Signaling molecules and cytokine production in T cells of patients with B-cell chronic lymphocytic leukemia (B-CLL): comparison of indolent and progressive disease. *Med Oncol* 2005;22:291-302.
165. Digel W, Stefanic M, Schoniger W, et al. Tumor necrosis factor induces proliferation of neoplastic B cells from chronic lymphocytic leukemia. *Blood* 1989;73:1242-6.
166. Buschle M, Campana D, Carding SR, Richard C, Hoffbrand AV, Brenner MK. Interferon gamma inhibits apoptotic cell death in B cell chronic lymphocytic leukemia. *J Exp Med* 1993;177:213-8.
167. Yan X-J, Dozmorov I, Li W, et al. Identification of outcome-correlated cytokine clusters in chronic lymphocytic leukemia. *Blood* 2011;118:5201-10.
168. Burger JA, Gribben JG. The microenvironment in chronic lymphocytic leukemia (CLL) and other B cell malignancies: Insight into disease biology and new targeted therapies. *Seminars in Cancer Biology* 2014;24:71-81.
169. DiLillo DJ, Weinberg JB, Yoshizaki A, et al. Chronic lymphocytic leukemia and regulatory B cells share IL-10 competence and immunosuppressive function. *Leukemia* 2013;27:170-82.
170. Garaud S, Morva A, Lemoine S, et al. CD5 Promotes IL-10 Production in Chronic Lymphocytic Leukemia B Cells through STAT3 and NFAT2 Activation. *The Journal of Immunology* 2011;186:4835-44.
171. Gorgun G, Holderried TAW, Zahrieh D, Neuberg D, Gribben JG. Chronic lymphocytic leukemia cells induce changes in gene expression of CD4 and CD8 T cells. *The Journal of Clinical Investigation* 2005;115:1797-805.
172. Di Ianni M, Moretti L, Terenzi A, et al. Activated autologous T cells exert an anti-B-cell chronic lymphatic leukemia effect in vitro and in vivo. *Cytotherapy* 2009;11:86-96.
173. Cha Z, Zang Y, Guo H, et al. Association of peripheral CD4+ CXCR5+ T cells with chronic lymphocytic leukemia. *Tumour biology : the journal of the International Society for Oncodevelopmental Biology and Medicine* 2013;34:3579-85.
174. Jadidi-Niaragh F, Ghalamfarsa G, Memarian A, et al. Downregulation of IL-17-producing T cells is associated with regulatory T cell expansion and disease progression in chronic lymphocytic leukemia. *Tumour biology : the journal of the International Society for Oncodevelopmental Biology and Medicine* 2013;34:929-40.
175. Hus I, Bojarska-Junak A, Chocholska S, et al. Th17/IL-17A might play a protective role in chronic lymphocytic leukemia immunity. *PLoS One* 2013;8:e78091.
176. D'Arena G, Laurenti L, Minervini MM, et al. Regulatory T-cell number is increased in chronic lymphocytic leukemia patients and correlates with progressive disease. *Leukemia Research* 2011;35:363-8.
177. Jadidi-Niaragh F, Yousefi M, Memarian A, et al. Increased frequency of CD8+ and CD4+ regulatory T cells in chronic lymphocytic leukemia: association with disease progression. *Cancer Invest* 2013;31:121-31.
178. Jak M, Mous R, Remmerswaal EB, et al. Enhanced formation and survival of CD4+ CD25hi Foxp3+ T-cells in chronic lymphocytic leukemia. *Leuk Lymphoma* 2009;50:788-801.
179. Motta M, Rassenti L, Shelvin BJ, et al. Increased expression of CD152 (CTLA-4) by normal T lymphocytes in untreated patients with B-cell chronic lymphocytic leukemia. *Leukemia* 2005;19:1788-93.
180. Linsley PS. CTLA-4 is a second receptor for the B cell activation antigen B7. *J Exp Med* 1991;174:561-9.
181. Wing K, Onishi Y, Prieto-Martin P, et al. CTLA-4 control over Foxp3+ regulatory T cell function. *Science* 2008;322:271-5.
182. Ziegler HW, Kay NE, Zarling JM. Deficiency of natural killer cell activity in patients with chronic lymphocytic leukemia. *International journal of cancer Journal international du cancer* 1981;27:321-7.
183. Kay NE, Zarling JM. Impaired natural killer activity in patients with chronic lymphocytic leukemia is associated with a deficiency of azurophilic cytoplasmic granules in putative NK cells. *Blood* 1984;63:305-9.
184. Kay NE, Zarling J. Restoration of impaired natural killer cell activity of B-chronic lymphocytic leukemia patients by recombinant interleukin-2. *Am J Hematol* 1987;24:161-7.
185. Le Garff-Tavernier M, Decocq J, de Romeuf C, et al. Analysis of CD16+CD56dim NK cells from CLL patients: evidence supporting a therapeutic strategy with optimized anti-CD20 monoclonal antibodies. *Leukemia* 2011;25:101-9.

186. Burton JD, Weitz CH, Kay NE. Malignant chronic lymphocytic leukemia B cells elaborate soluble factors that down-regulate T cell and NK function. *Am J Hematol* 1989;30:61-7.
187. Katrinakis G, Kyriakou D, Papadaki H, Kalokyri I, Markidou F, Eliopoulos GD. Defective natural killer cell activity in B-cell chronic lymphocytic leukaemia is associated with impaired release of natural killer cytotoxic factor(s) but not of tumour necrosis factor-alpha. *Acta haematologica* 1996;96:16-23.
188. Maki G, Hayes GM, Naji A, et al. NK resistance of tumor cells from multiple myeloma and chronic lymphocytic leukemia patients: implication of HLA-G. *Leukemia* 2008;22:998-1006.
189. Buechele C, Baessler T, Schmiedel BJ, et al. 4-1BB ligand modulates direct and Rituximab-induced NK-cell reactivity in chronic lymphocytic leukemia. *Eur J Immunol* 2012;42:737-48.
190. Palmer S, Hanson CA, Zent CS, et al. Prognostic importance of T and NK-cells in a consecutive series of newly diagnosed patients with chronic lymphocytic leukaemia. *Br J Haematol* 2008;141:607-14.
191. Bojarska-Junak A, Hus I, Sieklucka M, et al. Natural killer-like T CD3+/CD16+CD56+ cells in chronic lymphocytic leukemia: intracellular cytokine expression and relationship with clinical outcome. *Oncol Rep* 2010;24:803-10.
192. Itala M, Vainio O, Remes K. Functional abnormalities in granulocytes predict susceptibility to bacterial infections in chronic lymphocytic leukaemia. *Eur J Haematol* 1996;57:46-53.
193. Sawicka-Powierza J, Jablonska E, Kloczko J, Piszcz J, Garley M, Ratajczk-Wrona W. Evaluation of TNF superfamily molecules release by neutrophils and B leukemic cells of patients with chronic B - cell lymphocytic leukemia. *Neoplasma* 2011;58:45-50.
194. Kontoyiannis DP, Georgiadou SP, Wierda WG, et al. Impaired bactericidal but not fungicidal activity of polymorphonuclear neutrophils in patients with chronic lymphocytic leukemia. *Leuk Lymphoma* 2013;54:1730-3.
195. Saulep-Easton D, Vincent FB, Le Page M, et al. Cytokine-driven loss of plasmacytoid dendritic cell function in chronic lymphocytic leukemia. *Leukemia* 2014;28:2005-15.
196. Maffei R, Bulgarelli J, Fiorcari S, et al. The monocytic population in chronic lymphocytic leukemia shows altered composition and deregulation of genes involved in phagocytosis and inflammation. *Haematologica* 2013;98:1115-23.
197. Herishanu Y, Kay S, Sarid N, et al. Absolute monocyte count trichotomizes chronic lymphocytic leukemia into high risk patients with immune dysregulation, disease progression and poor survival. *Leuk Res* 2013;37:1222-8.
198. Gustafson MP, Abraham RS, Lin Y, et al. Association of an increased frequency of CD14+ HLA-DR lo/neg monocytes with decreased time to progression in chronic lymphocytic leukaemia (CLL). *Br J Haematol* 2012;156:674-6.
199. Jitschin R, Braun M, Buettner M, et al. CLL-cells induce IDOhi CD14+HLA-DRlo myeloid-derived suppressor cells that inhibit T-cell responses and promote TRegs. *Blood* 2014;124:750-60.
200. Reinart N, Nguyen P-H, Boucas J, et al. Delayed development of chronic lymphocytic leukemia in the absence of macrophage migration inhibitory factor. *Blood* 2013;121:812-21.
201. Audrito V, Serra S, Brusa D, et al. Extracellular nicotinamide phosphoribosyltransferase (NAMPT) promotes M2 macrophage polarization in chronic lymphocytic leukemia. *Blood* 2014; ePub ahead of print.
202. Burger J, Kipps TJ. Chemokine receptors and stromal cells in the homing and homeostasis of chronic lymphocytic leukemia B cells. *Leuk Lymphoma* 2002;43:461-6.
203. Burger JA, Tsukada N, Burger M, Zvaifler NJ, Dell'Aquila M, Kipps TJ. Blood-derived nurse-like cells protect chronic lymphocytic leukemia B cells from spontaneous apoptosis through stromal cell-derived factor-1. *Blood* 2000;96:2655-63.
204. Ysebaert L, Fournie JJ. Genomic and phenotypic characterization of nurse-like cells that promote drug resistance in chronic lymphocytic leukemia. *Leukemia and Lymphoma* 2011;52:1404-6.
205. Filip AA, B. C, Koczkodaj D, Wasik-Szczepanek E, Piersiak T, Dmoszynska A. Circulating microenvironment of CLL: Are nurse-like cells related to tumor-associated macrophages? *Blood Cells, Molecules, and Diseases* 2013;50:263-70.
206. Tsukada N, Burger JA, Zvaifler NJ, Kipps TJ. Distinctive features of nurse like cells that differentiate in the context of chronic lymphocytic leukemia. *Blood* 2002;99:1030-7.
207. Buerkle A, Niedermeier M, Schmitt-Gräff A, Wierda WG, Keating MJ, Burger JA. Overexpression of the CXCR5 chemokine receptor, and its ligand, CXCL13 in B-cell chronic lymphocytic leukemia. *Blood* 2007;110:3316-25.
208. Virgilio L, Isobe M, Narducci MG, et al. Chromosome walking on the TCL1 locus involved in T-cell neoplasia. *Proceedings of the National Academy of Sciences* 1993;90:9275-9.
209. Virgilio L, Narducci MG, Isobe M, et al. Identification of the TCL1 gene involved in T-cell malignancies. *Proceedings of the National Academy of Sciences* 1994;91:12530-4.
210. Pekarsky Y, Hallas C, Isobe M, Russo G, Croce CM. Abnormalities at 14q32.1 in T cell malignancies involve two oncogenes. *Proceedings of the National Academy of Sciences* 1999;96:2949-51.
211. Sugimoto J, Hatakeyama T, Narducci MG, Russo G, Isobe M. Identification of the TCL1/MTCP1-like 1 (TML1) Gene from the Region Next to the TCL1 Locus. *Cancer Research* 1999;59:2313-7.
212. Bichi R, Shinton SA, Martin ES, et al. Human chronic lymphocytic leukemia modeled in mouse by targeted TCL1 expression. *Proceedings of the National Academy of Sciences* 2002;99:6955-60.
213. Shaw AC, Swat W, Ferrini R, Davidson L, Alt FW. Activated Ras Signals Developmental Progression of Recombinase-activating Gene (RAG)-deficient Pro-B Lymphocytes. *The Journal of Experimental Medicine* 1999;189:123-9.

214. Zanesi N, Aqeilan R, Drusco A, et al. Effect of Rapamycin on Mouse Chronic Lymphocytic Leukemia and the Development of Nonhematopoietic Malignancies in Eu-TCL1 Transgenic Mice. *Cancer Research* 2006;66:915-20.
215. Johnson AJ, Lucas DM, Muthusamy N, et al. Characterization of the TCL-1 transgenic mouse as a preclinical drug development tool for human chronic lymphocytic leukemia. *Blood* 2006;108:1334-8.
216. Gorgun G, Ramsay AG, Holderried TAW, et al. Eu-TCL1 mice represent a model for immunotherapeutic reversal of chronic lymphocytic leukemia-induced T-cell dysfunction. *Proceedings of the National Academy of Sciences* 2009;106:6250-5.
217. Chen S, Batiwalla F, Holodick NE, et al. Autoantigen can promote progression to a more aggressive TCL1 leukemia by selecting variants with enhanced B-cell receptor signaling. *Proceedings of the National Academy of Sciences* 2013;110:E1500-E7.
218. Yan XJ, Albesiano E, Zanesi N, et al. B cell receptors in TCL1 transgenic mice resemble those of aggressive, treatment-resistant human chronic lymphocytic leukemia. *Proceedings of the National Academy of Sciences* 2006;103:11713-8.
219. Chen SS, Raval A, Johnson AJ, Hertlein E, Liu TH, Jin VX. Epigenetic changes during disease progression in a murine model of human chronic lymphocytic leukemia. *Proc Natl Acad Sci USA* 2009;106:13433-8.
220. Hofbauer JP, Heyder C, Denk U, et al. Development of CLL in the TCL1 transgenic mouse model is associated with severe skewing of the T-cell compartment homologous to human CLL. *Leukemia* 2011;25:1452-8.
221. Lutzny G, Kocher T, Schmidt-Suppran M, et al. Protein Kinase C- $\beta$ -Dependent Activation of NF- $\kappa$ B in Stromal Cells Is Indispensable for the Survival of Chronic Lymphocytic Leukemia B Cells In Vivo. *Cancer Cell* 2013;23:77-92.
222. Chinn IK, Blackburn CC, Manley NR, Sempowski GD. Changes in primary lymphoid organs with aging. *Seminars in Immunology* 2012;24:309-20.
223. Pinchuk L, Filipov N. Differential effects of age on circulating and splenic leukocyte populations in C57BL/6 and BALB/c male mice. *Immunity & Ageing* 2008;5:1.
224. Clementi M, Forabosco P, Amadori A, et al. CD4 and CD8 T lymphocyte inheritance. Evidence for major autosomal recessive genes. *Hum Genet* 1999;105:337-42.
225. Kraal G, Weissmann IL. Genetic control of T-cell subset representation in inbred mice. *Immunogenetics* 1983;18:585-92.
226. Merkel O, Wacht N, Siffert E, et al. Actinomycin D induces p53-independent cell death and prolongs survival in high-risk chronic lymphocytic leukemia. *Leukemia* 2012;26:2508-16.
227. Suljagic M, Longo PG, Bennardo S, et al. The Syk inhibitor fostamatinib disodium (R788) inhibits tumor growth in the Eu-TCL1 transgenic mouse model of CLL by blocking antigen-dependent B-cell receptor signaling. *Blood* 2010;116:4894-905.
228. Woyach JA, Bojnik E, Ruppert AS, et al. Bruton's tyrosine kinase (BTK) function is important to the development and expansion of chronic lymphocytic leukemia (CLL). *Blood* 2014;123:1207-13.
229. Lucas DM, Edwards RB, Lozanski G, et al. The novel plant-derived agent silvestrol has B-cell selective activity in chronic lymphocytic leukemia and acute lymphoblastic leukemia in vitro and in vivo. *Blood* 2009;113:4656-66.
230. Lapalombella R, Sun Q, Williams K, et al. Selective inhibitors of nuclear export show that CRM1/XPO1 is a target in chronic lymphocytic leukemia. *Blood* 2012;120:4621-34.
231. Hertlein E, Wagner AJ, Jones J, et al. 17-DMAG targets the nuclear factor-kappa B family of proteins to induce apoptosis in chronic lymphocytic leukemia: clinical implications of HSP90 inhibition. *Blood* 2010;116:45-53.
232. Wu Q-L, Buhtoiarov IN, Sondel PM, Rakhmilevich AL, Ranheim EA. Tumoricidal Effects of Activated Macrophages in a Mouse Model of Chronic Lymphocytic Leukemia. *The Journal of Immunology* 2009;182:6771-8.
233. Klein U, Lia M, Crespo M, et al. The DLEU2/miR-15a/16-1 Cluster Controls B Cell Proliferation and Its Deletion Leads to Chronic Lymphocytic Leukemia. *Cancer Cell* 2010;17:28-40.
234. Lia M, Carette A, Tang H, et al. Functional dissection of the chromosome 13q14 tumor-suppressor locus using transgenic mouse lines. *Blood* 2012;119:2981-90.
235. Zapata JM, Krajewska M, Morse HC, Choi Y, Reed JC. TNF receptor-associated factor (TRAF) domain and Bcl-2 cooperate to induce small B cell lymphoma/chronic lymphocytic leukemia in transgenic mice. *Proceedings of the National Academy of Sciences of the United States of America* 2004;101:16600-5.
236. Planelles L, Carvalho-Pinto CE, Hardenberg G, et al. APRIL promotes B-1 cell-associated neoplasm. *Cancer Cell* 2004;6:399-408.
237. Zhang W, Kater AP, Widhopf GF, et al. B-cell activating factor and v-Myc myelocytomatosis viral oncogene homolog (c-Myc) influence progression of chronic lymphocytic leukemia. *Proceedings of the National Academy of Sciences* 2010;107:18956-60.
238. Phillips JA, Mehta K, Fernandez C, Raveche ES. The NZB Mouse as a Model for Chronic Lymphocytic Leukemia. *Cancer Research* 1992;52:437-43.
239. Salerno E, Yuan Y, Scaglione BJ, et al. The New Zealand black mouse as a model for the development and progression of chronic lymphocytic leukemia. *Cytometry Part B: Clinical Cytometry* 2010;78B:S98-S109.

240. Raveche ES, Salerno E, Scaglione BJ, et al. Abnormal microRNA-16 locus with synteny to human 13q14 linked to CLL in NZB mice. *Blood* 2007;109:5079-86.
241. Santanam U, Zanesi N, Efanov A, et al. Chronic lymphocytic leukemia modeled in mouse by targeted miR-29 expression. *Proceedings of the National Academy of Sciences* 2010;107:12210-5.
242. Costinean S, Zanesi N, Pekarsky Y, et al. Pre-B cell proliferation and lymphoblastic leukemia/high-grade lymphoma in Eu-miR155 transgenic mice. *Proceedings of the National Academy of Sciences* 2006;103:7024-9.
243. Xiao C, Srinivasan L, Calado DP, et al. Lymphoproliferative disease and autoimmunity in mice with increased miR-17-92 expression in lymphocytes. *Nat Immunol* 2008;9:405-14.
244. Ventura A, Young AG, Winslow MM, et al. Targeted Deletion Reveals Essential and Overlapping Functions of the miR-17-92 Family of miRNA Clusters. *Cell* 2008;132:875-86.
245. Enomoto Y, Kitaura J, Hatakeyama K, et al. E[ $\mu$ ]/miR-125b transgenic mice develop lethal B-cell malignancies. *Leukemia* 2011;25:1849-56.
246. Widhopf GF, 2nd, Cui B, Ghia EM, et al. ROR1 can interact with TCL1 and enhance leukemogenesis in Emu-TCL1 transgenic mice. *Proc Natl Acad Sci U S A* 2014;111:793-8.
247. Shukla V, Ma S, Hardy RR, Joshi SS, Lu R. A role for IRF4 in the development of CLL. *2013* 2013;122:2848-55.
248. ter Brugge PJ, Ta VBT, de Bruijn MJW, et al. A mouse model for chronic lymphocytic leukemia based on expression of the SV40 large T antigen. *Blood* 2009;114:119-27.
249. Pekarsky Y, Koval A, Hallas C, et al. Tcl1 enhances Akt kinase activity and mediates its nuclear translocation. *Proceedings of the National Academy of Sciences* 2000;97:3028-33.
250. Pekarsky Y, Palamarchuk A, Maximov V, et al. Tcl1 functions as a transcriptional regulator and is directly involved in the pathogenesis of CLL. *Proceedings of the National Academy of Sciences* 2008;105:19643-8.
251. Zanesi N, Balatti V, Riordan J, et al. A Sleeping Beauty screen reveals NF- $\kappa$ B activation in CLL mouse model. *Blood* 2013;121:4355-8.
252. Palamarchuk A, Yan P, Zanesi N, et al. Tcl1 protein functions as an inhibitor of de novo DNA methylation in B-cell chronic lymphocytic leukemia (CLL). *Proc Natl Acad Sci U S A* 2012;109:2555-60.
253. Holler C, Pinon JD, Denk U, Heyder C, Hofbauer S, Greil R. PKC $\beta$  is essential for the development of chronic lymphocytic leukemia in the TCL1 transgenic mouse model: validation of PKC $\beta$  as a therapeutic target in chronic lymphocytic leukemia. *Blood* 2009;113:2791-4.
254. Nganga VK, Palmer VL, Naushad H, et al. Accelerated progression of chronic lymphocytic leukemia in Emu-TCL1 mice expressing catalytically inactive RAG1. *Blood* 2013;121:3855-66, S1-16.
255. Bertilaccio MTS, Simonetti G, Dagklis A, et al. Lack of TIR8/SIGIRR triggers progression of chronic lymphocytic leukemia in mouse models. *Blood* 2011;118:660-9.
256. Tang CH, Ranatunga S, Kriss CL, et al. Inhibition of ER stress-associated IRE-1/XBP-1 pathway reduces leukemic cell survival. *J Clin Invest* 2014;124:2585-98.
257. Liu J, Chen G, Feng L, et al. Loss of p53 and altered miR15-a/16-1 short right arrowMCL-1 pathway in CLL: insights from TCL1-Tg;p53(-/-) mouse model and primary human leukemia cells. *Leukemia* 2014;28:118-28.
258. Chen SS, Claus R, Lucas DM, et al. Silencing of the inhibitor of DNA binding protein 4 (ID4) contributes to the pathogenesis of mouse and human CLL. *Blood* 2011;117:862-71.
259. Lascano V, Guadagnoli M, Schot JG, et al. Chronic lymphocytic leukemia disease progression is accelerated by APRIL-TACI interaction in the TCL1 transgenic mouse model. *Blood* 2013;122:3960-3.
260. Enzler T, Kater AP, Zhang W, Widhopf GF, Chuang HY, Lee J. Chronic lymphocytic leukemia of Emu-TCL1 transgenic mice undergoes rapid cell turnover that can be offset by extrinsic CD257 to accelerate disease progression. *Blood* 2009;114:4469-76.
261. Fedorchenko O, Stiefelhagen M, Peer-Zada AA, et al. CD44 regulates the apoptotic response and promotes disease development in chronic lymphocytic leukemia. *Blood* 2013;121:4126-36.
262. Wu Q-L, Zierold C, Ranheim EA. Dysregulation of Frizzled 6 is a critical component of B-cell leukemogenesis in a mouse model of chronic lymphocytic leukemia. *Blood* 2009;113:3031-9.
263. Troeger A, Johnson A, Wood J, et al. RhoH is critical for cell-microenvironment interactions in chronic lymphocytic leukemia in mice and humans. *Blood* 2012.
264. Scielzo C, Bertilaccio MT, Simonetti G, et al. HS1 has a central role in the trafficking and homing of leukemic B cells. *Blood* 2010;116:3537-46.
265. Simonetti G, Bertilaccio MTS, Ghia P, Klein U. Mouse models in the study of chronic lymphocytic leukemia pathogenesis and therapy. *Blood* 2014.
266. Bertilaccio MT, Scielzo C, Simonetti G, et al. Xenograft models of chronic lymphocytic leukemia: problems, pitfalls and future directions. *Leukemia*;27:534-40.
267. Kobayashi R, Picchio G, Kirven M, et al. Transfer of human chronic lymphocytic leukemia to mice with severe combined immune deficiency. *Leukemia Research* 1992;16:1013-23.
268. Hummel JL, Lichty BD, Reis M, Dube I, Kamel-Reid S. Engraftment of human chronic lymphocytic leukemia cells in SCID mice: in vivo and in vitro studies. *Leukemia* 1996;10:1370-6.
269. Shimoni A, Marcus H, Canaan A, et al. A model for human B-chronic lymphocytic leukemia in human/mouse radiation chimera: evidence for tumor-mediated suppression of antibody production in low-stage disease. *Blood* 1997;89:2210-8.

270. Shimoni A, Marcus H, Dekel B, et al. Autologous T cells control B-chronic lymphocytic leukemia tumor progression in human->mouse radiation chimera. *Cancer Res* 1999;59:5968-74.
271. Durig J, Ebeling P, Grabellus F, Sorg UR, Mollmann M, Schutt P. A novel nonobese diabetic/severe combined immunodeficient xenograft model for chronic lymphocytic leukemia reflects important clinical characteristics of the disease. *Cancer Res* 2007;67:8653-61.
272. Aydin S, Grabellus F, Eisele L, et al. Investigating the role of CD38 and functionally related molecular risk factors in the CLL NOD/SCID xenograft model. *European Journal of Haematology* 2011;87:10-9.
273. Bagnara D, Kaufman MS, Calissano C, et al. A novel adoptive transfer model of chronic lymphocytic leukemia suggests a key role for T lymphocytes in the disease. *Blood* 2011;117:5463-72.
274. Kikushige Y, Ishikawa F, Miyamoto T, et al. Self-renewing hematopoietic stem cell is the primary target in pathogenesis of human chronic lymphocytic leukemia. *Cancer Cell*;20:246-59.
275. Herman SE, Sun X, McAuley EM, et al. Modeling tumor-host interactions of chronic lymphocytic leukemia in xenografted mice to study tumor biology and evaluate targeted therapy. *Leukemia* 2013;27:2311-21.
276. Rudd CE, Taylor A, Schneider H. CD28 and CTLA-4 coreceptor expression and signal transduction. *Immunol Rev* 2009;229:12-26.
277. Powell JD, Ragheb JA, Kitagawa-Sakakida S, Schwartz RH. Molecular regulation of interleukin-2 expression by CD28 co-stimulation and anergy. *Immunol Rev* 1998;165:287-300.
278. Ise W, Kohyama M, Nutsch KM, et al. CTLA-4 suppresses the pathogenicity of self antigen-specific T cells by cell-intrinsic and cell-extrinsic mechanisms. *Nat Immunol* 2010;11:129-35.
279. Ishida Y, Agata Y, Shibahara K, Honjo T. Induced expression of PD-1, a novel member of the immunoglobulin gene superfamily, upon programmed cell death. *EMBO J* 1992;11:3887-95.
280. Shinohara T, Taniwaki M, Ishida Y, Kawaichi M, Honjo T. Structure and Chromosomal Localization of the Human PD-1 Gene (PDCD1). *Genomics* 1994;23:704-6.
281. Finger LR, Pu J, Wasserman R, et al. The human PD-1 gene: complete cDNA, genomic organization, and developmentally regulated expression in B cell progenitors. *Gene* 1997;197:177-87.
282. Nishimura H, Agata Y, Kawasaki A, et al. Developmentally regulated expression of the PD-1 protein on the surface of double-negative (CD4-CD8-) thymocytes. *Int Immunol* 1996;8:773-80.
283. Agata Y, Kawasaki A, Nishimura H, et al. Expression of the PD-1 antigen on the surface of stimulated mouse T and B lymphocytes. *International Immunology* 1996;8:765-72.
284. Nishimura H, Minato N, Nakano T, Honjo T. Immunological studies on PD-1 deficient mice: implication of PD-1 as a negative regulator for B cell responses. *Int Immunol* 1998;10:1563-72.
285. Nishimura H, Nose M, Hiai H, Minato N, Honjo T. Development of lupus-like autoimmune diseases by disruption of the PD-1 gene encoding an ITIM motif-carrying immunoreceptor. *Immunity* 1999;11:141-51.
286. Nishimura H. Autoimmune dilated cardiomyopathy in PD-1 receptor-deficient mice. *Science* 2001;291:319-22.
287. Dong H, Zhu G, Tamada K, Chen L. B7-H1, a third member of the B7 family, co-stimulates T-cell proliferation and interleukin-10 secretion. *Nat Med* 1999;5:1365-9.
288. Freeman GJ, Long AJ, Iwai Y, et al. Engagement of the PD-1 immunoinhibitory receptor by a novel B7 family member leads to negative regulation of lymphocyte activation. *J Exp Med* 2000;192:1027-34.
289. Butte MJ, Keir ME, Phamduy TB, Sharpe AH, Freeman GJ. Programmed death-1 ligand 1 interacts specifically with the B7-1 costimulatory molecule to inhibit T cell responses. *Immunity* 2007;27:111-22.
290. Ishida M, Iwai Y, Tanaka Y, et al. Differential expression of PD-L1 and PD-L2, ligands for an inhibitory receptor PD-1, in the cells of lymphohematopoietic tissues. *Immunology Letters* 2002;84:57-62.
291. Yamazaki T, Akiba H, Iwai H, et al. Expression of programmed death 1 ligands by murine T cells and APC. *J Immunol* 2002;169:5538-45.
292. Latchman Y, Wood CR, Chernova T, et al. PD-L2 is a second ligand for PD-1 and inhibits T cell activation. *Nat Immunol* 2001;2:261-8.
293. Keir ME. Tissue expression of PD-L1 mediates peripheral T cell tolerance. *J Exp Med* 2006;203:883-95.
294. Dong H, Zhu G, Tamada K, Flies DB, van Deursen JMA, Chen L. B7-H1 Determines Accumulation and Deletion of Intrahepatic CD8+ T Lymphocytes. *Immunity* 2004;20:327-36.
295. Latchman YE, Liang SC, Wu Y, et al. PD-L1-deficient mice show that PD-L1 on T cells, antigen-presenting cells, and host tissues negatively regulates T cells. *Proc Natl Acad Sci U S A* 2004;101:10691-6.
296. Akbari O, Stock P, Singh AK, et al. PD-L1 and PD-L2 modulate airway inflammation and iNKT-cell-dependent airway hyperreactivity in opposing directions. *Mucosal Immunol* 2009;3:81-91.
297. Shin T. In vivo costimulatory role of B7-DC in tuning T helper cell 1 and cytotoxic T lymphocyte responses. *J Exp Med* 2005;201:1531-41.
298. Karwacz K, Bricogne C, MacDonald D, et al. PD-L1 co-stimulation contributes to ligand-induced T cell receptor down-modulation on CD8+ T cells. *EMBO Mol Med* 2011;3:581-92.
299. Sheppard K-A, Fitz LJ, Lee JM, et al. PD-1 inhibits T-cell receptor induced phosphorylation of the ZAP70/CD3 zeta signalosome and downstream signaling to PKC theta. *FEBS Letters* 2004;574:37-41.

300. Riley JL. PD-1 signaling in primary T cells. *Immunol Rev* 2009;229:114-25.
301. Chemnitz JM, Parry RV, Nichols KE, June CH, Riley JL. SHP-1 and SHP-2 associate with immunoreceptor tyrosine-based switch motif of programmed death 1 upon primary human T cell stimulation, but only receptor ligation prevents T cell activation. *J Immunol* 2004;173:945-54.
302. Yokosuka T, Takamatsu M, Kobayashi-Imanishi W, Hashimoto-Tane A, Azuma M, Saito T. Programmed cell death 1 forms negative costimulatory microclusters that directly inhibit T cell receptor signaling by recruiting phosphatase SHP2. *J Exp Med* 2012;209:1201-17.
303. Kwon J, Qu CK, Maeng JS, Falahati R, Lee C, Williams MS. Receptor-stimulated oxidation of SHP-2 promotes T-cell adhesion through SLP-76-ADAP. *EMBO J* 2005;24:2331-41.
304. Morgan MM, Labno CM, Van Seventer GA, Denny MF, Straus DB, Burkhardt JK. Superantigen-Induced T Cell:B Cell Conjugation Is Mediated by LFA-1 and Requires Signaling Through Lck, But Not ZAP-70. *The Journal of Immunology* 2001;167:5708-18.
305. Pentcheva-Hoang T, Chen L, Pardoll DM, Allison JP. Programmed death-1 concentration at the immunological synapse is determined by ligand affinity and availability. *Proc Natl Acad Sci U S A* 2007;104:17765-70.
306. Youngnak P, Kozono Y, Kozono H, et al. Differential binding properties of B7-H1 and B7-DC to programmed death-1. *Biochemical and Biophysical Research Communications* 2003;307:672-7.
307. Patsoukis N, Brown J, Petkova V, Liu F, Li L, Boussiotis VA. Selective effects of PD-1 on Akt and Ras pathways regulate molecular components of the cell cycle and inhibit T cell proliferation. *Sci Signal* 2012;5:ra46.
308. Patsoukis N, Sari D, Boussiotis VA. PD-1 inhibits T cell proliferation by upregulating p27 and p15 and suppressing Cdc25A. *Cell Cycle* 2012;11:4305-9.
309. Parry RV, Chemnitz JM, Frauwirth KA, et al. CTLA-4 and PD-1 receptors inhibit T-cell activation by distinct mechanisms. *Mol Cell Biol* 2005;25:9543-53.
310. Gibbons RM, Liu X, Pulko V, et al. B7-H1 limits the entry of effector CD8(+) T cells to the memory pool by upregulating Bim. *Oncol Immunology* 2012;1:1061-73.
311. Dong H. Tumor-associated B7-H1 promotes T-cell apoptosis: a potential mechanism of immune evasion. *Nature Med* 2002;8:793-800.
312. Nomi T, Sho M, Akahori T, et al. Clinical Significance and Therapeutic Potential of the Programmed Death-1 Ligand/Programmed Death-1 Pathway in Human Pancreatic Cancer. *Clinical Cancer Research* 2007;13:2151-7.
313. Ohigashi Y, Sho M, Yamada Y, et al. Clinical Significance of Programmed Death-1 Ligand-1 and Programmed Death-1 Ligand-2 Expression in Human Esophageal Cancer. *Clinical Cancer Research* 2005;11:2947-53.
314. Hamanishi J, Mandai M, Iwasaki M, et al. Programmed cell death 1 ligand 1 and tumor-infiltrating CD8+ T lymphocytes are prognostic factors of human ovarian cancer. *Proc Natl Acad Sci U S A* 2007;104:3360-5.
315. Wang L, Qian J, Lu Y, et al. Immune evasion of mantle cell lymphoma: expression of B7-H1 leads to inhibited T-cell response to and killing of tumor cells. *Haematologica* 2013;98:1458-66.
316. Yamamoto R, Nishikori M, Kitawaki T, et al. PD-1/PD-1 ligand interaction contributes to immunosuppressive microenvironment of Hodgkin lymphoma. *Blood* 2008;111:3220-4.
317. Steidl C, Shah SP, Woolcock BW, et al. MHC class II transactivator CIITA is a recurrent gene fusion partner in lymphoid cancers. *Nature* 2011;471:377-81.
318. Kondo A, Yamashita T, Tamura H, et al. Interferon- $\gamma$  and tumor necrosis factor- $\alpha$  induce an immunoinhibitory molecule, B7-H1, via nuclear factor- $\kappa$ B activation in blasts in myelodysplastic syndromes. *Blood* 2010;116:1124-31.
319. Yang H, Bueso-Ramos C, DiNardo C, et al. Expression of PD-L1, PD-L2, PD-1 and CTLA4 in myelodysplastic syndromes is enhanced by treatment with hypomethylating agents. *Leukemia* 2014;28:1280-8.
320. Chen X, Liu S, Wang L, Zhang W, Ji Y, Ma X. Clinical significance of B7-H1 (PD-L1) expression in human acute leukemia. *Cancer Biol Ther* 2008;7:622-7.
321. Liu J, Hamrouni A, Wolowiec D, et al. Plasma cells from multiple myeloma patients express B7-H1 (PD-L1) and increase expression after stimulation with IFN- $\gamma$  and TLR ligands via a MyD88-, TRAF6-, and MEK-dependent pathway. *Blood* 2007;110:296-304.
322. Norde WJ, Maas F, Hobo W, et al. PD-1/PD-L1 Interactions Contribute to Functional T-Cell Impairment in Patients Who Relapse with Cancer After Allogeneic Stem Cell Transplantation. *Cancer Research* 2011;71:5111-22.
323. Joos S, Otano-Joos M, Ziegler S, et al. Primary mediastinal (thymic) B-cell lymphoma is characterized by gains of chromosomal material including 9p and amplification of the REL gene; 1996.
324. Rosenwald A, Wright G, Leroy K, et al. Molecular diagnosis of primary mediastinal B cell lymphoma identifies a clinically favorable subgroup of diffuse large B cell lymphoma related to Hodgkin lymphoma. *J Exp Med* 2003;198:851-62.
325. Green MR, Monti S, Rodig SJ, et al. Integrative analysis reveals selective 9p24.1 amplification, increased PD-1 ligand expression, and further induction via JAK2 in nodular sclerosing Hodgkin lymphoma and primary mediastinal large B-cell lymphoma. *Blood* 2010;116:3268-77.
326. Marzec M. Oncogenic kinase NPM/ALK induces through STAT3 expression of immunosuppressive protein CD274 (PD-L1, B7-H1). *Proc Natl Acad Sci USA* 2008;105:20852-7.

327. Parsa AT. Loss of tumor suppressor PTEN function increases B7-H1 expression and immunoresistance in glioma. *Nature Med* 2007;13:84-8.
328. Gong A-Y, Zhou R, Hu G, et al. MicroRNA-513 Regulates B7-H1 Translation and Is Involved in IFN- $\gamma$ -induced B7-H1 Expression in Cholangiocytes. *The Journal of Immunology* 2009;182:1325-33.
329. Berthon C, Driss V, Liu J, et al. In acute myeloid leukemia, B7-H1 (PD-L1) protection of blasts from cytotoxic T cells is induced by TLR ligands and interferon-gamma and can be reversed using MEK inhibitors. *Cancer Immunology, Immunotherapy* 2010;59:1839-49.
330. Lee S-J, Jang B-C, Lee S-W, et al. Interferon regulatory factor-1 is prerequisite to the constitutive expression and IFN- $\gamma$ -induced upregulation of B7-H1 (CD274). *FEBS Letters* 2006;580:755-62.
331. Liu Y, Zeng B, Zhang Z, Zhang Y, Yang R. B7-H1 on myeloid-derived suppressor cells in immune suppression by a mouse model of ovarian cancer. *Clin Immunol* 2008;129:471-81.
332. Pardoll DM. The blockade of immune checkpoints in cancer immunotherapy. *Nat Rev Cancer* 2012;12:252-64.
333. Wang J, Cheng L, Wondimu Z, Swain M, Santamaria P, Yang Y. Cutting Edge: CD28 Engagement Releases Antigen-Activated Invariant NKT Cells from the Inhibitory Effects of PD-1. *The Journal of Immunology* 2009;182:6644-7.
334. Okazaki T, Maeda A, Nishimura H, Kurosaki T, Honjo T. PD-1 immunoreceptor inhibits B cell receptor-mediated signaling by recruiting src homology 2-domain-containing tyrosine phosphatase 2 to phosphotyrosine. *Proceedings of the National Academy of Sciences* 2001;98:13866-71.
335. Yao S, Wang S, Zhu Y, et al. PD-1 on dendritic cells impedes innate immunity against bacterial infection. *Blood* 2009;113:5811-8.
336. Hanahan D, Weinberg RA. The Hallmarks of Cancer. *Cell* 2000;100:57-70.
337. Hanahan D, Weinberg Robert A. Hallmarks of Cancer: The Next Generation. *Cell* 2011;144:646-74.
338. Schreiber RD, Old LJ, Smyth MJ. Cancer Immunoediting: Integrating Immunity's Roles in Cancer Suppression and Promotion. *Science* 2011;331:1565-70.
339. Gross G, Waks T, Eshhar Z. Expression of immunoglobulin-T-cell receptor chimeric molecules as functional receptors with antibody-type specificity. *Proceedings of the National Academy of Sciences* 1989;86:10024-8.
340. Cartellieri M, Bachmann M, Feldmann A, et al. Chimeric Antigen Receptor-Engineered T Cells for Immunotherapy of Cancer. *Journal of Biomedicine and Biotechnology* 2010;2010.
341. Brentjens RJ, Curran KJ. Novel cellular therapies for leukemia: CAR-modified T cells targeted to the CD19 antigen. *ASH Education Program Book* 2012;2012:143-51.
342. Porter DL, Levine BL, Kalos M, Bagg A, June CH. Chimeric Antigen Receptor Modified T Cells in Chronic Lymphoid Leukemia. *New England Journal of Medicine* 2011;365:725-33.
343. Kohn DB, Dotti G, Brentjens R, et al. CARs on Track in the Clinic. *Mol Ther* 2011;19:432-8.
344. Stauss HJ, Morris EC. Immunotherapy with gene-modified T cells: limiting side effects provides new challenges. *Gene Ther* 2013;20:1029-32.
345. Xu XJ, Tang YM. Cytokine release syndrome in cancer immunotherapy with chimeric antigen receptor engineered T cells. *Cancer letters* 2014;343:172-8.
346. Brentjens RJ, Riviere I, Park JH, et al. Safety and persistence of adoptively transferred autologous CD19-targeted T cells in patients with relapsed or chemotherapy refractory B-cell leukemias. *Blood* 2011;118:4817-28.
347. Porter DL, Levine BL, Kalos M, Bagg A, June CH. Chimeric antigen receptor-modified T cells in chronic lymphoid leukemia. *N Engl J Med* 2011;365:725-33.
348. Kalos M, Levine BL, Porter DL, et al. T cells with chimeric antigen receptors have potent antitumor effects and can establish memory in patients with advanced leukemia. *Sci Transl Med* 2011;3:95ra73.
349. Kochenderfer JN, Dudley ME, Carpenter RO, et al. Donor-derived CD19-targeted T cells cause regression of malignancy persisting after allogeneic hematopoietic stem cell transplantation. *Blood* 2013;122:4129-39.
350. Dubovsky JA, Beckwith KA, Natarajan G, et al. Ibrutinib is an irreversible molecular inhibitor of ITK driving a Th1-selective pressure in T lymphocytes. *Blood* 2013;122:2539-49.
351. Burger M, Hartmann T, Krome M, et al. Small peptide inhibitors of the CXCR4 chemokine receptor (CD184) antagonize the activation, migration, and antiapoptotic responses of CXCL12 in chronic lymphocytic leukemia B cells. *Blood* 2005;106:1824-30.
352. Buchner M, Brantner P, Stickel N, et al. The microenvironment differentially impairs passive and active immunotherapy in chronic lymphocytic leukaemia – CXCR4 antagonists as potential adjuvants for monoclonal antibodies. *British Journal of Haematology* 2010;151:167-78.
353. Buchner M, Baer C, Prinz G, et al. Spleen tyrosine kinase inhibition prevents chemokine- and integrin-mediated stromal protective effects in chronic lymphocytic leukemia. *Blood* 2010;115:4497-506.
354. Hoellenriegel J, Coffey GP, Sinha U, et al. Selective, novel spleen tyrosine kinase (Syk) inhibitors suppress chronic lymphocytic leukemia B-cell activation and migration. *Leukemia* 2012;26:1576-83.
355. Herman SEM, Gordon AL, Wagner AJ, et al. Phosphatidylinositol 3-kinase- $\gamma$  inhibitor CAL-101 shows promising preclinical activity in chronic lymphocytic leukemia by antagonizing intrinsic and extrinsic cellular survival signals. *Blood* 2010;116:2078-88.

356. Fecteau JF, Bharati IS, O'Hayre M, Handel TM, Kipps TJ, Messmer D. Sorafenib-induced apoptosis of chronic lymphocytic leukemia cells is associated with downregulation of RAF and myeloid cell leukemia sequence 1 (Mcl-1). *Mol Med* 2012;18:19-28.
357. Lopez-Guerra M, Xargay-Torrent S, Perez-Galan P, et al. Sorafenib targets BCR kinases and blocks migratory and microenvironmental survival signals in CLL cells. *Leukemia* 2012;26:1429-32.
358. Balakrishnan K, Burger JA, Wierda WG, Gandhi V. AT-101 induces apoptosis in CLL B cells and overcomes stromal cell-mediated Mcl-1 induction and drug resistance. *Blood* 2009;113:149-53.
359. Armand P, Nagler A, Weller EA, et al. Disabling Immune Tolerance by Programmed Death-1 Blockade With Pidilizumab After Autologous Hematopoietic Stem-Cell Transplantation for Diffuse Large B-Cell Lymphoma: Results of an International Phase II Trial. *Journal of Clinical Oncology* 2013;31:4199-206.
360. Westin JR, Chu F, Zhang M, et al. Safety and activity of PD1 blockade by pidilizumab in combination with rituximab in patients with relapsed follicular lymphoma: a single group, open-label, phase 2 trial. *The Lancet Oncology* 2014;15:69-77.
361. Brahmer JR, Tykodi SS, Chow LQM, et al. Safety and Activity of Anti-PD-L1 Antibody in Patients with Advanced Cancer. *New England Journal of Medicine* 2012;366:2455-65.
362. Berger R, Rotem-Yehudar R, Slama G, et al. Phase I Safety and Pharmacokinetic Study of CT-011, a Humanized Antibody Interacting with PD-1, in Patients with Advanced Hematologic Malignancies. *Clinical Cancer Research* 2008;14:3044-51.
363. Brahmer JR, Drake CG, Wollner I, et al. Phase I Study of Single-Agent Anti-Programmed Death-1 (MDX-1106) in Refractory Solid Tumors: Safety, Clinical Activity, Pharmacodynamics, and Immunologic Correlates. *Journal of Clinical Oncology* 2010;28:3167-75.
364. Topalian SL, Hodi FS, Brahmer JR, et al. Safety, Activity, and Immune Correlates of Anti-PD-1 Antibody in Cancer. *New England Journal of Medicine* 2012;366:2443-54.
365. Topalian SL, Sznol M, McDermott DF, et al. Survival, Durable Tumor Remission, and Long-Term Safety in Patients With Advanced Melanoma Receiving Nivolumab. *Journal of Clinical Oncology* 2014;32:1020-30.
366. Hamid O, Robert C, Daud A, et al. Safety and Tumor Responses with Lambrolizumab (Anti-PD-1) in Melanoma. *New England Journal of Medicine* 2013;369:134-44.
367. Robert C, Ribas A, Wolchok JD, et al. Anti-programmed-death-receptor-1 treatment with pembrolizumab in ipilimumab-refractory advanced melanoma: a randomised dose-comparison cohort of a phase 1 trial. *The Lancet* 2014;384:1109-17.
368. Russell WMS, Burch RL. *The principles of humane experimental technique*: Methuen; 1959.
369. European Union Directive 2010/63/EU of the European Parliament and of the Council of 22 September 2010 on the protection of animals used for scientific purposes. *OJEU L 276/33*. <http://eur-lex.europa.eu/legal-content/EN/TXT/?uri=CELEX:32010L0063#text> last accessed September 2014.
370. United States Code, 2012 Edition, Title 7 – agriculture, Chapter 54 – Transportation, Sale, and Handling of Certain Animals. <http://www.law.cornell.edu/uscode/text/7/chapter-54>. Last accessed September 2014.
371. Lundberg P, Skoda R. Hematology Testing in Mice. In: *Current Protocols in Mouse Biology*: John Wiley & Sons, Inc.; 2011.
372. Quah BJ, Warren HS, Parish CR. Monitoring lymphocyte proliferation in vitro and in vivo with the intracellular fluorescent dye carboxyfluorescein diacetate succinimidyl ester. *Nature protocols* 2007;2:2049-56.
373. Starborg M, Gell K, Brundell E, Hoog C. The murine Ki-67 cell proliferation antigen accumulates in the nucleolar and heterochromatic regions of interphase cells and at the periphery of the mitotic chromosomes in a process essential for cell cycle progression. *J Cell Sci* 1996;109 ( Pt 1):143-53.
374. Yu Y, Arora A, Min W, Roifman CM, Grunebaum E. EdU incorporation is an alternative non-radioactive assay to [3H]thymidine uptake for in vitro measurement of mice T-cell proliferations. *Journal of Immunological Methods* 2009;350:29-35.
375. Buck SB, Bradford J, Gee KR, Agnew BJ, Clarke ST, Salic A. Detection of S-phase cell cycle progression using 5-ethynyl-2'-deoxyuridine incorporation with click chemistry, an alternative to using 5-bromo-2'-deoxyuridine antibodies. *BioTechniques* 2008;44:927-29.
376. Cappella P, Gasparri F, Pulici M, Moll J. Cell Proliferation Method: Click Chemistry Based on BrdU Coupling for Multiplex Antibody Staining. *Current Protocols in Cytometry* 2008;Chapter 7.
377. Zaritskaya L, Shurin MR, Sayers TJ, Malyguine AM. New flow cytometric assays for monitoring cell-mediated cytotoxicity. *Expert Rev Vaccines* 2010;9:601-16.
378. Betts MR, Brenchley JM, Price DA, et al. Sensitive and viable identification of antigen-specific CD8+ T cells by a flow cytometric assay for degranulation. *Journal of Immunological Methods* 2003;281:65-78.
379. Linder CC. Mouse Nomenclature and Maintenance of Genetically Engineered Mice. *Comparative Medicine* 2003;53:119-25.
380. Mittal AK, Chaturvedi NK, Rai KJ, et al. Chronic lymphocytic leukemia cells in a lymph node microenvironment depict molecular signature associated with an aggressive disease. *Mol Med* 2014;20:290-301.
381. Lai L, Alaverdi N, Maltais L, Morse HC. Mouse Cell Surface Antigens: Nomenclature and Immunophenotyping. *The Journal of Immunology* 1998;160:3861-8.

382. Steeber DA, Green NE, Sato S, Tedder TF. Lymphocyte migration in L-selectin-deficient mice. Altered subset migration and aging of the immune system. *The Journal of Immunology* 1996;157:1096-106.
383. Lee WT, Vitetta EE. The differential expression of homing and adhesion molecules on virgin and memory T cells in the mouse. *Cell Immunol* 1991;132:125-222.
384. Kearney ER, Pape KA, Loh DY, Jenkins MK. Visualization of peptide-specific T cell immunity and peripheral tolerance induction in vivo. *Immunity* 1994;1:327-39.
385. Lee WT, Vitetta ES. Limiting dilution analysis of CD45Rhi and CD45Rlo T cells: further evidence that CD45Rlo cells are memory cells. *Cell Immunol* 1990;130:459-71.
386. Budd RC, Cerottini JC, MacDonald HR. Selectively increased production of interferon-gamma by subsets of Lyt-2+ and L3T4+ T cells identified by expression of Pgp-1. *The Journal of Immunology* 1987;138:3583-6.
387. Ernst DN, Weigle WO, Noonan DJ, McQuitty DN, Hobbs MV. The age-associated increase in IFN-gamma synthesis by mouse CD8+ T cells correlates with shifts in the frequencies of cell subsets defined by membrane CD44, CD45RB, 3G11, and MEL-14 expression. *The Journal of Immunology* 1993;151:575-87.
388. Sallusto F, Lenig D, Forster R, Lipp M, Lanzavecchia A. Two subsets of memory T lymphocytes with distinct homing potentials and effector functions. *Nature* 1999;401:708-12.
389. Henaio-Tamayo MI, Ordway DJ, Irwin SM, Shang S, Shanley C, Orme IM. Phenotypic Definition of Effector and Memory T-Lymphocyte Subsets in Mice Chronically Infected with *Mycobacterium tuberculosis*. *Clinical and Vaccine Immunology* 2010;17:618-25.
390. Mills KH, Worman CP, Cawley JC. T-cell subsets in B-chronic lymphocytic leukaemia (CLL). *Br J Haematol* 1982;50:710-2.
391. Lauria F, Foa R, Catovsky D. Increase in T gamma lymphocytes in B-cell chronic lymphocytic leukaemia. *Scand J Haematol* 1980;24:187-90.
392. Pizzolo G, Chilosi M, Ambrosetti A, Semenzato G, Fiore-Donati L, Perona G. Immunohistologic study of bone marrow involvement in B-chronic lymphocytic leukemia. *Blood* 1983;62:1289-96.
393. Klinker MW, Lizzio V, Reed TJ, Fox DA, Lundy SK. Human B cell-derived lymphoblastoid cell lines constitutively produce Fas ligand and secrete MHCII+ FasL+ killer exosomes. *Frontiers in Immunology* 2014;5:144.
394. Backteman K, Andersson C, Dahlin LG, Ernerudh J, Jonasson L. Lymphocyte subpopulations in lymph nodes and peripheral blood: a comparison between patients with stable angina and acute coronary syndrome. *PLoS One* 2012;7:e32691.
395. Al-Banna NA, Vaci M, Slauenwhite D, Johnston B, Issekutz TB. CCR4 and CXCR3 play different roles in the migration of T cells to inflammation in skin, arthritic joints, and lymph nodes. *European Journal of Immunology* 2014;44:1633-43.
396. Mu X, Kay NE, Gosland MP, Jennings CD. Analysis of blood T-cell cytokine expression in B-chronic lymphocytic leukaemia: evidence for increased levels of cytoplasmic IL-4 in resting and activated CD8 T cells. *Br J Haematol* 1997;96:733-5.
397. Bojarska-Junak A, Rolinski J, Wasik-Szczepaneko E, Kaluzny Z, Dmoszynska A. Intracellular tumor necrosis factor production by T- and B-cells in B-cell chronic lymphocytic leukemia. *Haematologica* 2002;87:490-9.
398. Gallego A, Vargas JA, Castejon R, et al. Production of intracellular IL-2, TNF-alpha, and IFN-gamma by T cells in B-CLL. *Cytometry B Clin Cytom* 2003;56:23-9.
399. Podhorecka M, Dmoszynska A, Rolinski J. Intracellular IFN-gamma expression by CD3+/CD8+ cell subset in B-CLL patients correlates with stage of the disease. *Eur J Haematol* 2004;73:29-35.
400. Zaki M, Douglas R, Patten N, et al. Disruption of the IFN-gamma cytokine network in chronic lymphocytic leukemia contributes to resistance of leukemic B cells to apoptosis. *Leuk Res* 2000;24:611-21.
401. Yoshizaki K, Nakagawa T, Kaieda T, Muraguchi A, Yamamura Y, Kishimoto T. Induction of proliferation and Ig production in human B leukemic cells by anti-immunoglobulins and T cell factors. *J Immunol* 1982;128:1296-301.
402. Kared H, Camous X, Larbi A. T cells and their cytokines in persistent stimulation of the immune system. *Current Opinion in Immunology* 2014;29:79-85.
403. Messmer BT, Messmer D, Allen SL, Koltz JE, Kudalkar P, Cesar D. In vivo measurements document the dynamic cellular kinetics of chronic lymphocytic leukemia B cells. *J Clin Invest* 2005;115:755-64.
404. Blackburn SD, Shin H, Haining WN, et al. Coregulation of CD8+ T cell exhaustion by multiple inhibitory receptors during chronic viral infection. *Nat Immunol* 2009;10:29-37.
405. Day CL, Kaufmann DE, Kiepiela P, et al. PD-1 expression on HIV-specific T cells is associated with T-cell exhaustion and disease progression. *Nature* 2006;443:350-4.
406. Barber DL, Wherry EJ, Masopust D, et al. Restoring function in exhausted CD8 T cells during chronic viral infection. *Nature* 2006;439:682-7.
407. Petrovas C, Casazza JP, Brenchley JM, et al. PD-1 is a regulator of virus-specific CD8+ T cell survival in HIV infection. *The Journal of Experimental Medicine* 2006;203:2281-92.
408. Freeman GJ. Engagement of the PD-1 immunoinhibitory receptor by a novel B7 family member leads to negative regulation of lymphocyte activation. *J Exp Med* 2000;192:1027-34.

409. Quigley M, Pereyra F, Nilsson B, et al. Transcriptional analysis of HIV-specific CD8+ T cells shows that PD-1 inhibits T cell function by upregulating BATF. *Nat Med* 2010;16:1147-51.
410. Zinselmeyer BH, Heydari S, Sacristán C, et al. PD-1 promotes immune exhaustion by inducing antiviral T cell motility paralysis. *The Journal of Experimental Medicine* 2013;210:757-74.
411. Matloubian M, Kolhekar SR, Somasundaram T, Ahmed R. Molecular determinants of macrophage tropism and viral persistence: importance of single amino acid changes in the polymerase and glycoprotein of lymphocytic choriomeningitis virus. *Journal of Virology* 1993;67:7340-9.
412. Wherry EJ, Ha S-J, Kaech SM, et al. Molecular Signature of CD8+ T Cell Exhaustion during Chronic Viral Infection. *Immunity* 2007;27:670-84.
413. Doering TA, Crawford A, Angelosanto JM, Paley MA, Ziegler CG, Wherry EJ. Network Analysis Reveals Centrally Connected Genes and Pathways Involved in CD8+ T Cell Exhaustion versus Memory. *Immunity* 2012;37:1130-44.
414. Rangachari M, Zhu C, Sakuishi K, et al. Bat3 promotes T cell responses and autoimmunity by repressing Tim-3-mediated cell death and exhaustion. *Nature Medicine* 2012;18:1394-400.
415. Shin H, Blackburn SD, Intlekofer AM, et al. A Role for the Transcriptional Repressor Blimp-1 in CD8+ T Cell Exhaustion during Chronic Viral Infection. *Immunity* 2009;31:309-20.
416. Utzschneider DT, Legat A, Furtos Marraco SA, et al. T cells maintain an exhausted phenotype after antigen withdrawal and population reexpansion. *Nature Immunology* 2013;14:603-10.
417. Blackburn SD, Shin H, Freeman GJ, Wherry EJ. Selective expansion of a subset of exhausted CD8 T cells by  $\alpha$ PD-L1 blockade. *Proceedings of the National Academy of Sciences of the United States of America* 2008;105:15016-21.
418. Mumprecht S, Schuerch C, Schwaller J, Solenthaler M, Ochsenbein AF. Programmed death 1 signaling on chronic myeloid leukemia-specific T cells results in T-cell exhaustion and disease progression. *Blood* 2009;114:1528-36.
419. Zhou Q, Munger ME, Veenstra RG, et al. Coexpression of Tim-3 and PD-1 identifies a CD8+ T-cell exhaustion phenotype in mice with disseminated acute myelogenous leukemia. *Blood* 2011;117:4501-10.
420. Woo SR, Turnis ME, Goldberg MV, et al. Immune inhibitory molecules LAG-3 and PD-1 synergistically regulate T-cell function to promote tumoral immune escape. *Cancer Research* 2012;72:917-27.
421. Grosso JF, Kelleher CC, Harris TJ, et al. LAG-3 regulates CD8+ T cell accumulation and effector function in murine self- and tumor-tolerance systems. *The Journal of Clinical Investigation* 2007;117:3383-92.
422. Sakuishi K, Apetoh L, Sullivan JM, Blazar BR, Kuchroo VK, Anderson AC. Targeting Tim-3 and PD-1 pathways to reverse T cell exhaustion and restore anti-tumor immunity. *The Journal of Experimental Medicine* 2010;207:2187-94.
423. Lasaro MO, Sazanovich M, Giles-Davis W, et al. Active Immunotherapy Combined With Blockade of a Coinhibitory Pathway Achieves Regression of Large Tumor Masses in Cancer-prone Mice. *Mol Ther* 2010;19:1727-36.
424. Duraiswamy J, Ibegbu CC, Masopust D, et al. Phenotype, Function, and Gene Expression Profiles of Programmed Death-1hi CD8 T Cells in Healthy Human Adults. *The Journal of Immunology* 2011;186:4200-12.
425. Kaech SM, Tan JT, Wherry EJ, Konieczny BT, Surh CD, Ahmed R. Selective expression of the interleukin 7 receptor identifies effector CD8 T cells that give rise to long-lived memory cells. *Nat Immunol* 2003;4:1191-8.
426. Yeo CJJ, Fearon DT. T-bet-mediated differentiation of the activated CD8+ T cell. *European Journal of Immunology* 2011;41:60-6.
427. Chen L, Flies DB. Molecular mechanisms of T cell co-stimulation and co-inhibition. *Nat Rev Immunol* 2013;13:227-42.
428. Taube JM, Klein A, Brahmer JR, et al. Association of PD-1, PD-1 Ligands, and Other Features of the Tumor Immune Microenvironment with Response to Anti-PD-1 Therapy. *Clinical Cancer Research* 2014.
429. Zhong X, Tumang JR, Gao W, Bai C, Rothstein TL. PD-L2 expression extends beyond dendritic cells/macrophages to B1 cells enriched for V(H)11/V(H)12 and phosphatidylcholine binding. *Eur J Immunol* 2007;37:2405-11.
430. Nelson BH. IL-2, Regulatory T Cells, and Tolerance. *The Journal of Immunology* 2004;172:3983-8.
431. Gowda A, Ramanunni A, Cheney C, et al. Differential effects of IL-2 and IL-21 on expansion of the CD4+ CD25+ Foxp3+ T regulatory cells with redundant roles in natural killer cell mediated antibody dependent cellular cytotoxicity in chronic lymphocytic leukemia. *MAbs* 2010;2:35-41.
432. West EE, Jin H-T, Rasheed A-U, et al. PD-L1 blockade synergizes with IL-2 therapy in reinvigorating exhausted T cells. *The Journal of Clinical Investigation* 2013;123:2604-15.
433. Kinter AL, Godbout EJ, McNally JP, et al. The common gamma-chain cytokines IL-2, IL-7, IL-15, and IL-21 induce the expression of programmed death-1 and its ligands. *J Immunol* 2008;181:6738-46.
434. Corral LG, Muller GW, Moreira AL, et al. Selection of novel analogs of thalidomide with enhanced tumor necrosis factor alpha inhibitory activity. *Mol Med* 1996;2:506-15.

435. Muller GW, Corral LG, Shire MG, et al. Structural modifications of thalidomide produce analogs with enhanced tumor necrosis factor inhibitory activity. *Journal of medicinal chemistry* 1996;39:3238-40.
436. Haslett PAJ, Corral LG, Albert M, Kaplan G. Thalidomide Costimulates Primary Human T Lymphocytes, Preferentially Inducing Proliferation, Cytokine Production, and Cytotoxic Responses in the CD8+ Subset. *The Journal of Experimental Medicine* 1998;187:1885-92.
437. Corral LG, Haslett PA, Muller GW, et al. Differential cytokine modulation and T cell activation by two distinct classes of thalidomide analogues that are potent inhibitors of TNF- $\alpha$ . *J Immunol* 1999;163:380-6.
438. Schafer PH, Gandhi AK, Loveland MA, et al. Enhancement of Cytokine Production and AP-1 Transcriptional Activity in T Cells by Thalidomide-Related Immunomodulatory Drugs. *Journal of Pharmacology and Experimental Therapeutics* 2003;305:1222-32.
439. Payvandi F, Wu L, Naziruddin SD, et al. Immunomodulatory drugs (IMiDs) increase the production of IL-2 from stimulated T cells by increasing PKC- $\theta$  activation and enhancing the DNA-binding activity of AP-1 but not NF- $\kappa$ B, OCT-1, or NF-AT. *Journal of Interferon & Cytokine Research: the official journal of the International Society for Interferon and Cytokine Research* 2005;25:604-16.
440. Rougerie P, Delon J. Rho GTPases: masters of T lymphocyte migration and activation. *Immunol Lett* 2012;142:1-13.
441. Gassner FJ, Zaborsky N, Neureiter D, et al. Chemotherapy-induced augmentation of T cells expressing inhibitory receptors is reversed by treatment with lenalidomide in chronic lymphocytic leukemia. *Haematologica* 2014;99:67-9.
442. Lee B-N, Gao H, Cohen EN, et al. Treatment with lenalidomide modulates T-cell immunophenotype and cytokine production in patients with chronic lymphocytic leukemia. *Cancer* 2011;117:3999-4008.
443. Idler I, Giannopoulos K, Zenz T, et al. Lenalidomide treatment of chronic lymphocytic leukaemia patients reduces regulatory T cells and induces Th17 T helper cells. *Br J Haematol* 2010;148:948-50.
444. Dauguet N, Fournié J-J, Poupot R, Poupot M. Lenalidomide down regulates the production of interferon- $\gamma$  and the expression of inhibitory cytotoxic receptors of human Natural Killer cells. *Cellular Immunology* 2010;264:163-70.
445. Davies FE, Raje N, Hideshima T, et al. Thalidomide and immunomodulatory derivatives augment natural killer cell cytotoxicity in multiple myeloma. *Blood* 2001;98:210-6.
446. Hayashi T, Hideshima T, Akiyama M, et al. Molecular mechanisms whereby immunomodulatory drugs activate natural killer cells: clinical application. *British Journal of Haematology* 2005;128:192-203.
447. Gorgun G, Calabrese E, Soydan E, et al. Immunomodulatory effects of lenalidomide and pomalidomide on interaction of tumor and bone marrow accessory cells in multiple myeloma. *Blood* 2010;116:3227-37.
448. Chanan-Khan AA, Chitta K, Ersing N, et al. Biological effects and clinical significance of lenalidomide-induced tumour flare reaction in patients with chronic lymphocytic leukaemia: in vivo evidence of immune activation and antitumour response. *British Journal of Haematology* 2011;155:457-67.
449. Rozewski DM, Herman SE, Towns WH, 2nd, et al. Pharmacokinetics and tissue disposition of lenalidomide in mice. *The AAPS journal* 2012;14:872-82.
450. Liu Q, Farley KL, Johnson AJ, et al. Development and Validation of a Highly Sensitive Liquid Chromatography/Mass Spectrometry Method for Simultaneous Quantification of Lenalidomide and Flavopiridol in Human Plasma. *Therapeutic Drug Monitoring* 2008;30:620-7  
10.1097/FTD.0b013e318185813d.
451. Davies F, Baz R. Lenalidomide mode of action: linking bench and clinical findings. *Blood Rev* 2010;24 Suppl 1:S13-9.
452. Lapalombella R, Andritsos L, Liu Q, et al. Lenalidomide treatment promotes CD154 expression on CLL cells and enhances production of antibodies by normal B cells through a PI3-kinase-dependent pathway. *Blood* 2010;115:2619-29.
453. Fecteau JF, Corral LG, Ghia EM, et al. Lenalidomide inhibits the proliferation of CLL cells via a cereblon/p21WAF1/Cip1-dependent mechanism independent of functional p53. *Blood* 2014;124:1637-44.
454. FDA Guidance for Industry. Estimating the Maximum Safe Starting Dose in Initial Clinical Trials for Therapeutics in Adult Healthy Volunteers. U.S. Department of Health and Human Services, Food and Drug Administration, Center for Drug Evaluation and Research (CDER). July 2005. <http://www.fda.gov/downloads/Drugs/GuidanceComplianceRegulatoryInformation/Guidances/ucm078932.pdf>. Accessed September 2014.
455. Brown JR, Abramson J, Hochberg E, et al. A phase I study of lenalidomide in combination with fludarabine and rituximab in previously untreated CLL/SLL. *Leukemia* 2010;24:1972-5.
456. Yang XX, Hu ZP, Xu AL, et al. A mechanistic study on reduced toxicity of irinotecan by coadministered thalidomide, a tumor necrosis factor- $\alpha$  inhibitor. *The Journal of pharmacology and experimental therapeutics* 2006;319:82-104.
457. Meyring M, Muhlbacher J, Messer K, et al. In vitro biotransformation of (R)- and (S)-thalidomide: application of circular dichroism spectroscopy to the stereochemical characterization of the hydroxylated metabolites. *Analytical chemistry* 2002;74:3726-35.
458. Ito T, Ando H, Suzuki T, et al. Identification of a primary target of thalidomide teratogenicity. *Science* 2010;327:1345-50.

459. Zhu YX, Braggio E, Shi CX, et al. Cereblon expression is required for the antimyeloma activity of lenalidomide and pomalidomide. *Blood* 2011;118:4771-9.
460. Lopez-Girona A, Mendy D, Ito T, et al. Cereblon is a direct protein target for immunomodulatory and antiproliferative activities of lenalidomide and pomalidomide. *Leukemia* 2012;26:2326-35.
461. Chamberlain PP, Lopez-Girona A, Miller K, et al. Structure of the human Cereblon–DDB1–lenalidomide complex reveals basis for responsiveness to thalidomide analogs. *Nat Struct Mol Biol* 2014;21:803-9.
462. Lu G, Middleton RE, Sun H, et al. The Myeloma Drug Lenalidomide Promotes the Cereblon-Dependent Destruction of Ikaros Proteins. *Science* 2014;343:305-9.
463. Gandhi AK, Kang J, Havens CG, et al. Immunomodulatory agents lenalidomide and pomalidomide co-stimulate T cells by inducing degradation of T cell repressors Ikaros and Aiolos via modulation of the E3 ubiquitin ligase complex CRL4CRBN. *British Journal of Haematology* 2014;164:811-21.
464. Quintana FJ, Jin H, Burns EJ, et al. Aiolos promotes TH17 differentiation by directly silencing IL2 expression. *Nat Immunol* 2012;13:770-7.
465. Duhamel M, Arrouss I, Merle-Beral H, Rebollo A. The Aiolos transcription factor is up-regulated in chronic lymphocytic leukemia. *Blood* 2008;111:3225-8.
466. Billot K, Soeur J, Chereau F, et al. Deregulation of Aiolos expression in chronic lymphocytic leukemia is associated with epigenetic modifications. *Blood* 2011;117:1917-27.
467. Chan AC, Carter PJ. Therapeutic antibodies for autoimmunity and inflammation. *Nat Rev Immunol* 2010;10:301-16.
468. US National Library of Medicine. Clinicaltrials.gov <http://clinicaltrials.gov/show/NCT01096602>, last accessed September 11, 2014. (Accessed September 11, at
469. US National Library of Medicine. Clinicaltrials.gov, <http://clinicaltrials.gov/show/NCT01067287>, last accessed September 11, 2014. (Accessed at
470. US National Library of Medicine. Clinicaltrials.gov, <http://clinicaltrials.gov/show/NCT02077959>, last accessed September 11, 2014.
471. US National Library of Medicine. Clinicaltrials.gov, <http://clinicaltrials.gov/show/NCT01953692> last accessed September 11, 2014.
472. US National Library of Medicine. Clinicaltrials.gov, <http://clinicaltrials.gov/show/NCT01375842> last accessed September 11, 2014.
473. US National Library of Medicine. Clinicaltrials.gov, <http://clinicaltrials.gov/show/NCT01452334> last accessed September 11, 2014.
474. Spranger S, Koblisch HK, Horton B, Scherle PA, Newton R, Gajewski TF. Mechanism of tumor rejection with doublets of CTLA-4, PD-1/PD-L1, or IDO blockade involves restored IL-2 production and proliferation of CD8(+) T cells directly within the tumor microenvironment. *J Immunother Cancer* 2014;2:eCollection 2014.
475. Yu P, Steel JC, Zhang M, et al. Simultaneous inhibition of two regulatory T-cell subsets enhanced Interleukin-15 efficacy in a prostate tumor model. *Proc Natl Acad Sci U S A* 2012;109:6187-92.
476. Wainwright DA, Chang AL, Dey M, et al. Durable therapeutic efficacy utilizing combinatorial blockade against IDO, CTLA-4 and PD-L1 in mice with brain tumors. *Clinical Cancer Research* 2014.
477. Noman MZ, Desantis G, Janji B, et al. PD-L1 is a novel direct target of HIF-1 $\alpha$ , and its blockade under hypoxia enhanced MDSC-mediated T cell activation. *The Journal of Experimental Medicine* 2014;211:781-90.
478. Kuang DM. Activated monocytes in peritumoral stroma of hepatocellular carcinoma foster immune privilege and disease progression through PD-L1. *J Exp Med* 2009;206:1327-37.
479. van der Heijden A, van Dijk JE, Lemmens AG, Beynen AC. Spleen pigmentation in young C57BL mice is caused by accumulation of melanin. *Laboratory Animals* 1995;29:459-63.
480. Butte MJ, Peña-Cruz V, Kim M-J, Freeman GJ, Sharpe AH. Interaction of human PD-L1 and B7-1. *Molecular Immunology* 2008;45:3567-72.
481. Paterson AM. The programmed death-1 ligand 1:B7-1 pathway restrains diabetogenic effector T cells in vivo. *J Immunol* 2011;187:1097-105.
482. McDermott DF, Atkins MB. PD-1 as a potential target in cancer therapy. *Cancer Medicine* 2013;2:662-73.
483. Rossille D, Gressier M, Damotte D, et al. High level of soluble programmed cell death ligand 1 in blood impacts overall survival in aggressive diffuse large B-Cell lymphoma: results from a French multicenter clinical trial. *Leukemia* 2014.
484. Matsuzaki J, Gnjjatic S, Mhawech-Fauceglia P, et al. Tumor-infiltrating NY-ESO-1-specific CD8+ T cells are negatively regulated by LAG-3 and PD-1 in human ovarian cancer. *Proceedings of the National Academy of Sciences of the United States of America* 2010;107:7875-80.
485. Butler NS, Moebius J, Pewe LL, et al. Therapeutic blockade of PD-L1 and LAG-3 rapidly clears established blood-stage Plasmodium infection. *Nat Immunol* 2012;13:188-95.
486. Hodi FS. Biologic activity of cytotoxic T lymphocyte-associated antigen 4 antibody blockade in previously vaccinated metastatic melanoma and ovarian carcinoma patients. *Proc Natl Acad Sci USA* 2003;100:4712-7.
487. Hodi FS, O'Day SJ, McDermott DF, et al. Improved Survival with Ipilimumab in Patients with Metastatic Melanoma. *New England Journal of Medicine* 2010;363:711-23.

488. Ansell SM, Hurvitz SA, Koenig PA, et al. Phase I Study of Ipilimumab, an Anti-CTLA-4 Monoclonal Antibody, in Patients with Relapsed and Refractory B-Cell Non-Hodgkin Lymphoma. *Clinical Cancer Research* 2009;15:6446-53.
489. Wolchok JD, Kluger H, Callahan MK, et al. Nivolumab plus Ipilimumab in Advanced Melanoma. *New England Journal of Medicine* 2013;369:122-33.
490. Pallasch CP, Ulbrich S, Brinker R, Hallek M, Uger RA, Wendtner C-M. Disruption of T cell suppression in chronic lymphocytic leukemia by CD200 blockade. *Leukemia Research* 2009;33:460-4.
491. Ge Y, Xi H, Zhang X. Blockade of PD-1/PD-L1 immune checkpoint during DC vaccination induces potent protective immunity against breast cancer in hu-SCID mice. *Cancer letters* 2013;336:253-9.
492. Hallett WH, Jing W, Drobyski WR, Johnson RD. Immunosuppressive effects of multiple myeloma are overcome by PD-L1 blockade. *Biology of blood and marrow transplantation : journal of the American Society for Blood and Marrow Transplantation* 2011;17:1133-45.
493. Haile ST, Dalal SP, Clements V, Tamada K, Ostrand-Rosenberg S. Soluble CD80 Restores T Cell Activation and Overcomes Tumor Cell Programmed Death Ligand 1-Mediated Immune Suppression. *The Journal of Immunology* 2013;191:2829-36.
494. Herling M, Patel KA, Khalili J, et al. TCL1 shows a regulated expression pattern in chronic lymphocytic leukemia that correlates with molecular subtypes and proliferative state. *Leukemia* 2006;20:280-5.
495. Herling M, Patel KA, Weit N, Lilienthal N, Hallek M, Keating MJ. High TCL1 levels are a marker of B-cell receptor pathway responsiveness and adverse outcome in chronic lymphocytic leukemia. *Blood* 2009;114:4675-86.
496. Kienle D, Benner A, Laeuffle C, et al. Gene expression factors as predictors of genetic risk and survival in chronic lymphocytic leukemia. *Haematologica* 2010;95:102-9.
497. Gaudio E, Spizzo R, Paduano F, et al. Tcl1 interacts with Atm and enhances NF-kB activation in hematological malignancies. *Blood* 2011.
498. Landau DA, Carter Scott L, Stojanov P, et al. Evolution and Impact of Subclonal Mutations in Chronic Lymphocytic Leukemia. *Cell* 2013;152:714-26.
499. Herishanu Y, Katz B-Z, Lipsky A, Wiestner A. Biology of Chronic Lymphocytic Leukemia in Different Microenvironments: Clinical and Therapeutic Implications. *Hematology/Oncology Clinics of North America* 2013;27:173-206.
500. Motz GT, Coukos G. Deciphering and reversing tumor immune suppression. *Immunity* 2013;39:61-73.
501. Fabbri M, Paone A, Calore F, et al. MicroRNAs bind to Toll-like receptors to induce prometastatic inflammatory response. *Proceedings of the National Academy of Sciences* 2012;109:E2110-E6.
502. Ntoufa S, Vardi A, Papakonstantinou N, et al. Distinct innate immunity pathways to activation and tolerance in subgroups of chronic lymphocytic leukemia with distinct immunoglobulin receptors. *Mol Med* 2012;18:1281-91.
503. Kubo S, Yamada T, Osawa Y, Ito Y, Narita N, Fujieda S. Cytosine-phosphate-guanosine-DNA induces CD274 expression in human B cells and suppresses T helper type 2 cytokine production in pollen antigen-stimulated CD4-positive cells. *Clin Exp Immunol* 2012;169:1-9.